SPIN DYNAMICS OF NUCLEAR SINGLET-STATES:

APPLICATION TO PARAHYDROGEN INDUCED HYPERPOLARIZATION

By

Chong Cai

Dissertation

Submitted to the Faculty of the

Graduate School of Vanderbilt University

in partial fulfillment of the requirements

for the degree of

DOCTOR OF PHILOSOPHY

in

Physics

December, 2013

Nashville, Tennessee

Approved

Kevin Waddell, PhD

John Gore, PhD

Thomas Weiler, PhD

Thomas Yankeelov, PhD

Zhaohua Ding, PhD

ACKNOWLEDGEMENTS

The doctoral work described in this dissertation was carried out at the Vanderbilt University Institute of Imaging Science over the course of approximately three years leading up to August 2013. I am grateful to the members of my committee for taking time from their busy schedules to help me along this journey. I would especially like to thank Dr. Kevin Waddell and feel very lucky to have him as my advisor. He led me into NMR technology when I knew little about this area, and came up with the idea of designing pulse sequences for manipulation of parahydrogen singlet-states, which became the major focus of my doctoral research. I also want to thank Dr. John Gore, co-chair of my committee, for providing a fertile environment to complete this work, and for discussion that helped to broaden my understanding of MRI. I am also grateful for the help of Dr. Thomas Yankeelov, Dr. Thomas Weiler and Dr. Zhaohua Ding for their guidance and communication that helped to deepen my understanding of this project. I am honored to have had the help of all of these people on my PhD committee.

I also want to thank the people in my research group. Raul Colon, Isaac Esteve Manzanera, Sasidhar Tadanki, and Jay Moore all helped with various aspects of my project. Their help in device set up and experiments improved the efficiency of the projects I worked on. This work would not be completed so smoothly without their cooperation.

I would like to thank Dr. Eduard Chekmenev, Aaron Coffey, and Dr. Roman

Shchepin, who were particularly helpful in chemical preparation and as collaborators on our experiments.

Finally, I owe a debt of gratitude to my family. When I chose to study in a place far away from home for a PhD career, my parents were very supportive. Their love and guidance accompany me wherever I am. They are always patient and supportive to me, and show great interest in the work I am doing. My PhD life would not have been so enjoyable without their support.

TABLE OF CONTENTS

Page

ACKNOWLEDGEMENTS ii

LIST OF TABLES vii

LIST OF FIGURES viii

CHAPTER

1. INTRODUCTION TO NUCLEAR MAGNETIC RESONANCE AND PARAHYDROGEN SINGLET-STATES 1

1.1. NMR Foundation 4
1.1.1. Zeeman effect 4
1.1.2. Chemical shift 6
1.1.3. Spin - spin coupling 7
1.1.4. Relaxation 8
1.2. Product Operator Basis 9
1.2.1. Spin states 10
1.2.2. Coherences 11
1.2.3. Hamiltonian 13
1.2.4. Evolution 14
1.3. NMR Sensitivity 15
1.3.1. Signal to noise ratio (SNR) 15
1.3.2. Thermal equilibrium 16
1.4. Dynamic Nuclear Polarization 19
1.4.1. DNP method 19
1.4.2. DNP applications 19
1.4.3. Pitfalls of DNP hyperpolarization 21
1.5. Parahydrogen singlet-state 21
1.6. Singlet-state populations 24
1.6.1. Dependence of singlet-state polarization on temperature 24
1.6.2. Angular momentum selection rules 27
1.6.3. Parahydrogen production devices 28
1.7. Operator basis of parahydrogen state 29
1.8. PASADENA and ALTADENA 32
1.8.1. PASADENA 32
1.8.2. ALTADENA 34
1.8.3. Parahydrogen hydrogenation device 36
1.9. Application of parahydrogen induced polarization 37
1.9.1. Setup and pulse sequences 37

1.9.2. Signal to noise ratio (SNR) 39
1.9.3. The optimal magnetic field for hyperpolarization imaging 40
1.9.4. Examples of hyperpolarized ^{13}C imaging 41

2. SPIN ORDER TRANSFER FROM PARAHYDROGEN SINGLET-STATES TO HETERONUCLEAR NET MAGNETIZATION IN AA'X SPIN SYSTEMS 43

2.1. Introduction to hyper - SHIELDED spin order transfer sequence 44
2.2. Mathematical basis analysis method for I_1I_2S spin systems 46
2.3. Methods: Evolution from singlet-state to net magnetization 50
2.3.1. Evolution under 3 spin I_1I_2S system Hamiltonians 50
2.3.2. Evolution of the initial singlet-states 52
2.3.3. Evolution into net heteronuclear magnetization 53
2.3.4. Hyper-SHIELDED pulse sequence 55
2.4. Experiment Section 57
2.4.1. Synthesis of parahydrogen gas 57
2.4.2. PASADENA precursor preparation 57
2.4.3. Catalytic hydrogenation 58
2.4.4. Detection of hyperpolarized ^{13}C 59
2.5. Discussion 59

3. SPIN ORDER TRANSFER FROM PARAHYDROGEN SINGLET-STATES INTO HETERONUCLEAR NET MAGNETIZATION IN AA'XY SPIN SYSTEMS 67

3.1. Introduction 69
3.2. Examples of molecules featuring I_1I_2SR spin systems 71
3.2.1. TCA cycle 71
3.2.2. Symmetrical spin system 73
3.3. Mathematical basis of I_1I_2SR systems 77
3.4. Methods: Evolution of parahydrogen singlet-state to heteronuclear net magnetization 79
3.4.1. Evolution of initial singlet-states 79
3.4.2. Evolution to heteronuclear net magnetization 81
3.4.3. Hyper-SHIELDED-4 pulse sequence 83
3.5. Discussion 85
3.6. Further studies: addition of a third channel 94

4. RESOLVING SCALAR COUPLINGS IN LOW INHOMOGENEOUS FIELDS BY INDIRECT DETECTION OF SINGLET-STATE EVOLUTION 98

4.1. Introduction 99
4.1.1. Conformations 100
4.1.2. PH dependence of scalar coupling constants 100
4.2. Method: High resolution scalar coupling spectra 102
4.2.1. Theoretical prediction of J-dependent polarization 102
4.2.2. Experimental 104

4.3. Experiment Results 106
4.4. Discussion 107
APPENDIX

A. PRODUCT OPERATORS FOR AA'X SPIN SYSTEMS 111

A.1. Matrix representation of product operators 111
A.1.1. Product operators for protons 111
A.1.2. Product operators for heteronuclei 113
A.2. Rotations operators 114
A.2.1. 90 degree rotations for protons 114
A.2.2. 180 degree rotations for protons 116
A.2.3. 90 degree rotations for a heteronucleus 118
A.2.4. 180 degree rotations for heteronucleus 119
A.3. Hamiltonian and related states 119
A.3.1. Hamiltonian 119
A.3.2. Related states 121

B. PRODUCT OPERATORS FOR I_1I_2SR SPIN SYSTEMS 124

B.1. Matrix representations of major product operators 124
B.1.1. Product operators for protons 124
B.1.2. Product operators for heteronuclei 128
B.2. Rotations of product operator states 131
B.2.1. 90 degree rotations for protons 131
B.2.2. 90 degree rotations for heteronuclei 132
B.2.3. 180 degree rotations for protons 135
B.2.4. 180 degree rotations for heteronuclei 136
B.3. Hamiltonians and related states 139
B.3.1. Hamiltonians 139
B.3.2. Related states 142

C. EVOLUTION OF STATES IN AA'XY SPIN SYSTEMS 151

C.1. Evolution of the initial singlet-state 151
C.2. Evolution to heteronuclear net magnetization 154

D. PROGRAM SOURCE CODES 159

D.1. Pulse programs for Hyper-SHIELDED 159
D.2. Pulse programs for I_1I_2SR spin system pulse sequence 167
D.3. Monte Carlo model for high resolution J spectroscopy and resolution 186

REFERENCES 193

LIST OF TABLES

TABLE 1.1. Product operator representation of the density matrix for a two spin system 11
TABLE 1.2. Correlations between rotational and spin wave function, and the forms of H_2 23
TABLE 1.3. Percentage of parahydrogen as a function of temperature 26
TABLE 4.1. Fraction of succinate ions as a function of pH. 101

LIST OF FIGURES

FIGURE 1.1. Zeeman Effect 6

FIGURE 1.2. Scheme of the rotational energy levels.....25

FIGURE 1.3. Schematic of parahydrogen production device 28

FIGURE 1.4. Proton spectrum of enriched parahydrogen gas 29

FIGURE 1.5. Reaction scheme for synthesizing parahydrogenated molecules 31

FIGURE 1.6. Schematic of the PASADENA experiment 33

FIGURE 1.7. Schematic of the ALTADENA experiment.....35

FIGURE 1.8. Schematic of the polarizer 36

FIGURE 2.1. Schematic of hyper-SHIELDED pulse sequence 55

FIGURE 2.2. Graphical depiction of evolution of density matrix of hyper - SHIELDED 56

FIGURE 2.3. Plot of polarization yield as a function of coupling constants 63

FIGURE 2.4. Polarization transfer efficiency of hyper-SHIELDED versus GPS 64

FIGURE 2.5. Experiment results of polarization yield of hype -SHIELDED sequence 65

FIGURE 3.1. Schematic of TCA cycle 72

FIGURE 3.2. Schematic of 1,4 - ^{13}C - labeled fumaric acid 73

FIGURE 3.3. Schematic of the Hyper-SHIELDED-4 polarization transfer pulse sequence 83

FIGURE 3.4. Evolution of density matrix components under the influence of hyper - SHIELDED pulse sequence 84

FIGURE 3.5. Graph of polarization yield from I_1I_2SR sequence for all three configurations 89

FIGURE 3.6. Plot of polarization yield from I_1I_2SR sequence with different durations 92

FIGURE 3.7. Three channel pulse sequence for four spin systems (I_1I_2SR) 95

FIGURE 3.8. Maximum polarization yields of 2 channel sequence and 3 channel sequences 96

FIGURE 4.1. Percentage of the asymetric ion in all three types of ions as a function of pH.....102

FIGURE 4.2. Schematic of multidimensional MR experiments to measure coupling constants.....105

FIGURE 4.3. Fitting of experimental polarization data to theory 107

FIGURE 4.4. Monte Carlo model to extract J coupling constants in 2 - hydroxyethyl 1 - ^{13}C - propionate - d_3.....109

FIGURE 4.5. Monte Carlo confidence interval with 5%, 10%, 15% standard deviation 110

FIGURE D.1. Graphical depiction of evolution of density matrix of hyper - SHIELDED 160

FIGURE D.2. Evolution of the density matrix and the pulse sequence for I_1I_2SR spin systems.....168

CHAPTER 1

INTRODUCTION TO NUCLEAR MAGNETIC RESONANCE AND PARAHYDROGEN SINGLET-STATES

Nuclear magnetic resonance (NMR) has been proven to be a diverse spectroscopic tool for probing molecular structure and their interactions with a broad array of surroundings. NMR was first reported in 1946 by Bloch and Purcell [1, 2], and new applications in biomedicine are still emerging. In fact, the emergence of hyperpolarization technologies that form the focus of this dissertation, are now opening windows into *in vivo* metabolism and providing a unique perspective that is difficult to obtain with traditional MR or alternative, non-MR technologies [3-8]. Although basic science applications in chemistry, molecular biology, and materials science are still growing, hyperpolarization methods have positioned NMR for rapid new growth in the field of biomedicine.

Nuclear magnetic moments resonate with applied fields in proximity to the Larmor precession frequency [9]. The chemical environment perturbs this characteristic Larmor precession of nuclei, as in conjunction with the correlated modulation in these offsets as reflected in scalar coupling networks, provide detailed information about the molecular structure in which the nucleus resides [10-12]. Given sufficient sensitivity, this enables observation of chemical reaction in general, and now allows a direct method of interrogating metabolism non-invasively *in vivo*.

The coherent modes of nuclear magnetism can be considered independent of

interaction with surrounding tissues, and the long lifetimes of these coherences enable comprehensive control over the quantum evolution of the systems. The applied fields necessary to perturb nuclear spins can also be applied safely so as to not physically alter or damage biological tissues. This is important for medical applications, and the lack of exposure to ionizing radiation or invasive surgery is often touted as an advantage of NMR for biomedicine [13-17].

In spite of these advantages, the application of NMR to metabolism has been traditionally limited by low equilibrium polarizations and poor sensitivity. For basic science applications, this inherent limitation can be partially overcome by extending scan time or improving the filling factor of the antennas to better match the biological tissue of interest. However, in biomedical applications, scan times are limited and Boltzmann polarization levels limit detection of protons to approximately 1 mM/mL. This detection threshold scales with gyromagnetic ratio and abundance. For example, the gyromagnetic ratio of ^{13}C (the observable carbon isotope) is 25% that of protons, and the abundance of this isotope is only 1.1% of all carbon in nature. For this reason, naturally abundant carbon-13 does not contribute significantly to background signal; hence carbon-13 NMR has the promise for high contrast *in vivo*. This has driven interest in polarization enhancement techniques, which aim to transiently increase the sensitivity of NMR on the time-scale of longitudinal relaxation. This dissertation will focus in particular, on the application of parahydrogen for polarizing nuclear magnetic moments.

This chapter starts by introducing NMR principles including the Zeeman effect,

chemical shift, and spin-spin coupling. Then tools to more efficiently manipulate spin operators are described, in the context of the spin density operator, spin Hamiltonians, and the evolution of spin coherences. NMR experiments are traditionally limited by low polarization level at thermal equilibrium, and in section 1.3 these principles are described quantitatively with respect to the NMR signal to noise ratio. Low sensitivity has driven interest in polarization level enhancement techniques - the most established of these techniques, called dynamic nuclear polarization (DNP), is presented in 1.4. Although DNP has proven useful and is becoming widespread, the technique requires bulky and expensive devices that are outside the reach of most laboratories. A complementary or alternative technique, referred to as parahydrogen induced polarization (PHIP), is the focus of this dissertation. With PHIP, high polarization can be generated at low fields using compact devices. Parahydrogen is the singlet-state of diatomic hydrogen gas, and this state is described quantitatively in section 1.5. In order to make use of parahydrogen state, highly enriched parahydrogen gas is necessary, and the method used to obtain parahydrogen gas with high purity at room temperature is discussed in section 1.6. In section 1.7, the spin operator basis representation of parahydrogen is described. Although obtaining high purity parahydrogen gas is possible, the state itself is invisible in NMR experiments; two major experiments to detect signal from the parahydrogen states, PASADENA and ALTADENA, are described in 1.8. Finally, some applications are discussed in section 1.9.

1.1. NMR Foundation

Upon being placed in a magnetic field, a nuclear ensemble generates a net magnetization along the direction of an external magnetic field. In a typical NMR experiment, this state is perturbed by rotating the net magnetization to an orthogonal plane. As it evolves to re-establish equilibrium, this net magnetization induces a current in an adjacent antenna, which can then be recorded and processed to reveal nuclear spin spectra. The underpinnings of this process were described over 100 years ago, when Pieter Zeeman first observed fine structure of nuclear spectra in the presence of a magnetic field [18].

1.1.1. Zeeman effect

The foundation of NMR rests on the intrinsic angular momentum referred to as spin. A spin *s* nucleus has 2s+1 energy levels, with spin angular momentum taking the values , $h\sqrt{s(s+1)}$, where s is restricted to half-integers:

$$s = 0, 1/2, 1, 3/2, \ldots \quad (1.1)$$

The azimuthal quantum number m_s, is used to label these 2s+1 states from m_s = -s, -s+1,…,s-1, to s. The magnetic moment of the nucleus can be written as:

$$\mu = h\gamma m_s , \quad (1.2)$$

where γ refers to the gyromagnetic ratio of the nucleus.

The nuclei most commonly used in NMR have s=½; this includes ^{1}H, ^{13}C, ^{15}N, ^{19}F, and ^{31}P. The states of these so-called spin -1/2 nuclei can be labeled as |α> and |β> [18]. In accord with the Zeeman effect, these two states have exactly the same energy

in the absence of an external magnetic field, and are equally populated at thermal equilibrium. However, in the presence of a magnetic field, +1/2 (|α>) state aligns with an external magnetic field and is lower in energy than -1/2 state, |β>, which is opposed to the magnetic field. At ambient conditions, the |α> state will be slightly more populated than the higher energy |β> state. The energy gap between these two states is proportional to the magnetic field.

$$\Delta E = h\upsilon = E_{-1/2} - E_{+1/2} = \frac{h\gamma B_0}{2\pi} \tag{1.3}$$

with

$$\upsilon = \frac{\gamma B_0}{2\pi} \tag{1.4}$$

where γ is the gyromagnetic ratio of the nucleus. The resonance frequency, ν, occurs in the radio frequency range at modern field strengths, and is known as the Larmor precession frequency [19]. Traditional NMR uses relatively weak electromagnetic radiation (radiofrequencies) delivered on resonance to perturb the equilibrium formed from a stronger static magnetic field. When the applied field is turned off, precession of the nuclear spins in the presence of the static field generates a time-dependent oscillation that can be Fourier transformed to the frequency.

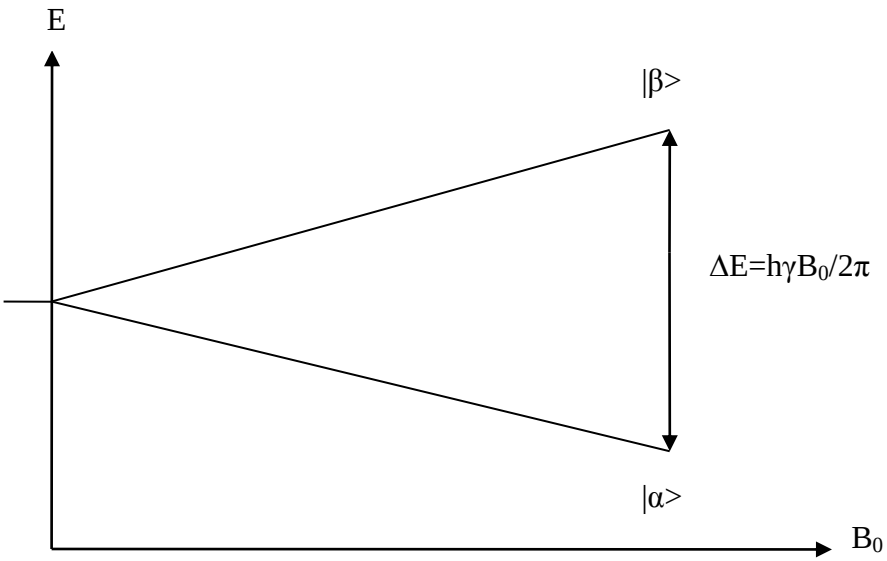

Figure 1.1. Schematic of the energy levels present due to the Zeeman effect. The degeneracy of the two states, |α> and |β>, is lifted in the presence of external magnetic fields, with the field-dependent splitting $\Delta E=h\gamma B_0/2\pi$.

1.1.2. Chemical shift

The diversity in application of NMR results in part from the sensitivity of nuclear precession and the availability of highly homogeneous static fields where small differences in precession can be measured. Larmor precession frequencies depend on the specific nucleus, and additionally on the electronic environment or molecular structure surrounding the nucleus. Each spin is surrounded by an electron distribution, which shields the external magnetic field and shifts the effective magnetic field experienced by the nucleus to $B_0(1-\sigma)$. Therefore the Larmor frequency of each spin is shifted to:

$$\upsilon = \frac{\gamma B_0(1-\sigma)}{2\pi} \tag{1.5}$$

The distribution of chemical environments results in a range of chemical shifts. The chemical shift is normally measured in parts per million (ppm) and is designated by delta (δ). In this representation, the resonance frequency for a particular nucleus in a

certain chemical position of a given molecule could be expressed as the fundamental frequency of the isotope times a factor that is very close to 1 due to the chemical shift, as follows:

$$\upsilon = \upsilon_0(1+\delta\times10^{-6}), \tag{1.6}$$

where $\upsilon_0=\gamma B_0/2\pi$. A typical NMR spectrum contains several peaks over a narrow range of frequencies centered on the fundamental resonance frequency of the nucleus of interest, each peak representing a unique chemical environment where the nucleus resides.

1.1.3. Spin-spin coupling

Apart from chemical shift, for systems with more than one spin there will be spin angular momentum couplings among the spins, referred to as spin-spin coupling [20, 21]. For two adjacent spins in liquids with different chemical shifts, whether the first spin is aligned (|α>) with the magnetic field or opposed (|β>) to the magnetic field influences the external magnetic field experienced by the other spins. Since the resonance frequency is proportional to the magnetic field experienced by the nucleus, the frequency of the second spin changes and now it resonates at one of the two frequencies quite close to each other. Since the two states of the first spin are almost evenly populated, the resonance of the second spin is split into two peaks of equal intensity. This effect works mutually, so the first spin is split into two identical peaks as well. The separation of the peaks is J Hz, which is called the J coupling constant. At fields greater than Earth's field or lower, J coupling normally occurs when the two

nuclei are in close proximity (three bonds or less). Spin-systems can be further characterized by the strength of the scalar coupling relative to chemical shielding. This is referred to as weak or strong coupling - strong coupling occurs mostly in homonuclear systems when $\delta \approx J$, and these systems are normally labeled as AB systems. Weak coupling occurs when $\delta >> J$, mostly in heteronuclear spin systems or in homonuclear systems at high magnetic fields, and are normally referred to as AX systems.

1.1.4. Relaxation

When placed in a magnetic field, the nucleus in the sample creates a net magnetization aligned with the external magnetic field due to Zeeman Effect. In typical NMR experiments the net magnetization is rotated to the transverse plane by a radio frequency pulse, and starts to rotate in the transverse plane at Larmor frequency, which is recorded as NMR signal. However, it does not stay in the transverse plane indefinitely. During evolution, the individual spins experience distinct magnetic fields (due to field inhomogeneity), and gradually lose phase coherence. Transverse components are also simultaneously spiraling around the axis of the magnetic field to re-establish equilibrium [22-27]. These relaxation rates are normally considered separately, as longitudinal relaxation [28-31] and transverse relaxation [32-36].

Longitudinal relaxation (T_1)

When the net magnetization is rotated to transverse plane, if the rotation is precisely 90°, at that moment there is zero magnetization in longitudinal direction.

The longitudinal magnetization starts to reform with time afterwards according to this expression:

$$M_z(t) = M_0[1 - \exp(-t / T_1)]. \quad (1.7)$$

Initially at t=0, M_z=0, and recovering with time according to Equation 1.7. The longitudinal relaxation constant, T_1, represents the rate of longitudinal recovery along the static field. T_1 values for protons are mostly in the range from 0.1 seconds to a few seconds, and much larger for other nuclei and depending on the environment. For example, ^{13}C T_1s in carboxyl groups are on the order of minutes in solution.

Transverse relaxation (T_2)

Once the magnetization is rotated to transverse plane, apart from the rotation in the transverse plane, the magnetization in transverse plane starts to decay as a function of time too, normally referred to as T_2 relaxation:

$$\begin{aligned} M_x(t) &= M_0\cos(2\pi\omega t)\exp(-t / T_2) \\ M_y(t) &= M_0\sin(2\pi\omega t)\exp(-t / T_2) \end{aligned} \quad (1.8)$$

NMR signals must be recorded within a few time periods of T_2, otherwise the signal will vanish.

1.2. Product Operator Basis

A useful tool for analyzing the dynamics of spin-systems with spin-spin interactions and applied fields (pulse sequences) is the density matrix [37]. A convenient basis to expand the density matrix for applications to NMR is the product operator basis first described by Sorenson and coworkers [38].

1.2.1. Spin states

In the product operator basis, the density operators are represented as N×N matrices and spanned by the Pauli operators [39]. The spin operators are formed by the external product of a ket and a bra, e.g. $\mathbf{I_x}=|I_x><I_x|$. For a single spin, the corresponding operators could be represented as:

$$\mathbf{I_0} = \begin{pmatrix} \frac{1}{2} & 0 \\ 0 & \frac{1}{2} \end{pmatrix} = \frac{1}{2}\sigma_0 \tag{1.9}$$

$$\mathbf{I_x} = \begin{pmatrix} 0 & \frac{1}{2} \\ \frac{1}{2} & 0 \end{pmatrix} = \frac{1}{2}\sigma_x \tag{1.10}$$

$$\mathbf{I_y} = \begin{pmatrix} 0 & -\frac{i}{2} \\ \frac{i}{2} & 0 \end{pmatrix} = \frac{1}{2}\sigma_y \tag{1.11}$$

$$\mathbf{I_z} = \begin{pmatrix} \frac{1}{2} & 0 \\ 0 & -\frac{1}{2} \end{pmatrix} = \frac{1}{2}\sigma_z \tag{1.12}$$

The letters I, S, R are traditionally used to represent the spins of the system. The density matrix of the single spin could always be represented by the combination of these the four states [39]:

$$\boldsymbol{\rho} = \frac{\mathbf{I_0}}{2} + \sum_{i=x,y,z} c_i \mathbf{I_i} \tag{1.13}$$

For a two spin system, the product operators expand to sixteen 4×4 matrices as follows [38, 40]:

$$\frac{\mathbf{I_0}}{2} \tag{1.14}$$

$$\mathbf{I_i}, i = x, y, z \tag{1.15}$$

$$\mathbf{S_j}, j = x, y, z \tag{1.16}$$

$$2\mathbf{I_i S_j}, i, j = x, y, z \tag{1.17}$$

Any two spin state could be represented by a combination of these 16 operators, as follows:

$$\boldsymbol{\rho} = \frac{\mathbf{I_0}}{4} + \sum_{i=x,y,z} c_i \mathbf{I_i} + \sum_{j=x,y,z} d_j \mathbf{S_j} + \sum_{i,j=x,y,z} e_{i,j} 2\mathbf{I_i S_j} \tag{1.18}$$

Each of the 16 operators has its own NMR symbol, as listed in Table 1.1.

Table 1.1. The 16 product operators for a two spin system.

Scalar Element	$\mathbf{I_0}/2$
Populations	$\mathbf{I_z}$, $\mathbf{S_z}$, $2\mathbf{I_z S_z}$
Single Quantum Coherence	$\mathbf{I_x}$, $\mathbf{I_y}$, $\mathbf{S_x}$, $\mathbf{S_y}$, $2\mathbf{I_x S_z}$, $2\mathbf{I_y S_z}$, $2\mathbf{S_x I_z}$, $2\mathbf{S_y I_z}$
Multiple Quantum Coherence	$2\mathbf{I_x S_x}$, $2\mathbf{I_y S_x}$, $2\mathbf{I_x S_y}$, $2\mathbf{I_y S_y}$

1.2.2. Coherences

In most NMR experiments, the population operators represent the population in difference between the two spin states of a given spin. The single quantum coherences are transverse components which could be observed and recorded as signal. It could also be represented in the density matrix view. The populations are those operators with only diagonal components, as:

$$\begin{pmatrix} \{\} & & & \\ & \{\} & & \\ & & \{\} & \\ & & & \{\} \end{pmatrix} \tag{1.19}$$

The zero and double quantum coherences are those operators with back diagonal components only, as:

$$\begin{pmatrix} & & & \{\} \\ & & \{\} & \\ & \{\} & & \\ \{\} & & & \end{pmatrix} \tag{1.20}$$

The single quantum coherences, on the other hand, are the operators with off-diagonal components only, as:

$$\begin{pmatrix} & \{\} & \{\} & \\ \{\} & & & \{\} \\ \{\} & & & \{\} \\ & \{\} & \{\} & \end{pmatrix} \tag{1.21}$$

A more common way to represent the multiple quantum coherence (zero and double coherence for two spin) is the expression of their linear combination:

$$ZQ_x = \frac{1}{2}(2\mathbf{I}_x\mathbf{S}_x + 2\mathbf{I}_y\mathbf{S}_y) \tag{1.22}$$

$$ZQ_y = \frac{1}{2}(2\mathbf{I}_y\mathbf{S}_x - 2\mathbf{I}_x\mathbf{S}_y) \tag{1.23}$$

$$DQ_x = \frac{1}{2}(2\mathbf{I}_x\mathbf{S}_x - 2\mathbf{I}_y\mathbf{S}_y) \tag{1.24}$$

$$DQ_y = \frac{1}{2}(2\mathbf{I}_y\mathbf{S}_x + 2\mathbf{I}_x\mathbf{S}_y) \tag{1.25}$$

This are the more commonly used expressions for multiple quantum coherence with populations, single quantum coherences and [ZQ_x, ZQ_y, DQ_x, DQ_y] representing multiple coherences.

Among all those operators, only single quantum coherences are directly observable:

$$\{\mathbf{I_x}, \mathbf{I_y}, \mathbf{S_x}, \mathbf{S_y}, 2\mathbf{I_xS_z}, 2\mathbf{I_yS_z}, 2\mathbf{S_xI_z}, 2\mathbf{S_yI_z}\}. \quad (1.26)$$

Among the single quantum coherence terms, $\{\mathbf{I_x}, \mathbf{I_y}, \mathbf{S_x}, \mathbf{S_y}\}$ represent in-phase while $\{2\mathbf{I_xS_z}, 2\mathbf{I_yS_z}, 2\mathbf{S_xI_z}, 2\mathbf{S_yI_z}\}$ represents anti-phase magnetization [41].

1.2.3. Hamiltonian

For a weakly coupled two spin system, the Hamiltonian can be written as:

$$\mathbf{H} = \upsilon_I\mathbf{I_z} + \upsilon_s\mathbf{S_z} + 2\pi J\mathbf{I_zS_z}, \quad (1.27)$$

where the value of h was set equal to 1. The Hamiltonian for a strongly coupled two spin system can be written as:

$$\mathbf{H} = \upsilon_I\mathbf{I_z} + \upsilon_s\mathbf{S_z} + 2\pi J\mathbf{I}\bullet\mathbf{S} = \upsilon_I\mathbf{I_z} + \upsilon_s\mathbf{S_z} + 2\pi J(\mathbf{I_xS_x} + \mathbf{I_yS_y} + \mathbf{I_zS_z}). \quad (1.28)$$

In these equations, υ represents the Larmor precession frequency of the two spins, while J refers to the magnitude of the coupling between spins. The density matrix of the system will evolve under the corresponding Hamiltonian. However, in NMR experiments, a series of pulses (pulse sequences) are typically used to tailor the response of the spin system for a particular application. In the presence of pulses, the Hamiltonian can be written as:

$$\mathbf{H_{RF}} = -\gamma B_1(\mathbf{I_x}\cos\varphi + \mathbf{I_y}\sin\varphi). \quad (1.29)$$

Here B_1 is the applied resonant control field, and φ is the phase of the pulse. While pulses are being applied, the total magnetization would be rotated under this Hamiltonian. The angle of rotation and phase is determined by the amplitude and duration of the applied pulse.

In summary, the density matrix of a two spin system evolves under following

Hamiltonians, depending on the type of the system:

$$\mathbf{H_z} = \sum_i \upsilon_i \mathbf{I_{iz}} \tag{1.30}$$

$$\mathbf{H_{Jz}} = \sum_{i,j} 2\pi J_{ij} \mathbf{I_{iz}} \mathbf{I_{jz}} \tag{1.31}$$

$$\mathbf{H_J} = \sum_{i,j} 2\pi J_{ij} (\mathbf{I_{ix}} \mathbf{I_{jx}} + \mathbf{I_{iy}} \mathbf{I_{jy}} + \mathbf{I_{iz}} \mathbf{I_{jz}}) \tag{1.32}$$

$$\mathbf{H_{rf}} = \gamma B_1 \sum_i (\mathbf{I_{ix}} \cos\varphi + \mathbf{I_{iy}} \sin\varphi), \tag{1.33}$$

where $\mathbf{H_z}$ refers to the Zeeman Hamiltonian, $\mathbf{H_{Jz}}$ to the truncated J-coupling Hamiltonian (weak coupling), $\mathbf{H_J}$ to the untruncated J-coupling Hamiltonian (strong coupling), and $\mathbf{H_{rf}}$ to the Hamiltonian for a hard pulse with phase angle φ [13].

1.2.4. Evolution

The evolution of a spin density matrix can be written as a similarity transformation:

$$\boldsymbol{\sigma}' = \mathbf{U}^{-1} \boldsymbol{\sigma} \mathbf{U}, \tag{1.34}$$

where the operator U is given by:

$$\mathbf{U} = \exp(-i\mathbf{H}t). \tag{1.35}$$

When pulses are applied, the evolution operator can be written as:

$$\mathbf{U} = \exp(-i\mathbf{H_{RF}}) \tag{1.36}$$

The rotation angle is varied by adjusting the power and duration of the applied pulse.

In the product operator basis, ideal pulses could be directly represented in the rotating frame. A 180 º pulse for spins with phase 0 º (x axis) represents a rotation of 180 º around x axis for all spin components, which implies that $\mathbf{I_x} \rightarrow \mathbf{I_x}$, $\mathbf{I_y} \rightarrow -\mathbf{I_y}$, and $\mathbf{I_z} \rightarrow -\mathbf{I_z}$. A 90 º pulse with phase 0 º also rotates all the vectors of the spin by 90 º, which

implies that $\mathbf{I_x \rightarrow I_x}$, $\mathbf{I_y \rightarrow I_z}$, and $\mathbf{I_z \rightarrow -I_y}$. The same principle applies to the pulses with different phases [42, 43].

1.3. NMR Sensitivity

Although a widely used tool in molecular and biomedical sciences, the application of NMR has traditionally been limited by low sensitivity. This low sensitivity is due to the fact that the population difference between the two spin states is low at thermal equilibrium.

1.3.1. Signal to noise ratio (SNR)

Signal to Noise Ratio (SNR) provides one metric to evaluate NMR sensitivity. In NMR, the SNR is typically given by [38, 44, 45]:

$$\mathrm{SNR} \propto \frac{N\gamma^{\frac{5}{2}}B_0^{\frac{3}{2}}}{T^{\frac{3}{2}}}\sqrt{\frac{N_s T_{read}}{T_R}}\ \delta_{Hz}. \tag{1.37}$$

In Equation 1.37, N represents numbers of spins, γ is the corresponding gyromagnetic ratio, B_0 the magnetic field strength, T the temperature, N_s is the number of transients acquired, T_{read} is the acquisition time, T_R the repetition time, and δ_{Hz} is the spectral resolution. This equation suggests several approaches to increasing SNR.

1) $\mathrm{SNR} \propto N$; $\mathrm{SNR} \propto \gamma^{5/2}$. Therefore, isotopes with higher natural abundance and larger gyromagnetic ratios will have higher sensitivities.
2) $\mathrm{SNR} \propto B^{3/2}$. Increasing the external magnetic field directly increases SNR, and comprises a major research field for NMR [46-49].

3) $SNR \propto (1/T^{3/2})$. SNR is inversely proportional to temperature. Unfortunately, it is not widely applicable since in many cases (especially in clinical application) the temperature of a biological sample is limited to a narrow range suitable to maintain life.

4) $SNR \propto N_s^{1/2}$. SNR increases with the square root of transients because noise adds incoherently while signals add coherently. Unfortunately, experimental durations are limited, and even in cases where periods of hours may be available, the time scale of metabolic events are on the order of seconds.

5) $SNR \propto \delta_{Hz}$. Better spectral resolution will lead to an increased SNR because the signal amplitude will be increased relative to noise.

1.3.2. Thermal equilibrium

As stated in 1.3.1, the sensitivity of NMR experiments is limited by the low population difference between the two spin states, which leads to a low net magnetization. In this section the net magnetization and the approaches to improve it will be described quantitatively.

The net magnetization, M_0, could be defined from statistical mechanics:

$$M_0 = h\gamma \sum_{m=-I}^{I} m_I N_m = Nh\gamma \sum_{m=-I}^{I} m_I P_m = Nh\gamma < m_I >= Nh\gamma Ip\,. \qquad (1.38)$$

In Eq 1.38, M_0 refers to the net magnetization, m_I to the azimuthal quantum number, N_m is the number of nuclei in the m_I state, P_m to the probability of the nucleus in m_I state. Nuclear spin polarization can be written as normalized population difference:

$$p = \frac{|P(|\alpha>) - P(|\beta>)|}{P(|\alpha>) + P(|\beta>)}, \tag{1.39}$$

where P(|α>) and P(|β>) refer to the population of the two spin states. The maximum net magnetization is obtained when the nuclei are fully polarized in one of the spin states, and alternatively net magnetization vanishes when the states are evenly populated.

It follows from statistical mechanics that the polarization level of the system at thermal equilibrium is [50]:

$$\begin{aligned} p &= \frac{\exp(\frac{-E_{+1/2}}{kT}) - \exp(\frac{-E_{-1/2}}{kT})}{\exp(\frac{-E_{+1/2}}{kT}) + \exp(\frac{-E_{-1/2}}{kT})} \\ &= \frac{\exp(\frac{\theta}{2T}) - \exp(-\frac{\theta}{2T})}{\exp(\frac{\theta}{2T}) + \exp(-\frac{\theta}{2T})} \\ &= \frac{\sinh(\frac{\theta}{2T})}{\cosh(\frac{\theta}{2T})} \\ &= \tanh(\frac{\theta}{2T}) \\ &\approx \frac{\theta}{2T} \end{aligned} \tag{1.40}$$

In this expression, θ is given by:

$$\theta = \frac{\Delta E}{k} = \frac{h\gamma B_0}{2\pi k}. \tag{1.41}$$

Therefore:

$$p = \frac{h\gamma B_0}{4\pi kT}, \tag{1.42}$$

and the net magnetization could be represented as:

$$M_0 = \frac{Nh^2\gamma^2 B_0}{16\pi^2 kT}. \tag{1.43}$$

Considering protons at room temperature and a magnetic field of 7.0 Tesla, the polarization level p is on the level of 10^{-4}. Therefore the polarization level at thermal equilibrium is low, mostly due to the fact that the energy splitting due to the Zeeman Effect is similarly small.

Equation 1.43 shows that the net magnetization is proportional to the external magnetic field and inversely proportional to the temperature. Therefore a straightforward approach to increase SNR is to increase the magnetic field and decrease temperature. However, even at a high field (around 7T), the polarization approaches unity only when the temperature is in the mK range. Therefore, other methods are necessary to enhance polarization.

Methods for producing polarized magnetic moments are collectively referred to as hyperpolarization, and are aimed at generating higher polarizations at room temperature. The most commonly used techniques for potential application to metabolism are: 1) dynamic nuclear polarization (DNP) [51] which produces polarization by transferring magnetization from electrons at ~2K to nuclei, and 2) parahydrogen induced polarization (PHIP) [52], which makes use of the symmetry of H_2 singlet-states to generate large polarizations at room temperature and low magnetic field. A brief review of DNP is given in the next section.

1.4. Dynamic Nuclear Polarization

The DNP method (dynamic nuclear polarization) transfers spin polarization from electrons at low temperature to coupled nuclei by microwave irradiation, thereby aligning the nuclear spins to the extent that electron spins are aligned.

1.4.1. DNP method

At 100K, the polarization level of electrons is 10.541%, while the polarization level of protons is only 0.016%. Therefore, DNP transfers polarization from electrons to protons with a maximum theoretical enhancement achievable given by γ_e/γ_n, being ~660 for protons [53]. Nowadays with advanced devices that enables low temperature and high-frequency microwave sources, in DNP experiments electrons are polarized at low temperature (around 2K) and high magnetic field (>5T range) [53]. The polarization is then transferred to the coupled nucleus by microwave irradiation, including protons and other heteronuclei such as ^{13}C.

1.4.2. DNP applications

Modulation of cancer cell metabolism with drugs

Hyperpolarized fumarate has been reported to be useful at detecting cell necrosis. Hyperpolarized fumarate was initially polarized to between 26% and 35% (by DNP), and then injected to mice with implanted lymphoma tumors both before and after treatment with etoposide. The result shows a 2.4 fold increase in hyperpolarized 1,4 - labeled malate production in mice that are etoposide treated comparing to those

untreated, which suggests that the production of malate from fumarate could be a marker of tumor cell death [54].

Imaging of intracellular pH

Since the ionization level of a labeled weak acid could be reflected as the change in chemical shift and J-coupling, and it is very sensitive to pH around the range close to its own Pk_a. Because of this, the recorded NMR signal may be sensitive to pH *in vivo*, and used as a surrogate to detect cancer or other diseases which are pH related. CO_2 and $NaHCO_3$ (^{13}C - labeled) have indeed been used successfully as a source of signal for this purpose. The pH can be calculated from the Henderson-Hasselbalch equation [55]:

$$PH = PKa + \log_{10} \frac{[HCO_3^-]}{[CO_2]} \tag{1.44}$$

This ratio has been extracted from hyperpolarized chemical shift images, and the *in vitro* experimental results were similar to measured pH (less than 0.1%) [56].

General DNP applications

Apart from the applications mentioned above, there are a wide range of potential applications for hyperpolarized DNP [57, 58]. Hyperpolarized pyruvate has been found useful to assess tumor grade [59], and to detect response to therapy [60]. Applications of imaging in cancer by direct and indirect assays of pyruvate metabolism have also been reported [61], due to the fact that compared to normal cells, a disproportionate conversion of pyruvate to lactate is commonly observed in tumors. These examples represent a small cross section of DNP applications for diagnostic purposes.

1.4.3. Pitfalls of DNP hyperpolarization

DNP is an advanced hyperpolarization technique and has a broad area of application. The primary downside of DNP is that it requires 1) bulky, expensive equipment. High-frequency microwave sources are required, 2) low temperatures near 2K to enable efficient transfer, 3) high fields to polarize electrons, and 4) the output solutions need to be rapidly warmed up to biological temperature for detection.

In conclusion, the DNP experiments require a set of advanced and expensive devices, which are not widely available commercially. This dissertation focuses on a less mature, but potentially less expensive and less bulky alternative, referred to as parahydrogen induced polarization (PHIP). PHIP achieves hyperpolarization at room temperature and low magnetic field.

1.5. Parahydrogen Singlet-States

It was recently reported that parahydrogen singlet-states could be used to generate hyperpolarized NMR samples through chemical interaction [52]. Compared to the much smaller Zeeman splitting, parahydrogen states have two essential advantages: 1) higher populations and 2) longer lifetimes.

According to statistical mechanics, nuclei with whole integer spins(I = 0, 1, 2, … ,), are called bosons and obey Bose-Einstein statistics; while nuclei with half integer spins(I = 1/2, 3/2, 5/2, … ,), are called fermions and obey Fermi-Dirac statistics. ^{1}H nuclei, with spin 1/2, as well as most other nuclei used in NMR experiments, are fermions with Pauli principle applied [62-64], which imposes the

criterion that the total wave function must be anti-symmetric under the exchange of particles.

$$\Psi_{tot}(A, B) = -\Psi_{tot}(B, A) \tag{1.45}$$

We study the anti-symmetry of the system by expanding it to the whole expression [65]. For the H_2 molecule, which is composed of two fermions, the total wave function is a combination of electronic, translational, vibrational, rotational, and nuclear spin wave functions.

$$\Psi_{tot} = \psi_e \psi_t \psi_v \psi_r \psi_{ns} \tag{1.46}$$

The ground state electronic and translation wave functions, ψ_e and ψ_t, are both symmetric under particle interchange [66, 67].The vibrational wave function, ψ_v, should not change either when the two nuclei are exchanged, in direct analogy to exchanging opposed masses connected by a spring. Therefore we are left with the rotational wave function, ψ_r , and the spin wave function, ψ_{ns}.

The rotational wave function transforms under rotations like a spherical harmonic function $Y_{J,m}$, which is symmetric with even J (J=0, 2, 4, … ,) or anti-symmetrical with odd J (J=1, 3, 5, … ,).

Since the spin wave function ψ_{ns} should be either symmetric or anti-symmetric, the simple product basis $|\alpha\alpha\rangle$, $|\alpha\beta\rangle$, $|\beta\alpha\rangle$, $|\beta\beta\rangle$ is insufficient to represent the basis set of H_2, because $|\alpha\beta\rangle \neq \pm|\beta\alpha\rangle$. However, a suitable basis could be represented by the linear combination of these states.

$$
\begin{aligned}
|T_1> &= |\alpha\alpha> \\
|T_{-1}> &= \beta\beta> \\
|T_0> &= \frac{1}{\sqrt{2}}(|\alpha\beta> + |\beta\alpha>) \\
|S_0> &= \frac{1}{\sqrt{2}}(|\alpha\beta> - |\beta\alpha>)
\end{aligned}
\tag{1.47}
$$

The first three states, $|T_1>$, $|T_{-1}>$, and $|T_0>$, correspond to odd angular momentum J, and are symmetric under exchange of the two nuclei – they form a triplet state and the corresponding hydrogen gas molecules in this spin state are called ortho-hydrogen (o-H_2). The last state, $|S_0>$, corresponds to even angular momentum J, and is anti-symmetric under exchange of the two nuclei. It forms a singlet-state [65] and the corresponding hydrogen gas is called parahydrogen (p - H_2).

The symmetry of the four states could be summarized as:

$$
\begin{aligned}
|T_1> &= |\alpha\alpha> \xrightarrow{\text{exchanging}} |\alpha\alpha> = |T_1> \\
|T_{-1}> &= |\beta\beta> \xrightarrow{\text{exchanging}} |\beta\beta> = |T_{-1}> \\
|T_0> &= \frac{1}{\sqrt{2}}(|\alpha\beta> + |\beta\alpha>) \xrightarrow{\text{exchanging}} \frac{1}{\sqrt{2}}(|\alpha\beta> + |\beta\alpha>) = |T_0> \\
|S_0> &= \frac{1}{\sqrt{2}}(|\alpha\beta> - |\beta\alpha>) \xrightarrow{\text{exchanging}} \frac{1}{\sqrt{2}}(|\beta\alpha> - |\alpha\beta>) = -|S_0>
\end{aligned}
\tag{1.48}
$$

Below is a table that summarizes the relation between rotational and spin wave functions.

Table 1.2. Correlations between rotational wave function and spin wave function, and the forms of H_2 gas.

J	Parity of ψ_r	Spin State	Parity of ψ_{ns}	Forms of H_2
Odd	Odd	$\|T_1>$	even	ortho
Odd	Odd	$\|T_{-1}>$	even	ortho
Odd	Odd	$\|T_0>$	even	ortho
Even	Even	$\|S_0>$	odd	para

Table 1.2 shows that due to the symmetry requirement, the freedom of rotation and spin are coupled. This relation can be used to induce spin states through manipulation of the rotational states.

1.6. Singlet-State Population

1.6.1. Dependence of singlet-state polarization on temperature

According to Table 1.2, to obtain parahydrogen state, an even J of the rotational function is necessary. It is common to consider the rotational ground state, J = 0. If the molecules are cooled to be locked in the rotational ground states, then they are constrained in the parahydrogen state at the same time. Since the energy spacing for rotational states is much larger than Zeeman effect, manipulating the rotational states by adjusting temperature is much easier. According to quantum mechanics, the energy of the angular momentum P_J, is given by [62, 68]:

$$E_J = \frac{h^2}{2I} J(J+1) \tag{1.49}$$

Therefore the rotational temperature could be defined as:

$$\theta_R = \frac{h^2}{2Ik} \tag{1.50}$$

This temperature, θ_R, for H_2, is roughly 86K [69].

The energy gap between the two levels, J and J+1, is:

$$\begin{aligned} \Delta E &= k\theta_R((J+1)(J+2) - J(J+1)) \\ &= 2k\theta_R(J+1) \end{aligned} \tag{1.51}$$

The energy splitting between the ground state, J = 0, and the state with J = 1, is then

$2k\theta_R$. Since θ_R is 86K, this is a more accessible temperature. Figure 1.2 depicts the energy level of J = 0 and J = 1.

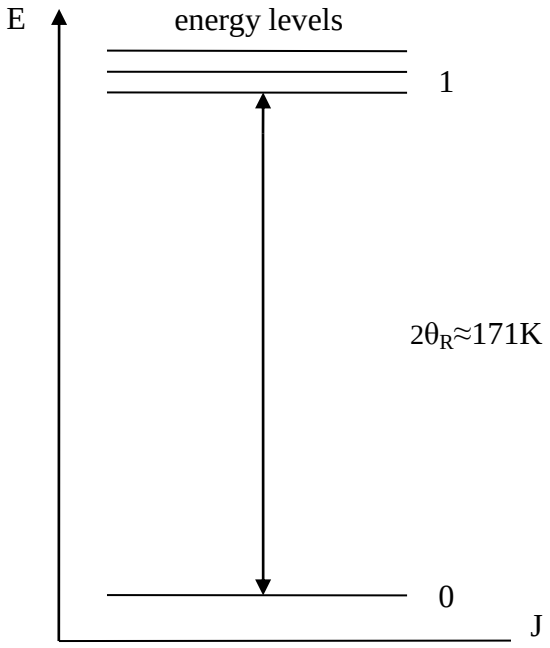

Figure 1.2. Schematic of the rotational energy levels. The molecules at ground state with J = 0 are parahydrogen. The rotational level with J = 1 has 3-fold degeneracy (triplet states). The energy spacing between the two levels is $2k\theta_R$.

It is then straightforward to get the partition function of the H_2 molecule. The J^{th} level rotational state is (2J+1)-fold degenerate (m_J = -J, -J+1,… J-1, J), and all the states with odd J are furthermore 3 - fold degenerate.

$$Z = \sum_{J\,even} (2J+1)\exp(-J(J+1)\theta_R / T) + 3\sum_{Jodd} (2J+1)\exp(-J(J+1)\theta_R / T) \qquad (1.52)$$

And the fraction of parahydrogen, defined as the ratio of parahydrogen of all the molecules, could then be calculated as:

$$P = \frac{\sum_{J\,even} (2J+1)\exp(-J(J+1)\theta_R / T)}{\sum_{J\,even} (2J+1)\exp(-J(J+1)\theta_R / T) + 3\sum_{Jodd} (2J+1)\exp(-J(J+1)\theta_R / T)} \qquad (1.53)$$

At high temperature, $T >> \theta_R$, the discrete levels could be treated as continuous levels. And the sum could be replaced by continuous integrals. Therefore we obtain that at high temperature limit:

$$P = \frac{N_{para}}{N_{para} + N_{ortho}} = \frac{1}{4}. \quad (1.54)$$

In the low temperature limit, $T << \theta_R$, only the ground state with J = 0 will be significantly populated, and the fraction of parahydrogen will approach100%.At the temperature $T \approx \theta_R$, it is easy to find that with the increase of J, the factor $\exp(-J(J+1)\theta_R/T)$ vanishes quickly. So it is reasonable to consider only the first several terms and calculate the polarization level. The more detailed data is showed in Table 1.3 [70].

Table 1.3. Percentage of parahydrogen at various temperatures.

Temperature (K)	Parahydrogen fraction (%)
300	25.06
200	25.25
150	28.58
100	38.51
80	46.4
77(liquid N_2)	50.33
60	65.17
40	88.5
20	99.79
18	99.9

Note that at 300K, P = 25%; at T = 77K, P ≈ 50%; and at T = 20K, P > 99%.

1.6.2. Angular momentum selection rules

Table 1.3 shows that high parahydrogen enrichments can be created by cooling the molecules to 77K (50%) or even 20K (~ 100 %) to populate the ground state with J = 0 (singlet-state). However, until now only the thermodynamics of the rotational and spin states have been accounted for. According to quantum mechanics, the conversion from ortho to para hydrogen, which requires both angular momentum quantum number J changed by ± 1 and at the same time the nuclear spin reoriented from S = 1 triplet-state to S = 0 singlet-state, is forbidden by angular momentum selection rules [62, 71-73]. This conversion can only take place with the presence of dipolar coupling to the other molecules or electrons during a collision. To increase the rate of conversion, the nuclear symmetry of ortho molecules needs to be broken and several types of ortho/para catalysts that lead to fast equilibration of the nuclear spin states have been identified [74, 75].

With the presence of catalysts, the ortho↔para conversion takes place on the surface of the catalysts rapidly. For example, if the temperature is cooled to near 20K, almost 100% pure parahydrogen is obtained rapidly [76]. The molecules persist in this parahydrogen state because of the angular momentum selection rule. By warming the molecules, they start to redistribute themselves in all the rotational states with even J according to Boltzmann distribution, but they remain in the singlet-state. Practically, this parahydrogen gas could be stored for several hours or even days.

1.6.3. Parahydrogen production devices

The device our group developed to produce high purity parahydrogen gas operates with a closed-cycle cryostat which is maintained at a nominal set-point of 15K (with operation between 15K and 20K) and enriches parahydrogen with high pressure, pulsed injections of ambient [76]. When operated to achieve a final fill pressure of 240 psi, this system generates highly enriched parahydrogen (> 98 %) at 0.9 SLM (standard liters per minute). A schematic of the device is shown in Figure 1.3.

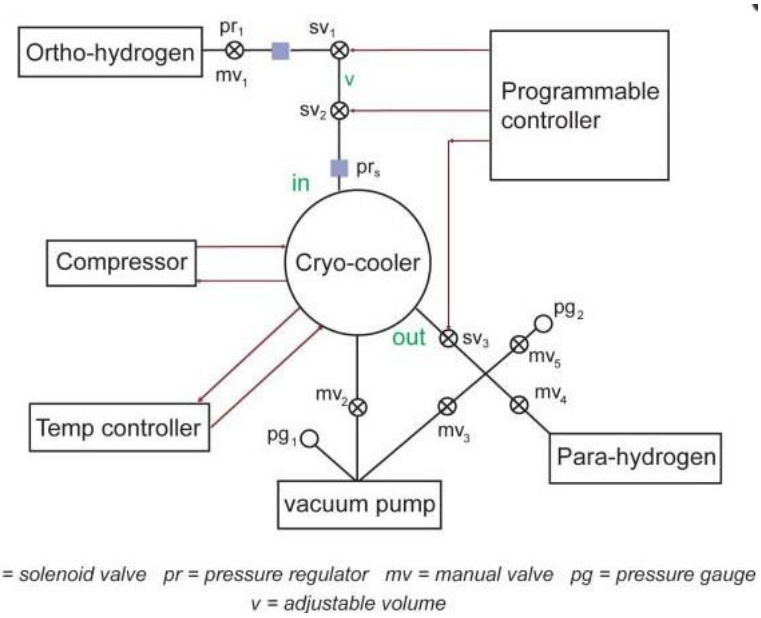

Figure 1.3. Schematic of parahydrogen production device. The valves are manually controlled to evacuate the cooler or the parahydrogen container. The helium cryo-cooler cools hydrogen gas to ~ 15-20K, and at this temperature parahydrogen is routinely generated with a purity of ~98% [76].

Parahydrogen singlet-states are completely evenly distributed between the two spin states, 50% |α> state and 50% |β>state. Therefore, pure singlet-states are not observable in NMR experiments since zero net magnetization is generated. Hence the

purity of parahydrogen gas can be calculated by comparing the NMR spectrum of the enriched gas to ambient hydrogen gas. Figure 1.4 shows the immediately recorded signal of parahydrogen gas produced using the device in shown in Figure 1.3, compared to the signal after four days [76].

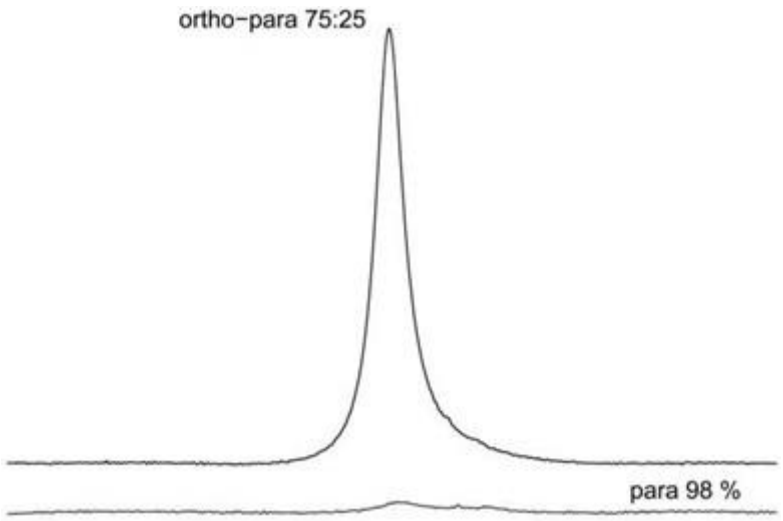

Figure 1.4. Proton spectrum acquired from approximately 98% enriched parahydrogen gas, compared to the same (relaxed) sample acquired from the same tank several days later [76].

1.7. Operator Basis of Parahydrogen State

To describe the ortho- and parahydrogen states, it is convenient to use density operators introduced in section 1.2. The four spin states for hydrogen gas are shown in Equation 1.55.

$$
\begin{aligned}
&\mathbf{T}_1 = |\alpha\alpha> = \{1,0,0,0\} \\
&\mathbf{T}_{-1} = |\beta\beta> = \{0,0,0,1\} \\
&\mathbf{T}_0 = \frac{1}{\sqrt{2}}(|\alpha\beta> + |\beta\alpha>) = \frac{1}{\sqrt{2}}\{0,1,1,0\} \\
&\mathbf{S}_0 = \frac{1}{\sqrt{2}}(|\alpha\beta> - |\beta\alpha>) = \frac{1}{\sqrt{2}}\{0,1,-1,0\} \\
&\mathbf{T}_1 = |T_1><T_1| = \begin{pmatrix} 1 & 0 & 0 & 0 \\ 0 & 0 & 0 & 0 \\ 0 & 0 & 0 & 0 \\ 0 & 0 & 0 & 0 \end{pmatrix} \\
&\mathbf{T}_{-1} = |T_{-1}><T_{-1}| = \begin{pmatrix} 0 & 0 & 0 & 0 \\ 0 & 0 & 0 & 0 \\ 0 & 0 & 0 & 0 \\ 0 & 0 & 0 & 1 \end{pmatrix} \\
&\mathbf{T}_0 = |T_0><T_0| = \frac{1}{2}\begin{pmatrix} 0 & 0 & 0 & 0 \\ 0 & 1 & 1 & 0 \\ 0 & 1 & 1 & 0 \\ 0 & 0 & 0 & 0 \end{pmatrix} \\
&\mathbf{S}_0 = |S_0><S_0| = \frac{1}{2}\begin{pmatrix} 0 & 0 & 0 & 0 \\ 0 & 1 & -1 & 0 \\ 0 & -1 & 1 & 0 \\ 0 & 0 & 0 & 0 \end{pmatrix}
\end{aligned}
\tag{1.55}
$$

Refer to the matrix of the product operator basis, these states could also be written in product operator notation [18]:

$$
\begin{aligned}
&\mathbf{T}_{\pm 1} = \frac{\mathbf{I}}{4} + \frac{1}{2}(\pm\mathbf{I}_{1z} \pm \mathbf{I}_{2z} + 2\mathbf{I}_{1z}\mathbf{I}_{2z}) \\
&\mathbf{T}_0 = \frac{\mathbf{I}}{4} + (\mathbf{I}_{1x}\mathbf{I}_{2x} + \mathbf{I}_{1y}\mathbf{I}_{2y} - \mathbf{I}_{1z}\mathbf{I}_{2z}) \\
&\mathbf{S}_0 = \frac{\mathbf{I}}{4} - (\mathbf{I}_{1x}\mathbf{I}_{2x} + \mathbf{I}_{1y}\mathbf{I}_{2y} + \mathbf{I}_{1z}\mathbf{I}_{2z})
\end{aligned}
\tag{1.56}
$$

where **I** represents unit matrix.

Using these equations, the pure parahydrogen state can be written as:

$$
\rho_{para} = \frac{\mathbf{I}}{4} - (\mathbf{I}_{1x}\mathbf{I}_{2x} + \mathbf{I}_{1y}\mathbf{I}_{2y} + \mathbf{I}_{1z}\mathbf{I}_{2z}) \tag{1.57}
$$

A pure ortho-hydrogen state can be written as:

$$\begin{aligned}\rho_{ortho} &= \frac{1}{3}(\mathbf{T_1} + \mathbf{T_{-1}} + \mathbf{T_0}) \\ &= \frac{\mathbf{I}}{4} + \frac{1}{3}(\mathbf{I_{1x}I_{2x}} + \mathbf{I_{1y}I_{2y}} + \mathbf{I_{1z}I_{2z}})\end{aligned} \tag{1.58}$$

Therefore the mixed state with parahydrogen fraction P will have the form:

$$\begin{aligned}\rho_{mix} &= P\rho_{para} + (1-P)\rho_{ortho} \\ &= \frac{\mathbf{I}}{4} + \frac{1-4P}{3}(\mathbf{I_{1x}I_{2x}} + \mathbf{I_{1y}I_{2y}} + \mathbf{I_{1z}I_{2z}})\end{aligned} \tag{1.59}$$

In this mixed state, $\mathbf{I_{1x}I_{2x}} + \mathbf{I_{1y}I_{2y}}$ is normally referred to as a zero quantum coherence. This term, together with the $\mathbf{I_{1z}I_{2z}}$ term, commutes with the Hamiltonian and is unobservable in NMR experiments as Equation 1.60.

$$[\rho, H] = 0 \tag{1.60}$$

To make the state observable, the two hydrogen molecules need to be placed in a chemical environment capable of breaking the symmetry (Figure 1.5). The requirements are:

1) The hydrogenation occurs via molecule addition so the two molecule spins remain correlated.
2) The two hydrogen atoms are placed in different chemical environment after the reaction.

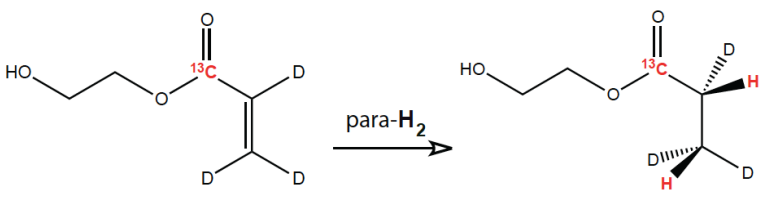

2-hydroxyethyl 1-^{13}C-acrylate-d$_3$ (HEA)

2-hydroxyethyl 1-^{13}C-propionate-d$_3$ (HEP)

Figure 1.5. Reaction schematic for adding parahydrogen across a double bond.

1.8. PASADENA and ALTADENA

As discussed in the previous sections, although high purity parahydrogen gas could be preserved at room temperature, the state is invisible in NMR experiments. To make the state useful, the two protons must be placed in different chemical environments.

1.8.1. PASADENA

The PASADENA effect (Parahydrogen And Synthesis Allows Dramatic Enhancement of Nuclear Alignment) [52] uses hydrogenation in a strong magnetic field to cause a sudden change of Hamiltonian from an $\mathbf{A_2}$ system to an **AX** system. Thus the density matrix, ρ_0, then evolves and is projected onto the eigenstates of **AX** system.

$$\boldsymbol{\rho}(t > 0) = \exp(-i\mathbf{H}t)\,\boldsymbol{\rho_0}\exp(i\mathbf{H}t) \tag{1.61}$$

A mixed state with an excess of parahydrogen will lead to polarization of the center states with $m_I = 0$, $|\alpha\beta\rangle$ and $|\beta\alpha\rangle$, resulting in a spectrum consisting of anti-phase doublets, as shown in Figure1.6.

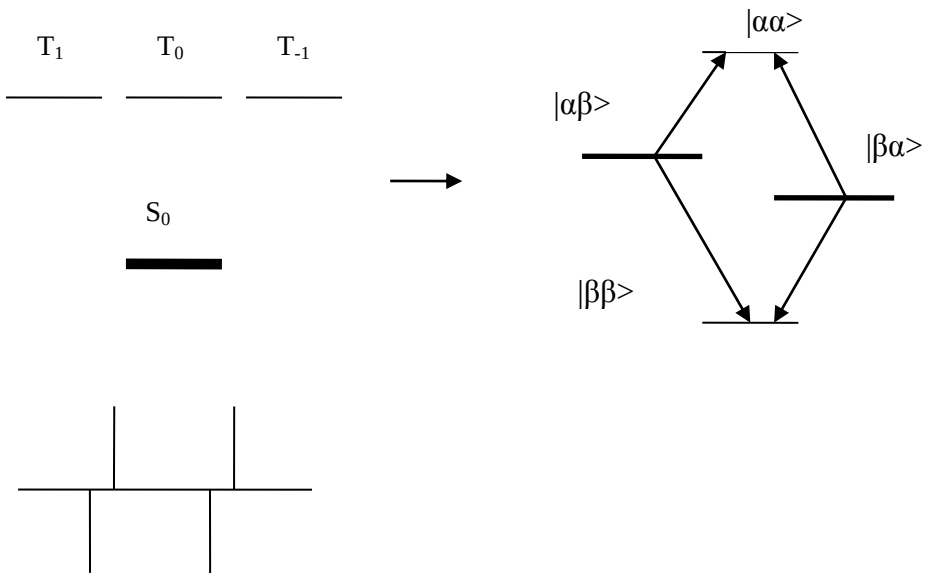

Figure 1.6. Schematic of the PASADENA experiment. The parahydrogen state is projected to the eigenstates of AX system, leading to a net excess of |αβ> and |βα> states that yields a spectrum of anti-phase doublets.

However, unless the signal recording starts instantaneously after the hydrogenation, the hydrogenated states will start to evolve since the two protons are now not in the equivalent chemical environment.

The initial singlet-state is:

$$\boldsymbol{\rho_0} = \frac{\mathbf{I}}{4} - (\mathbf{I_{1x}I_{2x}} + \mathbf{I_{1y}I_{2y}} + \mathbf{I_{1z}I_{2z}}) \tag{1.62}$$

After hydrogenation, the first and second terms start to evolve:

$$\begin{aligned} \mathbf{I_{1x}I_{2x}} &\rightarrow [\cos(\omega_1 t)\mathbf{I_{1x}} + \sin(\omega_1 t)\mathbf{I_{1y}}][\cos(\omega_2 t)\mathbf{I_{2x}} + \sin(\omega_2 t)\mathbf{I_{2y}}] \\ \mathbf{I_{1y}I_{2y}} &\rightarrow [\cos(\omega_1 t)\mathbf{I_{1y}} - \sin(\omega_1 t)\mathbf{I_{1x}}][\cos(\omega_2 t)\mathbf{I_{2y}} - \sin(\omega_2 t)\mathbf{I_{2x}}] \end{aligned} \tag{1.63}$$

As each molecule finishes hydrogenation reaction at different time and the initial states start to evolve at different time, the initial phase will be a complete mixture. The result is cancellation of both terms. Therefore, after hydrogenation the first and second terms vanish, leaving the initial state to be:

$$\boldsymbol{\rho_0} = \frac{\mathbf{I}}{4} - \mathbf{I_{1z}}\mathbf{I_{2z}} \tag{1.64}$$

Decoupling can be used while the hydrogenation reaction is occurring to synchronize density matrix evolution of individual molecules [77]. The effect of the waves is to flip the spin direction of the protons constantly and quickly, resulting in a changing of Hamiltonian which commutes with the density matrix.

$$\begin{aligned} \mathbf{H} &\propto \mathbf{I_1} \bullet \mathbf{I_2} \\ [\boldsymbol{\rho_0}, \mathbf{H}] &= 0 \end{aligned} \tag{1.65}$$

Therefore, the full expression of the initial state could be preserved and only after the reaction is finished and the applied field is removed that the states of each molecule starts to evolve in the same time [78].

1.8.2. ALTADENA

PASADENA uses applied pulses to transform parahydrogen singlet-states to observable magnetization, whereas the alternative, ALTADENA (adiabatic longitudinal transport and dissociation engenders nuclear alignment), uses field cycling between zero and high field to create observable signal [84, 85]. In this case, the singlet-state is preserved during reaction, since there exists no difference between the chemical shifts of the two atoms, and the Hamiltonian commutes with the initial states. If the sample is then transported to a magnetic field, the result is a smooth transformation of the Hamiltonian. As the Hamiltonian changes smoothly, the state will be projected to each instantaneous eigenstate of the corresponding Hamiltonian. Therefore the quantum states conserve their respective projection onto the instantaneous eigenstates of the transforming Hamiltonian [86, 87]. $|S_0\rangle$ and $|T_0\rangle$

transform to |αβ> and |βα> (or |βα> and |αβ>, depending on the sign of (ν_i - ν_s)). Therefore the polarized parahydrogen leads to a occupation of either the |αβ> or |βα> state. This results in in-phase absorptive or emissive peaks, as shown in Figure 1.7.

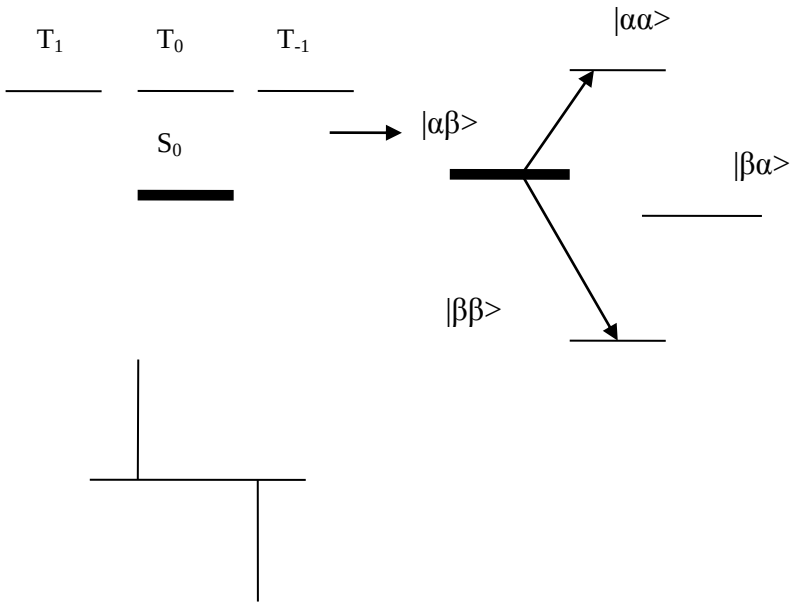

Figure 1.7. Schematic of the ALTADENA experiment. The parahydrogen state is projected to either eigenstate of the AX system, leading to a net excess of |αβ> or |βα> states. The resulting spectrum contains in-phase absorptive and emissive peaks.

ALTADENA experiments require that the Hamiltonian be changed slowly to meet the adiabatic condition [13]:

$$\begin{aligned} \left|\frac{dT}{dt}\right| &= 1 \\ \frac{1}{\omega_0 B_0}\frac{dB_0}{dt} &= 1 \\ \frac{\vec{G}\times\vec{v}}{B_0\omega_0} &= 1 \\ |\vec{v}| &= \frac{\omega_0 B_0}{|\vec{G}|} \end{aligned} \tag{1.66}$$

In Equation 2.22, $T = (1/\omega_0) = (1/\gamma B_0)$. And v is the velocity of gas. G is the magnetic

field gradient.

1.8.3. Parahydrogen hydrogenation device

The devices for PASADENA experiments need to provide a low magnetic field, radiofrequency pulses, with injection of high purity parahydrogen and molecular precursors. A scheme of the device developed in our group to achieve this is shown in Figure 1.8.

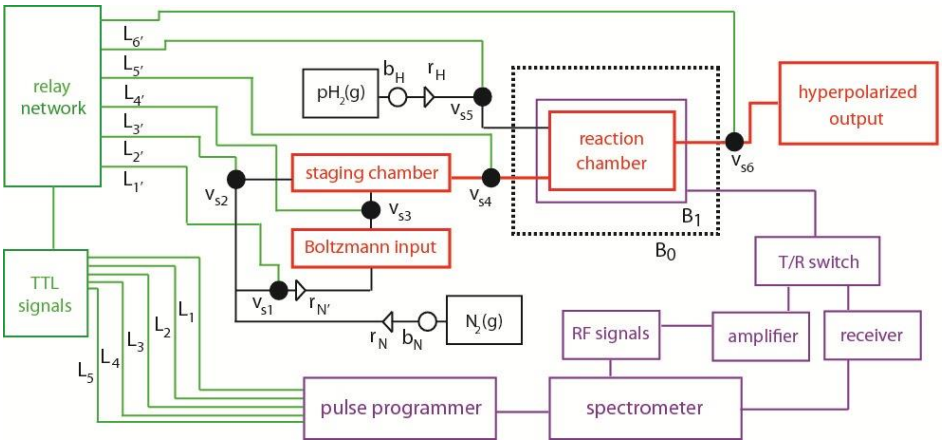

Figure 1.8. Schematic of the polarizer developed to generate observable signal from parahydrogen singlet-states. The long-lasting high purity parahydrogen gas is stored in a tank which is in turn connected to the polarizer. The molecular precursor gets hydrogenated by parahydrogen and RF pulses are applied to transfer polarization [89].

The parahydrogen induced polarization experiments have the advantage of requiring only low fields in the mT regime and room temperature. Therefore, compared to DNP, parahydrogen induced polarization technique could be used in compact, inexpensive and portable devices.

1.9. Application of Parahydrogen Induced Polarization

A wide range of applications of parahydrogen induced polarization (PHIP) have been reported [85, 90, 91]. Typical applications of PHIP includes homogeneous catalysis [92-94], magnetic resonance imaging [95, 96], and heteronuclear polarization [77].

In conventional MRI, the ability to differentiate between soft tissues and to detect pathology depends on the differential relaxation times (T_1, T_2, T_2^*) and proton density between the target molecules and the background (mostly protons in water). Paramagnetic contrast agents are used to decrease the relaxation times of adjacent protons, which will result in an increase or decrease in signal depending on the pulse sequence, so as to enhance the contrast [97]. The imaging of hyperpolarized molecules is fundamentally different. The injected agents themselves act as the source of signal, rather than modulating proton relaxation only.

1.9.1. Setup and pulse sequences

One of the most apparent differences in ^{13}C imaging from proton is the much lower gyromagnetic constant, $\gamma_C \approx (1/4)\gamma_H$. Therefore, the MRI scanner frequency needs to be adjusted to ^{13}C resonance frequency (15MHz at 1.5T) rather than proton resonance frequency (60MHz at 1.5T) [98].

A low gyromagnetic constant also leads to insensitivity to magnetic gradients of ^{13}C spins. If the same magnetic gradient is applied as in proton imaging, echo times (TE) and repetition times (TR) need to be elongated to achieve a comparable

resolution with proton imaging. This is not an acceptable option in most cases since the longer delays correspond to more loss in polarization due to relaxation. Therefore a higher magnetic gradient would be a necessary.

Hyperpolarized imaging also faces the problem of unrecoverable longitudinal magnetization since it is not a thermal equilibrium state. First, the loss of longitudinal magnetization due to T_1 relaxation is inevitable. Second, the longitudinal magnetization that converts to transverse magnetization by RF pulses is not recoverable either. The sequences used to image hyperpolarized agents would then be required to complete the image in a single shot, compared to the conventional multi-shots sequences which reuse longitudinal magnetization. The much longer T_2 relaxation of ^{13}C makes the single shot sequences feasible. The available pulse sequences include single-shot sequences based on true fast imaging with steady-state free-precession (true FISP), rapid acquisition with relaxation enhancement (RARE), or echo planar imaging (EPI), which convert almost 100% of the longitudinal magnetization to transverse [99].

An example of the available sequences, true FISP sequence, is shown below in Figure 1.6 [100]. A true FISP sequence is T_2/T_1-weighted, which makes it very useful in imaging of heart due to the excellent contrast between blood and myocardium. In a typical true FISP sequence, balanced gradient echo refocusing is applied in all directions to maintain steady-states of both longitudinal and transverse magnetization. If we apply a single-shot sequence based on true FISP, it is both impossible and unnecessary to maintain steady states of longitudinal magnetization. Therefore only

gradient echo refocusing in the transverse direction needs to be applied, which maintains the transverse magnetization at steady state each time before adjusting gradient and recording signal. The very long T_2 of hyperpolarized ^{13}C permits the use of the single-shot sequence ($T_2 >> TR$).

1.9.2. Signal to noise ratio (SNR)

One of the advantages of ^{13}C imaging is the absence of background signal. The low gyromagnetic ratio and low natural abundance (1.1%) of ^{13}C make the background signal far below the detection limit. In this case, the only possible noise comes from patient or coils, and the signal to noise ratio (SNR) is proportional to the polarization (P) and concentration (c) of the molecule [98]:

$$SNR \propto \gamma Pc \tag{1.67}$$

The polarization level $P = \gamma B_0$ for thermal equilibrium. For example, the polarization level at 1.5T and body temperature is approximately 5×10^{-6} for protons and 1×10^{-6} for ^{13}C.

For a liquid hyperpolarized ^{13}C imaging agent, the concentration is normally 0.3-1.2M in the injection syringe, far below the ^{1}H concentration of 80M. It will then take 3-4 seconds to reach the lungs, 6-10 seconds to the heart and 15-40 seconds to the other major organs. The concentration after dilution could be around 10mM [100]. Besides, the relaxation of magnetization during this period will decrease the polarization level too. But even after T_1 of injection, the available signal in the vascular system should still be at least a factor of 2 larger than the one in proton

imaging at 3T [101]. In addition, for hyperpolarization imaging, the polarization levels do not depend on thermal equilibrium. This opens the possibility of low field imaging.

1.9.3. The optimal magnetic field for hyperpolarization imaging

It is stated previously that for hyperpolarized ^{13}C imaging, a higher field gradient would be a necessary, and the signal to noise ratio is independent of external magnetic field. This leads to the idea that the imaging could be undertaken in a low magnetic field but with high field gradient. However, when the low field is combined with high field gradients, the problem called concomitant gradient terms rises, which is the nonlinear component of magnetic field gradients [102].

According to this theory, there will be a phase shift by the concomitant gradient, due to the fact that the magnetic field must obey the rule that both div B=0 and curl B = 0. Assuming a cylindrical symmetry for z - coil, with x - coil and y - coil 90 ºto each other, if the slice plane is aligned along y - axis, z - axis is used as phase direction and readout is performed along x-axis, the phase evolution due to the concomitant gradient would be:

$$\phi = t_{samp}\gamma\frac{G_x^2}{2B_0}z^2 \tag{1.68}$$

Here t_{samp} is the sampling time, G_x represents readout gradient, and z is the distance in z-axis from the iso-center of the scanner. In the case that t_{samp} = 1ms, B_0 = 0.2T and G_x = 40mT/m, then the phase shift will result in a pixel shift already from a distance of about only 12cm from the iso-center of magnet [98]. If the magnetic field is even

lower, the effect would be more significant since field gradient cannot be simply reduced unless longer echo times and repetition time are applied.

Besides, if there are several ^{13}C peaks in the molecule that need to be differentiated, a high magnetic field might be necessary to make the difference in chemical shift observable. Until recently most hyperpolarization images were taken in a magnetic field around 1.5T.

1.9.4. Examples of hyperpolarized ^{13}C imaging

Field cycling experiments to generate ^{13}C imaging both *in vitro* and *in vivo* is reported by Haukur Jóhannesson [103]. In this experiment parahydrogen of 95% purity is obtained by catalyst at 14K, and then hydrogenated to hydroxyethyl acrylate at a pressure of 10 bar during 3s. The produced hydroxyethyl propionate is then transferred to low field chamber at 100μT. After 0.5s delay the field is reduced to 30nT in 1ms. Then the field is ramped up to 100μT in 1.2s. The observed ^{13}C polarization is 21%. For *in vivo* experiments, the FISP pulse sequence was used for data collection and a ^{13}C angiogram showing head and neck parts of a guinea pig, acquired in 230 ms, were presented with high resolution [103].

^{13}C polarized by pulse sequence method to generate images was also published [96]. The pulse sequence was carried out *in vivo* as well. The production of parahydrogen and hydrogenated molecule is similar to the field-cycling method. In this experiment the DC field is set at 1.76 mT. The continuous RF irradiation is applied for 3-4 seconds at a proton Larmor frequency of 75kHz during hydrogenation.

After applying the pulse sequence (along with the echo pulses), 5 ml of 0.5 M solution of the sample (hyperpolarized hydroxyethyl propionate) was injected to the leg of a pig. Successive ^{13}C imaging, still by the true FISP method, was taken at 1s intervals. The slice thickness is larger than the pig, with the scan time 470ms for each image. And the matrix used is 104×128, with the pixel size $2.5 \times 2.5 mm^2$. A series of angiographic images of the pig chest was presented with high resolution within 8 seconds [96].

CHAPTER 2

SPIN ORDER TRANSFER FROM PARAHYDROGEN SINGLET-STATES TO HETERONUCLEAR NET MAGNETIZATION IN AA'X SPIN SYSTEMS

Spin order in parahydrogen induced polarization (PHIP) is initially captured as an ensemble of nuclear singlet-states formed by addition of parahydrogen across an unsaturated bond. For applications to biomedicine, it is often an advantage to convert these initial singlet-states into longitudinal magnetization on a long-lived nucleus. A variety of traditional sequences such as INEPT or HMQC are available to interconvert heteronuclear single quantum coherences, but new approaches are required for converting singlet-states into heteronuclear single quantum coherences at low field in the strong coupling regime of protons. Introduced in this chapter is a consolidated pulse sequence that was designed to achieve this conversion of singlet-state spin order into heteronuclear magnetization across a wide range of scalar couplings in AA'X spin systems. Analytic solutions to the spin evolution are presented, and performance was validated experimentally in the parahydrogen addition product, 2-hydroxyethyl 1 - ^{13}C – propionate - d_3. Hyperpolarized carbon-13 signals were enhanced by a factor of approximately 5,000,000 relative to Boltzmann polarization in a static magnetic field of 47.5 mT. It is anticipated that this pulse sequence will enable efficient conversion of spin order over a broad range of emerging PHIP agents that feature I_1I_2S spin systems.

The operators used to describe dynamic states in 3 spin I_1I_2S spin systems can be

represented by 8×8 matrices. After a brief introduction of related study and our approach in section 2.1, expressions of the spin operators are described in section 2.2, with the full expressions described in Appendix A. A pulse sequence designed to transfer polarization from an initial parahydrogen singlet-state to a heteronucleus is presented in 2.3. Experiment validation follows in section 2.4. Discussion about the sequence, including the efficiency across various spin systems, and comparison to previous approaches, is presented in section 2.5.

2.1. Introduction to Hyper-SHIELDED Spin Order Transfer Sequence

Hyperpolarization of nuclear spin ensembles has increased NMR sensitivity to a level that is now enabling detection of metabolism in biological tissue on a time-scale of seconds [104, 105]. The most developed of these technologies, DNP (dynamic nuclear polarization) [51, 106, 107], in particular has already been used to detect, grade, and monitor response to therapy in tumors [108-110]. These encouraging developments have demonstrated the overall viability of NMR based hyperpolarized methods for the study of *in vivo* metabolism, and have naturally spurred development in alternative methods of hyperpolarization, such as parahydrogen induced polarization (PHIP) [111-113]. Polarization yields from the less mature PHIP technology are similar to DNP in cases where precursors are available, and accessed at significantly reduced instrumental complexity and expense. An array of complementary advances is still required, however, for PHIP to reach its potential as a diagnostic imaging modality.

Efficient methods for transforming parahydrogen spin order into net magnetization at low magnetic fields using pulsed methods would be helpful for translating emerging PHIP contrast agents to biomedical applications. Parahydrogen spin order will generally evolve when added to a molecule by PASADENA [111, 112] if the singlet-state symmetry is broken, yielding a detectable antiphase NMR spectrum. For applications of PHIP biomedicine, it is advantageous to convert this parahydrogen spin order into net magnetization on a coupled heteronucleus. Aside from the standard benefits of heteronuclear detection arising from increased spectral dispersion and low background signals *in vivo*, producing carbonyl ^{13}C magnetization for example eliminates the need to synchronize subsequent imaging procedures with the ongoing evolution of an initial parahydrogen singlet-state. While spin order transfer has been demonstrated by field cycling to create ^{13}C angiograms in rats at 2.4T, pulsed methods offer a simple and equally efficient alternative when low field NMR consoles are available [114].

Determining the timing, frequency, and magnitude of these applied electromagnetic fields to efficiently transform parahydrogen spin order into heteronuclear magnetization in the strong coupling regime of protons is a challenging problem though, even for small AA'X spin systems. Two prior sequences have been reported for pulsed transformation of parahydrogen spin order into heteronuclear net magnetization in this field regime [114, 115]. Most recently, Kadlecek and coworkers reported a series of sequences that yield piecewise optimal polarization in three distinct coupling regimes [115]. The earlier and most frequently cited sequence developed by

Goldman and coworkers, offers unity efficiency for the targeted molecules and a recursive procedure for pumping polarization yields when outside of those coupling regimes [114]. We sought to build on those earlier works by developing a streamlined sequence that could achieve optimal polarization in a single implementation without the use of iterative pumping.

In this study, we describe a consolidated pulse sequence that transforms parahydrogen spin order into heteronuclear magnetization in I_1I_2S spin systems with a yield near unity and independent of spin couplings. The sequence affords a unified solution across scalar coupling topologies by flanking a heteronuclear excitation with two asymmetric proton refocusing intervals to provide four unique evolution intervals. These delay intervals are in turn optimized using prior knowledge of the spin couplings to sequentially transform the initial parahydrogen spin order into pure heteronuclear magnetization. We anticipate that the streamlined construction will be well-suited to multidimensional experiments and for efficient preparation of existing and emerging PHIP contrast agents.

2.2. Mathematical Basis Analysis Method for AA'X Spin Systems

For a three-spin system (I_1I_2S system, two protons in singlet-state and one heteronucleus), since each spin has two possible states (|α> and |β), 8×8 matrices are necessary to express the states of the system. The eight possible states of three spin-systems could be labeled as |ααα>, |ααβ>, |αβα>, |βαα>, |αββ>, |βαβ>, |ββα> and |βββ>. States and pulses from the product operator basis could be expressed in

matrices form. For example, the $\mathbf{I_{1x}}$ term, which is the x component magnetization for one of the protons, could be expressed as:

$$\mathbf{I_{1x}} = \frac{1}{2}\begin{pmatrix} 0 & 0 & 0 & 1 & 0 & 0 & 0 & 0 \\ 0 & 0 & 0 & 0 & 0 & 1 & 0 & 0 \\ 0 & 0 & 0 & 0 & 0 & 0 & 1 & 0 \\ 1 & 0 & 0 & 0 & 0 & 0 & 0 & 0 \\ 0 & 0 & 0 & 0 & 0 & 0 & 0 & 1 \\ 0 & 1 & 0 & 0 & 0 & 0 & 0 & 0 \\ 0 & 0 & 1 & 0 & 0 & 0 & 0 & 0 \\ 0 & 0 & 0 & 0 & 1 & 0 & 0 & 0 \end{pmatrix} \tag{2.1}$$

Pulses with any phase and any rotation angle could be represented by 8×8 matrices as well. For example, a pulse that rotates the ^{13}C magnetization around the x-axis by angle θ could be expressed as:

$$\mathbf{R_x^S}(\theta) = \begin{pmatrix} \cos\frac{\theta}{2} & i\sin\frac{\theta}{2} & 0 & 0 & 0 & 0 & 0 & 0 \\ i\sin\frac{\theta}{2} & \cos\frac{\theta}{2} & 0 & 0 & 0 & 0 & 0 & 0 \\ 0 & 0 & \cos\frac{\theta}{2} & 0 & i\sin\frac{\theta}{2} & 0 & 0 & 0 \\ 0 & 0 & 0 & \cos\frac{\theta}{2} & 0 & i\sin\frac{\theta}{2} & 0 & 0 \\ 0 & 0 & i\sin\frac{\theta}{2} & 0 & \cos\frac{\theta}{2} & 0 & 0 & 0 \\ 0 & 0 & 0 & i\sin\frac{\theta}{2} & 0 & \cos\frac{\theta}{2} & 0 & 0 \\ 0 & 0 & 0 & 0 & 0 & 0 & \cos\frac{\theta}{2} & i\sin\frac{\theta}{2} \\ 0 & 0 & 0 & 0 & 0 & 0 & i\sin\frac{\theta}{2} & \cos\frac{\theta}{2} \end{pmatrix} \tag{2.2}$$

Therefore the initial density matrix of the parahydrogen state, $\boldsymbol{\sigma_0} = \frac{\mathbf{I}}{4} - (\mathbf{I_{1x}I_{2x}} + \mathbf{I_{1y}I_{2y}} + \mathbf{I_{1z}I_{2z}})$, (assuming 100% polarization) can be expressed as:

$$\boldsymbol{\sigma_0} = \frac{1}{2}\begin{pmatrix} 0 & 0 & 0 & 0 & 0 & 0 & 0 & 0 \\ 0 & 0 & 0 & 0 & 0 & 0 & 0 & 0 \\ 0 & 0 & 1 & -1 & 0 & 0 & 0 & 0 \\ 0 & 0 & -1 & 1 & 0 & 0 & 0 & 0 \\ 0 & 0 & 0 & 0 & 1 & -1 & 0 & 0 \\ 0 & 0 & 0 & 0 & -1 & 1 & 0 & 0 \\ 0 & 0 & 0 & 0 & 0 & 0 & 0 & 0 \\ 0 & 0 & 0 & 0 & 0 & 0 & 0 & 0 \end{pmatrix} . \qquad (2.3)$$

The matrix representations for three spin systems (I_1I_2S) used in the following calculations are fully described in Appendix A.

In the strong coupling regime as obtained in fields used for this study, the Hamiltonian can be written as:

$$\begin{aligned} \mathbf{H} = 2\pi[&\omega_1\mathbf{I_{1z}} + \omega_2\mathbf{I_{2z}} + \omega_s\mathbf{S_z} \\ &+J_{12}(\mathbf{I_{1x}I_{2x}} + \mathbf{I_{1y}I_{2y}} + \mathbf{I_{1z}I_{2z}}) + J_{1S}\mathbf{I_{1z}S_z} + J_{2S}\mathbf{I_{2z}S_z}] \end{aligned} \qquad (2.4)$$

In Equation 2.4, ω_1, ω_2, and ω_S represent the Larmor frequencies of proton I_1, proton I_2, and S. J_{12} is the homonuclear coupling constant between the protons, J_{1S} is the heteronuclear coupling constant between proton I_1 and S, and J_{2S} is the heteronuclear coupling constant between proton I_2 and S. Here we only consider only J coupling terms of the Hamiltonian since offsets are cancelled by through the application of refocusing pulses at ¼ and ¾ of each evolution delay [77]. The Hamiltonian neglecting offset evolution can be written as:

$$\mathbf{H} = 2\pi[J_{12}(\mathbf{I_{1x}I_{2x}} + \mathbf{I_{1y}I_{2y}} + \mathbf{I_{1z}I_{2z}}) + J_{1S}\mathbf{I_{1z}S_z} + J_{2S}\mathbf{I_{2z}S_z}]. \qquad (2.5)$$

By substituting the operators of $\mathbf{I_{1x}}$, $\mathbf{I_{2x}}$, $\mathbf{I_{1y}}$, $\mathbf{I_{2y}}$, $\mathbf{I_{1z}}$, $\mathbf{I_{2z}}$ and $\mathbf{S_z}$ (See Appendix A), the Hamiltonian could be described by the follow matrix:

$$\mathbf{H} = 2\pi \begin{pmatrix} \frac{1}{4}(J_{12} + J_{1S} + J_{2S}) & 0 & 0 & 0 \\ 0 & \frac{1}{4}(J_{12} - J_{1S} - J_{2S}) & 0 & 0 \\ 0 & 0 & \frac{1}{4}(-J_{12} + J_{1S} - J_{2S}) & \frac{1}{2}J_{12} \\ 0 & 0 & \frac{1}{2}J_{12} & \frac{1}{4}(-J_{12} - J_{1S} + J_{2S}) \\ 0 & 0 & 0 & 0 \\ 0 & 0 & 0 & 0 \\ 0 & 0 & 0 & 0 \\ 0 & 0 & 0 & 0 \end{pmatrix}$$

$$\begin{pmatrix} 0 & 0 & 0 & 0 \\ 0 & 0 & 0 & 0 \\ 0 & 0 & 0 & 0 \\ 0 & 0 & 0 & 0 \\ \frac{1}{4}(-J_{12} - J_{1S} + J_{2S}) & \frac{1}{2}J_{12} & 0 & 0 \\ \frac{1}{2}J_{12} & \frac{1}{4}(-J_{12} + J_{1S} - J_{2S}) & 0 & 0 \\ 0 & 0 & \frac{1}{4}(J_{12} - J_{1S} - J_{2S}) & 0 \\ 0 & 0 & 0 & \frac{1}{4}(J_{12} + J_{1S} + J_{2S}) \end{pmatrix} \quad (2.6)$$

At this point, all operators needed to study the three spin system have been established. After hydrogenation, the initial state, $\boldsymbol{\rho_0}$, does not generally commute with the Hamiltonian and therefore begins to evolve. If the state is left evolving for time t, the evolution becomes [116]:

$$\boldsymbol{\rho} = \mathbf{U}^{-1}\boldsymbol{\rho_0}\mathbf{U} \quad (2.7)$$

In which

$$\mathbf{U} = \exp(i\mathbf{H}t) \quad (2.8)$$

If a pulse is applied, assuming the pulse operator is labeled as **R**, the state will evolve to:

$$\boldsymbol{\rho} = \mathbf{R}^{-1}\boldsymbol{\rho_0}\mathbf{R} \quad (2.9)$$

By using this basis, the evolution of the states could be represented by density matrix, while pulses and time evolutions could all be represented by matrix evolution.

2.3. Methods: Evolution from Singlet-state to Net Magnetization

In this section a pulse sequence designed to achieve unitary polarization level independent of coupling topology in 3-spin I_1I_2S systems is described.

2.3.1. Evolution under 3 spin I_1I_2S system Hamiltonians

At low field, the evolution of $\mathbf{I_{1x}}$, $\mathbf{I_{2x}}$ and $\mathbf{I_{1y}}$, $\mathbf{I_{2y}}$ terms are completely entangled, and $\mathbf{I_{1z}}$ and $\mathbf{I_{2z}}$ terms will also evolve as they do not commute with the Hamiltonian. Here the calculated evolutions of $\mathbf{I_{1x}}$ and $\mathbf{I_{2x}}$ are shown as examples:

$$
\begin{aligned}
\mathbf{I_{1x}} \rightarrow\ & \cos(\pi J_{12}t)\{\cos[\frac{\pi}{2}(J_{1S}+J_{2S})t]\cos(\pi\Omega t) - \frac{1-\gamma^2}{1+\gamma^2}\sin[\frac{\pi}{2}(J_{1S}+J_{2S})t]\sin(\pi\Omega t)\}\mathbf{I_{1x}} \\
& -\sin(\pi J_{12}t)\{\sin[\frac{\pi}{2}(J_{1S}+J_{2S})t]\cos(\pi\Omega t) + \frac{1-\gamma^2}{1+\gamma^2}\cos[\frac{\pi}{2}(J_{1S}+J_{2S})t]\sin(\pi\Omega t)\}4\mathbf{I_{1x}I_{2z}S_z} \\
& +\sin(\pi J_{12}t)\{\cos[\frac{\pi}{2}(J_{1S}+J_{2S})t]\cos(\pi\Omega t) - \frac{1-\gamma^2}{1+\gamma^2}\sin[\frac{\pi}{2}(J_{1S}+J_{2S})t]\sin(\pi\Omega t)\}2\mathbf{I_{1y}I_{2z}} \\
& +\cos(\pi J_{12}t)\{\sin[\frac{\pi}{2}(J_{1S}+J_{2S})t]\cos(\pi\Omega t) + \frac{1-\gamma^2}{1+\gamma^2}\cos[\frac{\pi}{2}(J_{1S}+J_{2S})t]\sin(\pi\Omega t)\}2\mathbf{I_{1y}S_z} \\
& +\frac{2\gamma}{1+\gamma^2}\sin(\pi J_{12}t)\cos[\frac{\pi}{2}(J_{1S}+J_{2S})t]\sin(\pi\Omega t)\mathbf{I_{2x}} \\
& +\frac{2\gamma}{1+\gamma^2}\cos(\pi J_{12}t)\sin[\frac{\pi}{2}(J_{1S}+J_{2S})t]\sin(\pi\Omega t)4\mathbf{I_{2x}I_{1z}S_z} \\
& -\frac{2\gamma}{1+\gamma^2}\cos(\pi J_{12}t)\cos[\frac{\pi}{2}(J_{1S}+J_{2S})t]\sin(\pi\Omega t)2\mathbf{I_{2y}I_{1z}} \\
& +\frac{2\gamma}{1+\gamma^2}\sin(\pi J_{12}t)\sin[\frac{\pi}{2}(J_{1S}+J_{2S})t]\sin(\pi\Omega t)\mathbf{I_{2y}S_z}
\end{aligned}
\tag{2.10}
$$

$$\mathbf{I_{2x}} \rightarrow \cos(\pi J_{12}t)\{\cos[\frac{\pi}{2}(J_{1S}+J_{2S})t]\cos(\pi\Omega t)+\frac{1-\gamma^2}{1+\gamma^2}\sin[\frac{\pi}{2}(J_{1S}+J_{2S})t]\sin(\pi\Omega t)\}\mathbf{I_{2x}}$$

$$-\sin(\pi J_{12}t)\{\sin[\frac{\pi}{2}(J_{1S}+J_{2S})t]\cos(\pi\Omega t)-\frac{1-\gamma^2}{1+\gamma^2}\cos[\frac{\pi}{2}(J_{1S}+J_{2S})t]\sin(\pi\Omega t)\}4\mathbf{I_{2x}I_{1z}S_z}$$

$$+\sin(\pi J_{12}t)\{\cos[\frac{\pi}{2}(J_{1S}+J_{2S})t]\cos(\pi\Omega t)+\frac{1-\gamma^2}{1+\gamma^2}\sin[\frac{\pi}{2}(J_{1S}+J_{2S})t]\sin(\pi\Omega t)\}2\mathbf{I_{2y}I_{1z}}$$

$$+\cos(\pi J_{12}t)\{\sin[\frac{\pi}{2}(J_{1S}+J_{2S})t]\cos(\pi\Omega t)-\frac{1-\gamma^2}{1+\gamma^2}\cos[\frac{\pi}{2}(J_{1S}+J_{2S})t]\sin(\pi\Omega t)\}2\mathbf{I_{2y}S_z}$$

$$+\frac{2\gamma}{1+\gamma^2}\sin(\pi J_{12}t)\cos[\frac{\pi}{2}(J_{1S}+J_{2S})t]\sin(\pi\Omega t)\mathbf{I_{1x}}$$

$$+\frac{2\gamma}{1+\gamma^2}\cos(\pi J_{12}t)\sin[\frac{\pi}{2}(J_{1S}+J_{2S})t]\sin(\pi\Omega t)4\mathbf{I_{1x}I_{2z}S_z}$$

$$-\frac{2\gamma}{1+\gamma^2}\cos(\pi J_{12}t)\cos[\frac{\pi}{2}(J_{1S}+J_{2S})t]\sin(\pi\Omega t)2\mathbf{I_{1y}I_{2z}}$$

$$+\frac{2\gamma}{1+\gamma^2}\sin(\pi J_{12}t)\sin[\frac{\pi}{2}(J_{1S}+J_{2S})t]\sin(\pi\Omega t)\mathbf{I_{1y}S_z}$$

(2.11)

$$(\gamma=-\Delta+\sqrt{1+\Delta^2},\Omega=J_{12}\sqrt{1+\Delta^2},\Delta=\frac{J_{1S}-J_{2S}}{2J_{12}})$$

The evolution is approximately symmetric, except for the only difference in signs of the term $(1-\gamma^2)/(1+\gamma^2)\sin[(\pi/2)(J_{1S}+J_{2S})t]\sin(\pi\Omega t)$. Therefore, unless this term is significant, it will not be possible to break the symmetry and create pure ^{13}C polarization magnetization ($\mathbf{S_z}$). Taking HEP as an example, $\sin[(\pi/2)(J_{1S}+J_{2S})t]\sin(\pi\Omega t) = \sin[(7.24-5.62)\pi t] = \sin(0.81\pi t)$ evolves very slowly with time (period T=2.47s). Therefore, unless a time delay that lasts for seconds is applied (which is not feasible due to the relaxation), this term is very close to zero and negligible. Then the $\mathbf{I_{1x}}$ and $\mathbf{I_{2x}}$ terms evolve almost exactly symmetrically, which makes the coupling immune to any pulse sequence and impossible to obtain a pure S polarization state. However, the $\mathbf{S_z}(\mathbf{I}-4\mathbf{I_{1z}I_{2z}})$ state could be generated, which represents S net magnetization too, as the $4\mathbf{I_{1z}I_{2z}}$ term commutes with the Hamiltonian

and hence does not evolve with time.

2.3.2. Evolution of the initial singlet-states

The initial parahydrogen singlet-state evolves upon addition as:

$$\boldsymbol{\sigma_0}(t) \rightarrow [\sin^2\theta + \cos^2\theta\cos(2\pi\Omega t)](\mathbf{I_{1x}I_{2x}} + \mathbf{I_{1y}I_{2y}}) \quad (2.12a)$$

$$+\cos\theta\sin(2\pi\Omega t)2(\mathbf{I_{1y}I_{2x}} - \mathbf{I_{1x}I_{2y}})\mathbf{S_z} \quad (2.12b)$$

$$+\sin\theta\cos\theta[1-\cos(2\pi\Omega t)](\mathbf{I_{1z}} - \mathbf{I_{2z}})\mathbf{S_z}\,, \quad (2.12c)$$

where the $\mathbf{I_{1z}I_{2z}}$ term was neglected since it does not evolve.
In this expression, theta, delta, and omega are defined as:

$$\cos\theta = \frac{\Delta}{\sqrt{1+\Delta^2}}, \sin\theta = \frac{1}{\sqrt{1+\Delta^2}}, \Omega = J_{12}\sqrt{1+\Delta^2}, \Delta = \frac{J_{1S} - J_{2S}}{2J_{12}}\,.$$

The last two terms are coupled with S. However, due to the existence of the constant θ, it is not possible to generate a pure state of either term by a single time interval. The method employed here to solve this problem was to apply a 180 ºpulse on either I or S. The first term is not affected by the pulse and keeps evolving, while the signs of the other two terms will be reversed, which leads to cancellation and makes it possible to generate pure states. Here after a t_1 interval, a 180 $^{o}_{x}$ pulse on S is applied, followed by another interval t_2. The final evolution can be described as:

$$\boldsymbol{\sigma_0}(t_1,t_2) \rightarrow \{-\cos2\theta\sin^2\theta + \cos2\theta\cos^2\theta\cos(2\pi\Omega t_1)\cos(2\pi\Omega t_2) + \frac{1}{2}\sin^2 2\theta$$
$$[\cos(2\pi\Omega t_1) + \cos(2\pi\Omega t_1)] + \cos^2\theta\sin(2\pi\Omega t_1)\sin(2\pi\Omega t_2)\}(\mathbf{I_{1x}I_{2x}} + \mathbf{I_{1y}I_{2y}}) \quad (2.13a)$$

$$+[\sin\theta\sin2\theta\sin(2\pi\Omega t_2) + \cos\theta\cos2\theta\cos(2\pi\Omega t_1)\sin(2\pi\Omega t_2)$$
$$-\cos\theta\sin(2\pi\Omega t_1)\cos(2\pi\Omega t_2)]2(\mathbf{I_{1y}I_{2x}} - \mathbf{I_{1x}I_{2y}})\mathbf{S_z} \quad (2.13b)$$

$$-\frac{1}{2}\sin2\theta[\cos2\theta + 2\sin^2\theta\cos(2\pi\Omega t_2) - 2\cos^2\theta\cos(2\pi\Omega t_1)$$
$$+\cos2\theta\cos(2\pi\Omega t_1)\cos(2\pi\Omega t_2) + \sin(2\pi\Omega t_1)\sin(2\pi\Omega t_2)](\mathbf{I_{1z}} - \mathbf{I_{2z}})\mathbf{S_z} \quad (2.13c)$$

Therefore, to get a pure $(\mathbf{I_{1z}} - \mathbf{I_{2z}})\mathbf{S_z}$ state, the set of equations need to be solved:

$$-\cos2\theta\sin^2\theta + \cos2\theta\cos^2\theta\cos(2\pi\Omega t_1)\cos(2\pi\Omega t_2) + \frac{1}{2}\sin^2 2\theta$$
$$[\cos(2\pi\Omega t_1) + \cos(2\pi\Omega t_2)] + \cos^2\theta\sin(2\pi\Omega t_1)\sin(2\pi\Omega t_2) = 0 \quad (2.14a)$$

$$\sin\theta\sin2\theta\sin(2\pi\Omega t_2) + \cos\theta\cos2\theta\cos(2\pi\Omega t_1)\sin(2\pi\Omega t_2)$$
$$-\cos\theta\sin(2\pi\Omega t_1)\cos(2\pi\Omega t_2) = 0 \quad (2.14b)$$

$$-\frac{1}{2}\sin2\theta[\cos2\theta + 2\sin^2\theta\cos(2\pi\Omega t_2) - 2\cos^2\theta\cos(2\pi\Omega t_1)$$
$$+\cos2\theta\cos(2\pi\Omega t_1)\cos(2\pi\Omega t_2) + \sin(2\pi\Omega t_1)\sin(2\pi\Omega t_2) = 1 \quad (2.14c)$$

This is a system of two unknowns and three equations. However, since the coefficients must satisfy the unitary condition that the square of each equation sums up to unity, choosing t_1 and t_2 satisfying any two equations guarantee that the third will be satisfied automatically. Therefore, by appropriate choice of t_1 and t_2 intervals, the initial state is successfully evolved to a pure $(\mathbf{I_{1z}} - \mathbf{I_{2z}})\mathbf{S_z}$ state, which then concludes the first phase of the sequence.

2.3.3. Evolution into net heteronuclear magnetization

After generating the pure $(\mathbf{I_{1z}} - \mathbf{I_{2z}})\mathbf{S_z}$ state, a 90°_{y} pulse on S channel is applied to obtain $(\mathbf{I_{1z}} - \mathbf{I_{2z}})\mathbf{S_x}$ state ($\boldsymbol{\sigma}_{\mathbf{int}}$), followed by another interval, this term evolves to:

$$\boldsymbol{\sigma}_{\mathbf{int}}(t) = \cos(2\pi\Omega t)(\mathbf{I_{1z}} - \mathbf{I_{2z}})\mathbf{S_x} \quad (2.15a)$$

$$+\cos\theta\sin(2\pi\Omega t)\frac{1}{2}\mathbf{S_y}(\mathbf{I} - 4\mathbf{I_{1z}}\mathbf{I_{2z}}) \quad (2.15b)$$

$$-\sin\theta\sin(2\pi\Omega t)2(\mathbf{I_{1x}}\mathbf{I_{2y}} - \mathbf{I_{1y}}\mathbf{I_{2x}})\mathbf{S_x}\,. \quad (2.15c)$$

As before, it is not possible to obtain a pure $\mathbf{S_y}(\mathbf{I} - 4\mathbf{I_{1z}}\mathbf{I_{2z}})$ state, due to the existence of the constant θ. The same strategy is used to constrain the problem as in the first phase

of the sequence; a 180°_{x} pulse is applied on the S channel after the interval t_3, followed by another interval t_4. The evolution then becomes:

$$\begin{aligned}&\boldsymbol{\sigma}_{\mathbf{int}}(t_3, t_4)\\&= [\cos(2\pi\Omega t_3)\cos(2\pi\Omega t_4) + \cos 2\theta \sin(2\pi\Omega t_3)\sin(2\pi\Omega t_4)]\mathbf{S}_x(\mathbf{I}_{1z} - \mathbf{I}_{2z})\end{aligned} \tag{2.16a}$$

$$\begin{aligned}&+[\cos\theta\cos(2\pi\Omega t_3)\sin(2\pi\Omega t_4) - \sin\theta\sin 2\theta\sin(2\pi\Omega t_3)\\&-\cos\theta\cos 2\theta\sin(2\pi\Omega t_3)\cos(2\pi\Omega t_4)]\frac{1}{2}\mathbf{S}_y(\mathbf{I} - 4\mathbf{I}_{1z}\mathbf{I}_{2z})\end{aligned} \tag{2.16b}$$

$$\begin{aligned}&+[\sin\theta\cos 2\theta in(2\pi\Omega t_3)\cos(2\pi\Omega t_4) - \sin\theta\cos(2\pi\Omega t_3)\sin(2\pi\Omega t_4)\\&-\cos\theta\sin 2\theta\sin(2\pi\Omega t_3)]2\mathbf{S}_x(\mathbf{I}_{1y}\mathbf{I}_{2x} - \mathbf{I}_{1x}\mathbf{I}_{2y})\end{aligned} \tag{2.16c}$$

To generate a pure $\mathbf{S_y}(\mathbf{I} - 4\mathbf{I_{1z}I_{2z}})$ term, which represents a transverse S component, the coefficients must satisfy the following equations:

$$\cos(2\pi\Omega t_3)\cos(2\pi\Omega t_4) + \cos 2\theta \sin(2\pi\Omega t_3)\sin(2\pi\Omega t_4) = 0 \tag{2.17a}$$

$$\begin{aligned}&\cos\theta\cos(2\pi\Omega t_3)\sin(2\pi\Omega t_4) - \sin\theta\sin 2\theta\sin(2\pi\Omega t_3)\\&-\cos\theta\cos 2\theta\sin(2\pi\Omega t_3)\cos(2\pi\Omega t_4) = 1\end{aligned} \tag{2.17b}$$

$$\begin{aligned}&\sin\theta\cos 2\theta in(2\pi\Omega t_3)\cos(2\pi\Omega t_4) - \sin\theta\cos(2\pi\Omega t_3)\sin(2\pi\Omega t_4)\\&-\cos\theta\sin 2\theta\sin(2\pi\Omega t_3) = 0\end{aligned} \tag{2.17c}$$

The solution of the time delays could then be calculated as:

$$\begin{cases}\tan(2\pi\Omega t_3) = -\dfrac{1}{\sqrt{1+2\cos 2\theta}}\\[2ex]\tan(\pi\Omega t_4) = \dfrac{1}{\sqrt{1+2\cos 2\theta}}\end{cases}. \tag{2.18}$$

After the t_4 interval, a 90°_{x} on S will lead to an $\mathbf{S_z}(\mathbf{I} - 4\mathbf{I_{1z}I_{2z}})$ state, which represents the final desired polarization state on S. Application of this pulse sequence with appropriately chosen evolution delays will generate 100% S polarization in most I_1I_2S spin systems independent of J (Figure 2.3). For HEP (2-hydroxy, 1-^{13}C-ethylpropionate-d_3) the optimal intervals are (J_{12} = 7.57Hz, J_{1S} = 7.24Hz, J_{2S} = -5.62Hz):

$$t_1 = 9.75\text{ms},\ t_2 = 58.47\text{ms},\ t_3 = 36.20\text{ms},\ t_4 = 28.28\text{ms}\ . \qquad (2.19)$$

2.3.4. Hyper-SHIELDED pulse sequence

The sequence described here provides a streamlined solution to the problem of polarization transfer. A complete form of the sequence is given in Figure 2.1.

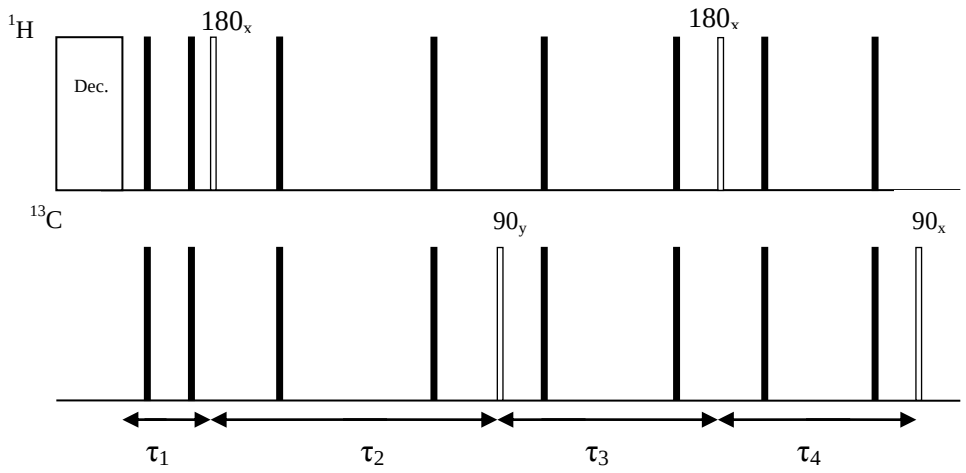

Figure 2.1. Schematic of hyper-SHIELDED pulse sequence. The sequence consists of 4 effective pulses (white pulses, 180° (+x) on I, 90° (+y) on S, 180° (+x) on I, and 90° (+x) on S), while the black bars are echo pulses applied at 1/4 and 3/4 of each time interval.

As shown in Figure 2.1, the effective pulses are the white pulses (180_x, 90_y, 180_x, 90_x). The decoupling sequences are applied during hydrogenation to prevent evolution during reaction, which leads to a loss in initial states. Also, the refocusing pulses at 1/4 and 3/4 of each time interval are applied to cancel the effect of field inhomogeneity [77].

The evolution pattern is summarized in Figure 2.2. The initial state 2 evolves to 3 states under Hamiltonian with time. Term 3a represents the ($\mathbf{I_{1x}I_{2x}} + \mathbf{I_{1y}I_{2y}}$) term (as

Equation 2.12a); 3b is $2(\mathbf{I_{1y}I_{2x}} - \mathbf{I_{1x}I_{2y}})\mathbf{S_z}$ term (as Equation 2.12b); 3c is $(\mathbf{I_{1z}} - \mathbf{I_{2z}})\mathbf{S_z}$ term (as Equation 2.12c). After the first step the three terms are focused to a pure 3c term. A 90_y pulse on S channel is followed to convert 3c to $(\mathbf{I_{1z}} - \mathbf{I_{2z}})\mathbf{S_x}$ term. Then in the second step, 3c evolves to 3 new terms, 4a, 4b, and 4c. Here 4a represents $(\mathbf{I_{1z}} - \mathbf{I_{2z}})\mathbf{S_x}$ term (as Equation 2.15a); 4b represents $\frac{1}{2}\mathbf{S_y}(\mathbf{I} - 4\mathbf{I_{1z}I_{2z}})$ term (as Equation 2.15b); 4c represents $2\mathbf{S_x}(\mathbf{I_{1y}I_{2x}} - \mathbf{I_{1x}I_{2y}})$ term(as Equation 2.15c). The three terms are focused to pure 4b term in the second term. Finally, a 90_y pulse on S channel rotates the state to $\frac{1}{2}\mathbf{S_z}(\mathbf{I} - 4\mathbf{I_{1z}I_{2z}})$ term and hyperpolarized S net magnetization could be stored along the direction of the static magnetic field.

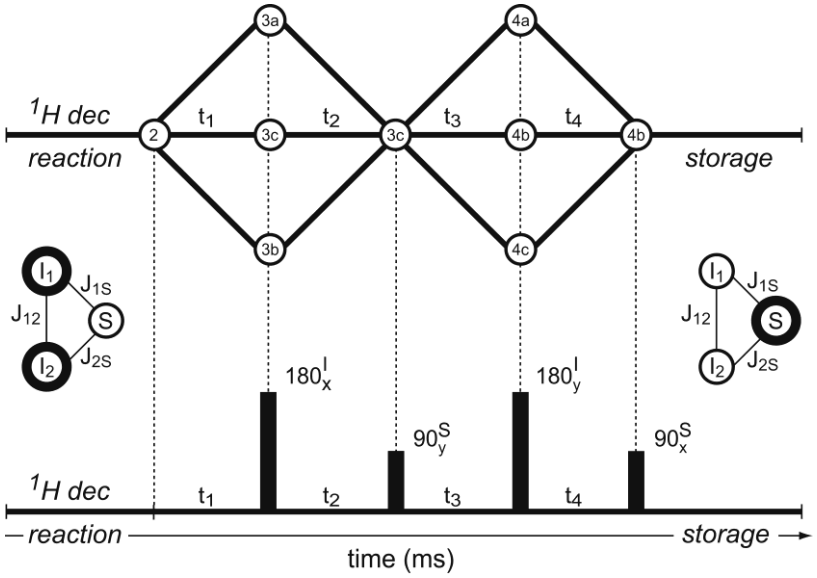

Figure 2.2. Graphical depiction of evolution of density matrix components (upper graph) and the hyper-SHIELDED sequence (lower graph) for focusing parahydrogen singlet-states ($\mathbf{I_1} \cdot \mathbf{I_2}$) into pure magnetization on an adjacent coupled (S) nucleus for strongly coupled I_1I_2S spin-systems. Symbols ($3_{a\text{-}c}$, $4_{a\text{-}c}$) correspond to components of the density operator.

The shorthand hyper-SHIELDED (Singlet to Heteronuclei by Iterative Evolution Locks Dramatic Enhancement for Delivery) was adopted for quick referencing the

sequence because it has the effect of protecting hyperpolarized spin order. The final polarization level of the pulse sequence could be calculated from Equation 2.20:

$$\begin{aligned}
\mathrm{Pol} = {} & [\sin\theta\sin2\theta\sin(2\pi\Omega t_2) + \cos\theta\cos2\theta\cos(2\pi\Omega t_1)\sin(2\pi\Omega t_2) \\
& -\cos\theta\sin(2\pi\Omega t_1)\cos(2\pi\Omega t_2)] \\
& \times[\frac{1}{4}\sin4\theta + \frac{1}{4}\sin4\theta\cos(2\pi\Omega t_3)\cos(2\pi\Omega t_4) \\
& +\sin2\theta(\sin^2\theta\cos(2\pi\Omega t_3) - \cos^2\theta\cos(2\pi\Omega t_4)) \\
& +\cos\theta\sin\theta\sin(2\pi\Omega t_3)\sin(2\pi\Omega t_4)] \\
& -\frac{1}{2}\sin2\theta[(\cos2\theta + 2\sin^2\theta\cos(2\pi\Omega t_2) - 2\cos^2\theta\cos(2\pi\Omega t_1) \\
& +\cos2\theta\cos(2\pi\Omega t_1)\cos(2\pi\Omega t_2) + \sin(2\pi\Omega t_1)\sin(2\pi\Omega t_2)] \\
& \times[\cos\theta\cos(2\pi\Omega t_3)\sin(2\pi\Omega t_4) - \sin\theta\sin2\theta\sin(2\pi\Omega t_3) \\
& \cos\theta\cos2\theta\sin(2\pi\Omega t_3)\cos(2\pi\Omega t_4)]
\end{aligned} \quad . \qquad (2.20)$$

2.4. Experimental Section

2.4.1. Synthesis of parahydrogen gas

Approximately 98% parahydrogen gas was synthesized by pulsing ambient hydrogen gas at 14 bar (200 psi) into a catalyst-filled (iron oxide) copper chamber held at 14 K using a previously described semi-automated parahydrogen generator. Fresh batches of parahydrogen were collected in 10 L aluminum storage tanks (14745-SHF-GNOS, Holley, KY, USA), used without Teflon lining or additional modification.

2.4.2. PASADENA precursor preparation

The preparation of PASADENA precursor molecules was similar to those previously [117] with the exception that water was used in place of 99.8% D_2O as a

solvent. Briefly, 1,4-bis- (phenyl-3-propane sulfonate) phosphine (0.180 g, 0.32 mmol, Q36333, Isotec, OH, USA) was combined with 100 mL H_2O in a 1 L flask. This ambient solution was then degassed with a rotary evaporator (model R-215 equipped with V-710 pump, Buchi, New Castle DE) by decrementing the onboard pressure slowly to avoid boiling, from 70 to 25 mbar over approximately 10 minutes. The rhodium catalyst, bis(norbornadiene)rhodium (I) tetrafluoroborate (0.10 g, 0.27 mmol, 45-0230, CAS 36620-11-8, Strem Chemicals, MA, USA) was dissolved in 7 mL acetone and was added drop-wise to the phosphine ligand solution to limit undesirable precipitation. After repeating the prior degassing procedure, this catalyst solution was mixed with 2-hydroxyethyl acrylate-1-^{13}C,2,3,3-d_3 (HEA, 97% chemical purity, 99 atom % ^{13}C, 98 atom % D (20 mg, 0.16 mmol, Sigma-Aldrich 676071) in a 150 mL square bottle (431430, Corning Life Sciences, NY, USA).

2.4.3. Catalytic hydrogenation

The precursor solution held in this 150 mL square bottle was connected to a previously described, automated parahydrogen polarizer [117], equipped with a dual-tuned ^{1}H/^{13}C coil [118]. Briefly, the chemical reaction was pulse programmed with a commercial NMR console, to synchronize chemical reaction parameters, decoupling fields, polarization transfer sequences, and detection of NMR signals. PASADENA precursors were sprayed from an external location into a plastic (polysulfone) reactor located within a 48 mT static magnetic field. The external solution was equilibrated at 65 $^{\circ}$C prior to spraying, and 16.5 bar (240 psi) nitrogen

gas was used to inject this heated PASADENA precursor solution into a pressurized atmosphere of **7** bar (100 psi) parahydrogen, and proton continuous wave decoupling was applied immediately at a frequency of 2.02 MHz (B_0 = 47.5 mT) with a magnitude of **5** kHz. This decoupling field was maintained for 4 seconds to lock the parahydrogen spin ensemble while the hydrogenation reaction went to completion.

2.4.4. Detection of hyperpolarized ^{13}C

The polarization transfer sequence was applied immediately after CW decoupling was turned off. For the HEP molecule, the t_1, t_2, t_3, and t_4 intervals were 9.75ms, 58.47ms, 36.20ms, and 28.28ms, respectively. These delays were calculated from the density matrix expressions above assuming a proton-proton coupling of 7.57 Hz, and a carbon-proton scalar coupling asymmetry of 12.86 Hz [119]. The actual couplings could vary somewhat from these values depending on pH and specific attributes of the polarization process such as temperature and pressure. After polarization transfer, the free induction decay (single shot) was sampled with 512 points at a receiver bandwidth of 5 kHz for a digital resolution of ~10 Hz per point.

2.5. Discussion

Described here is a new pulse sequence (hyper-SHIELDED) for transforming parahydrogen spin order in the strong coupling regime of protons into net heteronuclear magnetization. Hyper-SHIELDED operates at nearly unity efficiency with yields that are approximately independent of scalar coupling topology in three

spin systems (I_1I_2S). The I_1I_2S moiety is a widespread and important spin system in PHIP experiments formed for example, by molecular addition of parahydrogen to perdeuterated and unsaturated molecular backbones.

Hyper-SHIELDED flanks two asymmetric proton refocusing intervals about a heteronuclear excitation pulse to generate four unique delays ($t_1 - t_4$). Optimization of these delays to spin couplings in the molecule of interest sequentially converts the initial parahydrogen singlet-state into pure heteronuclear magnetization (Figure 2.2). Density matrix evolution under the influence of hyper-SHIELDED is depicted graphically in Figure 2.2 and linked directly to equations in section 2.3.

The analysis of spin dynamics under the influence of hyper-SHIELDED assumed strongly coupled protons and weak heteronuclear scalar couplings (Equation 2.5). The initial parahydrogen density operator was retained without truncation and proportional to $\mathbf{I_1} \cdot \mathbf{I_2}$ (Equation 2.3). Chemical shifts were not considered because the effects are small compared to homonuclear proton couplings at targeted fields in the vicinity of 47.5 mT or lower, and we note that offsets were refocused with 180 ° pulses on both channels placed at 1/4 and 3/4 of each evolution interval [119]. Evolution of the strongly coupled parahydrogen density operator of Equation 2.3 is relatively complicated compared to (truncated) high field density operators proportional to $\mathbf{I_{1z}I_{2z}}$. While analytical solutions to the spin dynamics are more tedious, heteronuclear magnetization yields from parahydrogen spin order are increased by a factor of 2 at low field in the strong coupling regime of protons.

Hyper-SHIELDED was applied immediately following the hydrogenation

reaction. During the fast catalytic hydrogenation [120], proton decoupling was used to maintain equivalence of the parahydrogen protons and freeze evolution of the spin density operator until reaction completion [77]. After this period of decoupling and chemical addition, with hyper-SHIELDED the initial density matrix evolved from the parahydrogen singlet-state (Equation 2.3) to three terms (Equations 3.12a−3.12c, symbols 3a−c in Figure 2.2) in the Cartesian product basis during the first interval (t_1). A 180 ℉(x) proton pulse then focused these three terms of the density matrix into term 4c during the interval t_2. A 90 ℉(y) pulse on the S nucleus then allowed term 4c to evolve into an additional three terms (Equation 3.15a-3.15c, symbols 4a−c, Figure 2) during the interval t_3. Following a proton 180 °pulse, these three terms (symbols 4a−c, Figure 2) collapse into a single term during t_4 (symbol 4b, Figure 2).

Note that since $\mathbf{I_{1z}I_{2z}}$ commutes with the Hamiltonian, $\mathbf{I_{1z}I_{2z}}(t = 0) = \mathbf{I_{1z}I_{2z}}$ (t). Since $\mathbf{I_{1z}}(t = 0) + \mathbf{I_{2z}}(t = 0) = 0$ for the parahydrogen singlet-state, $4\mathbf{I_{1z}I_{2z}}$ reduces to $-\mathbf{I}$. Therefore, when the τ intervals are chosen to satisfy Equations 2.17a and 2.17b, Equation 2.16b reduces to a pure $\mathbf{S_y}$ term. Rotating this heteronuclear magnetization then locks the original parahydrogen spin order along $\mathbf{S_z}$, where it will persist according to relaxation kinetics specific to the storage nucleus. Alternatively, if left unperturbed in the transverse plane this term could be detected directly at the field where the PHIP preparation was performed [117]. Nonselective refocusing pulses were interleaved at 1/4 and 3/4 on both channels in each evolution interval to refocus offsets and mitigate the deleterious impact of static field inhomogeneities [119].

Two prior sequences have been reported to transform parahydrogen spin order

into heteronuclear magnetization in the strong proton coupling regime where the process is most efficient [119, 121]. Most recently, Kadlecek and co-workers reported a set of sequences that can be selectively applied to yield optimal transfer efficiency in three distinct scalar coupling regimes [121]. Goldman and co-workers reported the first pulsed transfer method which yields near unity singlet-state transformation efficiency in proximity to the scalar couplings of the design molecule. They also described a recursion procedure to pump polarization yields with GPS toward unity when outside of those targeted coupling regimes [119]. With hyper-SHIELDED, we sought to build on these efficient earlier works by developing a streamlined sequence that could achieve optimal conversion efficiency in a single streamlined sequence without recursive application and with minimal sensitivity to scalar coupling.

To characterize sensitivity of hyper-SHIELDED to scalar couplings, transfer efficiency was calculated with respect to proton−proton scalar couplings (J_{12}) and coupling asymmetry ($|J_{1S}-J_{2S}|$) over a range spanning known and conceivable PHIP reaction products (Figures 2.3 and 2.4). For each unique set of couplings (J_{12}, $|J_{1S}-J_{2S}|$), the set of evolution intervals yielding maximum efficiency was determined by inverting the density matrix equations subject to a 300 ms total sequence duration constraint. As illustrated in Figure 2.3, a broad plateau of unity transformation efficiency was obtained with as little as ∼6 Hz heteronuclear coupling asymmetry ($|J_{1S}-J_{2S}|$) and ∼2 Hz homonuclear proton coupling (J_{12}). If application warranted and relaxation times were favorable, expanding the total pulse sequence duration constraint beyond 300 ms would enable sharper transitions from valley to plateau.

To validate the sequence, experimental heteronuclear ^{13}C signals were compared between hyper-SHIELDED and GPS [119] for a PHIP reaction product where both sequences were predicted to perform with identical efficiency (Figures 2.4 and 2.5).

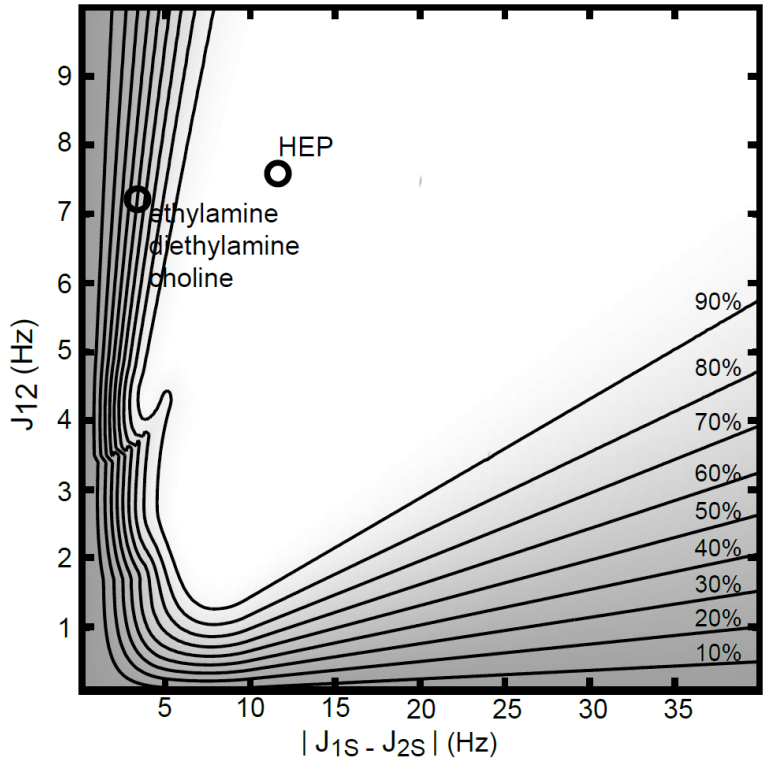

Figure 2.3. Polarization yield as a function of homonuclear proton coupling (J_{12}) and heteronuclear coupling asymmetry ($|J_{1S} - J_{2S}|$) for hyper-SHIELDED. Contours levels are annotated at right and superposed onto a gradient map calculated at a resolution of $(0.1\ Hz)^2$. For each point, the density matrix equations were inverted to find tau intervals corresponding to maximum polarization and normalized to the global maximum. The total duration of the sequence is fixed to be within 300 ms. Coupling coordinates are annotated for the test molecule (HEP) in addition to a series of molecules with small asymmetries expected to differentially benefit from hyper-SHIELDED.

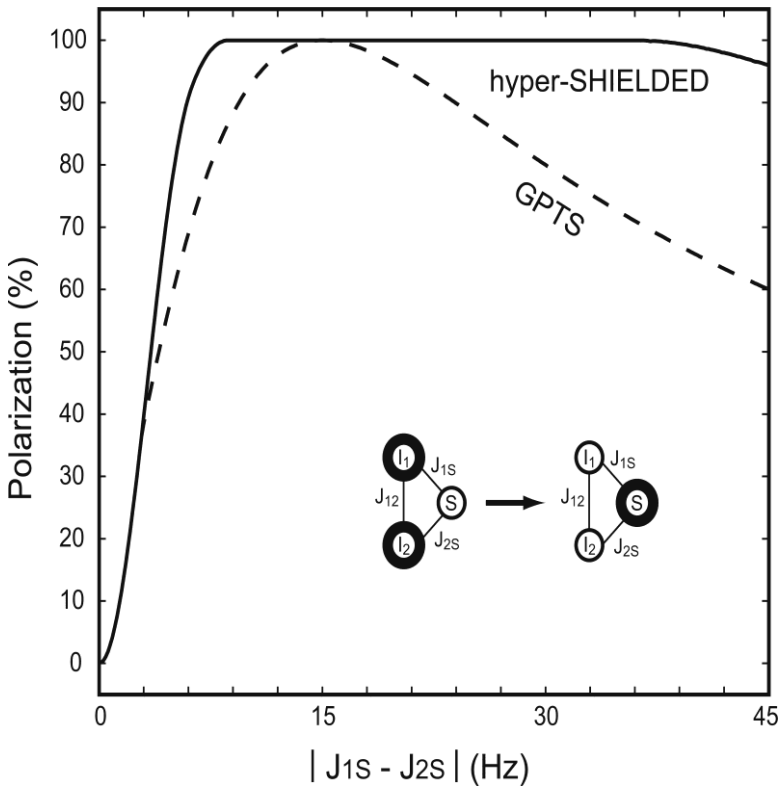

Figure 2.4. Dependence of theoretical polarization transfer efficiency on heteronuclear coupling constant asymmetry $|J_{1S} - J_{2S}|$ in 3 spin systems (I_1, I_2, S) starting from an initial singlet-state density operator ($I_1 \cdot I_2$)using the hyper-SHIELDED sequence (solid) versus a non-recursive implementation of a comparison sequence (dotted, GPS). For each point, the equations governing the evolution of the density matrix were solved for the optimal pulse sequence delays to produce maximum polarization. The tau parameter space was search over the range from zero to 300 ms.

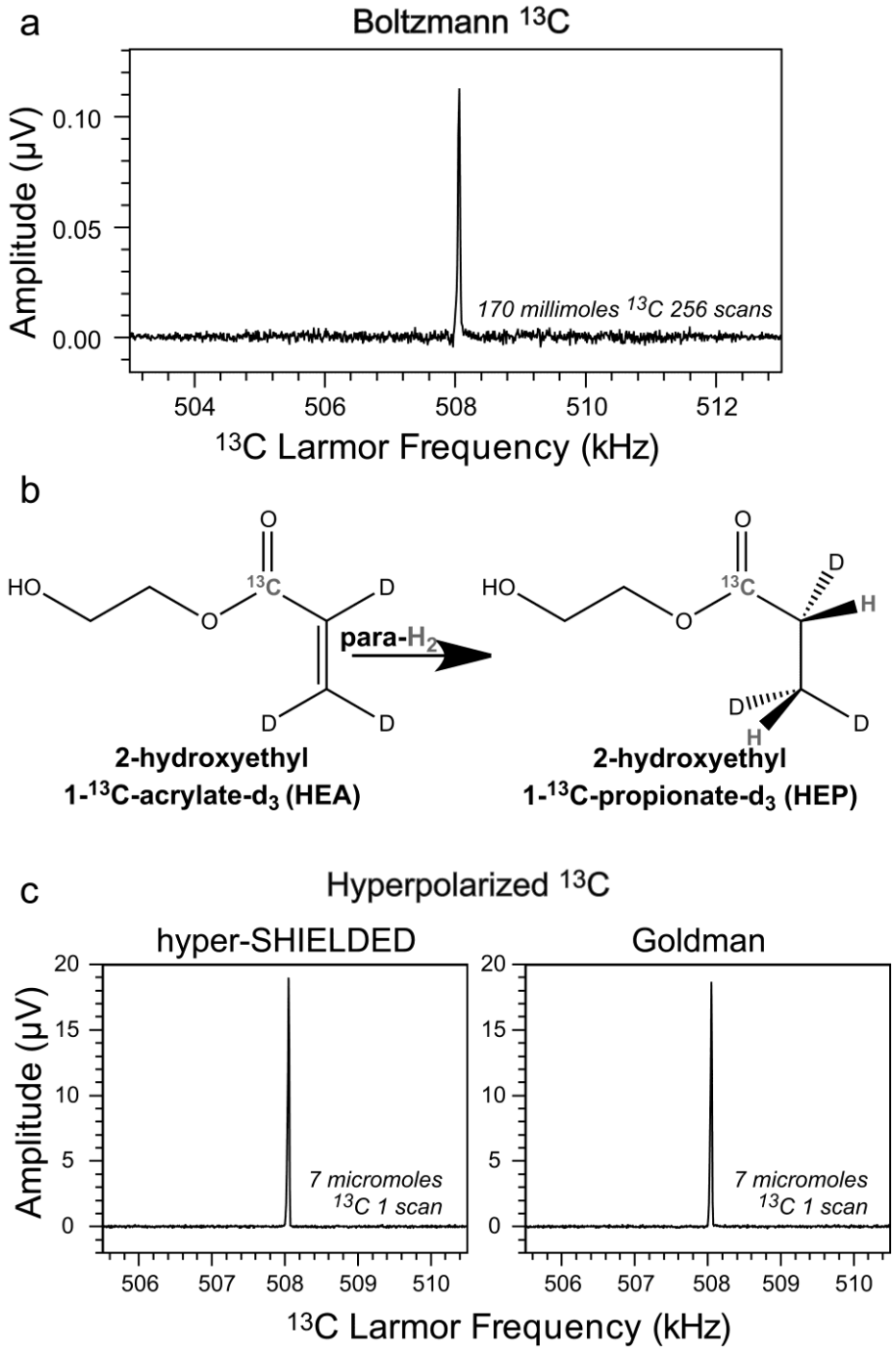

Figure 2.5. Polarization yield of the hyper-SHIELDED sequence versus Goldman measured at the respective optimal timing parameters in a PASADENA parahydrogenation reaction. Experimentally determined yields were nearly identical (c) and in accord with theory for the parahydrogenated reaction product, 2-hydroxy, 1-^{13}C-ethylpropionate-d_3 (b). A Boltzmann polarized carbon-13 spectrum was acquired from an aqueous solution containing 170 millimoles of the reaction product for comparison (a).

As shown in Figure 2.5 and in accord with theoretical expectations, ^{13}C magnetization yield in a 7 μmol sample of the PHIP reaction product, 2-hydroxyethyl 1-^{13}C-propionate-d_3, was enhanced by a large and equivalent factor of several million with both sequences. Hyper-SHIELDED builds on earlier advances [119, 121] by creating a single streamlined sequence that could achieve high transfer efficiencies independent of scalar couplings. Implementation of hyper-SHIELDED is experimentally compact and because the sequence does not rely on condition or recursive application for broadband efficiency, and it can be readily extended to multidimensional experiments on mixtures containing molecules with a range of couplings.

Theoretical conversion efficiency was also analyzed at a specific J_{12} (7.5 Hz) and compared to the nonrecursive application of GPS [77]. As illustrated in Figure 2.3, the dependence of polarization yield in the small asymmetry regime is relatively insensitive to J_{12}. Polarization yields reach uniform efficiency more rapidly as a function of asymmetry in hyper-SHIELDED versus the nonrecursive application of GPS, and high levels of polarization are sustained across a broad range of asymmetries (Figure 2.4). Although the calculated data points in Figure 2.4 were not parsed by sequence duration, hyper-SHIELDED was slightly longer (17.88 ms) at the HEP optimum. For the heteronuclear relaxation constants of HEP, the increased duration of the hyper-SHIELDED sequence did not reduce polarization yield (Figure 2.5). Hyper-SHIELDED should perform particularly well in molecules with small asymmetries such as ethylamine, diethyamine, and choline (Figure 2.4) [122, 123].

CHAPTER 3

SPIN ORDER TRANSFER FROM PARAHYDROGEN SINGLET-STATES INTO HETERONUCLEAR NET MAGNETIZATION IN AA'XY SPIN SYSTEMS

Parahydrogen based methods of hyperpolarization have the potential to enhance MR sensitivity to a level sufficient for observing metabolism *in vivo* at approximately physiologic substrate concentrations. While these chemically synthesized, ordered spin states can be long-lived and useful in many applications without additional processing, when applied to biomedicine they require transformation into net magnetization on long-lived heteronuclei to facilitate subsequent MR imaging by standard techniques. Efficient methods for transforming singlet-state spin order into net heteronuclear magnetization have been previously developed for parahydrogenated three-spin systems [77, 121, 124], but these methods are expected from theory to perform poorly when applied to four spin systems featuring strong proton-proton and weak, heteronuclear scalar couplings (I_1I_2SR).

In this chapter, a sequence is described for efficiently transferring parahydrogen spin order in four-spin systems. The method used to design the sequence is an extension of that used to develop the 3-spin hyper-SHIELDED sequences. Global analytic solutions to the spin evolution are found by embedding iterative refocusing pulses. These pulses act to selectively invert terms in the density matrix and taken together, a sufficient number allow global analytical solutions to be found. Specifically, the initial parahydrogen density matrix was transformed across three

independent time intervals to distill a six term product operator space into a single term. This desired S magnetization component was then rotated to the transverse plane and three additional tau intervals were used to distill the resulting eight term product operator space into a pure heteronuclear (S) magnetization term. Each interval provides a constraint, and together an approximately global solution could be found. This term could then either be directly observed *in situ* or more commonly for biomedical applications, stored along z for subsequent delivery and imaging. Although precursor molecules are not yet available to test experimentally, we anticipate that this sequence will provide an efficient method to transform parahydrogen singlet-states in four spin (I_1I_2SR) systems into net heteronuclear magnetization.

The aim of the sequence is presented in section 3.1. Four spin systems with two protons and two heteronuclei are likely to become significant because they include molecules in the TCA cycle, including 1,4-labeled succinic acid, which are introduced in 3.2. The detailed properties of four spin system, including product basis representation, are outlined in 3.3. The four spin analog of hyper-SHIELDED designed to transfer spin order from parahydrogen singlet-states to heteronuclear net magnetization is described in section 3.4. The discussions about the sequence, including the efficiency of the pulse sequence across various spin systems are described in section 3.5. Further studies for improving the efficiency of the spin order transfer sequence, are discussed in section 3.6.

3.1. Introduction

Hyperpolarization of nuclear spin ensembles has increased NMR sensitivity to a level that is now enabling detection of metabolism in biological tissue on a time-scale of seconds [51, 106]. The goal of this work was to address in particular, the absence of pulse sequences for efficiently transforming singlet-states into net heteronuclear magnetization in the important class of four spin systems formed by addition of parahydrogen to an unsaturated molecular backbone. While raw singlet-states can be long-lived and useful themselves for basic science applications and particularly at Earth's field or below, when applied to biomedicine it is useful to convert these states into net magnetization on a long-lived heteronucleus for both storage and to facilitate subsequent imaging by standard methods. To our knowledge, the analogous sequences for use in four spin systems have not yet been addressed in the literature.

Whether by covalent addition (PASADENA) or reversible interaction (SABRE), parahydrogen methods of hyperpolarization operate by creating ordered ensembles of singlet-states. In the strong proton coupling, these singlet-states evolve under special symmetry conditions are met within the larger spin network formed by the interaction of parahydrogen. For example, adding parahydrogen to a perdeuterated 1-^{13}C phosphoenolpyruvate molecule would create a four spin system ($^{1}H_1$, $^{1}H_2$,^{31}P,^{13}C) which in turn will evolve unless $J_{1S} - J_{1R} - J_{2S} + J_{2R} = 0$ and $J_{1S} + J_{1R} - J_{2S} - J_{2R} = 0$ (where S and R refer only to arbitrary, weakly coupled heteronuclei). In contrast to three spin systems formed analogously, the expressions that describe the four spin evolution are much more complicated. Therefore finding optimal spin trajectories

between the initial parahydrogen singlet-state and terms with nearly pure net heteronuclear magnetization, is more difficult.

In this study, we describe a consolidated pulse sequence that transforms parahydrogen spin order into heteronuclear magnetization in I_1I_2SR spin systems with a yield near unity and independent of spin couplings. The sequence provides efficient conversion across a broad range of coupling topologies by flanking a heteronuclear excitation with two asymmetric proton refocusing intervals to provide four unique evolution intervals. These delay intervals are in turn optimized using prior knowledge of the spin couplings to efficiently transform the initial parahydrogen spin order into pure heteronuclear magnetization. We anticipate that this hyper-SHIELDED-4 sequence will provide an efficient method to transform parahydrogen singlet-states in four spin (I_1I_2SR) systems into net heteronuclear magnetization.

Transforming these states into net heteronuclear magnetization maximizes spectral dispersion and reduces interference from the intense proton background arising from water proton signals. It has recently been demonstrated that parahydrogen singlet-states can themselves be long-lived at Earth's field [125], but even in cases where the parahydrogen proton lifetimes are similar to or even more favorable than carbonyl ^{13}C for example, locking the initial spin order also eliminates the need to synchronize subsequent imaging acquisitions to accrued singlet-state evolution.

3.2. Examples of m0olecules featuring the I_1I_2SR spin systems

As stated above, there are many important four spin systems in NMR. Many molecules in TCA cycle are likely to be formed into I_1I_2SR spin systems by PHIP. For example, a precursor for PHIP lactate (phospholactate) has recently been developed, and efficient utilization of PHIP spin order in this molecule will require a sequence tailored to transforming spin order in four spin sequences.

3.2.1. TCA cycle

The TCA cycle (tricarboxylic acid cycle), also referred to as citric acid cycle, stands for a series of chemical reactions by aerobic organisms to generate energy through the oxidization of acetate derived from carbohydrates, fats and proteins into carbon dioxide (Figure 3.1) [126-129].

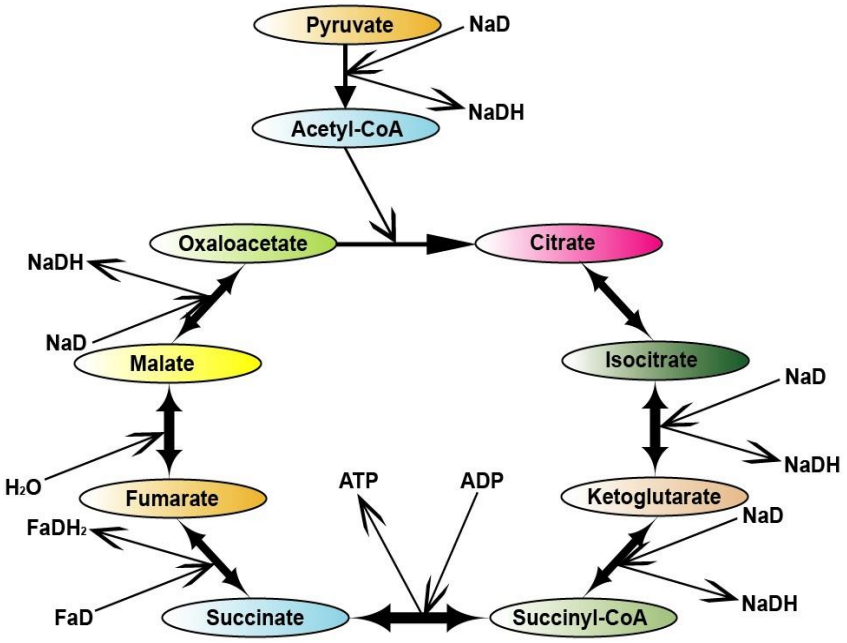

Figure 3.1. Schematic of the TCA cycle. A series of chemical reactions by aerobic organisms to generate energy through the oxidization of acetate derived from carbohydrates, fats and proteins into carbon dioxide.

TCA cycle molecules generate energy in the form of ATP through a series of chemical conversions, therefore the NMR signal between pairs of molecules adjacent in this cycle have the potential for tracking *in vivo* metabolism. From DNP, the conversion rate of the molecules (like fumarate to malate) in tumors has been shown to depend on treatment [54]. Fumarate and succinate are highly symmetric spin systems, and one of the primary goals of developing a four spin hyper-SHIELDED sequence was selectively modulate and observe these states in a manner dependent on TCA cycle chemical triggers.

3.2.2. Symmetrical spin system

Prior to hydrogenation, the 1,4-^{13}C fumaric acid molecule is a completely symmetrical molecule (Figure 3.2) and remains symmetric when converted to 1,4-^{13}C succinic acid after hydrogenation.

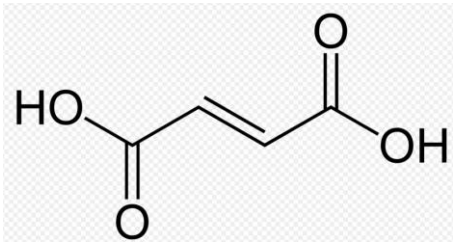

Figure 3.2. Stick diagram of 1,4-^{13}C-labeled fumaric acid. After labeling both carbons the molecule becomes a symmetric spin system.

The succinic acid is also a common molecule in TCA cycle. It possesses the property of adjacent couplings, double bond, and long lifetimes, making it a potentially ideal candidate for spin order transfer too. And the molecule is within a symmetric spin system, which could allow the singlet-states to be stored after hydrogenation.

The method used in Chapter II to transfer spin order from parahydrogen singlet-states to heteronuclear net magnetization requires the process (hydrogenation → spin order transfer → signal recording) to be continuous without any significant time lag. Otherwise, either the ^{13}C relaxation destroys the obtained hyperpolarized state, or the singlet-state will be projected to the eigenstates of the new Hamiltonian which relaxes quickly into thermal equilibrium. In this section we focus on the study of hyperpolarized state lifetimes.

Angular momentum selection rules prevent parahydrogen states from being relaxed to ortho states, which preserves singlet-states for durations much longer than would be expected from transverse or longitudinal relaxation. However, when the parahydrogen H_2 gas is added to other molecules in order to transfer spin order and to generate observable signals, it appears that the parahydrogen state will evolve to other states under the new Hamiltonian since the symmetry is broken. This will lead to a loss of polarization especially *in vivo* if the sample needs to be stored before recording signals.

Examining the low field Hamiltonian of the two protons and S spins (again neglecting chemical shifts):

$$\mathbf{H} = 2\pi(J_{12}\mathbf{I_1}\cdot\mathbf{I_2} + J_{1S}\mathbf{I_{1z}}\mathbf{S_z} + J_{2S}\mathbf{I_{2z}}\mathbf{S_z}) \tag{3.1}$$

The eigenstates of this Hamiltonian are:

$$\begin{aligned}
&\psi_1 = |\alpha\alpha\alpha> \qquad \psi_2 = |\alpha\alpha\beta> \\
&\psi_3 = |\beta\beta\alpha> \qquad \psi_4 = |\beta\beta\beta> \\
&\psi_5 = a|\alpha\beta\alpha> - b|\beta\alpha\alpha> \qquad \psi_6 = b|\alpha\beta\alpha> + a|\beta\alpha\alpha> \\
&\psi_7 = b|\alpha\beta\beta> - a|\beta\alpha\beta> \qquad \psi_8 = a|\alpha\beta\beta> + b|\beta\alpha\beta> \\
&a = \frac{\gamma_a}{\sqrt{1+\gamma_a^2}}, \gamma_a = \frac{\frac{J_{1S}-J_{2S}}{2} - \sqrt{(\frac{J_{1S}-J_{2S}}{2})^2 + J_{12}^2}}{J_{12}} \\
&b = \frac{\gamma_b}{\sqrt{1+\gamma_b^2}}, \gamma_b = \frac{\frac{J_{1S}-J_{2S}}{2} + \sqrt{(\frac{J_{1S}-J_{2S}}{2})^2 + J_{12}^2}}{J_{12}}
\end{aligned} \tag{3.2}$$

The initial density matrix, projected to the eigenstates of this Hamiltonian can be written as:

$$\boldsymbol{\rho} = \frac{1}{8}[\mathbf{I} - 4\mathbf{I_{1z}}\mathbf{I_{2z}} + \frac{1}{\sqrt{1+\Delta^2}}(\mathbf{I_{1x}}\mathbf{I_{2x}} + \mathbf{I_{1y}}\mathbf{I_{2y}}) + \frac{\Delta}{\sqrt{1+\Delta^2}}(\mathbf{I_{1z}} - \mathbf{I_{2z}})\mathbf{S_z}], \tag{3.3}$$

where $\Delta = (J_{1S}-J_{2S})/2J_{12}$

It follows that if $\Delta = 0$, the density matrix is stationary and remains in the singlet-state. Here $\Delta = 0$ implies that $J_{1S} = J_{2S}$. Examining the eigenstates, when $J_{1S} = J_{2S}$, $\Delta_a = \Delta_b$, $a = b = \frac{1}{\sqrt{2}}$, the last four eigenstates become:

$$\psi_5 = \frac{1}{\sqrt{2}}|\alpha\beta\alpha> - \frac{1}{\sqrt{2}}|\beta\alpha\alpha> \qquad \psi_6 = \frac{1}{\sqrt{2}}|\alpha\beta\alpha> + \frac{1}{\sqrt{2}}|\beta\alpha\alpha>$$
$$\psi_7 = \frac{1}{\sqrt{2}}|\alpha\beta\beta> - \frac{1}{\sqrt{2}}|\beta\alpha\beta> \qquad \psi_8 = \frac{1}{\sqrt{2}}|\alpha\beta\beta> + \frac{1}{\sqrt{2}}|\beta\alpha\beta> \quad . \qquad (3.4)$$

This expression shows that ψ_5 and ψ_7 are represented as singlet-states of protons coupled to either $|\alpha>$ or $|\beta>$ state of the heteronucleus. This implies that provided $J_{1S} = J_{2S}$, the singlet-state will be projected to 50% ψ_5 and 50% ψ_7, remaining in the singlet-state and preserved for long time. If $J_{1S} \neq J_{2S}$, then the larger $J_{1S} - J_{2S}$ is, the difference between the projected density matrix and the initial singlet-state density matrix becomes correspondingly larger. When $J_{1S} = J_{2S}$, the spin system is completely symmetric. This suggests that the singlet-state lifetime is proportional to asymmetry of the system, $\Delta=(J_{1S} - J_{2S})/2J_{12}$, with commensurate effects on lifetimes. The smaller $J_{1S} - J_{2S}$ is, the longer the singlet-state could be preserved. This hypothesis can be supported by the coherent evolution of singlet-states (See Section 2.3):

$$\boldsymbol{\sigma_0}(t) = [\sin^2\theta + \cos^2\theta\cos(2\pi\Omega t)](\mathbf{I_{1x}I_{2x}} + \mathbf{I_{1y}I_{2y}}) \qquad (3.5a)$$

$$+\cos\theta\sin(2\pi\Omega t)2(\mathbf{I_{1y}I_{2x}} - \mathbf{I_{1x}I_{2y}})\mathbf{S_z} \qquad (3.5b)$$

$$+\sin\theta\cos\theta[1-\cos(2\pi\Omega t)](\mathbf{I_{1z}} - \mathbf{I_{2z}})\mathbf{S_z} \qquad (3.5c)$$

If $J_{1S} = J_{2S}$, then $\Delta = 0$, $\sin\theta = 1$, $\cos\theta = 0$, so the coefficients for the last two terms vanish, and the singlet-state will not evolve with time. The larger the factor Δ is, the

faster singlet-state decays. The lifetime is therefore proportional to the factor $(1/\Delta)$.

However, if the molecule is prepared by hydrogenation through double-bonds, the two protons are always one bond away and J_{1S} - J_{2S} is never zero, therefore it is generally not feasible to obtain symmetric molecules in three spin systems (I_1I_2S). But if the molecule consists of two labeled carbons, like 1,4-^{13}C succinic acid, it becomes possible to create a symmetrical chemical environment for hydrogenation.

It is recently reported that the lifetime of the hyperpolarized state is related to magnetic field as well (a low field preserves longer lifetime rather than zero-field, the precise magnetic field needs to be selected from the spin system) [130].

As discussed above, singlet-states could be preserved for relatively long intervals after hydrogenation. Succinate is not completely symmetric, since for this molecule $J_{HaCb}=J_{HbCa}$, $J_{HaCa}=J_{HbCb}$, instead of the perfectly symmetric case, $J_{HaCa}=J_{HbCa}$ and $J_{HaCb}=J_{HbCb}$. In summary, it should be possible to generate signal in this molecule (detailed calculation provided in 3.3).

Further calculation of the evolution shows that the lifetime of the singlet-states in this molecule should be proportional to the factor of $\frac{1}{2}(\Delta_a + \Delta_b)$, in which $\Delta_a = (J_{HaCa} + J_{HaCb} - J_{HbCa} - J_{HbCb})/2J_{HaHb}$, $\Delta_b = (J_{HaCa} - J_{HaCb} - J_{HbCa} + J_{HbCb})/2J_{HaHb}$. If $\Delta_a = \Delta_b = 0$, the singlet-state will not evolve with time. For this molecule $\Delta_b=0$, therefore half of the spin system would stay in singlet-states while the lifetime of the other half will be proportional to $(J_{HaCa} + J_{HaCb} - J_{HbCa} - J_{HbCb})/2J_{HaHb}$. This part will likely to decay to thermal equilibrium on time scale of seconds.

In the view of eigenstates, after hydrogenation, the probability is 50% that the

initial singlet-state $(1/\sqrt{2})$ (|αβ>-|βα>), would be projected to the states $(1/\sqrt{2})$ (|αβ,αα>-|βα,αα>) or $(1/\sqrt{2})$ (|αβ,ββ>-|βα,ββ>) and remain in these states (the last two symbols represent the two heteronuclei). The other 50% probability is that the initial singlet-state will be projected to the states $(1/\sqrt{2})$ (|αβ, αβ>-|βα,αβ>) or $(1/\sqrt{2})$ (|αβ, βα>-|βα, βα>), and decay with time since it is longer in a singlet-state ($\gamma_a=\sqrt{(1+\Delta_a^2)}-\Delta_a$).

Therefore, after hydrogenation and relaxation, 50% polarized singlet-states could still be preserved in this spin system. This state could be made observable by breaking the symmetry and the pulse sequence presented later in 3.4. One possible method of breaking the symmetry would be to adjust pH, since the J coupling constants of succinic acid depend on pH.

3.3. Mathematical Basis of I_1I_2SR Systems

In product operator basis, since the I_1I_2SR spin system consists of four spin $1/2$ nuclei, each spin state could be represented by a 16×16 matrix. In the rest of this chapter, the two protons of parahydrogen will be labeled as I_1 and I_2, while the two heteronuclei will be labeled as S and R.

The 16 states formed by products of the individual spin ½ states could be labeled as: |αααα>, |ααaβ>, |ααβα>, |αβαα>, |βααα>, |ααββ>, |αβαβ>, |αββα>, |βααβ>, |βαβα>, |ββαα>, |αβββ>, |βαββ>, |ββαβ>, |βββα>, and |ββββ>. Full expressions of the operators can be found in Appendix B.

The initial density matrix is the parahydrogen singlet-state:

$$\boldsymbol{\sigma_0} = \mathbf{I_{1x}I_{2x}} + \mathbf{I_{1y}I_{2y}} + \mathbf{I_{1z}I_{2z}} \tag{3.6}$$

The matrix representation of the initial singlet-state is then (neglecting $\mathbf{I_{1z}I_{2z}}$ term, which does not evolve with time):

$$\boldsymbol{\sigma_0} = \frac{1}{2}\begin{pmatrix}
0&0&0&0&0&0&0&0&0&0&0&0&0&0&0&0\\
0&0&0&0&0&0&0&0&0&0&0&0&0&0&0&0\\
0&0&0&0&0&0&0&0&0&0&0&0&0&0&0&0\\
0&0&0&0&1&0&0&0&0&0&0&0&0&0&0&0\\
0&0&0&1&0&0&0&0&0&0&0&0&0&0&0&0\\
0&0&0&0&0&0&0&0&0&0&0&0&0&0&0&0\\
0&0&0&0&0&0&0&0&1&0&0&0&0&0&0&0\\
0&0&0&0&0&0&0&0&0&1&0&0&0&0&0&0\\
0&0&0&0&0&0&1&0&0&0&0&0&0&0&0&0\\
0&0&0&0&0&0&0&1&0&0&0&0&0&0&0&0\\
0&0&0&0&0&0&0&0&0&0&0&0&0&0&0&0\\
0&0&0&0&0&0&0&0&0&0&0&0&1&0&0&0\\
0&0&0&0&0&0&0&0&0&0&0&1&0&0&0&0\\
0&0&0&0&0&0&0&0&0&0&0&0&0&0&0&0\\
0&0&0&0&0&0&0&0&0&0&0&0&0&0&0&0\\
0&0&0&0&0&0&0&0&0&0&0&0&0&0&0&0
\end{pmatrix} \tag{3.7}$$

Any pulse applied to the spin system could be represented in this basis by a rotational operator (also 8x8 density matrix), calculated from:

$$\mathbf{R_i}(\theta,\varphi) = \cos(\frac{\theta}{2})\mathbf{I} + 2i\sin(\frac{\theta}{2})[\cos(\varphi)\mathbf{I_{ix}} + \sin(\varphi)\mathbf{I_{iy}}]. \tag{3.8}$$

For the I_1I_2SR spin systems with two protons and two heteronuclei, in low field the homonuclear coupling between the protons is considered strong coupling ($\delta \approx J$), while the other heteronuclear couplings are considered all weak couplings ($\delta >> J$), the coupling Hamiltonian is then (as in Chapter II, only coupling Hamiltonian is considered):

$$\begin{aligned}\mathbf{H} = 2\pi[&J_{12}(\mathbf{I_{1x}I_{2x}} + \mathbf{I_{1y}I_{2y}} + \mathbf{I_{1z}I_{2z}})\\ &+J_{1S}\mathbf{I_{1z}S_z} + J_{1R}\mathbf{I_{1z}R_z} + J_{2S}\mathbf{I_{2z}S_z} + J_{2R}\mathbf{I_{1z}R_z} + J_{SR}\mathbf{S_zR_z}]\end{aligned}. \tag{3.9}$$

Matrix expressions of this Hamiltonian are included in Appendix B. All the necessary

operators to analyze the spin order of I_1I_2RS spin systems have now been constructed. The initial parahydrogen singlet-state will evolve under the Hamiltonian as:

$$\begin{aligned}\boldsymbol{\rho} &= \mathbf{U}^{-1}\boldsymbol{\rho}_0\mathbf{U} \\ \mathbf{U} &= \exp(i\mathbf{H}t)\end{aligned} \tag{3.10}$$

3.4 Methods: evolution of parahydrogen singlet-state to heteronuclear net magnetization

Using a similar strategy as in Chapter II, the evolution of states under the Hamiltonian can be analyzed in two independent phases.

3.4.1. Evolution of initial singlet-states

The formation of the initial state is given in Sections 3.6 and 3.7. The evolution of the initial parahydrogen singlet-state could be calculated after numerical calculation in the mathematical basis constructed in Section 3.2 (detailed evolution of the systems is given in Appendix C).

$$\boldsymbol{\sigma}_0(t) = \frac{1}{2}[\sin^2\theta_1 + \cos^2\theta_1\cos(2\pi\Omega_1 t) + \sin^2\theta_2 + \cos^2\theta_2\cos(2\pi\Omega_2 t)](\mathbf{I_{1x}I_{2x}} + \mathbf{I_{1y}I_{2y}}) \tag{3.11a}$$

$$+\frac{1}{2}[\sin^2\theta_1 + \cos^2\theta_1\cos(2\pi\Omega_1 t) - \sin^2\theta_2 - \cos^2\theta_2\cos(2\pi\Omega_2 t)] \\ 4(\mathbf{I_{1x}I_{2x}} + \mathbf{I_{1y}I_{2y}})\mathbf{S_zR_z} \tag{3.11b}$$

$$+\frac{1}{2}[\cos\theta_1\sin(2\pi\Omega_1 t) + \cos\theta_2\sin(2\pi\Omega_2 t)]2(\mathbf{I_{1y}I_{2x}} - \mathbf{I_{1x}I_{2y}})\mathbf{S_z} \tag{3.11c}$$

$$+\frac{1}{2}[\cos\theta_1\sin(2\pi\Omega_1 t) - \cos\theta_2\sin(2\pi\Omega_2 t)]2(\mathbf{I_{1y}I_{2x}} - \mathbf{I_{1x}I_{2y}})\mathbf{R_z} \tag{3.11d}$$

$$+\frac{1}{4}[\sin2\theta_1(1-\cos(2\pi\Omega_1 t)) + \sin2\theta_2(1-\cos(2\pi\Omega_2 t))](\mathbf{I_{1z}} - \mathbf{I_{2z}})\mathbf{S_z} \tag{3.11e}$$

$$+\frac{1}{4}[\sin2\theta_1(1-\cos(2\pi\Omega_1 t)) - \sin2\theta_2(1-\cos(2\pi\Omega_2 t))](\mathbf{I_{1z}} - \mathbf{I_{2z}})\mathbf{R_z} \tag{3.11f}$$

There are six terms in the evolution. The first term represents the initial state, the second is the initial state coupled to both heteronuclei. The third and fifth terms are coupled with heteronucleus S, while the fourth and sixth are coupled with heteronucleus R. Here S is chosen as the receptor of PHIP spin order. The fifth term (3.11e), $(\mathbf{I_{1z}}\text{-}\mathbf{I_{2z}})\mathbf{S_z}$ is chosen as the node, or destination for the first phase in the spin order transfer. In contrast to the 3-spin I_1I_2S spin system, with this 4-spin problem there are six terms, so a simple 180 °pulse will not be sufficient to maximize the fifth term. The expression of the evolved terms shows that if a 180 ℵ pulse is applied on protons, the 3rd (3.11c), 4th (3.11d), 5th (3.11e), 6th (3.11f) terms all change signs. If a 180 ℵ pulse on heteronucleus S channel is applied, the 2nd (3.11b), 3rd (3.11c), 5th (3.11e) terms change signs. Also, a 180 ℵ pulse on heteronucleus R channel will change signs of the 2nd (3.11b), 4th (3.11d), 6th (3.11f) terms. It could be proven by calculation that applying a combination of 180 ℵ pulses on any two of the three channels will be sufficient to transfer spin order, only changing the time intervals of the sequence. Here proton and S channels are chosen, which are feasible in two-channel NMR facilities. Therefore, the first step of evolution contains three time intervals (t_1-t_3) and two 180 ℵ pulses on proton/heteronucleus S channels to evolve the initial singlet-state closest to the state coupled with heteronucleus S ($(\mathbf{I_{1z}} - \mathbf{I_{2z}})\mathbf{S_z}$). The density matrix after the evolution then becomes:

$$\boldsymbol{\sigma}_{\mathbf{N}}(t_1, t_2, t_3) = e^{-i\mathbf{H}t_3}[\mathbf{R}_{\mathbf{x}}^{\mathbf{I}}(\pi)]^{-1}e^{-i\mathbf{H}t_2}[\mathbf{R}_{\mathbf{x}}^{\mathbf{S}}(\pi)]^{-1}e^{-i\mathbf{H}t_1}\sigma_0 e^{i\mathbf{H}t_1}\mathbf{R}_{\mathbf{x}}^{\mathbf{S}}(\pi)e^{i\mathbf{H}t_2}\mathbf{R}_{\mathbf{x}}^{\mathbf{I}}(\pi)e^{i\mathbf{H}t_3}. \quad (3.12)$$

The time intervals t_1, t_2, and t_3 are modified simultaneously to evolve the state closest to $(\mathbf{I_{1z}}\text{-}\mathbf{I_{2z}})\mathbf{S_z}$ state (Equation 3.11e), to minimize the following expression:

$$\min[\boldsymbol{\sigma}_{\mathbf{N}}(t_1, t_2, t_3) - (3.11e)] \tag{3.13}$$

3.4.2. Evolution to heteronuclear net magnetization

After the first step, a 90 ℽ pulse is applied on heteronucleus S channel to obtain a transverse component of heteronucleus S:

$$\mathbf{S_z}(\mathbf{I_{1z}} - \mathbf{I_{2z}}) \xrightarrow{90^{o}\,y(S)} \mathbf{S_x}(\mathbf{I_{1z}} - \mathbf{I_{2z}}). \tag{3.14}$$

To generate net magnetization of heteronucleus S, the evolution of this state is then calculated:

$$\begin{aligned}&\boldsymbol{\sigma}_{\mathbf{N}}(t) = \cos(\pi J_{SR} t)\\ &[\cos(\pi\Omega_1 t)\cos(\pi\Omega_2 t) - \cos(\theta_1 - \theta_2)\sin(\pi\Omega_1 t)\sin(\pi\Omega_2 t)]\mathbf{S_x}(\mathbf{I_{1z}} - \mathbf{I_{2z}})\end{aligned} \tag{3.15a}$$

$$\begin{aligned}&-\sin(\pi J_{SR} t)[\cos\theta_1 \sin(\pi\Omega_1 t)\cos(\pi\Omega_2 t)\\ &+\cos\theta_2 \cos(\pi\Omega_1 t)\sin(\pi\Omega_2 t)]\mathbf{S_x}(\mathbf{I} - 4\mathbf{I_{1z}}\mathbf{I_{2z}})\mathbf{R_z}\end{aligned} \tag{3.15b}$$

$$\begin{aligned}&+\cos(\pi J_{SR} t)[\cos\theta_1 \sin(\pi\Omega_1 t)\cos(\pi\Omega_2 t)\\ &+\cos\theta_2 \cos(\pi\Omega_1 t)\sin(\pi\Omega_2 t)]\frac{1}{2}\mathbf{S_y}(\mathbf{I} - 4\mathbf{I_{1z}}\mathbf{I_{2z}})\end{aligned} \tag{3.15c}$$

$$\begin{aligned}&+\sin(\pi J_{SR} t)[\cos(\pi\Omega_1 t)\cos(\pi\Omega_2 t)\\ &-\cos(\theta_1 - \theta_2)\sin(\pi\Omega_1 t)\sin(\pi\Omega_2 t)]2\mathbf{S_y}(\mathbf{I_{1z}} - \mathbf{I_{2z}})\mathbf{R_z}\end{aligned} \tag{3.15d}$$

$$\begin{aligned}&-\cos(\pi J_{SR} t)[\sin(\theta_1 - \theta_2)\\ &\sin(\pi\Omega_1 t)\sin(\pi\Omega_2 t)]4\mathbf{S_x}(\mathbf{I_{1x}}\mathbf{I_{2x}} + \mathbf{I_{1y}}\mathbf{I_{2y}})\mathbf{R_z}\end{aligned} \tag{3.15e}$$

$$\begin{aligned}&-\sin(\pi J_{SR} t)[\sin\theta_1 \sin(\pi\Omega_1 t)\cos(\pi\Omega_2 t)\\ &+\sin\theta_2 \cos(\pi\Omega_1 t)\sin(\pi\Omega_2 t)]4\mathbf{S_y}(\mathbf{I_{1y}}\mathbf{I_{2x}} - \mathbf{I_{1x}}\mathbf{I_{2y}})\mathbf{R_z}\end{aligned} \tag{3.15f}$$

$$\begin{aligned}&-\cos(\pi J_{SR} t)[\sin\theta_1 \sin(\pi\Omega_1 t)\cos(\pi\Omega_2 t)\\ &+\sin\theta_2 \cos(\pi\Omega_1 t)\sin(\pi\Omega_2 t)]2\mathbf{S_x}(\mathbf{I_{1y}}\mathbf{I_{2x}} - \mathbf{I_{1x}}\mathbf{I_{2y}})\end{aligned} \tag{3.15g}$$

$$\begin{aligned}&-\sin(\pi J_{SR} t)[\sin(\theta_1 - \theta_2)\\ &\sin(\pi\Omega_1 t)\sin(\pi\Omega_2 t)]2\mathbf{S_y}(\mathbf{I_{1x}}\mathbf{I_{2x}} + \mathbf{I_{1y}}\mathbf{I_{2y}})\end{aligned} \tag{3.15h}$$

The state evolves into eight different terms. The term representing the heteronucleus S transverse component is the 3rd term (Equation 3.15c), $\frac{1}{2}\mathbf{S_y}(\mathbf{I} - 4\mathbf{I_{1z}}\mathbf{I_{2z}})$ term. The same

technique as the first step is applied to this evolution. Here if a 180 °x pulse is applied on protons, the terms that change signs are the 1st (Equation 3.15a), 4th (Equation 3.15d), 6th (Equation 3.15f), 7th (Equation 3.12g) terms. If a 180 °x pulse is applied on heteronucleus S channel, the terms that change signs are the 3rd (Equation 3.15c), 4th (Equation 3.15d), 6th (Equation 3.15e), 8th (Equation 3.15h) terms. Also, a 180 °x pulse on the heteronucleus R channel changes the signs of the 2nd (Equation 3.15b), 4th (Equation 3.15d), 5th (Equation 3.15e), 6th (Equation 3.15f) terms. It could also be proven that applying a combination of 180 °x pulses on any two of the three channels will transfer spin order with same efficiency by adjusting the time intervals in the sequence. Again proton and heteronucleus S channels are chosen as the channels that 180 °x pulses are applied to. The density matrix after this step then becomes:

$$\boldsymbol{\sigma}_{\mathbf{F}}(t_4, t_5, t_6) = e^{-i\mathbf{H}t_6}[\mathbf{R}_{\mathbf{x}}^{\mathbf{I}}(\pi)]^{-1}e^{-i\mathbf{H}t_5}[\mathbf{R}_{\mathbf{x}}^{\mathbf{S}}(\pi)]^{-1}e^{-i\mathbf{H}t_4}\sigma_{int}e^{i\mathbf{H}t_4}\mathbf{R}_{\mathbf{x}}^{\mathbf{S}}(\pi)e^{i\mathbf{H}t_5}\mathbf{R}_{\mathbf{x}}^{\mathbf{I}}(\pi)e^{i\mathbf{H}t_6}. \quad (3.16)$$

The time intervals t_4, t_5, and t_6 are modified simultaneously to get the state closest to $\frac{1}{2}\mathbf{S_y}(\mathbf{I} - 4\mathbf{I_{1z}I_{2z}})$ state (Equation 3.15c), to again minimize the difference between the target and final state:

$$\min[\boldsymbol{\sigma}_{\mathbf{F}}(t_4, t_5, t_6) - (3.15c)] \quad (3.17)$$

After evolving to the state with the least difference to the 3rd term (Equation 3.15c), a 90 °x pulse is applied to S channel to obtain pure heteronucleus S net magnetization.

$$\mathbf{S_y}(\mathbf{I} - 4\mathbf{I_{1z}I_{2z}}) \xrightarrow{90^o\,x(S)} \mathbf{S_z}(\mathbf{I} - 4\mathbf{I_{1z}I_{2z}}) \quad (3.18)$$

3.4.3. Hyper-SHIELDED-4 pulse sequence

The complete form of the pulse sequence that transfers spin order from a parahydrogen singlet-state to heteronuclear net magnetization for I_1I_2SR spin systems is described in this chapter (Figure 3.3).

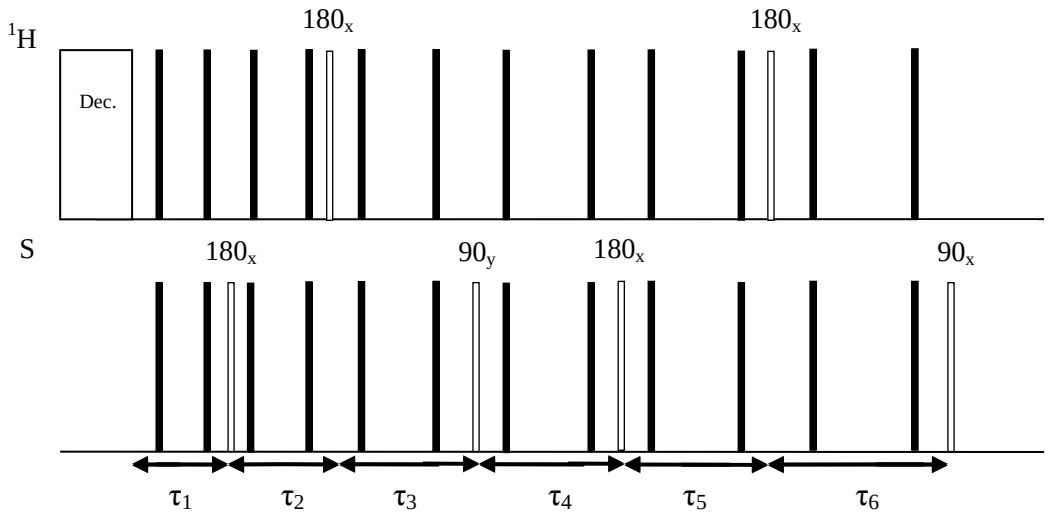

Figure 3.3. The 4-spin hyper-SHIELDED sequence for transferring spin order from a singlet-state to heteronuclear net magnetization in I_1I_2SR spin systems. The sequence consists of 6 effective pulses (white pulses, 180(+x) on S, 180° (+x) on I, 90° (+y) on S, 180° (+x) on S, 180° (+x) on I, and 90° (+x) on S), while the black pulses are refocusing pulses placed at 1/4 and 3/4 of each time interval.

In Figure 3.3, the white pulses are effective pulses. As in Chapter II, initially a decoupling field is applied during reaction to avoid the evolution and possible loss of polarization level during reaction. And 180 °refocusing pulses are applied at 1/4 and 3/4 of each time interval to cancel the effect of filed inhomogeneity [77]. In analogy to the 3-spin sequence, since a similar technique was used to design the sequence, and since the overall impact is similar (to protect PHIP spin order), the shorthand hyper-SHIELDED-4 was adopted for quick referencing.

A detailed diagram in Figure 3.4 depicts the pulse sequence and evolution of states.

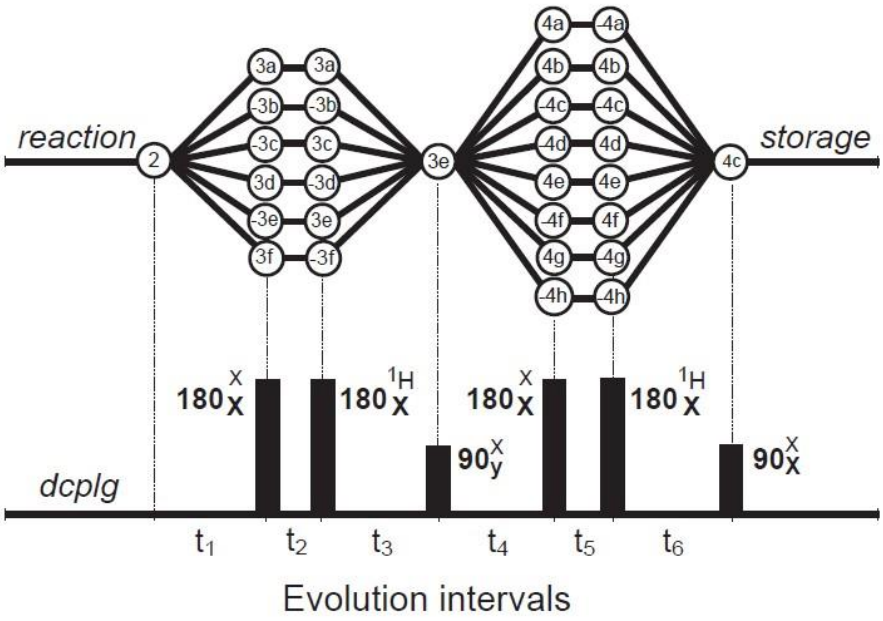

Figure 3.4. Evolution of density matrix components (upper graph) and the associated pulse sequence (lower graph) for focusing parahydrogen singlet-states ($\mathbf{I_1 \cdot I_2}$) into pure magnetization on an adjacent coupled (S) nucleus for I_1I_2SR spin-systems in the strong coupling regime. Labels S and P refer generally to coupled S-nucleus (for example, ^{13}C or ^{31}P). Symbols (3a-f, 4a-g) correspond to components of the density operator.

As shown in Figure 3.4, state 2 is the initial state. 3a-f represents the six states the initial term evolves into, including ($\mathbf{I_{1x}I_{2x}} + \mathbf{I_{1y}I_{2y}}$), 4($\mathbf{I_{1x}I_{2x}} + \mathbf{I_{1y}I_{2y}}$)$\mathbf{S_zR_z}$, 2($\mathbf{I_{1y}I_{2x}} - \mathbf{I_{1x}I_{2y}}$)$\mathbf{S_z}$, 2($\mathbf{I_{1y}I_{2x}} - \mathbf{I_{1x}I_{2y}}$)$\mathbf{R_z}$, ($\mathbf{I_{1z}} - \mathbf{I_{2z}}$)$\mathbf{S_z}$, and ($\mathbf{I_{1z}} - \mathbf{I_{2z}}$)$\mathbf{R_z}$ terms (as Equation 3.11a-f). After the initial state evolves for time t_1, a 180_x pulse on heteronucleus S channel coverts signs of the 3b, 3c, 3e terms. Then the state evolves again for interval t_2, a 180_x pulse is followed on proton channel that converts signs of 3c, 3d, 3e, 3f terms, the state then evolves for another time period t_3. After the pulses, the evolution pattern

for each term is different, making it possible to obtain the state closest to the desired term, 3e.

A 90° (+y) pulse on heteronucleus S channel is then followed to rotate $\mathbf{S_z}$ to $\mathbf{S_x}$ and generate S transverse component (3e to 4a). The 4_a state is left evolving for a time period of t_4 and evolves to eight new terms (4a-h). Those terms (4a-h) represents the 8 states of $\mathbf{S_x(I_{1z} - I_{2z})}$, $\mathbf{S_x(I - 4I_{1z}I_{2z})R_z}$, $\frac{1}{2}\mathbf{S_y(I - 4I_{1z}I_{2z})}$, $2\mathbf{S_y(I_{1z} - I_{2z})R_z}$, $4\mathbf{S_x(I_{1x}I_{2x} + I_{1y}I_{2y})R_z}$, $4\mathbf{S_y(I_{1y}I_{2x} - I_{1x}I_{2y})R_z}$, $2\mathbf{S_x(I_{1y}I_{2x} - I_{1x}I_{2y})}$, $2\mathbf{S_y(I_{1x}I_{2x} + I_{1y}I_{2y})}$ (as Equation 3.15a-h). A 180_x pulse on heteronucleus S channel then reverses signs of 4c, 4d, 4f, 4h terms. After another evolution of t_5, a 180_x pulse on proton channel then converts signs of 4a, 4d, 4f, 4g terms. Again by creating different evolution pattern for each term, the state closest to the desired term, 4c, could be obtained. In the end a 90_x pulse is applied on heteronucleus S channel to rotate it to net S longitudinal magnetization.

3.5. Discussion

Described here is a pulse sequence (hyper-SHIELDED-4) designed to efficiently transform parahydrogen singlet-state spin order into heteronuclear magnetization in hyperpolarized four spin systems that feature strong proton-proton, and weak heteronuclear scalar couplings. Although new molecules are emerging for applications to biomedicine that will require efficient transfer sequences, to our knowledge none have yet been described. We showed earlier that selective refocusing could be used to generate constraints sufficient to enable streamlined, approximately global analytic solutions to be identified in three spin systems. While applying the three spin

sequence generated earlier to four spin systems yields suboptimal results, we found that extending the earlier design process by introducing additional selective refocusing pulses would allow efficient, nearly global analytic solutions to be found in four spin systems.

The initial density matrix was transformed sequentially in two independent intervals, separated by a heteronuclear 90° pulse. Within each of these intervals, 180° pulses were applied on protons and a selected heteronucleus to generate sufficient constraints so as to enable an approximately global analytic solution to be found for transforming the initial singlet-state into net heteronuclear magnetization. Hyper-SHIELDED flanks two asymmetric proton refocusing intervals about a heteronuclear excitation pulse to generate six unique delays (t_1-t_6). Optimization of these delays to spin couplings in the molecule of interest sequentially converts the initial parahydrogen singlet-state into pure heteronuclear magnetization (Figure 3.4).

The analysis of spin dynamics under the influence of hyper-SHIELDED-4 assumed strongly coupled protons and weak heteronuclear scalar couplings. The initial parahydrogen density operator was retained without truncation and proportional to $\mathbf{I_1 \cdot I_2}$. Chemical shifts were not considered because the effects are small compared to homonuclear proton couplings at targeted fields in the vicinity of 47.5 mT or lower, and we note that offsets were refocused with 180° pulses on both channels placed at 1/4 and 3/4 of each evolution interval. Evolution of the strongly coupled parahydrogen density operator is relatively complicated compared to (truncated) high field density operators proportional to $\mathbf{I_{1z}I_{2z}}$. While analytical solutions to the spin dynamics are more tedious,

heteronuclear magnetization yields from parahydrogen spin order are increased by a factor of two at low field in the strong coupling regime of protons.

This sequence is meant to be applied immediately following the hydrogenation reaction. During the fast catalytic hydrogenation, Proton decoupling would be used to maintain equivalence of the parahydrogen protons therefore freezing evolution of the spin density operator until reaction completion. After this period of decoupling and chemical addition, with hyper-SHIELDED-4 the initial density matrix evolved from the parahydrogen singlet-state to six terms (Equation 3.11a-f, symbols 3a-f in Figure 3.4) in the Cartesian product basis during the first interval (t_1). Two 180_x proton/S-nucleus pulses then focused these six terms of the density matrix into term 3.11e during the intervals t_2 and t_3. A 90_y pulse on the S-nucleus then allowed term $\boldsymbol{\sigma_N}$ to evolve into an additional eight terms (Equation 3.15a-h, symbols 7a-h, Figure 3.4) during the interval t_4. Following two proton/S-nucleus 180° pulse, these eight terms (symbols 7a-h, Figure 3.4) collapse into a single term during t_5 and t_6 (symbol 7c, Figure 3.4).

Note that since $\mathbf{I_{1z}I_{2z}}$ commutes with the Hamiltonian, $\mathbf{I_{1z}I_{2z}}(t = 0) = \mathbf{I_{1z}I_{2z}}(t)$. Since $\mathbf{I_{1z}}(t = 0) + \mathbf{I_{2z}}(t = 0) = 0$ for the parahydrogen singlet-state, $4\mathbf{I_{1z}I_{2z}}$ reduces to $-\mathbf{I}$. Therefore when the tau intervals are chosen to satisfy Equation 3.17, Equation 3.15c reduces to a pure $\mathbf{S_y}$ term. Rotating this heteronuclear magnetization then locks the original parahydrogen spin order along $\mathbf{S_z}$, where it will persist according to relaxation kinetics specific to the storage nucleus. Alternatively, if left unperturbed in the transverse plane this term could be detected directly at the field where the PHIP

preparation was performed. Nonselective refocusing pulses could be interleaved at 1/4 and 3/4 on both channels in each evolution interval to refocus offsets and mitigate the deleterious impact of static field inhomogeneities.

To characterize sensitivity of hyper-SHIELDED-4 to scalar couplings, transfer efficiency was calculated with respect to both coupling asymmetry ($|J_{1S} - J_{2S}|$ and $|J_{1R} - J_{2R}|$) over a range spanning known and conceivable PHIP reaction products for the three major conformations - gauche, eclipse and anti (Figures 3.5). For each unique set of couplings ($|J_{1S} - J_{2S}|$, $|J_{1R} - J_{2R}|$), the set of evolution intervals yielding maximum efficiency was determined by inverting the density matrix equations subject to a 500 ms total sequence duration constraint. As illustrated in Figure 3.5, a broad plateau of unity transformation efficiency was obtained with heteronuclear coupling asymmetry ($|J_{1S}-J_{2S}|$) as little as half of the proton-proton scalar couplings. If application warranted and relaxation times were favorable, expanding the total pulse sequence duration constraint beyond 500 ms would enable sharper transitions from valley to plateau.

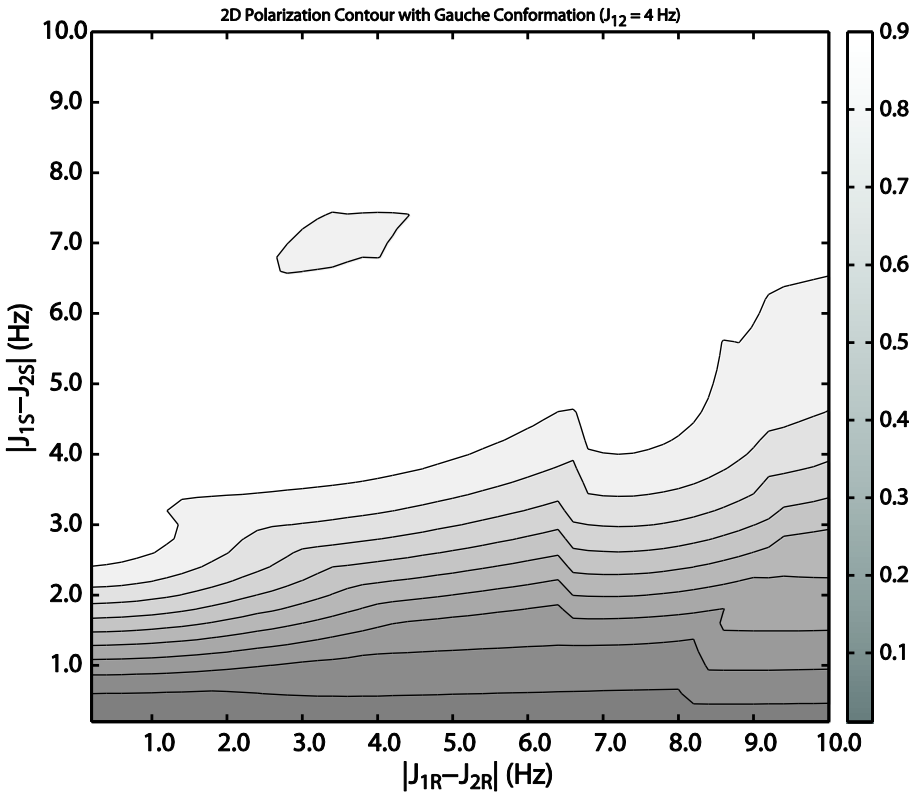

Figure 3.5. 2D contour of maximum polarization level from four spin system (I_1I_2SR) pulse sequence as a function of both J_{1S}-J_{2S} and J_{1R}-J_{2R} for all three major configurations (eclipsed with J_{12}=11Hz, anti with J_{12}=13Hz, and gauche with J_{12}=4Hz) while the total duration of the pulse sequence limited within 500ms. Here J_{SR} is both fixed at 6.52Hz.

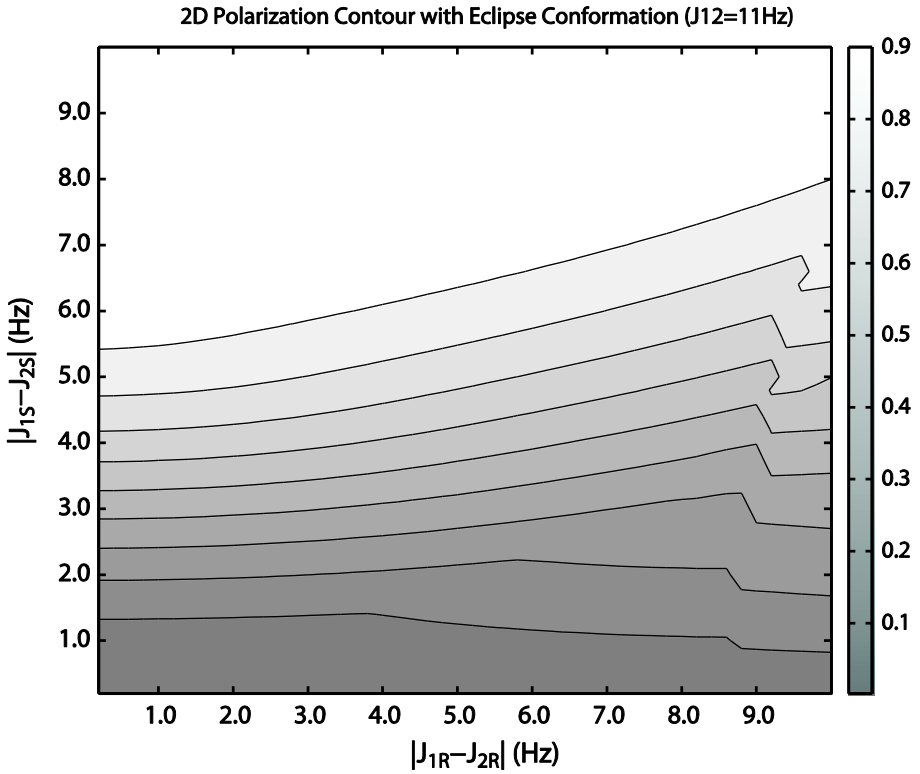

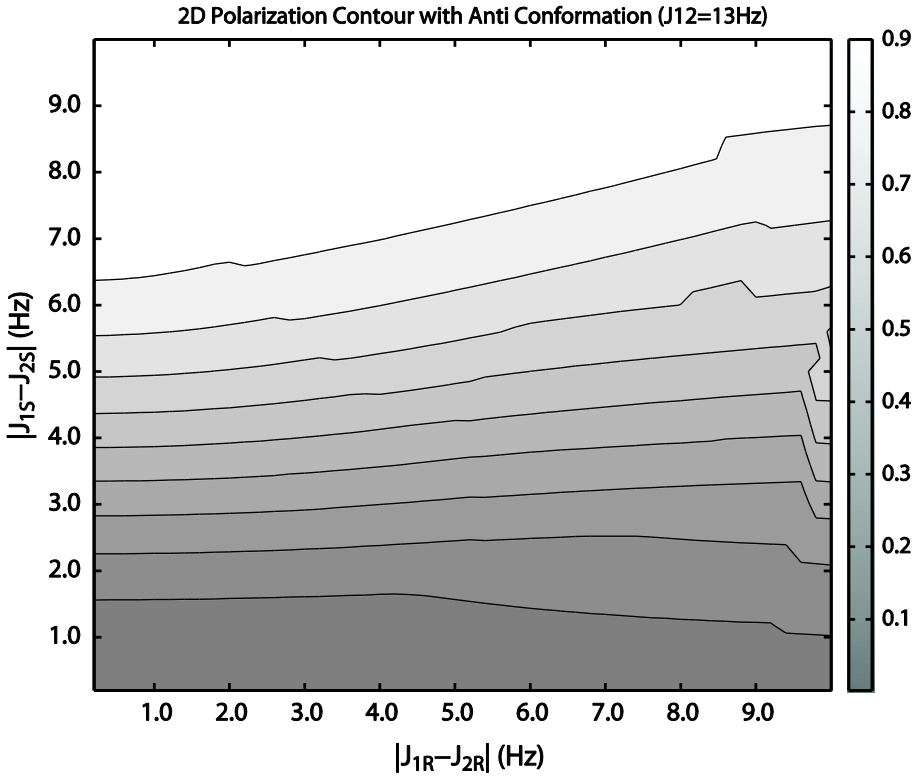

Figure 3.5, Continued

Similar as the three spin case, as the maximum time duration increases, the maximum polarization level increases too. As discussed in section 3.3, in the four I_1I_2SR systems, the more symmetric the spin system is, the longer lifetime singlet-states could be preserved. Figure 3.5 shows that the maximum polarization level is low when the symmetrical level of the spin system is high (both J_{1S} - J_{2S} and J_{1R} - J_{2R} approaches 0). In those spin systems it is possible that the singlet-states could be preserved longer and a longer sequence would be possible. So the maximum polarization level of the sequence with longer time duration is calculated, as shown in Figure 3.6, both J_{12} and J_{SR} are fixed at 5 Hz. Clearly the maximum polarization level increases as the total duration increases. If the sequence duration is fixed at 2 or 4 seconds, the sequence yields nearly unitary polarization level for a wide range of molecules, including those highly symmetric molecules.

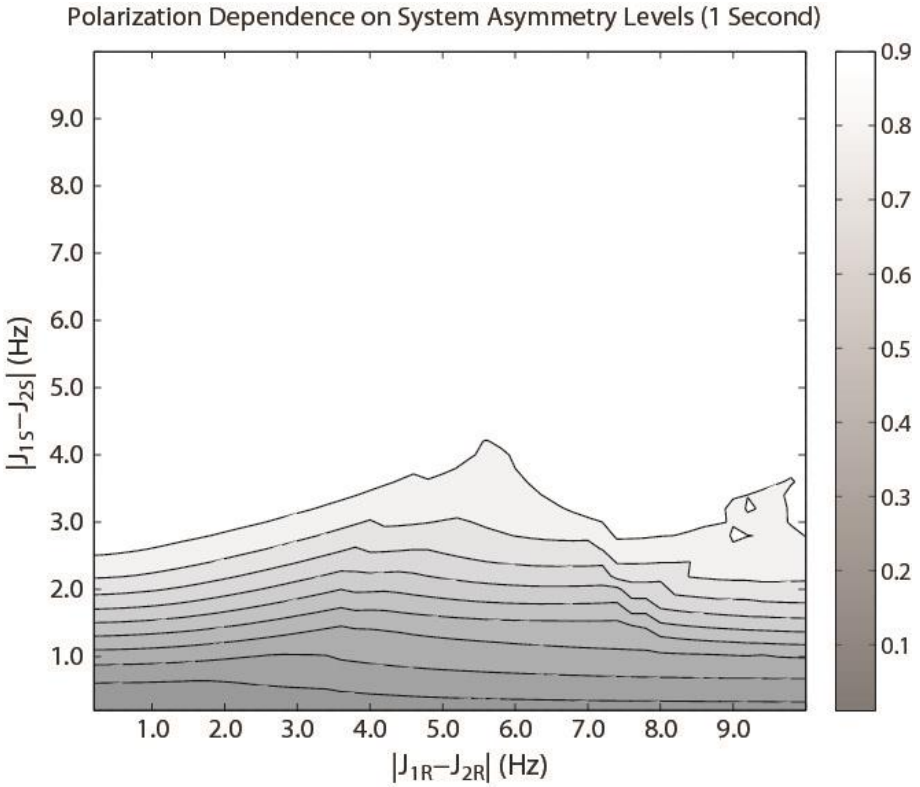

Figure 3.6. 2D contour of maximum polarization level from four spin system (I_1I_2SR) pulse sequence as a function of both J_{1S}-J_{2S} and J_{1R}-J_{2R} while the proton-proton scalar coupling is fixed to be 5 Hz and the total duration of the pulse sequence limited within 1 second (upper graph), 2 seconds (middle graph), and 4 seconds (lower graph). The maximum polarization level increases as the total duration increases. If the sequence duration is fixed at 2 or 4 seconds, the sequence would be expected to yield nearly unitary polarization level for a wide range of molecules, including those highly symmetric molecules.

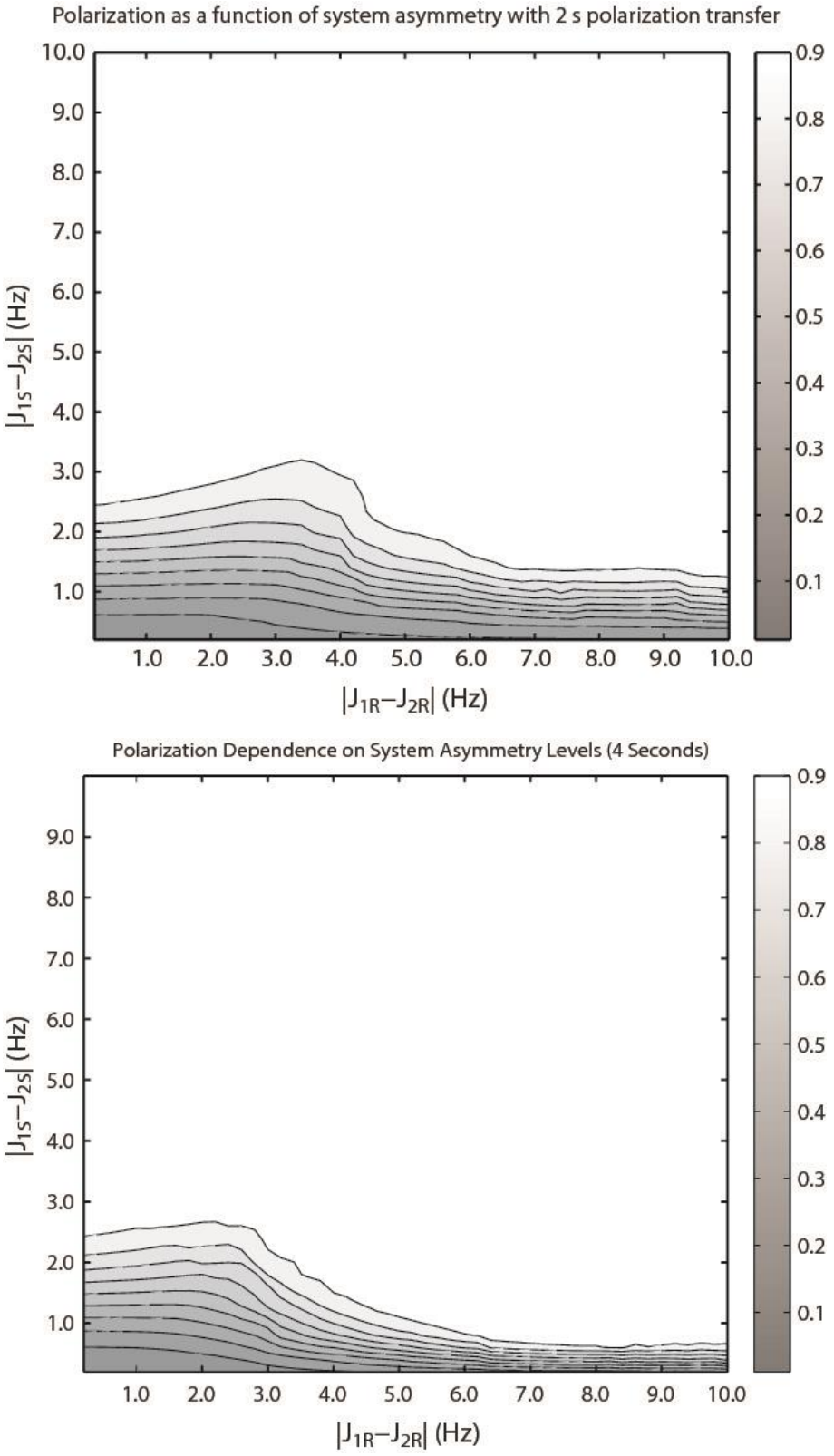

Figure 3.6, Continued

3.6. Further studies: a third channel

Although hyper-SHIELDED-4 sequence is expected to yield high polarization level for most I_1I_2SR spin systems, in cases where S and R have significantly different chemical shifts, a third channel would be necessary to eliminate the influence of chemical shift evolution completely. In hyper-SHIELDED-4 pulse sequence only pulses on proton and heteronucleus S channel are provided, if pulses on all three channels could be applied, the performance of the sequence will be improved. Those 3-channel devices are not quite common in MR labs nowadays yet, but the PANAROMIC sequence our group developed [131] would be able to address this type of problem to provide pulses on three channels using a two channel device (single channel as well). The modified sequence is shown in Figure 3.7. There are no refocusing pulses on the heteronucleus R channel since we are only using the longitudinal components of heteronucleus R.

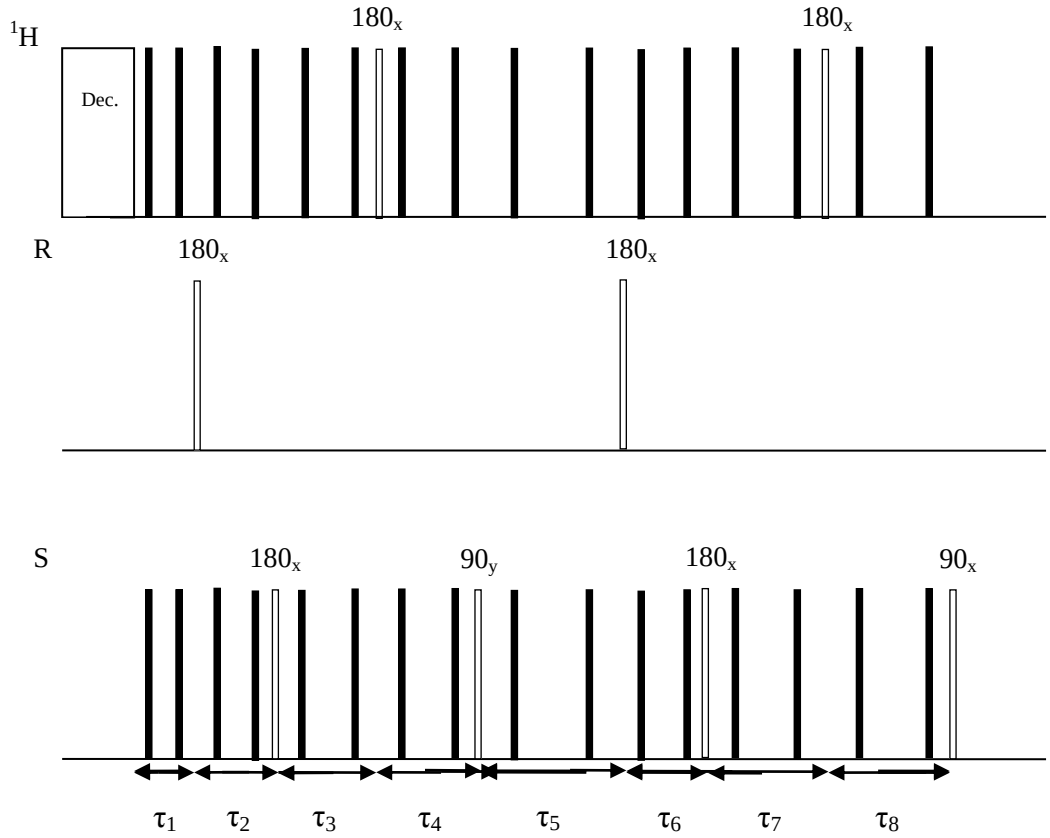

Figure 3.7. The 3-channel pulse sequence for 4 spin systems (I_1I_2SR). The sequence consists of 8 effective pulses (white pulses, 180_x on R, 180_x on S, 180_x on ^{1}H, 90_y on S, 180_x on R, 180_x on S, 180_x on ^{1}H, and 90_x on S). The black pulses are refocusing pulses applied at 1/4 and 3/4 of each time interval. There are no refocusing pulses on R channel since we are only using the longitudinal components of R and on transverse R component is generated.

There are eight time intervals in this sequence, which increases the level of freedom to manipulate the spin states. Below is the comparison of maximum polarization level of three channels versus two, Figure 3.8. The other J coupling constants are fixed at [J_{1S} = -3.8Hz, J_{1R} = 8.6Hz, J_{2S} = 4.07Hz, J_{2R} = 0Hz, J_{SR} = 6.52Hz] while varying J_{12}, [J_{12} = 6.9Hz, J_{1R} = 8.6Hz, J_{2S} = 4.07Hz,J_{2R} = 0Hz, J_{SR} = 6.52Hz] while varying J_{1S}, [J_{12} = 6.9Hz, J_{1S} = -3.8Hz, J_{2S} = 4.07Hz,J_{2R} = 0Hz, J_{SR} = 6.52Hz] while varying J_{1R}.

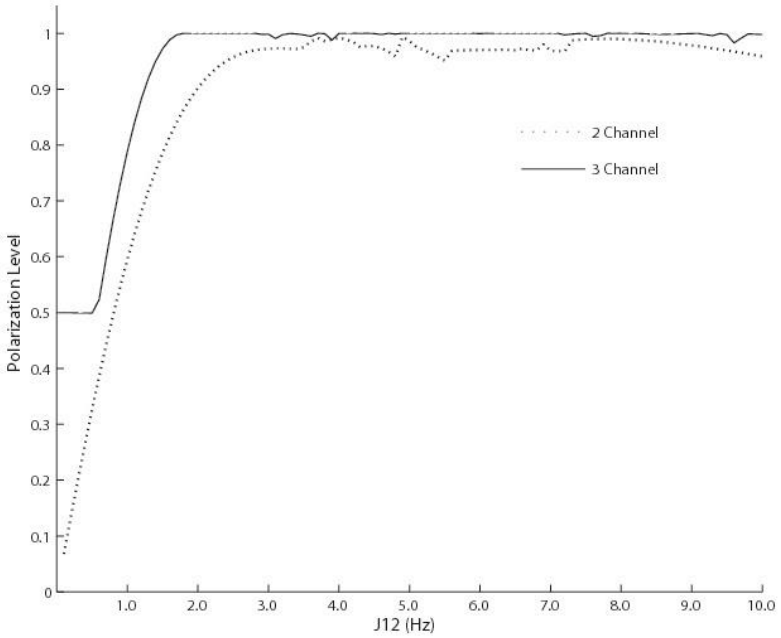

Figure3.8. The maximum polarization level of 2 channel sequence (dotted line) and 3 channel sequence (solid line) as a function of proton-proton coupling J_{12} (upper graph), proton-S coupling J_{1S} (middle graph), and proton-R coupling J_{1R} (lower graph). While varying one of the coupling constants, the other J coupling constants are fixed at [J_{1S} = -3.8Hz, J_{1R} = 8.6Hz, J_{2S} = 4.07Hz, J_{2R} = 0Hz, J_{SR} = 6.52Hz] while varying J_{12}, [J_{12} = 6.9Hz, J_{1R} = 8.6Hz, J_{2S} = 4.07Hz, J_{2R} = 0Hz, J_{SR} = 6.52Hz] while varying J_{1S}, [J_{12} = 6.9Hz, J_{1S} = -3.8Hz, J_{2S} = 4.07Hz, J_{2R} = 0Hz, J_{SR} = 6.52Hz] while varying J_{1R}. The duration of both sequences are fixed to be within 500 ms. The dependence of polarization level on J_{2S} (J_{2R}) is similar as J_{1S} (J_{1R}), and is not sensitive to J_{SR}.

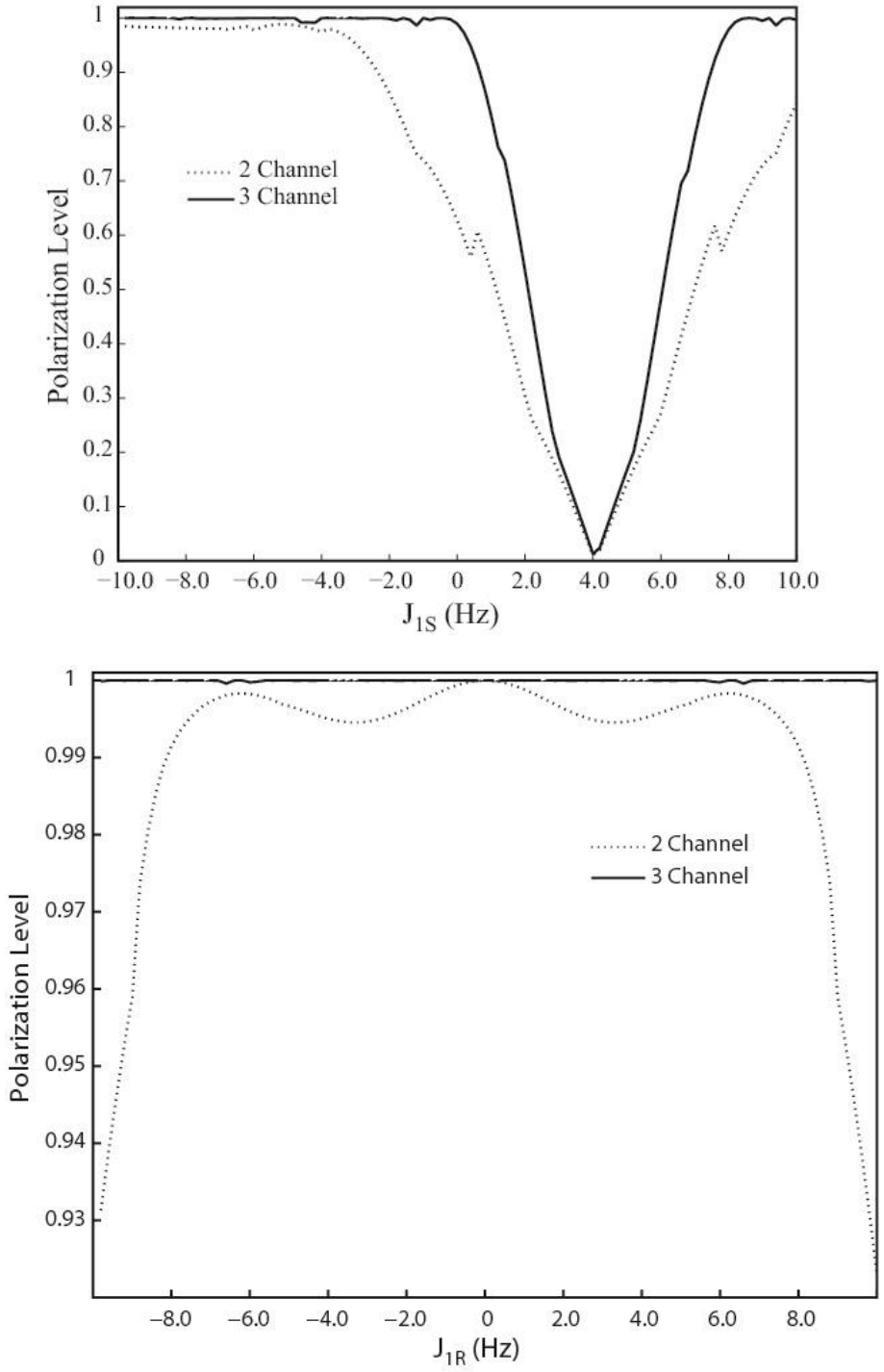

Figure 3.8, Continued

CHAPTER 4

RESOLVING SCALAR COUPLINGS IN LOW INHOMOGENEOUS FIELDS BY INDIRECT DETECTION OF SINGLET-STATE EVOLUTION

The efficiency of spin order transfer in hyper-SHIELDED-3 and hyper-SHIELDED-4 depends on accurate prior knowledge of accurate scalar coupling constants. Apart from spin order transfer sequences, precisely measured scalar coupling constants are also important in many NMR experiments. For example, APT (attached proton test) provides a simple and elegant method to distinguish the number of protons attached to a carbon atom by distinguishing the numbers of couplings of the carbon [132-134]. INEPT (Insensitive Nuclei Enhanced by Polarization Transfer) is an experiment that makes use of the high gyromagnetic ratio of protons to enhance signals of other heteronuclei by coherence transfer through coupling [135-141]. DEPT (Distortionless Enhancement by Polarization Transfer) is an NMR tool that distinguishes the CH_3, CH_2, CH and other groups of the observed molecules by making use of the different coupling of the groups [142-144]. It is also the basic character used in the experiments of HECTOR [145], COSY [146-153], and TOCSY [154-159].

Therefore, accurately measuring the scalar coupling constants is very important for hyperpolarization sequences and other experiments. There are several approaches to measure scalar coupling constants. However, although the spin order transfer experiments could be conducted at low fields, in most cases precisely measuring

scalar coupling constants requires a high magnetic field. Besides, precisely measuring scalar coupling constants will make high resolution NMR experiments possible at low inhomogeneous fields. Described in this chapter is a new method that measures scalar coupling constants of spin systems at low inhomogeneous fields by indirect detection of singlet-state evolution. The potential application of special cases for molecules that contain more than one set of scalar coupling constants are studied in 4.1, while the method developed to obtain high resolution coupling spectra is given in 4.2. The experiment results of sample HEP is stated in 4.3, while the resolution of the method is discussed in 4.4.

4.1. Introduction

Precisely measuring scalar coupling constants in low inhomogeneous fields potentially enables NMR experiments including hyper-SHIELDED parameters, but also plays a vital role in studying the behavior of many special and important molecules. Examples are molecules like 1-labelled succinic acid. Although the molecule is also a simple three spin system (I_1I_2S) after deuteration and labeling one of the carbons, the behavior of the molecule in NMR is not similar to other three spin systems since the molecule has two sets of conformations, hence two sets of J coupling constants. Moreover, the scalar coupling constants of the molecule depend on pH as well.

4.1.1. Conformations

Succinic acid normally exists in a superposition of three different conformations depending on pH [160-162]. Conformation I is called anti-periplanar conformation and II & III are called syn - clinal conformations. Different types of conformations lead to different chemical structures, in turn resulting in different sets of scalar coupling constants. For succinic acid molecules conformation II & III have the same scalar coupling constants, while conformation I has another set of scalar coupling constants.

4.1.2. pH dependence of scalar coupling constants

The scalar coupling constants of the molecule (also the chemical shift) appear to depend on environment pH, due to the fact that the molecule itself is an acid. While the environment pH increases, the molecule tends to lose protons on either side, or both sides when the pH is significantly higher. When the molecule gets ionized, the spin system changes since there is one less spin in the system and coupling constants get affected too.

Succinic acid is dibasic weak acid with $pk_{a1} = 4.2$, $pk_{a2} = 5.6$. When placed in solvent like water, the molecule will start to ionize:

$$\begin{aligned} C_4H_6O_4 &\leftrightarrow C_4H_5O_4^- + H^+ \\ C_4H_5O_4^- &\leftrightarrow C_4H_4O_4^{2-} + H^+ \end{aligned} \tag{4.1}$$

Since $pk_{a1} = 4.2$ and $pk_{a2} = 5.6$, we get:

$$\frac{a(H^+)\times a(C_4H_5O_4^-)}{a(C_4H_6O_4)} = 10^{-4.2} = 6.31\times10^{-5}$$
$$\frac{a(H^+)\times a(C_4H_4O_4^{2-})}{a(C_4H_5O_4^-)} = 10^{-5.6} = 2.51\times10^{-6} \quad (4.2)$$

Here *a* represents the concentration of corresponding molecule or ions.

From these equations follows that, at pH = 1, only 0.063% of the molecules are ionized, and most of them remain symmetric. At pH = 4.2, 50% of the molecules are ionized. At PH = 6, 98.5% of the molecules will be ionized, but 71.5% of them will be further ionized to $C_4H_4O_4^{2-}$, which is still symmetric. So at pH = 6.0 about 28.1% of the molecule exists in the form of $C_4H_5O_4^-$. And at pH = 7.0, only 3.8% of the molecules exists in the form of $C_4H_5O_4^-$ (Table 4.1 and Figure 4.1).

Table 4.1. Percentage of theasymetric ion $C_4H_5O_4^-$in all three types of ions ($C_4H_6O_4$, $C_4H_5O_4^-$, and $C_4H_4O_4^{2-}$) at different PH.

pH	1	4.2	6.0	7.0
$C_4H_5O_4^-$ (%)	0.063	50.0	28.1	3.8

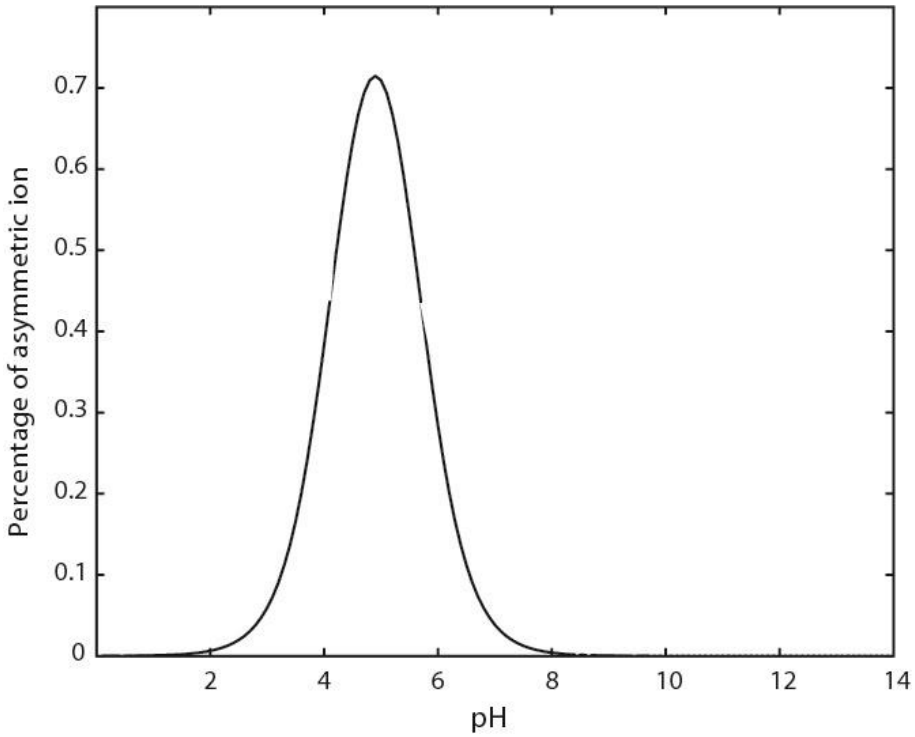

Fig 4.1. Percentage of the asymmetric ion $C_4H_5O_4^-$ in all three types of ions ($C_4H_6O_4$, $C_4H_5O_4^-$, and $C_4H_4O_4^{2-}$) as a function of pH.

It is also recently reported that the lifetime of the hyperpolarized ^{13}C states in succinic acid are strongly dependent on pH. This arises due to the different concentrations of neutral, anion, and dianion forms with different environment pH [163].

4.2. Method: high resolution scalar coupling spectra

4.2.1. Theoretical prediction of J-dependent polarization

Indirectly detecting scalar coupling constants from hyper-SHIELDED is feasible since the polarization level depends only on two parameters (proton-proton coupling J_{12}, and difference in proton-carbon-13 couplings $|J_{1S} - J_{2S}|$).

The polarization level dependence on each time interval has a period of (1/Ω). Therefore, if the experiment is conducted with one of the four time delays varying and the rest three fixed, the obtained data is supposed to be a periodic function with period $\frac{1}{\Omega}$. By Fourier transformation of the obtained data there will be a peak at Ω. The expression of Ω is:

$$\begin{aligned} \Omega &= J_{12}\sqrt{1+\Delta^2} \\ \Delta &= \frac{J_{1S} - J_{2S}}{2J_{12}} \end{aligned} \tag{4.3}$$

Apparently Ω depends on both scalar coupling constants (J_{12} and $|J_{1S} - J_{2S}|$). After Ω is found, we can adjust the other parameter θ to best fit the obtained data. θ is also a function of both parameters:

$$\begin{aligned} \sin\theta &= \frac{1}{\sqrt{1+\Delta^2}} \\ \cos\theta &= \frac{\Delta}{\sqrt{1+\Delta^2}} \end{aligned} \tag{4.4}$$

After both Ω and θ are obtained, both J coupling constants (J_{12} and $|J_{1S} - J_{2S}|$) could be calculated from the equations. The final polarization level of a given molecule with the four time intervals from hyper-SHIELDED could be calculated as:

$$\begin{aligned} Pol = {} & [\sin\theta\sin2\theta\sin(2\pi\Omega t_2) + \cos\theta\cos2\theta\cos(2\pi\Omega t_1)\sin(2\pi\Omega t_2) \\ & -\cos\theta\sin(2\pi\Omega t_1)\cos(2\pi\Omega t_2)] \\ & \times[\frac{1}{4}\sin4\theta + \frac{1}{4}\sin4\theta\cos(2\pi\Omega t_3)\cos(2\pi\Omega t_4) \\ & +\sin2\theta(\sin^2\theta\cos(2\pi\Omega t_3) - \cos^2\theta\cos(2\pi\Omega t_4)) \\ & +\cos\theta\sin\theta\sin(2\pi\Omega t_3)\sin(2\pi\Omega t_4)] \\ & -\frac{1}{2}\sin2\theta[(\cos2\theta + 2\sin^2\theta\cos(2\pi\Omega t_2) - 2\cos^2\theta\cos(2\pi\Omega t_1) \\ & +\cos2\theta\cos(2\pi\Omega t_1)\cos(2\pi\Omega t_2) + \sin(2\pi\Omega t_1)\sin(2\pi\Omega t_2)] \\ & \times[\cos\theta\cos(2\pi\Omega t_3)\sin(2\pi\Omega t_4) - \sin\theta\sin2\theta\sin(2\pi\Omega t_3) \\ & -\cos\theta\cos2\theta\sin(2\pi\Omega t_3)\cos(2\pi\Omega t_4)] \end{aligned} \tag{4.5}$$

Equation 4.7 shows how theoretical polarization varies with evolution delays in the hyper-SHIELDED sequence. Once the multidimensional experiment data is obtained, by fitting into this equation, both coupling constants (J_{12} and $|J_{1S} - J_{2S}|$) can be extracted. Since the evolution is independent of field homogeneities, the values of J can be determined with a resolution much higher than the native field homogeneity. This enables a version of high resolution NMR with even crude, inexpensive magnets.

4.2.2. Experimental section

The experiment for extracting J coupling constants of HEP uses a multidimensional implementation of hyper-SHIELDED to generate a curve of polarization level, which was then fit to theory to extract couplings.

The experiment steps of synthesis of parahydrogen gas, PASADENA precursor preparation, and catalytic hydrogenation are exactly the same as section 2.4. The difference is the pulse sequence applied.

The pulse sequence used to transfer polarization level was a sparsely sampled, multidimensional implementation of the hyper-SHIELDED pulse sequence where all four time intervals were varied (Figure 4.3). Briefly, the pulse sequence consisted of four major pulses. First, after the initial density matrix evolves during interval t_1, a 180_x pulse on proton is applied, and then let the density matrix evolve for another interval t_2. A 90_y pulse on the heteronucleus S spin then converted the ^{13}C signal of the test molecule to transverse plane. The state then evolves for time interval t_3, with a proton 180_x pulse applied afterwards, and the state then evolves for the last interval t_4. Finally,

a 90_x pulse converts the ^{13}C signal back to longitudinal magnetization on the heteronucleus for storage until subsequent detection. The pulse sequence diagram and schematic of spin evolution is illustrated in Figure 4.2. By carefully choosing the four time intervals the polarization level could reach unitary. Here, in order to effectively extract J coupling constants, we repeat the experiment n times with different time interval sets $(t_1, t_2, t_3, t_4)^k$ to obtain a series of polarization level data.

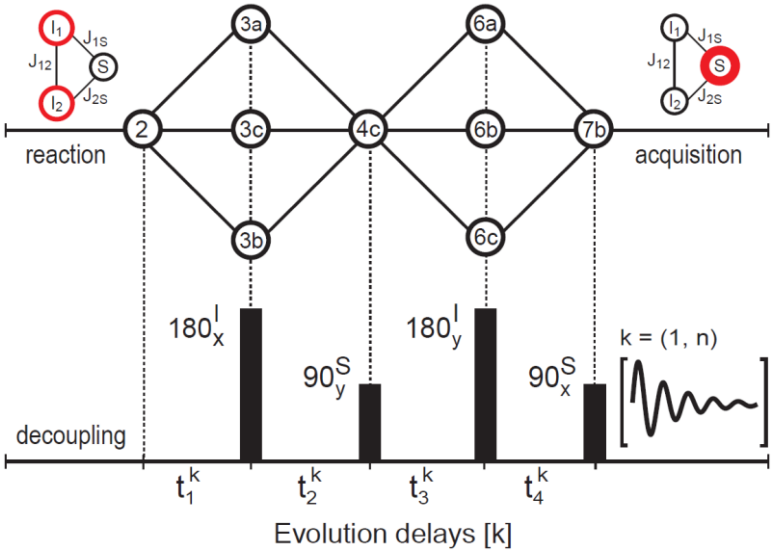

Figure 4.2. Schematic for the multidimensional NMR experiment used to measure scalar coupling constants, with evolution of density matrix components (upper graph) and the associated pulse sequence (lower graph) for focusing parahydrogen singlet-states ($I_1 \cdot I_2$) into magnetization on an adjacent coupled (S) nucleus for strongly coupled I_1I_2S spin systems. Symbols ($3_{a\text{-}c}$, $4_{a\text{-}c}$) correspond to components of the density operator (Appendix A). A multidimensional set of free induction decay (FID) is acquired with a set of evolution delays in hyper-SHIELDED sequence. The transfer of polarization from singlet-state to ^{13}C depends on both J_{12} (proton-proton coupling) and ΔJ (difference in proton-carbon-13 couplings, $|J_{1S} - J_{2S}|$).

The pulse sequences for transferring polarization were applied immediately after continuous wave decoupling was turned off (Figure 4.2) with a set of different time intervals. The polarization level depends on both time intervals and scalar coupling

constants. After each experiment, a single free induction decay was acquired with 512 points at a receiver bandwidth of 5 kHz, for a digital resolution of ~10 Hz per point. The process was repeated for 48 times with 48 different sets of intervals.

4.3. Experiment Results

With various time intervals from hyper-SHIELDED, a series of polarization levels was obtained, from which both scalar coupling constants can be detected (J_{12} and $|J_{1S} - J_{2S}|$) of the sample HEP.

Described here is a new method that indirectly detects scalar coupling constants of spin systems by the use of hyper-SHIELDED pulse sequence. Hyper-SHILEDED transforms parahydrogen spin order in the strong coupling regime of protons into net heteronuclear magnetization in three spin-systems (I_1I_2S). The I_1I_2S moiety is a widespread and important spin system in PHIP experiments formed for example, by molecular addition of parahydrogen to perdeuterated and unsaturated molecular backbones. The sequence flanks two asymmetric proton refocusing intervals about a heteronuclear excitation pulse to generate four unique intervals (t_1,t_2,t_3,t_4). Optimization of these delays to spin couplings in the molecule of interest sequentially converts the initial parahydrogen singlet-state into pure heteronuclear magnetization.

Therefore, the efficiency of hyper-SHIELDED depends on both scalar coupling constants of the spin system, and the set of intervals (t_1, t_2, t_3, t_4) (Equation 4.5). The method is to apply multidimensional experiments by the use of hyper - SHIELDED

with different sets of intervals, and acquire free induction decays (FID) for each set. Polarization level is calculated from each FID, and fitted to theory (Equation 4.5).

To validate the method, a set of experimental heteronuclear polarization level was compared to theory to extract scalar coupling constants (Figure 4.3). ^{13}C magnetization was yielded in a 7 micromole sample of the PHIP reaction product, 2 - hydroxyethyl 1-^{13}C-propionate-d_3. The fitting of experimental data to theory yields J coupling constants as J_{12} = 7.45 Hz and ΔJ = 11.30 Hz for the sample.

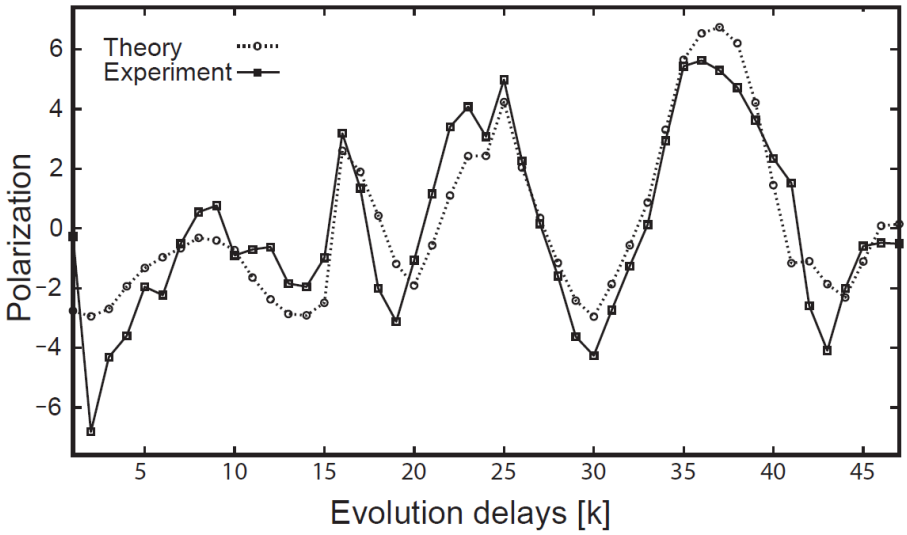

Figure 4.3. Fitting of experimental (solid squares) polarization data (48 sets) to theory (dash circles) using the hyper-SHIELDED sequence. Here we chose average polarization level as 0, and all results are shown with deviation from it. The fitting yielded J coupling constants for our sample as J_{12}=7.45 Hz and $|J_{1S}-J_{2S}|$=11.30 Hz.

4.4. Discussion

The method described here is to obtain sets of experimental polarization level data with different sets of time intervals from hyper-SHIELDED sequence, and fit to theory to extract scalar coupling constants. The resolution of the method depends on the precision of experiments. To characterize the resolution of our method to measure

scalar coupling constants, a Monte Carlo model was applied to determine the confidence interval of the obtained scalar coupling constants. The method makes use of a multidimensional implementation of the hyper-SHIELDED polarization transfer sequence and fits the resulting experimental polarization levels to theory in order to extract scalar coupling constants of the sample. The resolution of the method depends on the experimental error. Due to the differences in samples, devices, solvent, and experiment environment, the experimental results could randomly differ from the actual value. Here the Monte Carlo model is constructed to conduct 10^4 groups of fictitious experiments and measure corresponding scalar coupling constants with random experiment errors. In each group, there are 48 experiments. The experiment polarization level of each experiment though, is set at $\pm 5\%$ standard deviation error from theoretical values. Therefore, by fitting all 10^4 groups of randomly scattered data, the results are shown in Figure 4.4.

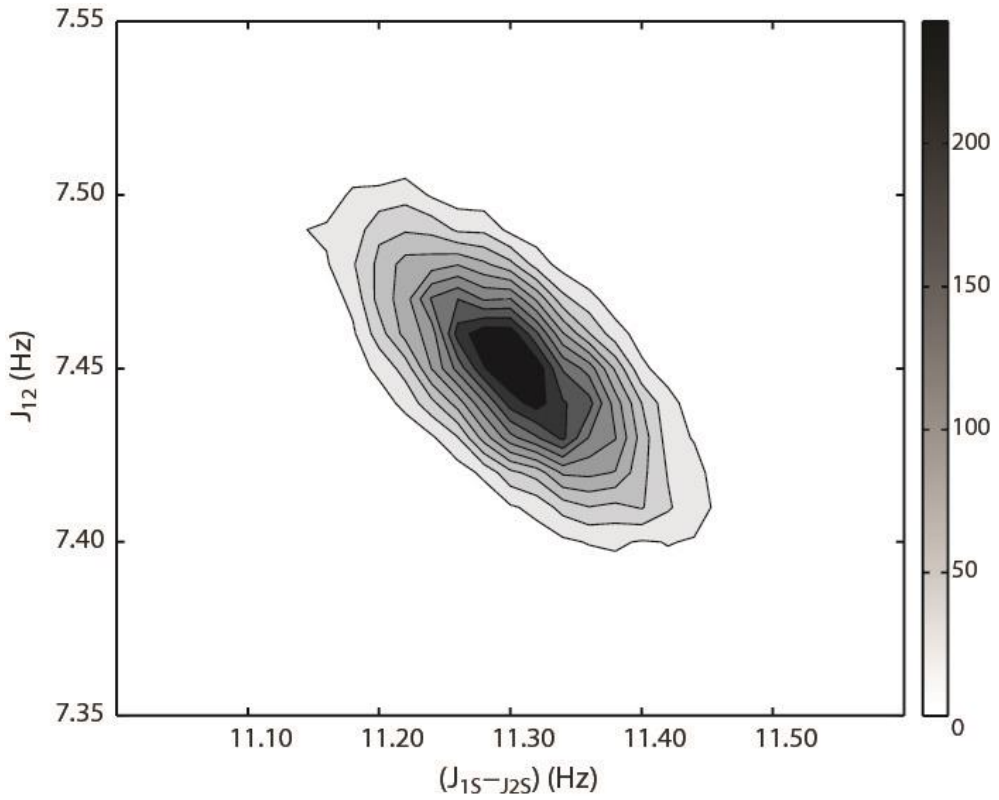

Figure 4.4. 2D contour of frequency as a function of both J_{12} and $|J_{1S}-J_{2S}|$. The Monte Carlo model for extracting J coupling constants of sample HEP shows dependence of frequency on both J coupling constants (J_{12} and $|J_{1S} - J_{2S}|$). The model conducts 10^4 fictitious experiments and extracts both coupling constants with random experiment error at standard experimental deviation of 5%. The calculated values and resolution of both J coupling constants are J_{12}=7.45 $\pm$ 0.05Hz and ($J_{1S} - J_{2S}$) =11.30 $\pm$ 0.12 Hz within 95% confidence interval.

As illustrated in Figure 4.4, it could be calculated that within 95% confidence interval, the value of J_{12} is 7.45 $\pm$ 0.05 Hz, while $|J_{1S} - J_{2S}|$ is 11.30 $\pm$ 0.12 Hz. This is the confidence interval for experiments within 5% standard deviation from theoretical values, and the resolution is within 0.1 Hz for both coupling constants (the resolution of $|J_{1S} - J_{2S}|$ results from both J_{1S} and J_{2S}).

The resolution decreases as the experiment standard error increases. If the experiment error increases to 10% or 15%, the corresponding error range increases as well. The calculated corresponding resolution of scalar coupling constants to

experiments with standard deviation 10% and 15% are J_{12}=7.45 ± 0.09Hz and (J_{1S} - J_{2S}) = 11.30 ± 0.26Hz (10% standard deviation), and J_{12}=7.45 ± 0.13Hz and (J_{1S} - J_{2S}) =11.30 ± 0.37Hz (15% standard deviation). The comparison graph for 5%, 10% and 15% standard deviation are provided in Figure 4.5.

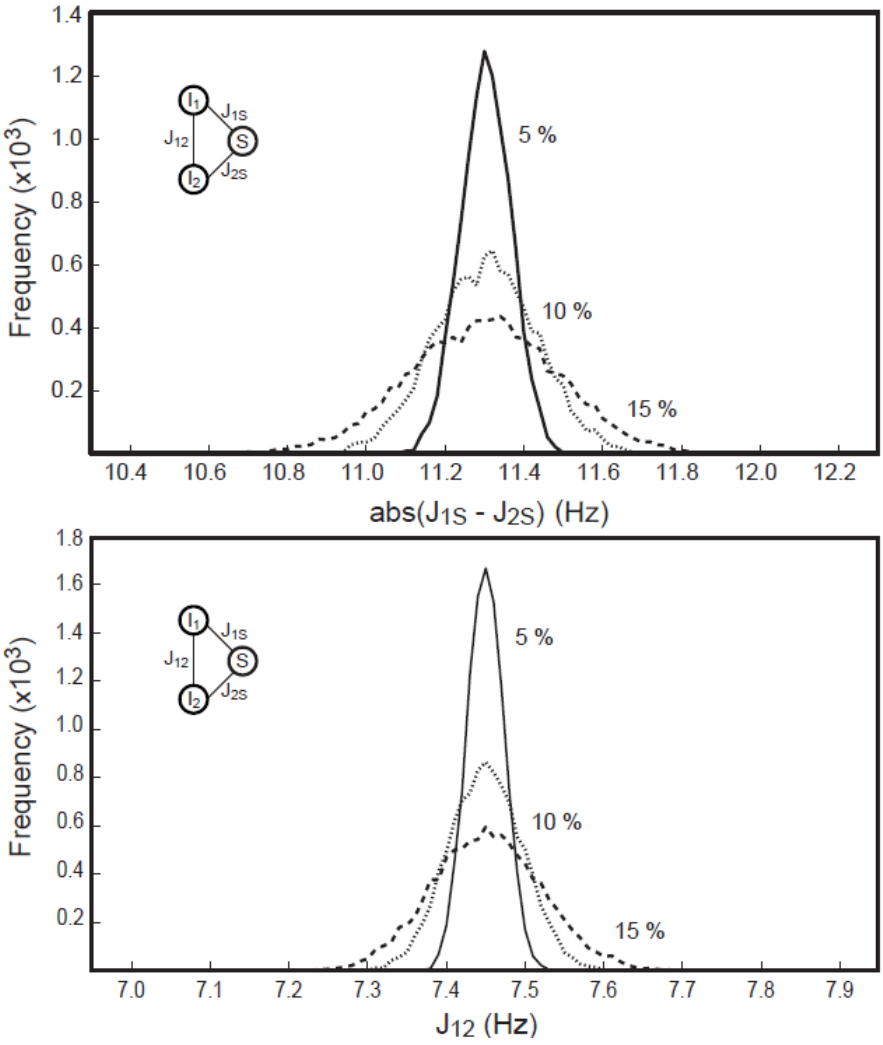

Figure 4.5. Monte Carlo model showing dependence of frequency on proton-proton coupling J_{12} (upper graph) and difference in proton-carbon-13 coupling $|J_{1S}-J_{2S}|$ (lower graph), with experiment standard deviation 5% (solid), 10% (dot), and 15% (dash). The model conducts 10^4 trial experiments and extracts both coupling constants with random experiment error. The calculated coupling constants are J_{12}=7.45 ± 0.05 Hz (5% standard deviation), 7.45 ± 0.09 Hz (10% standard deviation), and 7.45 ± 0.13 Hz (15% standard deviation); while $|J_{1S} - J_{2S}|$=11.30 ± 0.12 Hz (5% standard deviation), 11.30 ± 0.26 Hz (10% standard deviation), and 11.30 ± 0.37 Hz (15% standard deviation).

APPENDIX A

PRODUCT OPERATORS FOR AA'X SPIN SYSTEMS

Section 2.2 shows some examples of the product operators for I_1I_2S spin systems. To study the correct expression of evolution of each state and calculate the optimum method of polarization level transfer, the form of the entire product operator and most rotation operators are necessary.

A.1. Matrix Representation of Major Product Operators

The basic preparation before studying the I_1I_2S spin system is the complete form of all the major product operators. The list of major product operators is given in this section, including the x, y, and z components of two protons in parahydrogen singlet-state and a heteronucleus (^{13}C, for example). In all product operators the 8 spin states are ordered as |ααα>, |ααβ>, |αβα>, |βαα>, |αββ>, |βαβ>, |ββα>, |βββ>.

A.1.1. Product operators for protons

The two protons from parahydrogen are labeled as $\mathbf{I_1}$ and $\mathbf{I_2}$. Below is a list of product operators for both protons.

$$\mathbf{I}_{1x} = \frac{1}{2}\begin{pmatrix} 0 & 0 & 0 & 1 & 0 & 0 & 0 & 0 \\ 0 & 0 & 0 & 0 & 0 & 1 & 0 & 0 \\ 0 & 0 & 0 & 0 & 0 & 0 & 1 & 0 \\ 1 & 0 & 0 & 0 & 0 & 0 & 0 & 0 \\ 0 & 0 & 0 & 0 & 0 & 0 & 0 & 1 \\ 0 & 1 & 0 & 0 & 0 & 0 & 0 & 0 \\ 0 & 0 & 1 & 0 & 0 & 0 & 0 & 0 \\ 0 & 0 & 0 & 0 & 1 & 0 & 0 & 0 \end{pmatrix} \quad \text{(A.1)}$$

$$\mathbf{I}_{1y} = \frac{i}{2}\begin{pmatrix} 0 & 0 & 0 & -1 & 0 & 0 & 0 & 0 \\ 0 & 0 & 0 & 0 & 0 & -1 & 0 & 0 \\ 0 & 0 & 0 & 0 & 0 & 0 & -1 & 0 \\ 1 & 0 & 0 & 0 & 0 & 0 & 0 & 0 \\ 0 & 0 & 0 & 0 & 0 & 0 & 0 & -1 \\ 0 & 1 & 0 & 0 & 0 & 0 & 0 & 0 \\ 0 & 0 & 1 & 0 & 0 & 0 & 0 & 0 \\ 0 & 0 & 0 & 0 & 1 & 0 & 0 & 0 \end{pmatrix} \quad \text{(A.2)}$$

$$\mathbf{I}_{1z} = \frac{1}{2}\begin{pmatrix} 1 & 0 & 0 & 0 & 0 & 0 & 0 & 0 \\ 0 & 1 & 0 & 0 & 0 & 0 & 0 & 0 \\ 0 & 0 & 1 & 0 & 0 & 0 & 0 & 0 \\ 0 & 0 & 0 & -1 & 0 & 0 & 0 & 0 \\ 0 & 0 & 0 & 0 & 1 & 0 & 0 & 0 \\ 0 & 0 & 0 & 0 & 0 & -1 & 0 & 0 \\ 0 & 0 & 0 & 0 & 0 & 0 & -1 & 0 \\ 0 & 0 & 0 & 0 & 0 & 0 & 0 & -1 \end{pmatrix} \quad \text{(A.3)}$$

$$\mathbf{I}_{2x} = \frac{1}{2}\begin{pmatrix} 0 & 0 & 1 & 0 & 0 & 0 & 0 & 0 \\ 0 & 0 & 0 & 0 & 1 & 0 & 0 & 0 \\ 1 & 0 & 0 & 0 & 0 & 0 & 0 & 0 \\ 0 & 0 & 0 & 0 & 0 & 0 & 1 & 0 \\ 0 & 1 & 0 & 0 & 0 & 0 & 0 & 0 \\ 0 & 0 & 0 & 0 & 0 & 0 & 0 & 1 \\ 0 & 0 & 0 & 1 & 0 & 0 & 0 & 0 \\ 0 & 0 & 0 & 0 & 0 & 1 & 0 & 0 \end{pmatrix} \quad \text{(A.4)}$$

$$\mathbf{I}_{2y} = \frac{i}{2}\begin{pmatrix} 0 & 0 & -1 & 0 & 0 & 0 & 0 & 0 \\ 0 & 0 & 0 & 0 & -1 & 0 & 0 & 0 \\ 1 & 0 & 0 & 0 & 0 & 0 & 0 & 0 \\ 0 & 0 & 0 & 0 & 0 & 0 & -1 & 0 \\ 0 & 1 & 0 & 0 & 0 & 0 & 0 & 0 \\ 0 & 0 & 0 & 0 & 0 & 0 & 0 & -1 \\ 0 & 0 & 0 & 1 & 0 & 0 & 0 & 0 \\ 0 & 0 & 0 & 0 & 0 & 1 & 0 & 0 \end{pmatrix} \quad \text{(A.5)}$$

$$\mathbf{I}_{2z} = \frac{1}{2}\begin{pmatrix} 1 & 0 & 0 & 0 & 0 & 0 & 0 & 0 \\ 0 & 1 & 0 & 0 & 0 & 0 & 0 & 0 \\ 0 & 0 & -1 & 0 & 0 & 0 & 0 & 0 \\ 0 & 0 & 0 & 1 & 0 & 0 & 0 & 0 \\ 0 & 0 & 0 & 0 & -1 & 0 & 0 & 0 \\ 0 & 0 & 0 & 0 & 0 & 1 & 0 & 0 \\ 0 & 0 & 0 & 0 & 0 & 0 & -1 & 0 \\ 0 & 0 & 0 & 0 & 0 & 0 & 0 & -1 \end{pmatrix} \quad \text{(A.6)}$$

A.1.2. Product operators for heteronuclei

The basic product operators for the heteronucleus (labeled as S) are:

$$\mathbf{S}_x = \frac{1}{2}\begin{pmatrix} 0 & 1 & 0 & 0 & 0 & 0 & 0 & 0 \\ 1 & 0 & 0 & 0 & 0 & 0 & 0 & 0 \\ 0 & 0 & 0 & 0 & 1 & 0 & 0 & 0 \\ 0 & 0 & 0 & 0 & 0 & 1 & 0 & 0 \\ 0 & 0 & 1 & 0 & 0 & 0 & 0 & 0 \\ 0 & 0 & 0 & 1 & 0 & 0 & 0 & 0 \\ 0 & 0 & 0 & 0 & 0 & 0 & 0 & 1 \\ 0 & 0 & 0 & 0 & 0 & 0 & 1 & 0 \end{pmatrix} \quad \text{(A.7)}$$

$$\mathbf{S}_y = \frac{i}{2}\begin{pmatrix} 0 & -1 & 0 & 0 & 0 & 0 & 0 & 0 \\ 1 & 0 & 0 & 0 & 0 & 0 & 0 & 0 \\ 0 & 0 & 0 & 0 & -1 & 0 & 0 & 0 \\ 0 & 0 & 0 & 0 & 0 & -1 & 0 & 0 \\ 0 & 0 & 1 & 0 & 0 & 0 & 0 & 0 \\ 0 & 0 & 0 & 1 & 0 & 0 & 0 & 0 \\ 0 & 0 & 0 & 0 & 0 & 0 & 0 & -1 \\ 0 & 0 & 0 & 0 & 0 & 0 & 1 & 0 \end{pmatrix} \quad \text{(A.8)}$$

$$\mathbf{S}_z = \frac{1}{2}\begin{pmatrix} 1 & 0 & 0 & 0 & 0 & 0 & 0 & 0 \\ 0 & -1 & 0 & 0 & 0 & 0 & 0 & 0 \\ 0 & 0 & 1 & 0 & 0 & 0 & 0 & 0 \\ 0 & 0 & 0 & 1 & 0 & 0 & 0 & 0 \\ 0 & 0 & 0 & 0 & -1 & 0 & 0 & 0 \\ 0 & 0 & 0 & 0 & 0 & -1 & 0 & 0 \\ 0 & 0 & 0 & 0 & 0 & 0 & 1 & 0 \\ 0 & 0 & 0 & 0 & 0 & 0 & 0 & -1 \end{pmatrix} \quad \text{(A.9)}$$

A.2. Rotations

As described in section 3.1, all rotating pulses could be represented by a rotation matrix in the product operator basis. In this section the commonly used pulses (90 º and 180 º) for all AA'X spins are presented.

A.2.1. 90 degree rotations for protons

Propagators listed below are the operators that rotate the protons ($\mathbf{I_1}$ and $\mathbf{I_2}$) by 90 ºaround either x or y axis.

$$\mathbf{R}_{x}^{I_1}\left(\frac{\pi}{2}\right) = \frac{1}{\sqrt{2}}\begin{pmatrix} 1 & 0 & 0 & i & 0 & 0 & 0 & 0 \\ 0 & 1 & 0 & 0 & 0 & i & 0 & 0 \\ 0 & 0 & 1 & 0 & 0 & 0 & i & 0 \\ i & 0 & 0 & 1 & 0 & 0 & 0 & 0 \\ 0 & 0 & 0 & 0 & 1 & 0 & 0 & i \\ 0 & i & 0 & 0 & 0 & 1 & 0 & 0 \\ 0 & 0 & i & 0 & 0 & 0 & 1 & 0 \\ 0 & 0 & 0 & 0 & i & 0 & 0 & 1 \end{pmatrix} \tag{A.10}$$

$$\mathbf{R}_{x}^{I_2}\left(\frac{\pi}{2}\right) = \frac{1}{\sqrt{2}}\begin{pmatrix} 1 & 0 & i & 0 & 0 & 0 & 0 & 0 \\ 0 & 1 & 0 & 0 & i & 0 & 0 & 0 \\ i & 0 & 1 & 0 & 0 & 0 & 0 & 0 \\ 0 & 0 & 0 & 1 & 0 & 0 & i & 0 \\ 0 & i & 0 & 0 & 1 & 0 & 0 & 0 \\ 0 & 0 & 0 & 0 & 0 & 1 & 0 & i \\ 0 & 0 & 0 & i & 0 & 0 & 1 & 0 \\ 0 & 0 & 0 & 0 & 0 & i & 0 & 1 \end{pmatrix} \tag{A.11}$$

$$\mathbf{R}_{x}^{I}\left(\frac{\pi}{2}\right) = \frac{1}{2}\begin{pmatrix} 1 & 0 & 1 & i & 0 & 0 & -1 & 0 \\ 0 & 1 & 0 & 0 & i & i & 0 & -1 \\ i & 0 & 1 & -1 & 0 & 0 & i & 0 \\ i & 0 & -1 & 1 & 0 & 0 & i & 0 \\ 0 & i & 0 & 0 & 1 & -1 & 0 & i \\ 0 & i & 0 & 0 & -1 & 1 & 0 & i \\ -1 & 0 & i & -1 & 0 & 0 & i & 0 \\ 0 & -1 & 0 & 0 & i & i & 0 & 1 \end{pmatrix} \tag{A.12}$$

$$\mathbf{R}_{y}^{I_1}\left(\frac{\pi}{2}\right) = \frac{1}{\sqrt{2}}\begin{pmatrix} 1 & 0 & 0 & 1 & 0 & 0 & 0 & 0 \\ 0 & 1 & 0 & 0 & 0 & 1 & 0 & 0 \\ 0 & 0 & 1 & 0 & 0 & 0 & 1 & 0 \\ -1 & 0 & 0 & 1 & 0 & 0 & 0 & 0 \\ 0 & 0 & 0 & 0 & 1 & 0 & 0 & 1 \\ 0 & -1 & 0 & 0 & 0 & 1 & 0 & 0 \\ 0 & 0 & -1 & 0 & 0 & 0 & 1 & 0 \\ 0 & 0 & 0 & 0 & -1 & 0 & 0 & 1 \end{pmatrix} \tag{A.13}$$

$$\mathbf{R}_{y}^{I_2}(\frac{\pi}{2}) = \frac{1}{\sqrt{2}}\begin{pmatrix} 1 & 0 & 1 & 0 & 0 & 0 & 0 & 0 \\ 0 & 1 & 0 & 0 & 1 & 0 & 0 & 0 \\ -1 & 0 & 1 & 0 & 0 & 0 & 0 & 0 \\ 0 & 0 & 0 & 1 & 0 & 0 & 1 & 0 \\ 0 & -1 & 0 & 0 & 1 & 0 & 0 & 0 \\ 0 & 0 & 0 & 0 & 0 & 1 & 0 & 1 \\ 0 & 0 & 0 & -1 & 0 & 0 & 1 & 0 \\ 0 & 0 & 0 & 0 & 0 & -1 & 0 & 1 \end{pmatrix} \quad \text{(A.14)}$$

$$\mathbf{R}_{y}^{I}(\frac{\pi}{2}) = \frac{1}{2}\begin{pmatrix} 1 & 0 & 1 & 1 & 0 & 0 & 1 & 0 \\ 0 & 1 & 0 & 0 & 1 & 1 & 0 & 1 \\ -1 & 0 & 1 & -1 & 0 & 0 & 1 & 0 \\ -1 & 0 & -1 & 1 & 0 & 0 & 1 & 0 \\ 0 & -1 & 0 & 0 & 1 & -1 & 0 & 1 \\ 0 & -1 & 0 & 0 & -1 & 1 & 0 & 1 \\ 1 & 0 & -1 & -1 & 0 & 0 & 1 & 0 \\ 0 & 1 & 0 & 0 & -1 & -1 & 0 & 1 \end{pmatrix} \quad \text{(A.15)}$$

A.2.2. 180 degree rotations for protons

Propagators listed below are the operators that rotate the protons by 180 ºaround either x or y axis.

$$\mathbf{R}_{x}^{I_1}(\pi) = \begin{pmatrix} 0 & 0 & 0 & i & 0 & 0 & 0 & 0 \\ 0 & 0 & 0 & 0 & 0 & i & 0 & 0 \\ 0 & 0 & 0 & 0 & 0 & 0 & i & 0 \\ i & 0 & 0 & 0 & 0 & 0 & 0 & 0 \\ 0 & 0 & 0 & 0 & 0 & 0 & 0 & i \\ 0 & i & 0 & 0 & 0 & 0 & 0 & 0 \\ 0 & 0 & i & 0 & 0 & 0 & 0 & 0 \\ 0 & 0 & 0 & 0 & i & 0 & 0 & 0 \end{pmatrix} \quad \text{(A.16)}$$

$$\mathbf{R}_{x}^{I_2}(\pi) = \begin{pmatrix} 0 & 0 & i & 0 & 0 & 0 & 0 & 0 \\ 0 & 0 & 0 & 0 & i & 0 & 0 & 0 \\ i & 0 & 0 & 0 & 0 & 0 & 0 & 0 \\ 0 & 0 & 0 & 0 & 0 & 0 & i & 0 \\ 0 & i & 0 & 0 & 0 & 0 & 0 & 0 \\ 0 & 0 & 0 & 0 & 0 & 0 & 0 & i \\ 0 & 0 & 0 & i & 0 & 0 & 0 & 0 \\ 0 & 0 & 0 & 0 & 0 & i & 0 & 0 \end{pmatrix} \quad \text{(A.17)}$$

$$\mathbf{R}_{x}^{I}(\pi) = \begin{pmatrix} 0 & 0 & 0 & 0 & 0 & 0 & -1 & 0 \\ 0 & 0 & 0 & 0 & 0 & 0 & 0 & -1 \\ 0 & 0 & 0 & -1 & 0 & 0 & 0 & 0 \\ 0 & 0 & -1 & 0 & 0 & 0 & 0 & 0 \\ 0 & 0 & 0 & 0 & 0 & -1 & 0 & 0 \\ 0 & 0 & 0 & 0 & -1 & 0 & 0 & 0 \\ -1 & 0 & 0 & 0 & 0 & 0 & 0 & 0 \\ 0 & -1 & 0 & 0 & 0 & 0 & 0 & 0 \end{pmatrix} \quad \text{(A.18)}$$

$$\mathbf{R}_{y}^{I_1}(\pi) = \begin{pmatrix} 0 & 0 & 0 & 1 & 0 & 0 & 0 & 0 \\ 0 & 0 & 0 & 0 & 0 & 1 & 0 & 0 \\ 0 & 0 & 0 & 0 & 0 & 0 & 1 & 0 \\ -1 & 0 & 0 & 0 & 0 & 0 & 0 & 0 \\ 0 & 0 & 0 & 0 & 0 & 0 & 0 & 1 \\ 0 & -1 & 0 & 0 & 0 & 0 & 0 & 0 \\ 0 & 0 & -1 & 0 & 0 & 0 & 0 & 0 \\ 0 & 0 & 0 & 0 & -1 & 0 & 0 & 0 \end{pmatrix} \quad \text{(A.19)}$$

$$\mathbf{R}_{y}^{I_2}(\pi) = \begin{pmatrix} 0 & 0 & 1 & 0 & 0 & 0 & 0 & 0 \\ 0 & 0 & 0 & 0 & 1 & 0 & 0 & 0 \\ -1 & 0 & 0 & 0 & 0 & 0 & 0 & 0 \\ 0 & 0 & 0 & 0 & 0 & 0 & 1 & 0 \\ 0 & -1 & 0 & 0 & 0 & 0 & 0 & 0 \\ 0 & 0 & 0 & 0 & 0 & 0 & 0 & 1 \\ 0 & 0 & 0 & -1 & 0 & 0 & 0 & 0 \\ 0 & 0 & 0 & 0 & 0 & -1 & 0 & 0 \end{pmatrix} \quad \text{(A.20)}$$

$$\mathbf{R}_y^I(\pi) = \begin{pmatrix} 0 & 0 & 0 & 0 & 0 & 0 & 1 & 0 \\ 0 & 0 & 0 & 0 & 0 & 0 & 0 & 1 \\ 0 & 0 & 0 & -1 & 0 & 0 & 0 & 0 \\ 0 & 0 & -1 & 0 & 0 & 0 & 0 & 0 \\ 0 & 0 & 0 & 0 & 0 & -1 & 0 & 0 \\ 0 & 0 & 0 & 0 & -1 & 0 & 0 & 0 \\ 1 & 0 & 0 & 0 & 0 & 0 & 0 & 0 \\ 0 & 1 & 0 & 0 & 0 & 0 & 0 & 0 \end{pmatrix} \quad \text{(A.21)}$$

A.2.3. 90 degree rotations for a heteronucleus

Propagators listed below are the operators that rotate the heteronucleus S by 90 ^{o} around either x or y axis.

$$\mathbf{R}_x^s(\frac{\pi}{2}) = \frac{1}{\sqrt{2}} \begin{pmatrix} 1 & i & 0 & 0 & 0 & 0 & 0 & 0 \\ i & 1 & 0 & 0 & 0 & 0 & 0 & 0 \\ 0 & 0 & 1 & 0 & i & 0 & 0 & 0 \\ 0 & 0 & 0 & 1 & 0 & i & 0 & 0 \\ 0 & 0 & i & 0 & 1 & 0 & 0 & 0 \\ 0 & 0 & 0 & i & 0 & 1 & 0 & 0 \\ 0 & 0 & 0 & 0 & 0 & 0 & 1 & i \\ 0 & 0 & 0 & 0 & 0 & 0 & i & 1 \end{pmatrix} \quad \text{(A.22)}$$

$$\mathbf{R}_y^s(\frac{\pi}{2}) = \frac{1}{\sqrt{2}} \begin{pmatrix} 1 & 1 & 0 & 0 & 0 & 0 & 0 & 0 \\ -1 & 1 & 0 & 0 & 0 & 0 & 0 & 0 \\ 0 & 0 & 1 & 0 & 1 & 0 & 0 & 0 \\ 0 & 0 & 0 & 1 & 0 & 1 & 0 & 0 \\ 0 & 0 & -1 & 0 & 1 & 0 & 0 & 0 \\ 0 & 0 & 0 & -1 & 0 & 1 & 0 & 0 \\ 0 & 0 & 0 & 0 & 0 & 0 & 1 & 1 \\ 0 & 0 & 0 & 0 & 0 & 0 & -1 & 1 \end{pmatrix} \quad \text{(A.23)}$$

A.2.4. 180 degree rotations for heteronuclei

Propagators listed below are the operators that rotate the heteronucleus S by 180 º around either x or y axis.

$$\mathbf{R}_x^S(\pi) = \begin{pmatrix} 0 & i & 0 & 0 & 0 & 0 & 0 & 0 \\ i & 0 & 0 & 0 & 0 & 0 & 0 & 0 \\ 0 & 0 & 0 & 0 & i & 0 & 0 & 0 \\ 0 & 0 & 0 & 0 & 0 & i & 0 & 0 \\ 0 & 0 & i & 0 & 0 & 0 & 0 & 0 \\ 0 & 0 & 0 & i & 0 & 0 & 0 & 0 \\ 0 & 0 & 0 & 0 & 0 & 0 & 0 & i \\ 0 & 0 & 0 & 0 & 0 & 0 & i & 0 \end{pmatrix} \quad \text{(A.24)}$$

$$\mathbf{R}_y^S(\pi) = \begin{pmatrix} 0 & 1 & 0 & 0 & 0 & 0 & 0 & 0 \\ -1 & 0 & 0 & 0 & 0 & 0 & 0 & 0 \\ 0 & 0 & 0 & 0 & 1 & 0 & 0 & 0 \\ 0 & 0 & 0 & 0 & 0 & 1 & 0 & 0 \\ 0 & 0 & -1 & 0 & 0 & 0 & 0 & 0 \\ 0 & 0 & 0 & -1 & 0 & 0 & 0 & 0 \\ 0 & 0 & 0 & 0 & 0 & 0 & 0 & 1 \\ 0 & 0 & 0 & 0 & 0 & 0 & -1 & 0 \end{pmatrix} \quad \text{(A.25)}$$

A.3. Hamiltonian and Related State

A.3.1 Hamiltonian

The Hamiltonian of the three spin system, as stated in section 3.1, is:

$$\mathbf{H} = 2\pi \begin{pmatrix} \frac{1}{4}(J_{12} + J_{1S} + J_{2S}) & 0 & 0 & 0 \\ 0 & \frac{1}{4}(J_{12} - J_{1S} - J_{2S}) & 0 & 0 \\ 0 & 0 & \frac{1}{4}(-J_{12} + J_{1S} - J_{2S}) & \frac{1}{2}J_{12} \\ 0 & 0 & \frac{1}{2}J_{12} & \frac{1}{4}(-J_{12} - J_{1S} + J_{2S}) \\ 0 & 0 & 0 & 0 \\ 0 & 0 & 0 & 0 \\ 0 & 0 & 0 & 0 \\ 0 & 0 & 0 & 0 \end{pmatrix}$$

$$\begin{pmatrix} 0 & 0 & 0 & 0 \\ 0 & 0 & 0 & 0 \\ 0 & 0 & 0 & 0 \\ 0 & 0 & 0 & 0 \\ \frac{1}{4}(-J_{12} - J_{1S} + J_{2S}) & \frac{1}{2}J_{12} & 0 & 0 \\ \frac{1}{2}J_{12} & \frac{1}{4}(-J_{12} + J_{1S} - J_{2S}) & 0 & 0 \\ 0 & 0 & \frac{1}{4}(J_{12} - J_{1S} - J_{2S}) & 0 \\ 0 & 0 & 0 & \frac{1}{4}(J_{12} + J_{1S} + J_{2S}) \end{pmatrix}$$

(A.26)

The eigenvalues and eigenfunctions of the Hamiltonian, which is used to study the evolution of states, could be calculated. The eigenvalues of the J coupling Hamiltonian are:

$$\begin{aligned}
\lambda_1 &= \frac{1}{4}(J_{12} + J_{1S} + J_{2S}) \\
\lambda_2 &= \frac{1}{4}(J_{12} - J_{1S} - J_{2S}) \\
\lambda_3 &= -\frac{1}{4}J_{12} + \frac{1}{4}\sqrt{4J_{12}^2 + (J_{1S} - J_{2S})^2} \\
\lambda_4 &= -\frac{1}{4}J_{12} - \frac{1}{4}\sqrt{4J_{12}^2 + (J_{1S} - J_{2S})^2}
\end{aligned} \tag{A.27}$$

The corresponding eigenfunctions are:

$$\begin{aligned}
&\lambda_1 \begin{cases} j_1 = |\alpha\alpha\alpha> \\ j_2 = |\beta\beta\beta> \end{cases} \\
&\lambda_2 \begin{cases} j_3 = |\alpha\alpha\beta> \\ j_4 = |\beta\beta\alpha> \end{cases} \\
&\lambda_3 \begin{cases} j_5 = |\alpha\beta\alpha> + (\sqrt{1+\Delta^2} - \Delta)\,|\beta\alpha\alpha> \\ j_6 = (\sqrt{1+\Delta^2} - \Delta)\,|\alpha\beta\beta> + |\beta\alpha\beta> \end{cases} \\
&\lambda_4 \begin{cases} j_7 = |\alpha\beta\alpha> + (-\sqrt{1+\Delta^2} - \Delta)\,|\beta\alpha\alpha> \\ j_8 = (-\sqrt{1+\Delta^2} - \Delta)\,|\alpha\beta\beta> + |\beta\alpha\beta> \end{cases} \\
&\left(\Delta = \frac{J_{1S} - J_{2S}}{2J_{12}}\right)
\end{aligned} \tag{A.28}$$

By using the eigenvalues and eigenstates of the Hamiltonian, the evolution of states for I_1I_2S spin systems could be studied.

A.3.2. Related states

The initial state, $\boldsymbol{\sigma_0 = I_{1x}I_{2x} + I_{1y}I_{2y}}$, is (neglecting $\mathbf{I_{1z}I_{2z}}$ term which does not evolve under the Hamiltonian):

$$\boldsymbol{\sigma_0} = \frac{1}{2}\begin{pmatrix} 0 & 0 & 0 & 0 & 0 & 0 & 0 & 0 \\ 0 & 0 & 0 & 0 & 0 & 0 & 0 & 0 \\ 0 & 0 & 0 & 1 & 0 & 0 & 0 & 0 \\ 0 & 0 & 1 & 0 & 0 & 0 & 0 & 0 \\ 0 & 0 & 0 & 0 & 0 & 1 & 0 & 0 \\ 0 & 0 & 0 & 0 & 1 & 0 & 0 & 0 \\ 0 & 0 & 0 & 0 & 0 & 0 & 0 & 0 \\ 0 & 0 & 0 & 0 & 0 & 0 & 0 & 0 \end{pmatrix} \tag{A.29}$$

Other states in the first step include:

$$2(\mathbf{I_{1y}I_{2x}} - \mathbf{I_{1x}I_{2y}})\mathbf{S_z} = \frac{1}{2}\begin{pmatrix} 0 & 0 & 0 & 0 & 0 & 0 & 0 & 0 \\ 0 & 0 & 0 & 0 & 0 & 0 & 0 & 0 \\ 0 & 0 & 0 & -i & 0 & 0 & 0 & 0 \\ 0 & 0 & i & 0 & 0 & 0 & 0 & 0 \\ 0 & 0 & 0 & 0 & 0 & i & 0 & 0 \\ 0 & 0 & 0 & 0 & -i & 0 & 0 & 0 \\ 0 & 0 & 0 & 0 & 0 & 0 & 0 & 0 \\ 0 & 0 & 0 & 0 & 0 & 0 & 0 & 0 \end{pmatrix} \tag{A.30}$$

$$(\mathbf{I_{1z}} - \mathbf{I_{2z}})\mathbf{S_z} = \frac{1}{2}\begin{pmatrix} 0 & 0 & 0 & 0 & 0 & 0 & 0 & 0 \\ 0 & 0 & 0 & 0 & 0 & 0 & 0 & 0 \\ 0 & 0 & 1 & 0 & 0 & 0 & 0 & 0 \\ 0 & 0 & 0 & -1 & 0 & 0 & 0 & 0 \\ 0 & 0 & 0 & 0 & -1 & 0 & 0 & 0 \\ 0 & 0 & 0 & 0 & 0 & 1 & 0 & 0 \\ 0 & 0 & 0 & 0 & 0 & 0 & 0 & 0 \\ 0 & 0 & 0 & 0 & 0 & 0 & 0 & 0 \end{pmatrix} \tag{A.31}$$

The state in Equation A.31 is the state we chose to evolve in step 2. After evolving to this state, a 90 ^{o}pulse on S channel is applied to convert the state to:

$$\mathbf{S}_x(\mathbf{I}_{1z} - \mathbf{I}_{2z}) = \frac{1}{2}\begin{pmatrix} 0 & 0 & 0 & 0 & 0 & 0 & 0 & 0 \\ 0 & 0 & 0 & 0 & 0 & 0 & 0 & 0 \\ 0 & 0 & 0 & 0 & 1 & 0 & 0 & 0 \\ 0 & 0 & 0 & 0 & 0 & -1 & 0 & 0 \\ 0 & 0 & 1 & 0 & 0 & 0 & 0 & 0 \\ 0 & 0 & 0 & -1 & 0 & 0 & 0 & 0 \\ 0 & 0 & 0 & 0 & 0 & 0 & 0 & 0 \\ 0 & 0 & 0 & 0 & 0 & 0 & 0 & 0 \end{pmatrix} \quad \text{(A.32)}$$

The other states used in step 2 include:

$$2\mathbf{S}_x(\mathbf{I}_{1y}\mathbf{I}_{2x} - \mathbf{I}_{1x}\mathbf{I}_{2y}) = \frac{1}{2}\begin{pmatrix} 0 & 0 & 0 & 0 & 0 & 0 & 0 & 0 \\ 0 & 0 & 0 & 0 & 0 & 0 & 0 & 0 \\ 0 & 0 & 0 & 0 & 0 & -i & 0 & 0 \\ 0 & 0 & 0 & 0 & i & 0 & 0 & 0 \\ 0 & 0 & 0 & -i & 0 & 0 & 0 & 0 \\ 0 & 0 & i & 0 & 0 & 0 & 0 & 0 \\ 0 & 0 & 0 & 0 & 0 & 0 & 0 & 0 \\ 0 & 0 & 0 & 0 & 0 & 0 & 0 & 0 \end{pmatrix} \quad \text{(A.33)}$$

The final state we got from the sequence, representing carbon polarization, $\mathbf{S}_y(\mathbf{I} - 4\mathbf{I}_{1z}\mathbf{I}_{2z})$, is:

$$\boldsymbol{\sigma}_{final} = \frac{1}{2}\begin{pmatrix} 0 & 0 & 0 & 0 & 0 & 0 & 0 & 0 \\ 0 & 0 & 0 & 0 & 0 & 0 & 0 & 0 \\ 0 & 0 & 0 & 0 & -i & 0 & 0 & 0 \\ 0 & 0 & 0 & 0 & 0 & -i & 0 & 0 \\ 0 & 0 & i & 0 & 0 & 0 & 0 & 0 \\ 0 & 0 & 0 & i & 0 & 0 & 0 & 0 \\ 0 & 0 & 0 & 0 & 0 & 0 & 0 & 0 \\ 0 & 0 & 0 & 0 & 0 & 0 & 0 & 0 \end{pmatrix} \quad \text{(A.34)}$$

In the end a 90 ℅ pulse is applied on S channel to convert the state to S polarization $\mathbf{S}_z(\mathbf{I} - 4\mathbf{I}_{1z}\mathbf{I}_{2z})$.

APPENDIX B

PRODUCT OPERATORS FOR I_1I_2SR SPIN SYSTEMS

Section 3.2 describes how the lifetime could be determined from evolution. Section 3.3 shows some examples of the product operators for AA'XY spin systems. To study the correct expression of evolution of each state and calculate the optimum method of polarization level transfer, the form of the entire product operator and most rotation operators are necessary. As Appendix A, here we show a list of the basic operators that are essential to evolution analysis.

B.1. Matrix representation of major product operators

As in Appendix A, first the basic product operators are given in this section, including the x, y, and z components of both protons from parahydrogen and both heteronuclei (^{13}C, for example). For I_1I_2SR spin systems all matrix representation become 16×16 matrix instead of 8×8 in three spin cases. In all product operators the 16 spin states are ordered as |αααα>, |αααβ>, |ααβα>, |αβαα>, |βααα>, |ααββ>, |αβαβ>, |αββα>, |βααβ>, |βαβα>, |ββαα>, |αβββ>, |βαββ>, |ββαβ>, |βββα>, and |ββββ>.

B.1.1. Product operators for protons

The two protons from parahydrogen are labeled as $\mathbf{I_1}$ and $\mathbf{I_2}$. Below is a list of

product operators for both protons.

$$\mathbf{I}_{1x} = \frac{1}{2}\begin{pmatrix}
0 & 0 & 0 & 0 & 1 & 0 & 0 & 0 & 0 & 0 & 0 & 0 & 0 & 0 & 0 & 0 \\
0 & 0 & 0 & 0 & 0 & 0 & 0 & 0 & 1 & 0 & 0 & 0 & 0 & 0 & 0 & 0 \\
0 & 0 & 0 & 0 & 0 & 0 & 0 & 0 & 0 & 1 & 0 & 0 & 0 & 0 & 0 & 0 \\
0 & 0 & 0 & 0 & 0 & 0 & 0 & 0 & 0 & 0 & 1 & 0 & 0 & 0 & 0 & 0 \\
1 & 0 & 0 & 0 & 0 & 0 & 0 & 0 & 0 & 0 & 0 & 0 & 0 & 0 & 0 & 0 \\
0 & 0 & 0 & 0 & 0 & 0 & 0 & 0 & 0 & 0 & 0 & 0 & 1 & 0 & 0 & 0 \\
0 & 0 & 0 & 0 & 0 & 0 & 0 & 0 & 0 & 0 & 0 & 0 & 0 & 1 & 0 & 0 \\
0 & 0 & 0 & 0 & 0 & 0 & 0 & 0 & 0 & 0 & 0 & 0 & 0 & 0 & 1 & 0 \\
0 & 1 & 0 & 0 & 0 & 0 & 0 & 0 & 0 & 0 & 0 & 0 & 0 & 0 & 0 & 0 \\
0 & 0 & 1 & 0 & 0 & 0 & 0 & 0 & 0 & 0 & 0 & 0 & 0 & 0 & 0 & 0 \\
0 & 0 & 0 & 1 & 0 & 0 & 0 & 0 & 0 & 0 & 0 & 0 & 0 & 0 & 0 & 0 \\
0 & 0 & 0 & 0 & 0 & 0 & 0 & 0 & 0 & 0 & 0 & 0 & 0 & 0 & 0 & 1 \\
0 & 0 & 0 & 0 & 0 & 1 & 0 & 0 & 0 & 0 & 0 & 0 & 0 & 0 & 0 & 0 \\
0 & 0 & 0 & 0 & 0 & 0 & 1 & 0 & 0 & 0 & 0 & 0 & 0 & 0 & 0 & 0 \\
0 & 0 & 0 & 0 & 0 & 0 & 0 & 1 & 0 & 0 & 0 & 0 & 0 & 0 & 0 & 0 \\
0 & 0 & 0 & 0 & 0 & 0 & 0 & 0 & 0 & 0 & 0 & 1 & 0 & 0 & 0 & 0
\end{pmatrix} \tag{B.1}$$

$$\mathbf{I}_{1y} = \frac{i}{2}\begin{pmatrix}
0 & 0 & 0 & 0 & -1 & 0 & 0 & 0 & 0 & 0 & 0 & 0 & 0 & 0 & 0 & 0 \\
0 & 0 & 0 & 0 & 0 & 0 & 0 & 0 & -1 & 0 & 0 & 0 & 0 & 0 & 0 & 0 \\
0 & 0 & 0 & 0 & 0 & 0 & 0 & 0 & 0 & -1 & 0 & 0 & 0 & 0 & 0 & 0 \\
0 & 0 & 0 & 0 & 0 & 0 & 0 & 0 & 0 & 0 & -1 & 0 & 0 & 0 & 0 & 0 \\
1 & 0 & 0 & 0 & 0 & 0 & 0 & 0 & 0 & 0 & 0 & 0 & 0 & 0 & 0 & 0 \\
0 & 0 & 0 & 0 & 0 & 0 & 0 & 0 & 0 & 0 & 0 & 0 & -1 & 0 & 0 & 0 \\
0 & 0 & 0 & 0 & 0 & 0 & 0 & 0 & 0 & 0 & 0 & 0 & 0 & -1 & 0 & 0 \\
0 & 0 & 0 & 0 & 0 & 0 & 0 & 0 & 0 & 0 & 0 & 0 & 0 & 0 & -1 & 0 \\
0 & 1 & 0 & 0 & 0 & 0 & 0 & 0 & 0 & 0 & 0 & 0 & 0 & 0 & 0 & 0 \\
0 & 0 & 1 & 0 & 0 & 0 & 0 & 0 & 0 & 0 & 0 & 0 & 0 & 0 & 0 & 0 \\
0 & 0 & 0 & 1 & 0 & 0 & 0 & 0 & 0 & 0 & 0 & 0 & 0 & 0 & 0 & 0 \\
0 & 0 & 0 & 0 & 0 & 0 & 0 & 0 & 0 & 0 & 0 & 0 & 0 & 0 & 0 & -1 \\
0 & 0 & 0 & 0 & 0 & 1 & 0 & 0 & 0 & 0 & 0 & 0 & 0 & 0 & 0 & 0 \\
0 & 0 & 0 & 0 & 0 & 0 & 1 & 0 & 0 & 0 & 0 & 0 & 0 & 0 & 0 & 0 \\
0 & 0 & 0 & 0 & 0 & 0 & 0 & 1 & 0 & 0 & 0 & 0 & 0 & 0 & 0 & 0 \\
0 & 0 & 0 & 0 & 0 & 0 & 0 & 0 & 0 & 0 & 0 & 1 & 0 & 0 & 0 & 0
\end{pmatrix} \tag{B.2}$$

$$\mathbf{I}_{1z} = \frac{1}{2}\begin{pmatrix}
1 & 0 & 0 & 0 & 0 & 0 & 0 & 0 & 0 & 0 & 0 & 0 & 0 & 0 & 0 & 0 \\
0 & 1 & 0 & 0 & 0 & 0 & 0 & 0 & 0 & 0 & 0 & 0 & 0 & 0 & 0 & 0 \\
0 & 0 & 1 & 0 & 0 & 0 & 0 & 0 & 0 & 0 & 0 & 0 & 0 & 0 & 0 & 0 \\
0 & 0 & 0 & 1 & 0 & 0 & 0 & 0 & 0 & 0 & 0 & 0 & 0 & 0 & 0 & 0 \\
0 & 0 & 0 & 0 & -1 & 0 & 0 & 0 & 0 & 0 & 0 & 0 & 0 & 0 & 0 & 0 \\
0 & 0 & 0 & 0 & 0 & 1 & 0 & 0 & 0 & 0 & 0 & 0 & 0 & 0 & 0 & 0 \\
0 & 0 & 0 & 0 & 0 & 0 & 1 & 0 & 0 & 0 & 0 & 0 & 0 & 0 & 0 & 0 \\
0 & 0 & 0 & 0 & 0 & 0 & 0 & 1 & 0 & 0 & 0 & 0 & 0 & 0 & 0 & 0 \\
0 & 0 & 0 & 0 & 0 & 0 & 0 & 0 & -1 & 0 & 0 & 0 & 0 & 0 & 0 & 0 \\
0 & 0 & 0 & 0 & 0 & 0 & 0 & 0 & 0 & -1 & 0 & 0 & 0 & 0 & 0 & 0 \\
0 & 0 & 0 & 0 & 0 & 0 & 0 & 0 & 0 & 0 & -1 & 0 & 0 & 0 & 0 & 0 \\
0 & 0 & 0 & 0 & 0 & 0 & 0 & 0 & 0 & 0 & 0 & 1 & 0 & 0 & 0 & 0 \\
0 & 0 & 0 & 0 & 0 & 0 & 0 & 0 & 0 & 0 & 0 & 0 & -1 & 0 & 0 & 0 \\
0 & 0 & 0 & 0 & 0 & 0 & 0 & 0 & 0 & 0 & 0 & 0 & 0 & -1 & 0 & 0 \\
0 & 0 & 0 & 0 & 0 & 0 & 0 & 0 & 0 & 0 & 0 & 0 & 0 & 0 & -1 & 0 \\
0 & 0 & 0 & 0 & 0 & 0 & 0 & 0 & 0 & 0 & 0 & 0 & 0 & 0 & 0 & -1
\end{pmatrix} \tag{B.3}$$

$$\mathbf{I}_{2x} = \frac{1}{2}\begin{pmatrix}
0 & 0 & 0 & 1 & 0 & 0 & 0 & 0 & 0 & 0 & 0 & 0 & 0 & 0 & 0 & 0 \\
0 & 0 & 0 & 0 & 0 & 0 & 1 & 0 & 0 & 0 & 0 & 0 & 0 & 0 & 0 & 0 \\
0 & 0 & 0 & 0 & 0 & 0 & 0 & 1 & 0 & 0 & 0 & 0 & 0 & 0 & 0 & 0 \\
1 & 0 & 0 & 0 & 0 & 0 & 0 & 0 & 0 & 0 & 0 & 0 & 0 & 0 & 0 & 0 \\
0 & 0 & 0 & 0 & 0 & 0 & 0 & 0 & 0 & 0 & 1 & 0 & 0 & 0 & 0 & 0 \\
0 & 0 & 0 & 0 & 0 & 0 & 0 & 0 & 0 & 0 & 0 & 1 & 0 & 0 & 0 & 0 \\
0 & 1 & 0 & 0 & 0 & 0 & 0 & 0 & 0 & 0 & 0 & 0 & 0 & 0 & 0 & 0 \\
0 & 0 & 1 & 0 & 0 & 0 & 0 & 0 & 0 & 0 & 0 & 0 & 0 & 0 & 0 & 0 \\
0 & 0 & 0 & 0 & 0 & 0 & 0 & 0 & 0 & 0 & 0 & 0 & 0 & 1 & 0 & 0 \\
0 & 0 & 0 & 0 & 0 & 0 & 0 & 0 & 0 & 0 & 0 & 0 & 0 & 0 & 1 & 0 \\
0 & 0 & 0 & 0 & 1 & 0 & 0 & 0 & 0 & 0 & 0 & 0 & 0 & 0 & 0 & 0 \\
0 & 0 & 0 & 0 & 0 & 1 & 0 & 0 & 0 & 0 & 0 & 0 & 0 & 0 & 0 & 0 \\
0 & 0 & 0 & 0 & 0 & 0 & 0 & 0 & 0 & 0 & 0 & 0 & 0 & 0 & 0 & 1 \\
0 & 0 & 0 & 0 & 0 & 0 & 0 & 0 & 1 & 0 & 0 & 0 & 0 & 0 & 0 & 0 \\
0 & 0 & 0 & 0 & 0 & 0 & 0 & 0 & 0 & 1 & 0 & 0 & 0 & 0 & 0 & 0 \\
0 & 0 & 0 & 0 & 0 & 0 & 0 & 0 & 0 & 0 & 0 & 0 & 1 & 0 & 0 & 0
\end{pmatrix} \tag{B.4}$$

$$\mathbf{I}_{2y} = \frac{i}{2}\begin{pmatrix}
0 & 0 & 0 & -1 & 0 & 0 & 0 & 0 & 0 & 0 & 0 & 0 & 0 & 0 & 0 & 0 \\
0 & 0 & 0 & 0 & 0 & 0 & -1 & 0 & 0 & 0 & 0 & 0 & 0 & 0 & 0 & 0 \\
0 & 0 & 0 & 0 & 0 & 0 & 0 & -1 & 0 & 0 & 0 & 0 & 0 & 0 & 0 & 0 \\
1 & 0 & 0 & 0 & 0 & 0 & 0 & 0 & 0 & 0 & 0 & 0 & 0 & 0 & 0 & 0 \\
0 & 0 & 0 & 0 & 0 & 0 & 0 & 0 & 0 & 0 & -1 & 0 & 0 & 0 & 0 & 0 \\
0 & 0 & 0 & 0 & 0 & 0 & 0 & 0 & 0 & 0 & 0 & -1 & 0 & 0 & 0 & 0 \\
0 & 1 & 0 & 0 & 0 & 0 & 0 & 0 & 0 & 0 & 0 & 0 & 0 & 0 & 0 & 0 \\
0 & 0 & 1 & 0 & 0 & 0 & 0 & 0 & 0 & 0 & 0 & 0 & 0 & 0 & 0 & 0 \\
0 & 0 & 0 & 0 & 0 & 0 & 0 & 0 & 0 & 0 & 0 & 0 & 0 & -1 & 0 & 0 \\
0 & 0 & 0 & 0 & 0 & 0 & 0 & 0 & 0 & 0 & 0 & 0 & 0 & 0 & -1 & 0 \\
0 & 0 & 0 & 0 & 1 & 0 & 0 & 0 & 0 & 0 & 0 & 0 & 0 & 0 & 0 & 0 \\
0 & 0 & 0 & 0 & 0 & 1 & 0 & 0 & 0 & 0 & 0 & 0 & 0 & 0 & 0 & 0 \\
0 & 0 & 0 & 0 & 0 & 0 & 0 & 0 & 0 & 0 & 0 & 0 & 0 & 0 & 0 & -1 \\
0 & 0 & 0 & 0 & 0 & 0 & 0 & 0 & 1 & 0 & 0 & 0 & 0 & 0 & 0 & 0 \\
0 & 0 & 0 & 0 & 0 & 0 & 0 & 0 & 0 & 1 & 0 & 0 & 0 & 0 & 0 & 0 \\
0 & 0 & 0 & 0 & 0 & 0 & 0 & 0 & 0 & 0 & 0 & 0 & 1 & 0 & 0 & 0
\end{pmatrix} \tag{B.5}$$

$$\mathbf{I}_{2z} = \frac{1}{2}\begin{pmatrix}
1 & 0 & 0 & 0 & 0 & 0 & 0 & 0 & 0 & 0 & 0 & 0 & 0 & 0 & 0 & 0 \\
0 & 1 & 0 & 0 & 0 & 0 & 0 & 0 & 0 & 0 & 0 & 0 & 0 & 0 & 0 & 0 \\
0 & 0 & 1 & 0 & 0 & 0 & 0 & 0 & 0 & 0 & 0 & 0 & 0 & 0 & 0 & 0 \\
0 & 0 & 0 & -1 & 0 & 0 & 0 & 0 & 0 & 0 & 0 & 0 & 0 & 0 & 0 & 0 \\
0 & 0 & 0 & 0 & 1 & 0 & 0 & 0 & 0 & 0 & 0 & 0 & 0 & 0 & 0 & 0 \\
0 & 0 & 0 & 0 & 0 & 1 & 0 & 0 & 0 & 0 & 0 & 0 & 0 & 0 & 0 & 0 \\
0 & 0 & 0 & 0 & 0 & 0 & -1 & 0 & 0 & 0 & 0 & 0 & 0 & 0 & 0 & 0 \\
0 & 0 & 0 & 0 & 0 & 0 & 0 & -1 & 0 & 0 & 0 & 0 & 0 & 0 & 0 & 0 \\
0 & 0 & 0 & 0 & 0 & 0 & 0 & 0 & 1 & 0 & 0 & 0 & 0 & 0 & 0 & 0 \\
0 & 0 & 0 & 0 & 0 & 0 & 0 & 0 & 0 & 1 & 0 & 0 & 0 & 0 & 0 & 0 \\
0 & 0 & 0 & 0 & 0 & 0 & 0 & 0 & 0 & 0 & -1 & 0 & 0 & 0 & 0 & 0 \\
0 & 0 & 0 & 0 & 0 & 0 & 0 & 0 & 0 & 0 & 0 & -1 & 0 & 0 & 0 & 0 \\
0 & 0 & 0 & 0 & 0 & 0 & 0 & 0 & 0 & 0 & 0 & 0 & 1 & 0 & 0 & 0 \\
0 & 0 & 0 & 0 & 0 & 0 & 0 & 0 & 0 & 0 & 0 & 0 & 0 & -1 & 0 & 0 \\
0 & 0 & 0 & 0 & 0 & 0 & 0 & 0 & 0 & 0 & 0 & 0 & 0 & 0 & -1 & 0 \\
0 & 0 & 0 & 0 & 0 & 0 & 0 & 0 & 0 & 0 & 0 & 0 & 0 & 0 & 0 & -1
\end{pmatrix} \tag{B.6}$$

B.1.2. Product operators for heteronuclei

The basic product operators for the heteronuclei (labeled as S an R) are:

$$\mathbf{S}_x = \frac{1}{2}\begin{pmatrix}
0 & 0 & 1 & 0 & 0 & 0 & 0 & 0 & 0 & 0 & 0 & 0 & 0 & 0 & 0 & 0 \\
0 & 0 & 0 & 0 & 0 & 1 & 0 & 0 & 0 & 0 & 0 & 0 & 0 & 0 & 0 & 0 \\
1 & 0 & 0 & 0 & 0 & 0 & 0 & 0 & 0 & 0 & 0 & 0 & 0 & 0 & 0 & 0 \\
0 & 0 & 0 & 0 & 0 & 0 & 0 & 1 & 0 & 0 & 0 & 0 & 0 & 0 & 0 & 0 \\
0 & 0 & 0 & 0 & 0 & 0 & 0 & 0 & 0 & 1 & 0 & 0 & 0 & 0 & 0 & 0 \\
0 & 1 & 0 & 0 & 0 & 0 & 0 & 0 & 0 & 0 & 0 & 0 & 0 & 0 & 0 & 0 \\
0 & 0 & 0 & 0 & 0 & 0 & 0 & 0 & 0 & 0 & 0 & 1 & 0 & 0 & 0 & 0 \\
0 & 0 & 0 & 1 & 0 & 0 & 0 & 0 & 0 & 0 & 0 & 0 & 0 & 0 & 0 & 0 \\
0 & 0 & 0 & 0 & 0 & 0 & 0 & 0 & 0 & 0 & 0 & 0 & 1 & 0 & 0 & 0 \\
0 & 0 & 0 & 0 & 1 & 0 & 0 & 0 & 0 & 0 & 0 & 0 & 0 & 0 & 0 & 0 \\
0 & 0 & 0 & 0 & 0 & 0 & 0 & 0 & 0 & 0 & 0 & 0 & 0 & 0 & 1 & 0 \\
0 & 0 & 0 & 0 & 0 & 0 & 1 & 0 & 0 & 0 & 0 & 0 & 0 & 0 & 0 & 0 \\
0 & 0 & 0 & 0 & 0 & 0 & 0 & 0 & 1 & 0 & 0 & 0 & 0 & 0 & 0 & 0 \\
0 & 0 & 0 & 0 & 0 & 0 & 0 & 0 & 0 & 0 & 0 & 0 & 0 & 0 & 0 & 1 \\
0 & 0 & 0 & 0 & 0 & 0 & 0 & 0 & 0 & 0 & 1 & 0 & 0 & 0 & 0 & 0 \\
0 & 0 & 0 & 0 & 0 & 0 & 0 & 0 & 0 & 0 & 0 & 0 & 0 & 1 & 0 & 0
\end{pmatrix} \tag{B.7}$$

$$\mathbf{S}_y = \frac{i}{2}\begin{pmatrix}
0 & 0 & -1 & 0 & 0 & 0 & 0 & 0 & 0 & 0 & 0 & 0 & 0 & 0 & 0 & 0 \\
0 & 0 & 0 & 0 & 0 & -1 & 0 & 0 & 0 & 0 & 0 & 0 & 0 & 0 & 0 & 0 \\
1 & 0 & 0 & 0 & 0 & 0 & 0 & 0 & 0 & 0 & 0 & 0 & 0 & 0 & 0 & 0 \\
0 & 0 & 0 & 0 & 0 & 0 & 0 & -1 & 0 & 0 & 0 & 0 & 0 & 0 & 0 & 0 \\
0 & 0 & 0 & 0 & 0 & 0 & 0 & 0 & 0 & -1 & 0 & 0 & 0 & 0 & 0 & 0 \\
0 & 1 & 0 & 0 & 0 & 0 & 0 & 0 & 0 & 0 & 0 & 0 & 0 & 0 & 0 & 0 \\
0 & 0 & 0 & 0 & 0 & 0 & 0 & 0 & 0 & 0 & 0 & -1 & 0 & 0 & 0 & 0 \\
0 & 0 & 0 & 1 & 0 & 0 & 0 & 0 & 0 & 0 & 0 & 0 & 0 & 0 & 0 & 0 \\
0 & 0 & 0 & 0 & 0 & 0 & 0 & 0 & 0 & 0 & 0 & 0 & -1 & 0 & 0 & 0 \\
0 & 0 & 0 & 0 & 1 & 0 & 0 & 0 & 0 & 0 & 0 & 0 & 0 & 0 & 0 & 0 \\
0 & 0 & 0 & 0 & 0 & 0 & 0 & 0 & 0 & 0 & 0 & 0 & 0 & 0 & -1 & 0 \\
0 & 0 & 0 & 0 & 0 & 0 & 1 & 0 & 0 & 0 & 0 & 0 & 0 & 0 & 0 & 0 \\
0 & 0 & 0 & 0 & 0 & 0 & 0 & 0 & 1 & 0 & 0 & 0 & 0 & 0 & 0 & 0 \\
0 & 0 & 0 & 0 & 0 & 0 & 0 & 0 & 0 & 0 & 0 & 0 & 0 & 0 & 0 & -1 \\
0 & 0 & 0 & 0 & 0 & 0 & 0 & 0 & 0 & 0 & 1 & 0 & 0 & 0 & 0 & 0 \\
0 & 0 & 0 & 0 & 0 & 0 & 0 & 0 & 0 & 0 & 0 & 0 & 0 & 1 & 0 & 0
\end{pmatrix} \tag{B.8}$$

$$\mathbf{S}_z = \frac{1}{2}\begin{pmatrix}
1 & 0 & 0 & 0 & 0 & 0 & 0 & 0 & 0 & 0 & 0 & 0 & 0 & 0 & 0 & 0 \\
0 & 1 & 0 & 0 & 0 & 0 & 0 & 0 & 0 & 0 & 0 & 0 & 0 & 0 & 0 & 0 \\
0 & 0 & -1 & 0 & 0 & 0 & 0 & 0 & 0 & 0 & 0 & 0 & 0 & 0 & 0 & 0 \\
0 & 0 & 0 & 1 & 0 & 0 & 0 & 0 & 0 & 0 & 0 & 0 & 0 & 0 & 0 & 0 \\
0 & 0 & 0 & 0 & 1 & 0 & 0 & 0 & 0 & 0 & 0 & 0 & 0 & 0 & 0 & 0 \\
0 & 0 & 0 & 0 & 0 & -1 & 0 & 0 & 0 & 0 & 0 & 0 & 0 & 0 & 0 & 0 \\
0 & 0 & 0 & 0 & 0 & 0 & 1 & 0 & 0 & 0 & 0 & 0 & 0 & 0 & 0 & 0 \\
0 & 0 & 0 & 0 & 0 & 0 & 0 & -1 & 0 & 0 & 0 & 0 & 0 & 0 & 0 & 0 \\
0 & 0 & 0 & 0 & 0 & 0 & 0 & 0 & 1 & 0 & 0 & 0 & 0 & 0 & 0 & 0 \\
0 & 0 & 0 & 0 & 0 & 0 & 0 & 0 & 0 & -1 & 0 & 0 & 0 & 0 & 0 & 0 \\
0 & 0 & 0 & 0 & 0 & 0 & 0 & 0 & 0 & 0 & 1 & 0 & 0 & 0 & 0 & 0 \\
0 & 0 & 0 & 0 & 0 & 0 & 0 & 0 & 0 & 0 & 0 & -1 & 0 & 0 & 0 & 0 \\
0 & 0 & 0 & 0 & 0 & 0 & 0 & 0 & 0 & 0 & 0 & 0 & -1 & 0 & 0 & 0 \\
0 & 0 & 0 & 0 & 0 & 0 & 0 & 0 & 0 & 0 & 0 & 0 & 0 & 1 & 0 & 0 \\
0 & 0 & 0 & 0 & 0 & 0 & 0 & 0 & 0 & 0 & 0 & 0 & 0 & 0 & -1 & 0 \\
0 & 0 & 0 & 0 & 0 & 0 & 0 & 0 & 0 & 0 & 0 & 0 & 0 & 0 & 0 & -1
\end{pmatrix} \quad \text{(B.9)}$$

$$\mathbf{R}_x = \frac{1}{2}\begin{pmatrix}
0 & 1 & 0 & 0 & 0 & 0 & 0 & 0 & 0 & 0 & 0 & 0 & 0 & 0 & 0 & 0 \\
1 & 0 & 0 & 0 & 0 & 0 & 0 & 0 & 0 & 0 & 0 & 0 & 0 & 0 & 0 & 0 \\
0 & 0 & 0 & 0 & 0 & 1 & 0 & 0 & 0 & 0 & 0 & 0 & 0 & 0 & 0 & 0 \\
0 & 0 & 0 & 0 & 0 & 0 & 1 & 0 & 0 & 0 & 0 & 0 & 0 & 0 & 0 & 0 \\
0 & 0 & 0 & 0 & 0 & 0 & 0 & 0 & 1 & 0 & 0 & 0 & 0 & 0 & 0 & 0 \\
0 & 0 & 1 & 0 & 0 & 0 & 0 & 0 & 0 & 0 & 0 & 0 & 0 & 0 & 0 & 0 \\
0 & 0 & 0 & 1 & 0 & 0 & 0 & 0 & 0 & 0 & 0 & 0 & 0 & 0 & 0 & 0 \\
0 & 0 & 0 & 0 & 0 & 0 & 0 & 0 & 0 & 0 & 0 & 1 & 0 & 0 & 0 & 0 \\
0 & 0 & 0 & 0 & 1 & 0 & 0 & 0 & 0 & 0 & 0 & 0 & 0 & 0 & 0 & 0 \\
0 & 0 & 0 & 0 & 0 & 0 & 0 & 0 & 0 & 0 & 0 & 0 & 1 & 0 & 0 & 0 \\
0 & 0 & 0 & 0 & 0 & 0 & 0 & 0 & 0 & 0 & 0 & 0 & 0 & 1 & 0 & 0 \\
0 & 0 & 0 & 0 & 0 & 0 & 0 & 1 & 0 & 0 & 0 & 0 & 0 & 0 & 0 & 0 \\
0 & 0 & 0 & 0 & 0 & 0 & 0 & 0 & 0 & 1 & 0 & 0 & 0 & 0 & 0 & 0 \\
0 & 0 & 0 & 0 & 0 & 0 & 0 & 0 & 0 & 0 & 1 & 0 & 0 & 0 & 0 & 0 \\
0 & 0 & 0 & 0 & 0 & 0 & 0 & 0 & 0 & 0 & 0 & 0 & 0 & 0 & 0 & 1 \\
0 & 0 & 0 & 0 & 0 & 0 & 0 & 0 & 0 & 0 & 0 & 0 & 0 & 0 & 1 & 0
\end{pmatrix} \quad \text{(B.10)}$$

$$\mathbf{R}_y = \frac{i}{2}\begin{pmatrix}
0 & -1 & 0 & 0 & 0 & 0 & 0 & 0 & 0 & 0 & 0 & 0 & 0 & 0 & 0 & 0 \\
1 & 0 & 0 & 0 & 0 & 0 & 0 & 0 & 0 & 0 & 0 & 0 & 0 & 0 & 0 & 0 \\
0 & 0 & 0 & 0 & 0 & -1 & 0 & 0 & 0 & 0 & 0 & 0 & 0 & 0 & 0 & 0 \\
0 & 0 & 0 & 0 & 0 & 0 & -1 & 0 & 0 & 0 & 0 & 0 & 0 & 0 & 0 & 0 \\
0 & 0 & 0 & 0 & 0 & 0 & 0 & 0 & -1 & 0 & 0 & 0 & 0 & 0 & 0 & 0 \\
0 & 0 & 1 & 0 & 0 & 0 & 0 & 0 & 0 & 0 & 0 & 0 & 0 & 0 & 0 & 0 \\
0 & 0 & 0 & 1 & 0 & 0 & 0 & 0 & 0 & 0 & 0 & 0 & 0 & 0 & 0 & 0 \\
0 & 0 & 0 & 0 & 0 & 0 & 0 & 0 & 0 & 0 & 0 & -1 & 0 & 0 & 0 & 0 \\
0 & 0 & 0 & 0 & 1 & 0 & 0 & 0 & 0 & 0 & 0 & 0 & 0 & 0 & 0 & 0 \\
0 & 0 & 0 & 0 & 0 & 0 & 0 & 0 & 0 & 0 & 0 & 0 & -1 & 0 & 0 & 0 \\
0 & 0 & 0 & 0 & 0 & 0 & 0 & 0 & 0 & 0 & 0 & 0 & 0 & -1 & 0 & 0 \\
0 & 0 & 0 & 0 & 0 & 0 & 0 & 1 & 0 & 0 & 0 & 0 & 0 & 0 & 0 & 0 \\
0 & 0 & 0 & 0 & 0 & 0 & 0 & 0 & 0 & 1 & 0 & 0 & 0 & 0 & 0 & 0 \\
0 & 0 & 0 & 0 & 0 & 0 & 0 & 0 & 0 & 0 & 1 & 0 & 0 & 0 & 0 & 0 \\
0 & 0 & 0 & 0 & 0 & 0 & 0 & 0 & 0 & 0 & 0 & 0 & 0 & 0 & 0 & -1 \\
0 & 0 & 0 & 0 & 0 & 0 & 0 & 0 & 0 & 0 & 0 & 0 & 0 & 0 & 1 & 0
\end{pmatrix} \quad \text{(B.11)}$$

$$\mathbf{R}_z = \frac{1}{2}\begin{pmatrix}
1 & 0 & 0 & 0 & 0 & 0 & 0 & 0 & 0 & 0 & 0 & 0 & 0 & 0 & 0 & 0 \\
0 & -1 & 0 & 0 & 0 & 0 & 0 & 0 & 0 & 0 & 0 & 0 & 0 & 0 & 0 & 0 \\
0 & 0 & 1 & 0 & 0 & 0 & 0 & 0 & 0 & 0 & 0 & 0 & 0 & 0 & 0 & 0 \\
0 & 0 & 0 & 1 & 0 & 0 & 0 & 0 & 0 & 0 & 0 & 0 & 0 & 0 & 0 & 0 \\
0 & 0 & 0 & 0 & 1 & 0 & 0 & 0 & 0 & 0 & 0 & 0 & 0 & 0 & 0 & 0 \\
0 & 0 & 0 & 0 & 0 & -1 & 0 & 0 & 0 & 0 & 0 & 0 & 0 & 0 & 0 & 0 \\
0 & 0 & 0 & 0 & 0 & 0 & -1 & 0 & 0 & 0 & 0 & 0 & 0 & 0 & 0 & 0 \\
0 & 0 & 0 & 0 & 0 & 0 & 0 & 1 & 0 & 0 & 0 & 0 & 0 & 0 & 0 & 0 \\
0 & 0 & 0 & 0 & 0 & 0 & 0 & 0 & -1 & 0 & 0 & 0 & 0 & 0 & 0 & 0 \\
0 & 0 & 0 & 0 & 0 & 0 & 0 & 0 & 0 & 1 & 0 & 0 & 0 & 0 & 0 & 0 \\
0 & 0 & 0 & 0 & 0 & 0 & 0 & 0 & 0 & 0 & 1 & 0 & 0 & 0 & 0 & 0 \\
0 & 0 & 0 & 0 & 0 & 0 & 0 & 0 & 0 & 0 & 0 & -1 & 0 & 0 & 0 & 0 \\
0 & 0 & 0 & 0 & 0 & 0 & 0 & 0 & 0 & 0 & 0 & 0 & -1 & 0 & 0 & 0 \\
0 & 0 & 0 & 0 & 0 & 0 & 0 & 0 & 0 & 0 & 0 & 0 & 0 & -1 & 0 & 0 \\
0 & 0 & 0 & 0 & 0 & 0 & 0 & 0 & 0 & 0 & 0 & 0 & 0 & 0 & 1 & 0 \\
0 & 0 & 0 & 0 & 0 & 0 & 0 & 0 & 0 & 0 & 0 & 0 & 0 & 0 & 0 & -1
\end{pmatrix} \quad \text{(B.12)}$$

B.2. Rotations

In this section the commonly used pulses (90 º and 180 º) for all four spins are presented.

B.2.1. 90 degree rotations for protons

Propagators listed below are the operators that rotate the protons by 90 º around either x or y axis.

$$\mathbf{R}_x^{\mathbf{I}}(\frac{\pi}{2}) =$$

$$\frac{1}{2}\begin{pmatrix}
1 & 0 & 0 & i & i & 0 & 0 & 0 & 0 & 0 & -1 & 0 & 0 & 0 & 0 & 0 \\
0 & 1 & 0 & 0 & 0 & 0 & i & 0 & i & 0 & 0 & 0 & 0 & -1 & 0 & 0 \\
0 & 0 & 1 & 0 & 0 & 0 & 0 & i & 0 & i & 0 & 0 & 0 & 0 & -1 & 0 \\
i & 0 & 0 & 1 & -1 & 0 & 0 & 0 & 0 & 0 & i & 0 & 0 & 0 & 0 & 0 \\
i & 0 & 0 & -1 & 1 & 0 & 0 & 0 & 0 & 0 & i & 0 & 0 & 0 & 0 & 0 \\
0 & 0 & 0 & 0 & 0 & 1 & 0 & 0 & 0 & 0 & 0 & i & i & 0 & 0 & -1 \\
0 & i & 0 & 0 & 0 & 0 & 1 & 0 & -1 & 0 & 0 & 0 & 0 & i & 0 & 0 \\
0 & 0 & i & 0 & 0 & 0 & 0 & 1 & 0 & -1 & 0 & 0 & 0 & 0 & i & 0 \\
0 & i & 0 & 0 & 0 & 0 & -1 & 0 & 1 & 0 & 0 & 0 & 0 & i & 0 & 0 \\
0 & 0 & i & 0 & 0 & 0 & 0 & -1 & 0 & 1 & 0 & 0 & 0 & 0 & i & 0 \\
-1 & 0 & 0 & i & i & 0 & 0 & 0 & 0 & 0 & 1 & 0 & 0 & 0 & 0 & 0 \\
0 & 0 & 0 & 0 & 0 & i & 0 & 0 & 0 & 0 & 0 & 1 & -1 & 0 & 0 & i \\
0 & 0 & 0 & 0 & 0 & i & 0 & 0 & 0 & 0 & 0 & -1 & 1 & 0 & 0 & i \\
0 & -1 & 0 & 0 & 0 & 0 & i & 0 & i & 0 & 0 & 0 & 0 & 1 & 0 & 0 \\
0 & 0 & -1 & 0 & 0 & 0 & 0 & i & 0 & i & 0 & 0 & 0 & 0 & 1 & 0 \\
0 & 0 & 0 & 0 & 0 & -1 & 0 & 0 & 0 & 0 & 0 & i & i & 0 & 0 & 1
\end{pmatrix} \quad \text{(B.13)}$$

$$\mathbf{R}_y^{\mathbf{I}}\left(\frac{\pi}{2}\right) =$$

$$\frac{1}{2}\begin{pmatrix}
1 & 0 & 0 & 1 & 1 & 0 & 0 & 0 & 0 & 0 & 1 & 0 & 0 & 0 & 0 & 0 \\
0 & 1 & 0 & 0 & 0 & 0 & 1 & 0 & 1 & 0 & 0 & 0 & 0 & 1 & 0 & 0 \\
0 & 0 & 1 & 0 & 0 & 0 & 0 & 1 & 0 & 1 & 0 & 0 & 0 & 0 & 1 & 0 \\
-1 & 0 & 0 & 1 & -1 & 0 & 0 & 0 & 0 & 0 & 1 & 0 & 0 & 0 & 0 & 0 \\
-1 & 0 & 0 & -1 & 1 & 0 & 0 & 0 & 0 & 0 & 1 & 0 & 0 & 0 & 0 & 0 \\
0 & 0 & 0 & 0 & 0 & 1 & 0 & 0 & 0 & 0 & 0 & 1 & 1 & 0 & 0 & 1 \\
0 & -1 & 0 & 0 & 0 & 0 & 1 & 0 & -1 & 0 & 0 & 0 & 0 & 1 & 0 & 0 \\
0 & 0 & -1 & 0 & 0 & 0 & 0 & 1 & 0 & -1 & 0 & 0 & 0 & 0 & 1 & 0 \\
0 & -1 & 0 & 0 & 0 & 0 & -1 & 0 & 1 & 0 & 0 & 0 & 0 & 1 & 0 & 0 \\
0 & 0 & -1 & 0 & 0 & 0 & 0 & -1 & 0 & 1 & 0 & 0 & 0 & 0 & 1 & 0 \\
1 & 0 & 0 & -1 & -1 & 0 & 0 & 0 & 0 & 0 & 1 & 0 & 0 & 0 & 0 & 0 \\
0 & 0 & 0 & 0 & 0 & -1 & 0 & 0 & 0 & 0 & 0 & 1 & -1 & 0 & 0 & 1 \\
0 & 0 & 0 & 0 & 0 & -1 & 0 & 0 & 0 & 0 & 0 & -1 & 1 & 0 & 0 & 1 \\
0 & 1 & 0 & 0 & 0 & 0 & -1 & 0 & -1 & 0 & 0 & 0 & 0 & 1 & 0 & 0 \\
0 & 0 & 1 & 0 & 0 & 0 & 0 & -1 & 0 & -1 & 0 & 0 & 0 & 0 & 1 & 0 \\
0 & 0 & 0 & 0 & 0 & 1 & 0 & 0 & 0 & 0 & 0 & -1 & -1 & 0 & 0 & 1
\end{pmatrix} \tag{B.14}$$

B.2.2. 90 degree rotations for heteronuclei

Propagators listed below are the operators that rotate the heteronuclei (S or R) by 90 ºaround either x or y axis.

$$\mathbf{R}_x^s\left(\frac{\pi}{2}\right) = \frac{1}{\sqrt{2}}\begin{pmatrix}
1 & 0 & i & 0 & 0 & 0 & 0 & 0 & 0 & 0 & 0 & 0 & 0 & 0 & 0 & 0 \\
0 & 1 & 0 & 0 & 0 & i & 0 & 0 & 0 & 0 & 0 & 0 & 0 & 0 & 0 & 0 \\
i & 0 & 1 & 0 & 0 & 0 & 0 & 0 & 0 & 0 & 0 & 0 & 0 & 0 & 0 & 0 \\
0 & 0 & 0 & 1 & 0 & 0 & 0 & i & 0 & 0 & 0 & 0 & 0 & 0 & 0 & 0 \\
0 & 0 & 0 & 0 & 1 & 0 & 0 & 0 & 0 & i & 0 & 0 & 0 & 0 & 0 & 0 \\
0 & i & 0 & 0 & 0 & 1 & 0 & 0 & 0 & 0 & 0 & 0 & 0 & 0 & 0 & 0 \\
0 & 0 & 0 & 0 & 0 & 0 & 1 & 0 & 0 & 0 & 0 & i & 0 & 0 & 0 & 0 \\
0 & 0 & 0 & i & 0 & 0 & 0 & 1 & 0 & 0 & 0 & 0 & 0 & 0 & 0 & 0 \\
0 & 0 & 0 & 0 & 0 & 0 & 0 & 0 & 1 & 0 & 0 & 0 & i & 0 & 0 & 0 \\
0 & 0 & 0 & 0 & i & 0 & 0 & 0 & 0 & 1 & 0 & 0 & 0 & 0 & 0 & 0 \\
0 & 0 & 0 & 0 & 0 & 0 & 0 & 0 & 0 & 0 & 1 & 0 & 0 & 0 & i & 0 \\
0 & 0 & 0 & 0 & 0 & 0 & i & 0 & 0 & 0 & 0 & 1 & 0 & 0 & 0 & 0 \\
0 & 0 & 0 & 0 & 0 & 0 & 0 & 0 & i & 0 & 0 & 0 & 1 & 0 & 0 & 0 \\
0 & 0 & 0 & 0 & 0 & 0 & 0 & 0 & 0 & 0 & 0 & 0 & 0 & 1 & 0 & i \\
0 & 0 & 0 & 0 & 0 & 0 & 0 & 0 & 0 & 0 & i & 0 & 0 & 0 & 1 & 0 \\
0 & 0 & 0 & 0 & 0 & 0 & 0 & 0 & 0 & 0 & 0 & 0 & 0 & i & 0 & 1
\end{pmatrix} \tag{B.15}$$

$$\mathbf{R}_y^s\left(\frac{\pi}{2}\right) = \frac{1}{\sqrt{2}}\begin{pmatrix}
1 & 0 & 1 & 0 & 0 & 0 & 0 & 0 & 0 & 0 & 0 & 0 & 0 & 0 & 0 & 0 \\
0 & 1 & 0 & 0 & 0 & 1 & 0 & 0 & 0 & 0 & 0 & 0 & 0 & 0 & 0 & 0 \\
-1 & 0 & 1 & 0 & 0 & 0 & 0 & 0 & 0 & 0 & 0 & 0 & 0 & 0 & 0 & 0 \\
0 & 0 & 0 & 1 & 0 & 0 & 0 & 1 & 0 & 0 & 0 & 0 & 0 & 0 & 0 & 0 \\
0 & 0 & 0 & 0 & 1 & 0 & 0 & 0 & 0 & 1 & 0 & 0 & 0 & 0 & 0 & 0 \\
0 & -1 & 0 & 0 & 0 & 1 & 0 & 0 & 0 & 0 & 0 & 0 & 0 & 0 & 0 & 0 \\
0 & 0 & 0 & 0 & 0 & 0 & 1 & 0 & 0 & 0 & 0 & 1 & 0 & 0 & 0 & 0 \\
0 & 0 & 0 & -1 & 0 & 0 & 0 & 1 & 0 & 0 & 0 & 0 & 0 & 0 & 0 & 0 \\
0 & 0 & 0 & 0 & 0 & 0 & 0 & 0 & 1 & 0 & 0 & 0 & 1 & 0 & 0 & 0 \\
0 & 0 & 0 & 0 & -1 & 0 & 0 & 0 & 0 & 1 & 0 & 0 & 0 & 0 & 0 & 0 \\
0 & 0 & 0 & 0 & 0 & 0 & 0 & 0 & 0 & 0 & 1 & 0 & 0 & 0 & 1 & 0 \\
0 & 0 & 0 & 0 & 0 & 0 & -1 & 0 & 0 & 0 & 0 & 1 & 0 & 0 & 0 & 0 \\
0 & 0 & 0 & 0 & 0 & 0 & 0 & 0 & -1 & 0 & 0 & 0 & 1 & 0 & 0 & 0 \\
0 & 0 & 0 & 0 & 0 & 0 & 0 & 0 & 0 & 0 & 0 & 0 & 0 & 1 & 0 & 1 \\
0 & 0 & 0 & 0 & 0 & 0 & 0 & 0 & 0 & 0 & -1 & 0 & 0 & 0 & 1 & 0 \\
0 & 0 & 0 & 0 & 0 & 0 & 0 & 0 & 0 & 0 & 0 & 0 & 0 & -1 & 0 & 1
\end{pmatrix} \tag{B.16}$$

$$\mathbf{R}_{x}^{R}\left(\frac{\pi}{2}\right) = \frac{1}{\sqrt{2}}\begin{pmatrix}
1 & i & 0 & 0 & 0 & 0 & 0 & 0 & 0 & 0 & 0 & 0 & 0 & 0 & 0 & 0 \\
i & 1 & 0 & 0 & 0 & 0 & 0 & 0 & 0 & 0 & 0 & 0 & 0 & 0 & 0 & 0 \\
0 & 0 & 1 & 0 & 0 & i & 0 & 0 & 0 & 0 & 0 & 0 & 0 & 0 & 0 & 0 \\
0 & 0 & 0 & 1 & 0 & 0 & i & 0 & 0 & 0 & 0 & 0 & 0 & 0 & 0 & 0 \\
0 & 0 & 0 & 0 & 1 & 0 & 0 & 0 & i & 0 & 0 & 0 & 0 & 0 & 0 & 0 \\
0 & 0 & i & 0 & 0 & 1 & 0 & 0 & 0 & 0 & 0 & 0 & 0 & 0 & 0 & 0 \\
0 & 0 & 0 & i & 0 & 0 & 1 & 0 & 0 & 0 & 0 & 0 & 0 & 0 & 0 & 0 \\
0 & 0 & 0 & 0 & 0 & 0 & 0 & 1 & 0 & 0 & 0 & i & 0 & 0 & 0 & 0 \\
0 & 0 & 0 & 0 & i & 0 & 0 & 0 & 1 & 0 & 0 & 0 & 0 & 0 & 0 & 0 \\
0 & 0 & 0 & 0 & 0 & 0 & 0 & 0 & 0 & 1 & 0 & 0 & i & 0 & 0 & 0 \\
0 & 0 & 0 & 0 & 0 & 0 & 0 & 0 & 0 & 0 & 1 & 0 & 0 & i & 0 & 0 \\
0 & 0 & 0 & 0 & 0 & 0 & 0 & i & 0 & 0 & 0 & 1 & 0 & 0 & 0 & 0 \\
0 & 0 & 0 & 0 & 0 & 0 & 0 & 0 & 0 & i & 0 & 0 & 1 & 0 & 0 & 0 \\
0 & 0 & 0 & 0 & 0 & 0 & 0 & 0 & 0 & 0 & i & 0 & 0 & 1 & 0 & 0 \\
0 & 0 & 0 & 0 & 0 & 0 & 0 & 0 & 0 & 0 & 0 & 0 & 0 & 0 & 1 & i \\
0 & 0 & 0 & 0 & 0 & 0 & 0 & 0 & 0 & 0 & 0 & 0 & 0 & 0 & i & 1
\end{pmatrix} \tag{B.17}$$

$$\mathbf{R}_{y}^{R}\left(\frac{\pi}{2}\right) = \frac{1}{\sqrt{2}}\begin{pmatrix}
1 & 1 & 0 & 0 & 0 & 0 & 0 & 0 & 0 & 0 & 0 & 0 & 0 & 0 & 0 & 0 \\
-1 & 1 & 0 & 0 & 0 & 0 & 0 & 0 & 0 & 0 & 0 & 0 & 0 & 0 & 0 & 0 \\
0 & 0 & 1 & 0 & 0 & 1 & 0 & 0 & 0 & 0 & 0 & 0 & 0 & 0 & 0 & 0 \\
0 & 0 & 0 & 1 & 0 & 0 & 1 & 0 & 0 & 0 & 0 & 0 & 0 & 0 & 0 & 0 \\
0 & 0 & 0 & 0 & 1 & 0 & 0 & 0 & 1 & 0 & 0 & 0 & 0 & 0 & 0 & 0 \\
0 & 0 & -1 & 0 & 0 & 1 & 0 & 0 & 0 & 0 & 0 & 0 & 0 & 0 & 0 & 0 \\
0 & 0 & 0 & -1 & 0 & 0 & 1 & 0 & 0 & 0 & 0 & 0 & 0 & 0 & 0 & 0 \\
0 & 0 & 0 & 0 & 0 & 0 & 0 & 1 & 0 & 0 & 0 & 1 & 0 & 0 & 0 & 0 \\
0 & 0 & 0 & 0 & -1 & 0 & 0 & 0 & 1 & 0 & 0 & 0 & 0 & 0 & 0 & 0 \\
0 & 0 & 0 & 0 & 0 & 0 & 0 & 0 & 0 & 1 & 0 & 0 & 1 & 0 & 0 & 0 \\
0 & 0 & 0 & 0 & 0 & 0 & 0 & 0 & 0 & 0 & 1 & 0 & 0 & 1 & 0 & 0 \\
0 & 0 & 0 & 0 & 0 & 0 & 0 & -1 & 0 & 0 & 0 & 1 & 0 & 0 & 0 & 0 \\
0 & 0 & 0 & 0 & 0 & 0 & 0 & 0 & 0 & -1 & 0 & 0 & 1 & 0 & 0 & 0 \\
0 & 0 & 0 & 0 & 0 & 0 & 0 & 0 & 0 & 0 & -1 & 0 & 0 & 1 & 0 & 0 \\
0 & 0 & 0 & 0 & 0 & 0 & 0 & 0 & 0 & 0 & 0 & 0 & 0 & 0 & 1 & 1 \\
0 & 0 & 0 & 0 & 0 & 0 & 0 & 0 & 0 & 0 & 0 & 0 & 0 & 0 & -1 & 1
\end{pmatrix} \tag{B.18}$$

B.2.3. 180 degree rotations for protons

Propagators listed below are the operators that rotate the protons by 180 ºaround either x or y axis.

$$\mathbf{R}_x^{\mathbf{I}}(\pi) =$$

$$\begin{pmatrix}
0 & 0 & 0 & 0 & 0 & 0 & 0 & 0 & 0 & 0 & -1 & 0 & 0 & 0 & 0 & 0 \\
0 & 0 & 0 & 0 & 0 & 0 & 0 & 0 & 0 & 0 & 0 & 0 & 0 & -1 & 0 & 0 \\
0 & 0 & 0 & 0 & 0 & 0 & 0 & 0 & 0 & 0 & 0 & 0 & 0 & 0 & -1 & 0 \\
0 & 0 & 0 & 0 & -1 & 0 & 0 & 0 & 0 & 0 & 0 & 0 & 0 & 0 & 0 & 0 \\
0 & 0 & 0 & -1 & 0 & 0 & 0 & 0 & 0 & 0 & 0 & 0 & 0 & 0 & 0 & 0 \\
0 & 0 & 0 & 0 & 0 & 0 & 0 & 0 & 0 & 0 & 0 & 0 & 0 & 0 & 0 & -1 \\
0 & 0 & 0 & 0 & 0 & 0 & 0 & 0 & -1 & 0 & 0 & 0 & 0 & 0 & 0 & 0 \\
0 & 0 & 0 & 0 & 0 & 0 & 0 & 0 & 0 & -1 & 0 & 0 & 0 & 0 & 0 & 0 \\
0 & 0 & 0 & 0 & 0 & 0 & -1 & 0 & 0 & 0 & 0 & 0 & 0 & 0 & 0 & 0 \\
0 & 0 & 0 & 0 & 0 & 0 & 0 & -1 & 0 & 0 & 0 & 0 & 0 & 0 & 0 & 0 \\
-1 & 0 & 0 & 0 & 0 & 0 & 0 & 0 & 0 & 0 & 0 & 0 & 0 & 0 & 0 & 0 \\
0 & 0 & 0 & 0 & 0 & 0 & 0 & 0 & 0 & 0 & 0 & 0 & -1 & 0 & 0 & 0 \\
0 & 0 & 0 & 0 & 0 & 0 & 0 & 0 & 0 & 0 & 0 & -1 & 0 & 0 & 0 & 0 \\
0 & -1 & 0 & 0 & 0 & 0 & 0 & 0 & 0 & 0 & 0 & 0 & 0 & 0 & 0 & 0 \\
0 & 0 & -1 & 0 & 0 & 0 & 0 & 0 & 0 & 0 & 0 & 0 & 0 & 0 & 0 & 0 \\
0 & 0 & 0 & 0 & 0 & -1 & 0 & 0 & 0 & 0 & 0 & 0 & 0 & 0 & 0 & 0
\end{pmatrix} \quad \text{(B.19)}$$

$$\mathbf{R}_y^{\mathbf{I}}(\pi) =$$

$$\begin{pmatrix}
0 & 0 & 0 & 0 & 0 & 0 & 0 & 0 & 0 & 0 & 1 & 0 & 0 & 0 & 0 & 0 \\
0 & 0 & 0 & 0 & 0 & 0 & 0 & 0 & 0 & 0 & 0 & 0 & 0 & 1 & 0 & 0 \\
0 & 0 & 0 & 0 & 0 & 0 & 0 & 0 & 0 & 0 & 0 & 0 & 0 & 0 & 1 & 0 \\
0 & 0 & 0 & 0 & -1 & 0 & 0 & 0 & 0 & 0 & 0 & 0 & 0 & 0 & 0 & 0 \\
0 & 0 & 0 & -1 & 0 & 0 & 0 & 0 & 0 & 0 & 0 & 0 & 0 & 0 & 0 & 0 \\
0 & 0 & 0 & 0 & 0 & 0 & 0 & 0 & 0 & 0 & 0 & 0 & 0 & 0 & 0 & 1 \\
0 & 0 & 0 & 0 & 0 & 0 & 0 & 0 & -1 & 0 & 0 & 0 & 0 & 0 & 0 & 0 \\
0 & 0 & 0 & 0 & 0 & 0 & 0 & 0 & 0 & -1 & 0 & 0 & 0 & 0 & 0 & 0 \\
0 & 0 & 0 & 0 & 0 & 0 & -1 & 0 & 0 & 0 & 0 & 0 & 0 & 0 & 0 & 0 \\
0 & 0 & 0 & 0 & 0 & 0 & 0 & -1 & 0 & 0 & 0 & 0 & 0 & 0 & 0 & 0 \\
1 & 0 & 0 & 0 & 0 & 0 & 0 & 0 & 0 & 0 & 0 & 0 & 0 & 0 & 0 & 0 \\
0 & 0 & 0 & 0 & 0 & 0 & 0 & 0 & 0 & 0 & 0 & 0 & -1 & 0 & 0 & 0 \\
0 & 0 & 0 & 0 & 0 & 0 & 0 & 0 & 0 & 0 & 0 & -1 & 0 & 0 & 0 & 0 \\
0 & 1 & 0 & 0 & 0 & 0 & 0 & 0 & 0 & 0 & 0 & 0 & 0 & 0 & 0 & 0 \\
0 & 0 & 1 & 0 & 0 & 0 & 0 & 0 & 0 & 0 & 0 & 0 & 0 & 0 & 0 & 0 \\
0 & 0 & 0 & 0 & 0 & 1 & 0 & 0 & 0 & 0 & 0 & 0 & 0 & 0 & 0 & 0
\end{pmatrix} \qquad \text{(B.20)}$$

B.2.4. 180 degree rotations for heteronuclei

Propagators listed below are the operators that rotate the heteronuclei (S or R) by 180 ºaround either x or y axis.

$$\mathbf{R}_x^S(\pi) = \begin{pmatrix}
0 & 0 & i & 0 & 0 & 0 & 0 & 0 & 0 & 0 & 0 & 0 & 0 & 0 & 0 & 0 \\
0 & 0 & 0 & 0 & 0 & i & 0 & 0 & 0 & 0 & 0 & 0 & 0 & 0 & 0 & 0 \\
i & 0 & 0 & 0 & 0 & 0 & 0 & 0 & 0 & 0 & 0 & 0 & 0 & 0 & 0 & 0 \\
0 & 0 & 0 & 0 & 0 & 0 & 0 & i & 0 & 0 & 0 & 0 & 0 & 0 & 0 & 0 \\
0 & 0 & 0 & 0 & 0 & 0 & 0 & 0 & 0 & i & 0 & 0 & 0 & 0 & 0 & 0 \\
0 & i & 0 & 0 & 0 & 0 & 0 & 0 & 0 & 0 & 0 & 0 & 0 & 0 & 0 & 0 \\
0 & 0 & 0 & 0 & 0 & 0 & 0 & 0 & 0 & 0 & 0 & i & 0 & 0 & 0 & 0 \\
0 & 0 & 0 & i & 0 & 0 & 0 & 0 & 0 & 0 & 0 & 0 & 0 & 0 & 0 & 0 \\
0 & 0 & 0 & 0 & 0 & 0 & 0 & 0 & 0 & 0 & 0 & 0 & i & 0 & 0 & 0 \\
0 & 0 & 0 & 0 & i & 0 & 0 & 0 & 0 & 0 & 0 & 0 & 0 & 0 & 0 & 0 \\
0 & 0 & 0 & 0 & 0 & 0 & 0 & 0 & 0 & 0 & 0 & 0 & 0 & 0 & i & 0 \\
0 & 0 & 0 & 0 & 0 & 0 & i & 0 & 0 & 0 & 0 & 0 & 0 & 0 & 0 & 0 \\
0 & 0 & 0 & 0 & 0 & 0 & 0 & 0 & i & 0 & 0 & 0 & 0 & 0 & 0 & 0 \\
0 & 0 & 0 & 0 & 0 & 0 & 0 & 0 & 0 & 0 & 0 & 0 & 0 & 0 & 0 & i \\
0 & 0 & 0 & 0 & 0 & 0 & 0 & 0 & 0 & 0 & i & 0 & 0 & 0 & 0 & 0 \\
0 & 0 & 0 & 0 & 0 & 0 & 0 & 0 & 0 & 0 & 0 & 0 & 0 & i & 0 & 0
\end{pmatrix} \quad \text{(B.21)}$$

$$\mathbf{R}_y^S(\pi) = \begin{pmatrix}
0 & 0 & 1 & 0 & 0 & 0 & 0 & 0 & 0 & 0 & 0 & 0 & 0 & 0 & 0 & 0 \\
0 & 0 & 0 & 0 & 0 & 1 & 0 & 0 & 0 & 0 & 0 & 0 & 0 & 0 & 0 & 0 \\
-1 & 0 & 0 & 0 & 0 & 0 & 0 & 0 & 0 & 0 & 0 & 0 & 0 & 0 & 0 & 0 \\
0 & 0 & 0 & 0 & 0 & 0 & 0 & 1 & 0 & 0 & 0 & 0 & 0 & 0 & 0 & 0 \\
0 & 0 & 0 & 0 & 0 & 0 & 0 & 0 & 0 & 1 & 0 & 0 & 0 & 0 & 0 & 0 \\
0 & -1 & 0 & 0 & 0 & 0 & 0 & 0 & 0 & 0 & 0 & 0 & 0 & 0 & 0 & 0 \\
0 & 0 & 0 & 0 & 0 & 0 & 0 & 0 & 0 & 0 & 0 & 1 & 0 & 0 & 0 & 0 \\
0 & 0 & 0 & -1 & 0 & 0 & 0 & 0 & 0 & 0 & 0 & 0 & 0 & 0 & 0 & 0 \\
0 & 0 & 0 & 0 & 0 & 0 & 0 & 0 & 0 & 0 & 0 & 0 & 1 & 0 & 0 & 0 \\
0 & 0 & 0 & 0 & -1 & 0 & 0 & 0 & 0 & 0 & 0 & 0 & 0 & 0 & 0 & 0 \\
0 & 0 & 0 & 0 & 0 & 0 & 0 & 0 & 0 & 0 & 0 & 0 & 0 & 0 & 1 & 0 \\
0 & 0 & 0 & 0 & 0 & 0 & -1 & 0 & 0 & 0 & 0 & 0 & 0 & 0 & 0 & 0 \\
0 & 0 & 0 & 0 & 0 & 0 & 0 & 0 & -1 & 0 & 0 & 0 & 0 & 0 & 0 & 0 \\
0 & 0 & 0 & 0 & 0 & 0 & 0 & 0 & 0 & 0 & 0 & 0 & 0 & 0 & 0 & 1 \\
0 & 0 & 0 & 0 & 0 & 0 & 0 & 0 & 0 & 0 & -1 & 0 & 0 & 0 & 0 & 0 \\
0 & 0 & 0 & 0 & 0 & 0 & 0 & 0 & 0 & 0 & 0 & 0 & 0 & -1 & 0 & 0
\end{pmatrix} \quad \text{(B.22)}$$

$$\mathbf{R}_x^{\mathbf{R}}(\pi) =$$

$$\begin{pmatrix}
0 & i & 0 & 0 & 0 & 0 & 0 & 0 & 0 & 0 & 0 & 0 & 0 & 0 & 0 & 0 \\
i & 0 & 0 & 0 & 0 & 0 & 0 & 0 & 0 & 0 & 0 & 0 & 0 & 0 & 0 & 0 \\
0 & 0 & 0 & 0 & 0 & i & 0 & 0 & 0 & 0 & 0 & 0 & 0 & 0 & 0 & 0 \\
0 & 0 & 0 & 0 & 0 & 0 & i & 0 & 0 & 0 & 0 & 0 & 0 & 0 & 0 & 0 \\
0 & 0 & 0 & 0 & 0 & 0 & 0 & 0 & i & 0 & 0 & 0 & 0 & 0 & 0 & 0 \\
0 & 0 & i & 0 & 0 & 0 & 0 & 0 & 0 & 0 & 0 & 0 & 0 & 0 & 0 & 0 \\
0 & 0 & 0 & i & 0 & 0 & 0 & 0 & 0 & 0 & 0 & 0 & 0 & 0 & 0 & 0 \\
0 & 0 & 0 & 0 & 0 & 0 & 0 & 0 & 0 & 0 & 0 & i & 0 & 0 & 0 & 0 \\
0 & 0 & 0 & 0 & i & 0 & 0 & 0 & 0 & 0 & 0 & 0 & 0 & 0 & 0 & 0 \\
0 & 0 & 0 & 0 & 0 & 0 & 0 & 0 & 0 & 0 & 0 & 0 & i & 0 & 0 & 0 \\
0 & 0 & 0 & 0 & 0 & 0 & 0 & 0 & 0 & 0 & 0 & 0 & 0 & i & 0 & 0 \\
0 & 0 & 0 & 0 & 0 & 0 & 0 & i & 0 & 0 & 0 & 0 & 0 & 0 & 0 & 0 \\
0 & 0 & 0 & 0 & 0 & 0 & 0 & 0 & 0 & i & 0 & 0 & 0 & 0 & 0 & 0 \\
0 & 0 & 0 & 0 & 0 & 0 & 0 & 0 & 0 & 0 & i & 0 & 0 & 0 & 0 & 0 \\
0 & 0 & 0 & 0 & 0 & 0 & 0 & 0 & 0 & 0 & 0 & 0 & 0 & 0 & 0 & i \\
0 & 0 & 0 & 0 & 0 & 0 & 0 & 0 & 0 & 0 & 0 & 0 & 0 & 0 & i & 0
\end{pmatrix} \qquad \text{(B.23)}$$

$$\mathbf{R}_y^{\mathbf{R}}(\pi) =$$

$$\begin{pmatrix}
0 & 1 & 0 & 0 & 0 & 0 & 0 & 0 & 0 & 0 & 0 & 0 & 0 & 0 & 0 & 0 \\
-1 & 0 & 0 & 0 & 0 & 0 & 0 & 0 & 0 & 0 & 0 & 0 & 0 & 0 & 0 & 0 \\
0 & 0 & 0 & 0 & 0 & 1 & 0 & 0 & 0 & 0 & 0 & 0 & 0 & 0 & 0 & 0 \\
0 & 0 & 0 & 0 & 0 & 0 & 1 & 0 & 0 & 0 & 0 & 0 & 0 & 0 & 0 & 0 \\
0 & 0 & 0 & 0 & 0 & 0 & 0 & 0 & 1 & 0 & 0 & 0 & 0 & 0 & 0 & 0 \\
0 & 0 & -1 & 0 & 0 & 0 & 0 & 0 & 0 & 0 & 0 & 0 & 0 & 0 & 0 & 0 \\
0 & 0 & 0 & -1 & 0 & 0 & 0 & 0 & 0 & 0 & 0 & 0 & 0 & 0 & 0 & 0 \\
0 & 0 & 0 & 0 & 0 & 0 & 0 & 0 & 0 & 0 & 0 & 1 & 0 & 0 & 0 & 0 \\
0 & 0 & 0 & 0 & -1 & 0 & 0 & 0 & 0 & 0 & 0 & 0 & 0 & 0 & 0 & 0 \\
0 & 0 & 0 & 0 & 0 & 0 & 0 & 0 & 0 & 0 & 0 & 0 & 1 & 0 & 0 & 0 \\
0 & 0 & 0 & 0 & 0 & 0 & 0 & 0 & 0 & 0 & 0 & 0 & 0 & 1 & 0 & 0 \\
0 & 0 & 0 & 0 & 0 & 0 & 0 & -1 & 0 & 0 & 0 & 0 & 0 & 0 & 0 & 0 \\
0 & 0 & 0 & 0 & 0 & 0 & 0 & 0 & 0 & -1 & 0 & 0 & 0 & 0 & 0 & 0 \\
0 & 0 & 0 & 0 & 0 & 0 & 0 & 0 & 0 & 0 & -1 & 0 & 0 & 0 & 0 & 0 \\
0 & 0 & 0 & 0 & 0 & 0 & 0 & 0 & 0 & 0 & 0 & 0 & 0 & 0 & 0 & 1 \\
0 & 0 & 0 & 0 & 0 & 0 & 0 & 0 & 0 & 0 & 0 & 0 & 0 & 0 & -1 & 0
\end{pmatrix} \qquad \text{(B.24)}$$

B.3 Hamiltonian and related states

B.3.1. Hamiltonian

The Hamiltonian of the I_1I_2SR spin system, as stated in section 3.3, is:

$$
H = 2\pi \begin{pmatrix}
\frac{1}{4}(J_{12}+J_{1S}+J_{1R}+J_{2S}+J_{2R}+J_{SR}) & 0 & 0 & 0 \\
0 & \frac{1}{4}(J_{12}+J_{1S}-J_{1R}+J_{2S}-J_{2R}-J_{SR}) & 0 & 0 \\
0 & 0 & \frac{1}{4}(J_{12}-J_{1S}+J_{1R}-J_{2S}+J_{2R}-J_{SR}) & 0 \\
0 & 0 & 0 & \frac{1}{4}(-J_{12}+J_{1S}+J_{1R}-J_{2S}-J_{2R}+J_{SR}) \\
0 & 0 & 0 & \frac{1}{2}J_{12} \\
0 & 0 & 0 & 0 \\
0 & 0 & 0 & 0 \\
0 & 0 & 0 & 0 \\
0 & 0 & 0 & 0 \\
0 & 0 & 0 & 0 \\
0 & 0 & 0 & 0 \\
0 & 0 & 0 & 0 \\
0 & 0 & 0 & 0 \\
0 & 0 & 0 & 0 \\
0 & 0 & 0 & 0 \\
0 & 0 & 0 & 0
\end{pmatrix}
$$

$$
\begin{pmatrix}
0 & 0 & 0 & 0 \\
0 & 0 & 0 & 0 \\
0 & 0 & 0 & 0 \\
\frac{1}{2}J_{12} & 0 & 0 & 0 \\
\frac{1}{4}(-J_{12}-J_{1S}-J_{1R}+J_{2S}+J_{2R}+J_{SR}) & 0 & 0 & 0 \\
0 & \frac{1}{4}(J_{12}-J_{1S}-J_{1R}-J_{2S}-J_{2R}+J_{SR}) & 0 & 0 \\
0 & 0 & \frac{1}{4}(-J_{12}+J_{1S}-J_{1R}-J_{2S}+J_{2R}-J_{SR}) & 0 \\
0 & 0 & 0 & \frac{1}{4}(-J_{12}-J_{1S}+J_{1R}+J_{2S}+-J_{2R}-J_{SR}) \\
0 & 0 & \frac{1}{2}J_{12} & 0 \\
0 & 0 & 0 & \frac{1}{2}J_{12} \\
0 & 0 & 0 & 0 \\
0 & 0 & 0 & 0 \\
0 & 0 & 0 & 0 \\
0 & 0 & 0 & 0 \\
0 & 0 & 0 & 0 \\
0 & 0 & 0 & 0
\end{pmatrix}
$$

$$
\begin{pmatrix}
0 & 0 & 0 & 0 \\
0 & 0 & 0 & 0 \\
0 & 0 & 0 & 0 \\
0 & 0 & 0 & 0 \\
0 & 0 & 0 & 0 \\
0 & 0 & 0 & 0 \\
\frac{1}{2}J_{12} & 0 & 0 & 0 \\
0 & \frac{1}{2}J_{12} & 0 & 0 \\
\frac{1}{4}(-J_{12}-J_{1S}+J_{1R}+J_{2S}-J_{2R}-J_{SR}) & 0 & 0 & 0 \\
0 & \frac{1}{4}(-J_{12}+J_{1S}-J_{1R}-J_{2S}+J_{2R}-J_{SR}) & 0 & 0 \\
0 & 0 & \frac{1}{4}(J_{12}-J_{1S}-J_{1R}-J_{2S}-J_{2R}+J_{SR}) & 0 \\
0 & 0 & 0 & \frac{1}{4}(-J_{12}-J_{1S}-J_{1R}+J_{2S}+J_{2R}+J_{SR}) \\
0 & 0 & 0 & \frac{1}{2}J_{12} \\
0 & 0 & 0 & 0 \\
0 & 0 & 0 & 0 \\
0 & 0 & 0 & 0
\end{pmatrix}
$$

$$
\begin{pmatrix}
0 & 0 & 0 & 0 \\
0 & 0 & 0 & 0 \\
0 & 0 & 0 & 0 \\
0 & 0 & 0 & 0 \\
0 & 0 & 0 & 0 \\
0 & 0 & 0 & 0 \\
0 & 0 & 0 & 0 \\
0 & 0 & 0 & 0 \\
0 & 0 & 0 & 0 \\
0 & 0 & 0 & 0 \\
0 & 0 & 0 & 0 \\
\frac{1}{2}J_{12} & 0 & 0 & 0 \\
\frac{1}{4}(-J_{12}+J_{1S}+J_{1R}-J_{2S}-J_{2R}+J_{SR}) & 0 & 0 & 0 \\
0 & \frac{1}{4}(J_{12}-J_{1S}+J_{1R}-J_{2S}+J_{2R}-J_{SR}) & 0 & 0 \\
0 & 0 & \frac{1}{4}(J_{12}+J_{1S}-J_{1R}+J_{2S}-J_{2R}-J_{SR}) & 0 \\
0 & 0 & 0 & \frac{1}{4}(J_{12}+J_{1S}+J_{1R}+J_{2S}+J_{2R}+J_{SR})
\end{pmatrix}
$$

(B.25)

The eigenvalues and eigenfunctions of the Hamiltonian could then be calculated.

The eigenvalues of the J coupling Hamiltonian for the AA'XY spin systems are:

$$\lambda_1 = \frac{1}{4}(J_{12} + J_{1S} + J_{1R} + J_{2S} + J_{2R} + J_{SR})$$

$$\lambda_2 = \frac{1}{4}(J_{12} + J_{1S} - J_{1R} + J_{2S} - J_{2R} - J_{SR})$$

$$\lambda_3 = \frac{1}{4}(J_{12} - J_{1S} + J_{1R} - J_{2S} + J_{2R} - J_{SR})$$

$$\lambda_4 = \frac{1}{4}(J_{12} - J_{1S} - J_{1R} - J_{2S} - J_{2R} + J_{SR})$$

$$\lambda_5 = \frac{1}{4}[-J_{12} - \sqrt{4J_{12}^2 + (J_{1S} - J_{1R})^2 - 2J_{1S}J_{2S} + 2J_{1R}J_{2S} + (J_{2S} - J_{2R})^2 + 2J_{1S}J_{2R} - 2J_{1R}J_{2R}} - J_{SR}]$$

$$\lambda_6 = \frac{1}{4}[-J_{12} + \sqrt{4J_{12}^2 + (J_{1S} - J_{1R})^2 - 2J_{1S}J_{2S} + 2J_{1R}J_{2S} + (J_{2S} - J_{2R})^2 + 2J_{1S}J_{2R} - 2J_{1R}J_{2R}} - J_{SR}]$$

$$\lambda_7 = \frac{1}{4}[-J_{12} - \sqrt{4J_{12}^2 + (J_{1S} + J_{1R})^2 - 2J_{1S}J_{2S} - 2J_{1R}J_{2S} + (J_{2S} + J_{2R})^2 - 2J_{1S}J_{2R} - 2J_{1R}J_{2R}} - J_{SR}]$$

$$\lambda_8 = \frac{1}{4}[-J_{12} + \sqrt{4J_{12}^2 + (J_{1S} + J_{1R})^2 - 2J_{1S}J_{2S} - 2J_{1R}J_{2S} + (J_{2S} + J_{2R})^2 - 2J_{1S}J_{2R} - 2J_{1R}J_{2R}} - J_{SR}]$$

(B.26)

The corresponding eigenfunctions are:

$$
\begin{aligned}
&\lambda_1 \begin{cases} j_1 = |\alpha\alpha\alpha\alpha> \\ j_2 = |\beta\beta\beta\beta> \end{cases} \\
&\lambda_2 \begin{cases} j_3 = |\alpha\alpha\alpha\beta> \\ j_4 = |\beta\beta\beta\alpha> \end{cases} \\
&\lambda_3 \begin{cases} j_5 = |\alpha\alpha\beta\alpha> \\ j_6 = |\beta\beta\alpha\beta> \end{cases} \\
&\lambda_4 \begin{cases} j_7 = |\alpha\alpha\beta\beta> \\ j_8 = |\beta\beta\alpha\alpha> \end{cases} \\
&\lambda_5 \begin{cases} j_9 = \dfrac{\gamma_2}{\sqrt{1+\gamma_2^2}}|\alpha\beta\alpha\beta> - \dfrac{1}{\sqrt{1+\gamma_2^2}}|\beta\alpha\alpha\beta> \\ j_{10} = \dfrac{1}{\sqrt{1+\gamma_2^2}}|\alpha\beta\beta\alpha> - \dfrac{\gamma_2}{\sqrt{1+\gamma_2^2}}|\beta\alpha\beta\alpha> \end{cases} \\
&\lambda_6 \begin{cases} j_{11} = -\dfrac{1}{\sqrt{1+\gamma_2^2}}|\alpha\beta\alpha\beta> - \dfrac{\gamma_2}{\sqrt{1+\gamma_2^2}}|\beta\alpha\alpha\beta> \\ j_{12} = -\dfrac{\gamma_2}{\sqrt{1+\gamma_2^2}}|\alpha\beta\beta\alpha> - \dfrac{1}{\sqrt{1+\gamma_2^2}}|\beta\alpha\beta\alpha> \end{cases} \\
&\lambda_7 \begin{cases} j_{13} = \dfrac{\gamma_1}{\sqrt{1+\gamma_1^2}}|\alpha\beta\alpha\alpha> - \dfrac{1}{\sqrt{1+\gamma_1^2}}|\beta\alpha\alpha\alpha> \\ j_{14} = -\dfrac{1}{\sqrt{1+\gamma_1^2}}|\alpha\beta\beta\beta> + \dfrac{\gamma_1}{\sqrt{1+\gamma_1^2}}|\beta\alpha\beta\beta> \end{cases} \\
&\lambda_8 \begin{cases} j_{15} = -\dfrac{1}{\sqrt{1+\gamma_1^2}}|\alpha\beta\alpha\alpha> - \dfrac{\gamma_1}{\sqrt{1+\gamma_2^2}}|\beta\alpha\alpha\alpha> \\ j_{16} = \dfrac{\gamma_1}{\sqrt{1+\gamma_1^2}}|\alpha\beta\beta\beta> + \dfrac{1}{\sqrt{1+\gamma_1^2}}|\beta\alpha\beta\beta> \end{cases} \\
&\begin{pmatrix} \gamma_1 = \sqrt{1+\Delta_1^2} - \Delta_1 & \gamma_2 = \sqrt{1+\Delta_2^2} - \Delta_2 \\ \Delta_1 = \dfrac{J_{1S} + J_{1R} - J_{2S} - J_{2R}}{2J_{12}} & \Delta_2 = \dfrac{J_{1S} - J_{1R} - J_{2S} + J_{2R}}{2J_{12}} \end{pmatrix}
\end{aligned}
\tag{B.27}
$$

By using the eigenvalues and eigenfunctions the evolution of states for the I_1I_2SR spin systems can then be studied.

B.3.2. Related states

The initial singlet-state, $\boldsymbol{\sigma_0}$, is:

$$\boldsymbol{\sigma}_0 = \frac{1}{2}\begin{pmatrix}
0&0&0&0&0&0&0&0&0&0&0&0&0&0&0&0\\
0&0&0&0&0&0&0&0&0&0&0&0&0&0&0&0\\
0&0&0&0&0&0&0&0&0&0&0&0&0&0&0&0\\
0&0&0&0&1&0&0&0&0&0&0&0&0&0&0&0\\
0&0&0&1&0&0&0&0&0&0&0&0&0&0&0&0\\
0&0&0&0&0&0&0&0&0&0&0&0&0&0&0&0\\
0&0&0&0&0&0&0&0&1&0&0&0&0&0&0&0\\
0&0&0&0&0&0&0&0&0&1&0&0&0&0&0&0\\
0&0&0&0&0&0&1&0&0&0&0&0&0&0&0&0\\
0&0&0&0&0&0&0&1&0&0&0&0&0&0&0&0\\
0&0&0&0&0&0&0&0&0&0&0&0&0&0&0&0\\
0&0&0&0&0&0&0&0&0&0&0&0&1&0&0&0\\
0&0&0&0&0&0&0&0&0&0&0&1&0&0&0&0\\
0&0&0&0&0&0&0&0&0&0&0&0&0&0&0&0\\
0&0&0&0&0&0&0&0&0&0&0&0&0&0&0&0\\
0&0&0&0&0&0&0&0&0&0&0&0&0&0&0&0
\end{pmatrix} \tag{B.28}$$

The other states showing up in the first step are:

$$4(\mathbf{I}_{1x}\mathbf{I}_{2x} + \mathbf{I}_{1y}\mathbf{I}_{2y})\mathbf{S}_z\mathbf{R}_z =$$

$$\frac{1}{2}\begin{pmatrix}
0&0&0&0&0&0&0&0&0&0&0&0&0&0&0&0\\
0&0&0&0&0&0&0&0&0&0&0&0&0&0&0&0\\
0&0&0&0&0&0&0&0&0&0&0&0&0&0&0&0\\
0&0&0&0&1&0&0&0&0&0&0&0&0&0&0&0\\
0&0&0&1&0&0&0&0&0&0&0&0&0&0&0&0\\
0&0&0&0&0&0&0&0&0&0&0&0&0&0&0&0\\
0&0&0&0&0&0&0&0&-1&0&0&0&0&0&0&0\\
0&0&0&0&0&0&0&0&0&-1&0&0&0&0&0&0\\
0&0&0&0&0&0&-1&0&0&0&0&0&0&0&0&0\\
0&0&0&0&0&0&0&-1&0&0&0&0&0&0&0&0\\
0&0&0&0&0&0&0&0&0&0&0&0&0&0&0&0\\
0&0&0&0&0&0&0&0&0&0&0&0&1&0&0&0\\
0&0&0&0&0&0&0&0&0&0&0&1&0&0&0&0\\
0&0&0&0&0&0&0&0&0&0&0&0&0&0&0&0\\
0&0&0&0&0&0&0&0&0&0&0&0&0&0&0&0\\
0&0&0&0&0&0&0&0&0&0&0&0&0&0&0&0
\end{pmatrix} \tag{B.29}$$

$$2(\mathbf{I}_{1y}\mathbf{I}_{2x} - \mathbf{I}_{1x}\mathbf{I}_{2y})\mathbf{S}_z =$$

$$\frac{1}{2}\begin{pmatrix}
0 & 0 & 0 & 0 & 0 & 0 & 0 & 0 & 0 & 0 & 0 & 0 & 0 & 0 & 0 & 0 \\
0 & 0 & 0 & 0 & 0 & 0 & 0 & 0 & 0 & 0 & 0 & 0 & 0 & 0 & 0 & 0 \\
0 & 0 & 0 & 0 & 0 & 0 & 0 & 0 & 0 & 0 & 0 & 0 & 0 & 0 & 0 & 0 \\
0 & 0 & 0 & 0 & -i & 0 & 0 & 0 & 0 & 0 & 0 & 0 & 0 & 0 & 0 & 0 \\
0 & 0 & 0 & i & 0 & 0 & 0 & 0 & 0 & 0 & 0 & 0 & 0 & 0 & 0 & 0 \\
0 & 0 & 0 & 0 & 0 & 0 & 0 & 0 & 0 & 0 & 0 & 0 & 0 & 0 & 0 & 0 \\
0 & 0 & 0 & 0 & 0 & 0 & 0 & 0 & -i & 0 & 0 & 0 & 0 & 0 & 0 & 0 \\
0 & 0 & 0 & 0 & 0 & 0 & 0 & 0 & 0 & i & 0 & 0 & 0 & 0 & 0 & 0 \\
0 & 0 & 0 & 0 & 0 & 0 & i & 0 & 0 & 0 & 0 & 0 & 0 & 0 & 0 & 0 \\
0 & 0 & 0 & 0 & 0 & 0 & 0 & -i & 0 & 0 & 0 & 0 & 0 & 0 & 0 & 0 \\
0 & 0 & 0 & 0 & 0 & 0 & 0 & 0 & 0 & 0 & 0 & 0 & 0 & 0 & 0 & 0 \\
0 & 0 & 0 & 0 & 0 & 0 & 0 & 0 & 0 & 0 & 0 & 0 & i & 0 & 0 & 0 \\
0 & 0 & 0 & 0 & 0 & 0 & 0 & 0 & 0 & 0 & 0 & -i & 0 & 0 & 0 & 0 \\
0 & 0 & 0 & 0 & 0 & 0 & 0 & 0 & 0 & 0 & 0 & 0 & 0 & 0 & 0 & 0 \\
0 & 0 & 0 & 0 & 0 & 0 & 0 & 0 & 0 & 0 & 0 & 0 & 0 & 0 & 0 & 0 \\
0 & 0 & 0 & 0 & 0 & 0 & 0 & 0 & 0 & 0 & 0 & 0 & 0 & 0 & 0 & 0
\end{pmatrix} \tag{B.30}$$

$$2(\mathbf{I}_{1y}\mathbf{I}_{2x} - \mathbf{I}_{1x}\mathbf{I}_{2y})\mathbf{R}_z =$$

$$\frac{1}{2}\begin{pmatrix}
0 & 0 & 0 & 0 & 0 & 0 & 0 & 0 & 0 & 0 & 0 & 0 & 0 & 0 & 0 & 0 \\
0 & 0 & 0 & 0 & 0 & 0 & 0 & 0 & 0 & 0 & 0 & 0 & 0 & 0 & 0 & 0 \\
0 & 0 & 0 & 0 & 0 & 0 & 0 & 0 & 0 & 0 & 0 & 0 & 0 & 0 & 0 & 0 \\
0 & 0 & 0 & 0 & -i & 0 & 0 & 0 & 0 & 0 & 0 & 0 & 0 & 0 & 0 & 0 \\
0 & 0 & 0 & i & 0 & 0 & 0 & 0 & 0 & 0 & 0 & 0 & 0 & 0 & 0 & 0 \\
0 & 0 & 0 & 0 & 0 & 0 & 0 & 0 & 0 & 0 & 0 & 0 & 0 & 0 & 0 & 0 \\
0 & 0 & 0 & 0 & 0 & 0 & 0 & 0 & i & 0 & 0 & 0 & 0 & 0 & 0 & 0 \\
0 & 0 & 0 & 0 & 0 & 0 & 0 & 0 & 0 & -i & 0 & 0 & 0 & 0 & 0 & 0 \\
0 & 0 & 0 & 0 & 0 & 0 & -i & 0 & 0 & 0 & 0 & 0 & 0 & 0 & 0 & 0 \\
0 & 0 & 0 & 0 & 0 & 0 & 0 & i & 0 & 0 & 0 & 0 & 0 & 0 & 0 & 0 \\
0 & 0 & 0 & 0 & 0 & 0 & 0 & 0 & 0 & 0 & 0 & 0 & 0 & 0 & 0 & 0 \\
0 & 0 & 0 & 0 & 0 & 0 & 0 & 0 & 0 & 0 & 0 & 0 & i & 0 & 0 & 0 \\
0 & 0 & 0 & 0 & 0 & 0 & 0 & 0 & 0 & 0 & 0 & -i & 0 & 0 & 0 & 0 \\
0 & 0 & 0 & 0 & 0 & 0 & 0 & 0 & 0 & 0 & 0 & 0 & 0 & 0 & 0 & 0 \\
0 & 0 & 0 & 0 & 0 & 0 & 0 & 0 & 0 & 0 & 0 & 0 & 0 & 0 & 0 & 0 \\
0 & 0 & 0 & 0 & 0 & 0 & 0 & 0 & 0 & 0 & 0 & 0 & 0 & 0 & 0 & 0
\end{pmatrix} \tag{B.31}$$

$$(\mathbf{I}_{1z} - \mathbf{I}_{2z})\mathbf{S}_z =$$

$$\frac{1}{2}\begin{pmatrix}
0 & 0 & 0 & 0 & 0 & 0 & 0 & 0 & 0 & 0 & 0 & 0 & 0 & 0 & 0 & 0 \\
0 & 0 & 0 & 0 & 0 & 0 & 0 & 0 & 0 & 0 & 0 & 0 & 0 & 0 & 0 & 0 \\
0 & 0 & 0 & 0 & 0 & 0 & 0 & 0 & 0 & 0 & 0 & 0 & 0 & 0 & 0 & 0 \\
0 & 0 & 0 & 1 & 0 & 0 & 0 & 0 & 0 & 0 & 0 & 0 & 0 & 0 & 0 & 0 \\
0 & 0 & 0 & 0 & -1 & 0 & 0 & 0 & 0 & 0 & 0 & 0 & 0 & 0 & 0 & 0 \\
0 & 0 & 0 & 0 & 0 & 0 & 0 & 0 & 0 & 0 & 0 & 0 & 0 & 0 & 0 & 0 \\
0 & 0 & 0 & 0 & 0 & 0 & 1 & 0 & 0 & 0 & 0 & 0 & 0 & 0 & 0 & 0 \\
0 & 0 & 0 & 0 & 0 & 0 & 0 & -1 & 0 & 0 & 0 & 0 & 0 & 0 & 0 & 0 \\
0 & 0 & 0 & 0 & 0 & 0 & 0 & 0 & -1 & 0 & 0 & 0 & 0 & 0 & 0 & 0 \\
0 & 0 & 0 & 0 & 0 & 0 & 0 & 0 & 0 & 1 & 0 & 0 & 0 & 0 & 0 & 0 \\
0 & 0 & 0 & 0 & 0 & 0 & 0 & 0 & 0 & 0 & 0 & 0 & 0 & 0 & 0 & 0 \\
0 & 0 & 0 & 0 & 0 & 0 & 0 & 0 & 0 & 0 & 0 & -1 & 0 & 0 & 0 & 0 \\
0 & 0 & 0 & 0 & 0 & 0 & 0 & 0 & 0 & 0 & 0 & 0 & 1 & 0 & 0 & 0 \\
0 & 0 & 0 & 0 & 0 & 0 & 0 & 0 & 0 & 0 & 0 & 0 & 0 & 0 & 0 & 0 \\
0 & 0 & 0 & 0 & 0 & 0 & 0 & 0 & 0 & 0 & 0 & 0 & 0 & 0 & 0 & 0 \\
0 & 0 & 0 & 0 & 0 & 0 & 0 & 0 & 0 & 0 & 0 & 0 & 0 & 0 & 0 & 0
\end{pmatrix} \tag{B.32}$$

$$(\mathbf{I}_{1z} - \mathbf{I}_{2z})\mathbf{R}_z =$$

$$\frac{1}{2}\begin{pmatrix}
0 & 0 & 0 & 0 & 0 & 0 & 0 & 0 & 0 & 0 & 0 & 0 & 0 & 0 & 0 & 0 \\
0 & 0 & 0 & 0 & 0 & 0 & 0 & 0 & 0 & 0 & 0 & 0 & 0 & 0 & 0 & 0 \\
0 & 0 & 0 & 0 & 0 & 0 & 0 & 0 & 0 & 0 & 0 & 0 & 0 & 0 & 0 & 0 \\
0 & 0 & 0 & 1 & 0 & 0 & 0 & 0 & 0 & 0 & 0 & 0 & 0 & 0 & 0 & 0 \\
0 & 0 & 0 & 0 & -1 & 0 & 0 & 0 & 0 & 0 & 0 & 0 & 0 & 0 & 0 & 0 \\
0 & 0 & 0 & 0 & 0 & 0 & 0 & 0 & 0 & 0 & 0 & 0 & 0 & 0 & 0 & 0 \\
0 & 0 & 0 & 0 & 0 & 0 & -1 & 0 & 0 & 0 & 0 & 0 & 0 & 0 & 0 & 0 \\
0 & 0 & 0 & 0 & 0 & 0 & 0 & 1 & 0 & 0 & 0 & 0 & 0 & 0 & 0 & 0 \\
0 & 0 & 0 & 0 & 0 & 0 & 0 & 0 & 1 & 0 & 0 & 0 & 0 & 0 & 0 & 0 \\
0 & 0 & 0 & 0 & 0 & 0 & 0 & 0 & 0 & -1 & 0 & 0 & 0 & 0 & 0 & 0 \\
0 & 0 & 0 & 0 & 0 & 0 & 0 & 0 & 0 & 0 & 0 & 0 & 0 & 0 & 0 & 0 \\
0 & 0 & 0 & 0 & 0 & 0 & 0 & 0 & 0 & 0 & 0 & -1 & 0 & 0 & 0 & 0 \\
0 & 0 & 0 & 0 & 0 & 0 & 0 & 0 & 0 & 0 & 0 & 0 & 1 & 0 & 0 & 0 \\
0 & 0 & 0 & 0 & 0 & 0 & 0 & 0 & 0 & 0 & 0 & 0 & 0 & 0 & 0 & 0 \\
0 & 0 & 0 & 0 & 0 & 0 & 0 & 0 & 0 & 0 & 0 & 0 & 0 & 0 & 0 & 0 \\
0 & 0 & 0 & 0 & 0 & 0 & 0 & 0 & 0 & 0 & 0 & 0 & 0 & 0 & 0 & 0
\end{pmatrix} \tag{B.33}$$

Equation B.32 is the state chosen in the first step. After a 90_y pulse on S the state becomes:

$$\mathbf{S_x}(\mathbf{I_{1z}} - \mathbf{I_{2z}}) =$$

$$\frac{1}{2}\begin{pmatrix}
0 & 0 & 0 & 0 & 0 & 0 & 0 & 0 & 0 & 0 & 0 & 0 & 0 & 0 & 0 & 0 \\
0 & 0 & 0 & 0 & 0 & 0 & 0 & 0 & 0 & 0 & 0 & 0 & 0 & 0 & 0 & 0 \\
0 & 0 & 0 & 0 & 0 & 0 & 0 & 0 & 0 & 0 & 0 & 0 & 0 & 0 & 0 & 0 \\
0 & 0 & 0 & 0 & 0 & 0 & 0 & 1 & 0 & 0 & 0 & 0 & 0 & 0 & 0 & 0 \\
0 & 0 & 0 & 0 & 0 & 0 & 0 & 0 & 0 & -1 & 0 & 0 & 0 & 0 & 0 & 0 \\
0 & 0 & 0 & 0 & 0 & 0 & 0 & 0 & 0 & 0 & 0 & 0 & 0 & 0 & 0 & 0 \\
0 & 0 & 0 & 0 & 0 & 0 & 0 & 0 & 0 & 0 & 0 & 1 & 0 & 0 & 0 & 0 \\
0 & 0 & 0 & 1 & 0 & 0 & 0 & 0 & 0 & 0 & 0 & 0 & 0 & 0 & 0 & 0 \\
0 & 0 & 0 & 0 & 0 & 0 & 0 & 0 & 0 & 0 & 0 & 0 & -1 & 0 & 0 & 0 \\
0 & 0 & 0 & 0 & -1 & 0 & 0 & 0 & 0 & 0 & 0 & 0 & 0 & 0 & 0 & 0 \\
0 & 0 & 0 & 0 & 0 & 0 & 0 & 0 & 0 & 0 & 0 & 0 & 0 & 0 & 0 & 0 \\
0 & 0 & 0 & 0 & 0 & 0 & 1 & 0 & 0 & 0 & 0 & 0 & 0 & 0 & 0 & 0 \\
0 & 0 & 0 & 0 & 0 & 0 & 0 & 0 & -1 & 0 & 0 & 0 & 0 & 0 & 0 & 0 \\
0 & 0 & 0 & 0 & 0 & 0 & 0 & 0 & 0 & 0 & 0 & 0 & 0 & 0 & 0 & 0 \\
0 & 0 & 0 & 0 & 0 & 0 & 0 & 0 & 0 & 0 & 0 & 0 & 0 & 0 & 0 & 0 \\
0 & 0 & 0 & 0 & 0 & 0 & 0 & 0 & 0 & 0 & 0 & 0 & 0 & 0 & 0 & 0
\end{pmatrix} \tag{B.34}$$

The other states showing up in step two are:

$$\mathbf{S}_x(\mathbf{I} - 4\mathbf{I}_{1z}\mathbf{I}_{2z})\mathbf{R}_z =$$

$$\frac{1}{2}\begin{pmatrix}
0&0&0&0&0&0&0&0&0&0&0&0&0&0&0&0\\
0&0&0&0&0&0&0&0&0&0&0&0&0&0&0&0\\
0&0&0&0&0&0&0&0&0&0&0&0&0&0&0&0\\
0&0&0&0&0&0&0&1&0&0&0&0&0&0&0&0\\
0&0&0&0&0&0&0&0&0&1&0&0&0&0&0&0\\
0&0&0&0&0&0&0&0&0&0&0&0&0&0&0&0\\
0&0&0&0&0&0&0&0&0&0&0&-1&0&0&0&0\\
0&0&0&1&0&0&0&0&0&0&0&0&0&0&0&0\\
0&0&0&0&0&0&0&0&0&0&0&0&-1&0&0&0\\
0&0&0&0&1&0&0&0&0&0&0&0&0&0&0&0\\
0&0&0&0&0&0&0&0&0&0&0&0&0&0&0&0\\
0&0&0&0&0&0&-1&0&0&0&0&0&0&0&0&0\\
0&0&0&0&0&0&0&0&-1&0&0&0&0&0&0&0\\
0&0&0&0&0&0&0&0&0&0&0&0&0&0&0&0\\
0&0&0&0&0&0&0&0&0&0&0&0&0&0&0&0\\
0&0&0&0&0&0&0&0&0&0&0&0&0&0&0&0
\end{pmatrix} \qquad \text{(B.35)}$$

$$2\mathbf{S}_y(\mathbf{I}_{1z} - \mathbf{I}_{2z})\mathbf{R}_z =$$

$$\frac{1}{2}\begin{pmatrix}
0&0&0&0&0&0&0&0&0&0&0&0&0&0&0&0\\
0&0&0&0&0&0&0&0&0&0&0&0&0&0&0&0\\
0&0&0&0&0&0&0&0&0&0&0&0&0&0&0&0\\
0&0&0&0&0&0&0&-i&0&0&0&0&0&0&0&0\\
0&0&0&0&0&0&0&0&0&i&0&0&0&0&0&0\\
0&0&0&0&0&0&0&0&0&0&0&0&0&0&0&0\\
0&0&0&0&0&0&0&0&0&0&0&i&0&0&0&0\\
0&0&0&i&0&0&0&0&0&0&0&0&0&0&0&0\\
0&0&0&0&0&0&0&0&0&0&0&0&-i&0&0&0\\
0&0&0&0&-i&0&0&0&0&0&0&0&0&0&0&0\\
0&0&0&0&0&0&0&0&0&0&0&0&0&0&0&0\\
0&0&0&0&0&0&-i&0&0&0&0&0&0&0&0&0\\
0&0&0&0&0&0&0&0&i&0&0&0&0&0&0&0\\
0&0&0&0&0&0&0&0&0&0&0&0&0&0&0&0\\
0&0&0&0&0&0&0&0&0&0&0&0&0&0&0&0\\
0&0&0&0&0&0&0&0&0&0&0&0&0&0&0&0
\end{pmatrix} \qquad \text{(B.36)}$$

$$4\mathbf{S}_x(\mathbf{I}_{1x}\mathbf{I}_{2x} + \mathbf{I}_{1y}\mathbf{I}_{2y})\mathbf{R}_z =$$

$$\frac{1}{2}\begin{pmatrix}
0&0&0&0&0&0&0&0&0&0&0&0&0&0&0&0\\
0&0&0&0&0&0&0&0&0&0&0&0&0&0&0&0\\
0&0&0&0&0&0&0&0&0&0&0&0&0&0&0&0\\
0&0&0&0&0&0&0&0&0&1&0&0&0&0&0&0\\
0&0&0&0&0&0&0&1&0&0&0&0&0&0&0&0\\
0&0&0&0&0&0&0&0&0&0&0&0&0&0&0&0\\
0&0&0&0&0&0&0&0&0&0&0&0&-1&0&0&0\\
0&0&0&0&1&0&0&0&0&0&0&0&0&0&0&0\\
0&0&0&0&0&0&0&0&0&0&0&-1&0&0&0&0\\
0&0&0&1&0&0&0&0&0&0&0&0&0&0&0&0\\
0&0&0&0&0&0&0&0&0&0&0&0&0&0&0&0\\
0&0&0&0&0&0&0&0&-1&0&0&0&0&0&0&0\\
0&0&0&0&0&0&-1&0&0&0&0&0&0&0&0&0\\
0&0&0&0&0&0&0&0&0&0&0&0&0&0&0&0\\
0&0&0&0&0&0&0&0&0&0&0&0&0&0&0&0\\
0&0&0&0&0&0&0&0&0&0&0&0&0&0&0&0
\end{pmatrix} \qquad \text{(B.37)}$$

$$4\mathbf{S}_y(\mathbf{I}_{1y}\mathbf{I}_{2x} - \mathbf{I}_{1x}\mathbf{I}_{2y})\mathbf{R}_z =$$

$$\frac{1}{2}\begin{pmatrix}
0&0&0&0&0&0&0&0&0&0&0&0&0&0&0&0\\
0&0&0&0&0&0&0&0&0&0&0&0&0&0&0&0\\
0&0&0&0&0&0&0&0&0&0&0&0&0&0&0&0\\
0&0&0&0&0&0&0&0&0&-1&0&0&0&0&0&0\\
0&0&0&0&0&0&0&1&0&0&0&0&0&0&0&0\\
0&0&0&0&0&0&0&0&0&0&0&0&0&0&0&0\\
0&0&0&0&0&0&0&0&0&0&0&0&1&0&0&0\\
0&0&0&0&1&0&0&0&0&0&0&0&0&0&0&0\\
0&0&0&0&0&0&0&0&0&0&0&-1&0&0&0&0\\
0&0&0&-1&0&0&0&0&0&0&0&0&0&0&0&0\\
0&0&0&0&0&0&0&0&0&0&0&0&0&0&0&0\\
0&0&0&0&0&0&0&0&-1&0&0&0&0&0&0&0\\
0&0&0&0&0&0&1&0&0&0&0&0&0&0&0&0\\
0&0&0&0&0&0&0&0&0&0&0&0&0&0&0&0\\
0&0&0&0&0&0&0&0&0&0&0&0&0&0&0&0\\
0&0&0&0&0&0&0&0&0&0&0&0&0&0&0&0
\end{pmatrix} \qquad \text{(B.38)}$$

$$2\mathbf{S}_x(\mathbf{I}_{1y}\mathbf{I}_{2x} - \mathbf{I}_{1x}\mathbf{I}_{2y}) =$$

$$\frac{1}{2}\begin{pmatrix}
0&0&0&0&0&0&0&0&0&0&0&0&0&0&0&0\\
0&0&0&0&0&0&0&0&0&0&0&0&0&0&0&0\\
0&0&0&0&0&0&0&0&0&0&0&0&0&0&0&0\\
0&0&0&0&0&0&0&0&0&-i&0&0&0&0&0&0\\
0&0&0&0&0&0&0&i&0&0&0&0&0&0&0&0\\
0&0&0&0&0&0&0&0&0&0&0&0&0&0&0&0\\
0&0&0&0&0&0&0&0&0&0&0&0&-i&0&0&0\\
0&0&0&0&-i&0&0&0&0&0&0&0&0&0&0&0\\
0&0&0&0&0&0&0&0&0&0&0&i&0&0&0&0\\
0&0&0&i&0&0&0&0&0&0&0&0&0&0&0&0\\
0&0&0&0&0&0&0&0&0&0&0&0&0&0&0&0\\
0&0&0&0&0&0&0&0&-i&0&0&0&0&0&0&0\\
0&0&0&0&0&0&i&0&0&0&0&0&0&0&0&0\\
0&0&0&0&0&0&0&0&0&0&0&0&0&0&0&0\\
0&0&0&0&0&0&0&0&0&0&0&0&0&0&0&0\\
0&0&0&0&0&0&0&0&0&0&0&0&0&0&0&0
\end{pmatrix} \qquad \text{(B.39)}$$

$$2\mathbf{S}_y(\mathbf{I}_{1x}\mathbf{I}_{2x} + \mathbf{I}_{1y}\mathbf{I}_{2y}) =$$

$$\frac{1}{2}\begin{pmatrix}
0&0&0&0&0&0&0&0&0&0&0&0&0&0&0&0\\
0&0&0&0&0&0&0&0&0&0&0&0&0&0&0&0\\
0&0&0&0&0&0&0&0&0&0&0&0&0&0&0&0\\
0&0&0&0&0&0&0&0&0&-i&0&0&0&0&0&0\\
0&0&0&0&0&0&0&-i&0&0&0&0&0&0&0&0\\
0&0&0&0&0&0&0&0&0&0&0&0&0&0&0&0\\
0&0&0&0&0&0&0&0&0&0&0&0&-i&0&0&0\\
0&0&0&0&i&0&0&0&0&0&0&0&0&0&0&0\\
0&0&0&0&0&0&0&0&0&0&0&-i&0&0&0&0\\
0&0&0&i&0&0&0&0&0&0&0&0&0&0&0&0\\
0&0&0&0&0&0&0&0&0&0&0&0&0&0&0&0\\
0&0&0&0&0&0&0&0&i&0&0&0&0&0&0&0\\
0&0&0&0&0&0&i&0&0&0&0&0&0&0&0&0\\
0&0&0&0&0&0&0&0&0&0&0&0&0&0&0&0\\
0&0&0&0&0&0&0&0&0&0&0&0&0&0&0&0\\
0&0&0&0&0&0&0&0&0&0&0&0&0&0&0&0
\end{pmatrix} \qquad \text{(B.40)}$$

The final state after step two, $\mathbf{S}_y(\mathbf{I} - 4\mathbf{I}_{1z}\mathbf{I}_{2z})$, representing net magnetization on

heteronucleus S, is:

$$\frac{1}{2}\mathbf{S}_y(\mathbf{I} - 4\mathbf{I}_{1z}\mathbf{I}_{2z}) =$$

$$\frac{1}{2}\begin{pmatrix}
0 & 0 & 0 & 0 & 0 & 0 & 0 & 0 & 0 & 0 & 0 & 0 & 0 & 0 & 0 & 0 \\
0 & 0 & 0 & 0 & 0 & 0 & 0 & 0 & 0 & 0 & 0 & 0 & 0 & 0 & 0 & 0 \\
0 & 0 & 0 & 0 & 0 & 0 & 0 & 0 & 0 & 0 & 0 & 0 & 0 & 0 & 0 & 0 \\
0 & 0 & 0 & 0 & 0 & 0 & 0 & -i & 0 & 0 & 0 & 0 & 0 & 0 & 0 & 0 \\
0 & 0 & 0 & 0 & 0 & 0 & 0 & 0 & 0 & -i & 0 & 0 & 0 & 0 & 0 & 0 \\
0 & 0 & 0 & 0 & 0 & 0 & 0 & 0 & 0 & 0 & 0 & 0 & 0 & 0 & 0 & 0 \\
0 & 0 & 0 & 0 & 0 & 0 & 0 & 0 & 0 & 0 & 0 & -i & 0 & 0 & 0 & 0 \\
0 & 0 & 0 & i & 0 & 0 & 0 & 0 & 0 & 0 & 0 & 0 & 0 & 0 & 0 & 0 \\
0 & 0 & 0 & 0 & 0 & 0 & 0 & 0 & 0 & 0 & 0 & 0 & -i & 0 & 0 & 0 \\
0 & 0 & 0 & 0 & i & 0 & 0 & 0 & 0 & 0 & 0 & 0 & 0 & 0 & 0 & 0 \\
0 & 0 & 0 & 0 & 0 & 0 & 0 & 0 & 0 & 0 & 0 & 0 & 0 & 0 & 0 & 0 \\
0 & 0 & 0 & 0 & 0 & 0 & i & 0 & 0 & 0 & 0 & 0 & 0 & 0 & 0 & 0 \\
0 & 0 & 0 & 0 & 0 & 0 & 0 & 0 & i & 0 & 0 & 0 & 0 & 0 & 0 & 0 \\
0 & 0 & 0 & 0 & 0 & 0 & 0 & 0 & 0 & 0 & 0 & 0 & 0 & 0 & 0 & 0 \\
0 & 0 & 0 & 0 & 0 & 0 & 0 & 0 & 0 & 0 & 0 & 0 & 0 & 0 & 0 & 0 \\
0 & 0 & 0 & 0 & 0 & 0 & 0 & 0 & 0 & 0 & 0 & 0 & 0 & 0 & 0 & 0
\end{pmatrix} \qquad \text{(B.41)}$$

APPENDIX C

EVOLUTION OF ALL STATES IN AA'XY SPIN SYSTEMS

To find the optimum method to control the evolution of states by pulse sequence, it is necessary to study the precise evolution pattern for each state, which could be calculated by using the matrix and Hamiltonian mentioned in Appendix B. In this chapter the evolutions of each state from the initial singlet-state to the final heteronuclear polarization state are presented below.

C.1. Evolution of the initial singlet-state

Upon hydrogenation, the singlet-state starts to evolve from its initial form ($\mathbf{I_{1x}I_{2x}} + \mathbf{I_{1y}I_{2y}}$). The evolution pattern for this state and all other related states are listed below ($3_{a\text{-}f}$).

$$
\begin{aligned}
&(\mathbf{I_{1x}I_{2x}} + \mathbf{I_{1y}I_{2y}})(t) \\
&= \frac{1}{2}[\sin^2\theta_1 + \cos^2\theta_1\cos(2\pi\Omega_1 t) + \sin^2\theta_2 + \cos^2\theta_2\cos(2\pi\Omega_2 t)](\mathbf{I_{1x}I_{2x}} + \mathbf{I_{1y}I_{2y}}) \\
&+ \frac{1}{2}[\sin^2\theta_1 + \cos^2\theta_1\cos(2\pi\Omega_1 t) - \sin^2\theta_2 - \cos^2\theta_2\cos(2\pi\Omega_2 t)]4(\mathbf{I_{1x}I_{2x}} + \mathbf{I_{1y}I_{2y}})\mathbf{S_zR_z} \\
&+ \frac{1}{2}[\cos\theta_1\sin(2\pi\Omega_1 t) + \cos\theta_2\sin(2\pi\Omega_2 t)]2(\mathbf{I_{1y}I_{2x}} - \mathbf{I_{1x}I_{2y}})\mathbf{S_z} \\
&+ \frac{1}{2}[\cos\theta_1\sin(2\pi\Omega_1 t) - \cos\theta_2\sin(2\pi\Omega_2 t)]2(\mathbf{I_{1y}I_{2x}} - \mathbf{I_{1x}I_{2y}})\mathbf{R_z} \\
&+ \frac{1}{4}[\sin 2\theta_1(1 - \cos(2\pi\Omega_1 t)) + \sin 2\theta_2(1 - \cos(2\pi\Omega_2 t))](\mathbf{I_{1z}} - \mathbf{I_{2z}})\mathbf{S_z} \\
&+ \frac{1}{4}[\sin 2\theta_1(1 - \cos(2\pi\Omega_1 t)) - \sin 2\theta_2(1 - \cos(2\pi\Omega_2 t))](\mathbf{I_{1z}} - \mathbf{I_{2z}})\mathbf{R_z}
\end{aligned}
$$

$$
\begin{pmatrix}
\Omega_1 = J_{12}\sqrt{1+\Delta_1^2} & \Omega_2 = J_{12}\sqrt{1+\Delta_2^2} \\
\sin\theta_1 = \dfrac{1}{\sqrt{1+\Delta_1^2}} & \sin\theta_2 = \dfrac{1}{\sqrt{1+\Delta_2^2}} \\
\cos\theta_1 = \dfrac{\Delta}{\sqrt{1+\Delta_1^2}} & \cos\theta_2 = \dfrac{\Delta}{\sqrt{1+\Delta_2^2}} \\
\Delta_1 = \dfrac{J_{1S} + J_{1R} - J_{2S} - J_{2R}}{2J_{12}} & \Delta_2 = \dfrac{J_{1S} - J_{1R} - J_{2S} + J_{2R}}{2J_{12}}
\end{pmatrix} \tag{C.1}
$$

$$
\begin{aligned}
&4(\mathbf{I_{1x}I_{2x}} + \mathbf{I_{1y}I_{2y}})\mathbf{S_zR_z}(t) \\
&= \frac{1}{2}[\sin^2\theta_1 + \cos^2\theta_1\cos(2\pi\Omega_1 t) + \sin^2\theta_2 + \cos^2\theta_2\cos(2\pi\Omega_2 t)]4(\mathbf{I_{1x}I_{2x}} + \mathbf{I_{1y}I_{2y}})\mathbf{S_zR_z} \\
&+ \frac{1}{2}[\sin^2\theta_1 + \cos^2\theta_1\cos(2\pi\Omega_1 t) - \sin^2\theta_2 - \cos^2\theta_2\cos(2\pi\Omega_2 t)](\mathbf{I_{1x}I_{2x}} + \mathbf{I_{1y}I_{2y}}) \\
&+ \frac{1}{2}[\cos\theta_1\sin(2\pi\Omega_1 t) + \cos\theta_2\sin(2\pi\Omega_2 t)]2(\mathbf{I_{1y}I_{2x}} - \mathbf{I_{1x}I_{2y}})\mathbf{R_z} \\
&+ \frac{1}{2}[\cos\theta_1\sin(2\pi\Omega_1 t) - \cos\theta_2\sin(2\pi\Omega_2 t)]2(\mathbf{I_{1y}I_{2x}} - \mathbf{I_{1x}I_{2y}})\mathbf{S_z} \\
&+ \frac{1}{4}[\sin 2\theta_1(1 - \cos(2\pi\Omega_1 t)) + \sin 2\theta_2(1 - \cos(2\pi\Omega_2 t))](\mathbf{I_{1z}} - \mathbf{I_{2z}})\mathbf{R_z} \\
&+ \frac{1}{4}[\sin 2\theta_1(1 - \cos(2\pi\Omega_1 t)) - \sin 2\theta_2(1 - \cos(2\pi\Omega_2 t))](\mathbf{I_{1z}} - \mathbf{I_{2z}})\mathbf{S_z}
\end{aligned} \tag{C.2}
$$

$$
\begin{aligned}
&2(\mathbf{I_{1y}I_{2x}} - \mathbf{I_{1x}I_{2y}})\mathbf{S_z}(t) \\
&= \frac{1}{2}[\cos(2\pi\Omega_1 t) + \cos(2\pi\Omega_2 t)]2(\mathbf{I_{1y}I_{2x}} - \mathbf{I_{1x}I_{2y}})\mathbf{S_z} \\
&+ \frac{1}{2}[\cos(2\pi\Omega_1 t) - \cos(2\pi\Omega_2 t)]2(\mathbf{I_{1y}I_{2x}} - \mathbf{I_{1x}I_{2y}})\mathbf{R_z} \\
&- \frac{1}{2}[\cos\theta_1\sin(2\pi\Omega_1 t) + \cos\theta_2\sin(2\pi\Omega_2 t)](\mathbf{I_{1x}I_{2x}} + \mathbf{I_{1y}I_{2y}}) \\
&- \frac{1}{2}[\cos\theta_1\sin(2\pi\Omega_1 t) - \cos\theta_2\sin(2\pi\Omega_2 t)]4(\mathbf{I_{1x}I_{2x}} + \mathbf{I_{1y}I_{2y}})\mathbf{S_zR_z} \\
&+ \frac{1}{2}[\sin\theta_1\sin(2\pi\Omega_1 t) + \sin\theta_2\sin(2\pi\Omega_2 t)](\mathbf{I_{1z}} - \mathbf{I_{2z}})\mathbf{S_z} \\
&+ \frac{1}{2}[\sin\theta_1\sin(2\pi\Omega_1 t) - \sin\theta_2\sin(2\pi\Omega_2 t)](\mathbf{I_{1z}} - \mathbf{I_{2z}})\mathbf{R_z}
\end{aligned}
\tag{C.3}
$$

$$
\begin{aligned}
&2(\mathbf{I_{1y}I_{2x}} - \mathbf{I_{1x}I_{2y}})\mathbf{R_z}(t) \\
&= \frac{1}{2}[\cos(2\pi\Omega_1 t) + \cos(2\pi\Omega_2 t)]2(\mathbf{I_{1y}I_{2x}} - \mathbf{I_{1x}I_{2y}})\mathbf{R_z} \\
&+ \frac{1}{2}[\cos(2\pi\Omega_1 t) - \cos(2\pi\Omega_2 t)]2(\mathbf{I_{1y}I_{2x}} - \mathbf{I_{1x}I_{2y}})\mathbf{S_z} \\
&- \frac{1}{2}[\cos\theta_1\sin(2\pi\Omega_1 t) + \cos\theta_2\sin(2\pi\Omega_2 t)]4(\mathbf{I_{1x}I_{2x}} + \mathbf{I_{1y}I_{2y}})\mathbf{S_zR_z} \\
&- \frac{1}{2}[\cos\theta_1\sin(2\pi\Omega_1 t) - \cos\theta_2\sin(2\pi\Omega_2 t)](\mathbf{I_{1x}I_{2x}} + \mathbf{I_{1y}I_{2y}}) \\
&+ \frac{1}{2}[\sin\theta_1\sin(2\pi\Omega_1 t) + \sin\theta_2\sin(2\pi\Omega_2 t)](\mathbf{I_{1z}} - \mathbf{I_{2z}})\mathbf{R_z} \\
&+ \frac{1}{2}[\sin\theta_1\sin(2\pi\Omega_1 t) - \sin\theta_2\sin(2\pi\Omega_2 t)](\mathbf{I_{1z}} - \mathbf{I_{2z}})\mathbf{S_z}
\end{aligned}
\tag{C.4}
$$

$$
\begin{aligned}
&(\mathbf{I_{1z}} - \mathbf{I_{2z}})\mathbf{S_z}(t) \\
&= \frac{1}{2}[\cos^2\theta_1 + \sin^2\theta_1\cos(2\pi\Omega_1 t) + \cos^2\theta_2 + \sin^2\theta_2\cos(2\pi\Omega_2 t)](\mathbf{I_{1z}} - \mathbf{I_{2z}})\mathbf{S_z} \\
&+ \frac{1}{2}[\cos^2\theta_1 + \sin^2\theta_1\cos(2\pi\Omega_1 t) - \cos^2\theta_2 - \sin^2\theta_2\cos(2\pi\Omega_2 t)](\mathbf{I_{1z}} - \mathbf{I_{2z}})\mathbf{R_z} \\
&+ \frac{1}{4}[\sin 2\theta_1(1 - \cos(2\pi\Omega_1 t)) + \sin 2\theta_2(1 - \cos(2\pi\Omega_2 t))](\mathbf{I_{1x}}\mathbf{I_{2x}} + \mathbf{I_{1y}}\mathbf{I_{2y}}) \\
&+ \frac{1}{4}[\sin 2\theta_1(1 - \cos(2\pi\Omega_1 t)) - \sin 2\theta_2(1 - \cos(2\pi\Omega_2 t))]4(\mathbf{I_{1x}}\mathbf{I_{2x}} + \mathbf{I_{1y}}\mathbf{I_{2y}})\mathbf{S_z}\mathbf{R_z} \\
&- \frac{1}{2}[\sin\theta_1\sin(2\pi\Omega_1 t) + \sin\theta_2\sin(2\pi\Omega_2 t)]2(\mathbf{I_{1y}}\mathbf{I_{2x}} - \mathbf{I_{1x}}\mathbf{I_{2y}})\mathbf{S_z} \\
&- \frac{1}{2}[\sin\theta_1\sin(2\pi\Omega_1 t) - \sin\theta_2\sin(2\pi\Omega_2 t)]2(\mathbf{I_{1y}}\mathbf{I_{2x}} - \mathbf{I_{1x}}\mathbf{I_{2y}})\mathbf{R_z}
\end{aligned}
\tag{C.5}
$$

$$
\begin{aligned}
&(\mathbf{I_{1z}} - \mathbf{I_{2z}})\mathbf{R_z}(t) \\
&= \frac{1}{2}[\cos^2\theta_1 + \sin^2\theta_1\cos(2\pi\Omega_1 t) + \cos^2\theta_2 + \sin^2\theta_2\cos(2\pi\Omega_2 t)](\mathbf{I_{1z}} - \mathbf{I_{2z}})\mathbf{R_z} \\
&+ \frac{1}{2}[\cos^2\theta_1 + \sin^2\theta_1\cos(2\pi\Omega_1 t) - \cos^2\theta_2 - \sin^2\theta_2\cos(2\pi\Omega_2 t)](\mathbf{I_{1z}} - \mathbf{I_{2z}})\mathbf{S_z} \\
&+ \frac{1}{4}[\sin 2\theta_1(1 - \cos(2\pi\Omega_1 t)) + \sin 2\theta_2(1 - \cos(2\pi\Omega_2 t))]4(\mathbf{I_{1x}}\mathbf{I_{2x}} + \mathbf{I_{1y}}\mathbf{I_{2y}})\mathbf{S_z}\mathbf{R_z} \\
&+ \frac{1}{4}[\sin 2\theta_1(1 - \cos(2\pi\Omega_1 t)) - \sin 2\theta_2(1 - \cos(2\pi\Omega_2 t))](\mathbf{I_{1x}}\mathbf{I_{2x}} + \mathbf{I_{1y}}\mathbf{I_{2y}}) \\
&- \frac{1}{2}[\sin\theta_1\sin(2\pi\Omega_1 t) + \sin\theta_2\sin(2\pi\Omega_2 t)]2(\mathbf{I_{1y}}\mathbf{I_{2x}} - \mathbf{I_{1x}}\mathbf{I_{2y}})\mathbf{R_z} \\
&- \frac{1}{2}[\sin\theta_1\sin(2\pi\Omega_1 t) - \sin\theta_2\sin(2\pi\Omega_2 t)]2(\mathbf{I_{1y}}\mathbf{I_{2x}} - \mathbf{I_{1x}}\mathbf{I_{2y}})\mathbf{S_z}
\end{aligned}
\tag{C.6}
$$

Equation C.5, the state of $(I_{1z} - I_{2z})S_z$, is the state we chose to start step two.

C.2. Evolution to heteronuclear net magnetization

After extracting the maximum of the state we chose above, $(\mathbf{I_{1z}} - \mathbf{I_{2z}})\mathbf{S_z}$, a 90_y pulse on S channel is applied to rotate the state to $(\mathbf{I_{1z}} - \mathbf{I_{2z}})\mathbf{S_x}$. In this section we study the evolution pattern of this state and other related states in step 2.

$$
\begin{aligned}
&\mathbf{S}_x(\mathbf{I}_{1z}-\mathbf{I}_{2z})(t)\\
&=\cos(\pi J_{SR}t)[\cos(\pi\Omega_1 t)\cos(\pi\Omega_2 t)-\cos(\theta_1-\theta_2)\sin(\pi\Omega_1 t)\sin(\pi\Omega_2 t)]\mathbf{S}_x(\mathbf{I}_{1z}-\mathbf{I}_{2z})\\
&-\sin(\pi J_{SR}t)[\cos\theta_1\sin(\pi\Omega_1 t)\cos(\pi\Omega_2 t)+\cos\theta_2\cos(\pi\Omega_1 t)\sin(\pi\Omega_2 t)]\mathbf{S}_x(\mathbf{I}-4\mathbf{I}_{1z}\mathbf{I}_{2z})\mathbf{R}_z\\
&+\cos(\pi J_{SR}t)[\cos\theta_1\sin(\pi\Omega_1 t)\cos(\pi\Omega_2 t)+\cos\theta_2\cos(\pi\Omega_1 t)\sin(\pi\Omega_2 t)]\frac{1}{2}\mathbf{S}_y(\mathbf{I}-4\mathbf{I}_{1z}\mathbf{I}_{2z})\\
&+\sin(\pi J_{SR}t)[\cos(\pi\Omega_1 t)\cos(\pi\Omega_2 t)-\cos(\theta_1-\theta_2)\sin(\pi\Omega_1 t)\sin(\pi\Omega_2 t)]2\mathbf{S}_y(\mathbf{I}_{1z}-\mathbf{I}_{2z})\mathbf{R}_z\\
&-\cos(\pi J_{SR}t)[\sin(\theta_1-\theta_2)\sin(\pi\Omega_1 t)\sin(\pi\Omega_2 t)]4\mathbf{S}_x(\mathbf{I}_{1x}\mathbf{I}_{2x}+\mathbf{I}_{1y}\mathbf{I}_{2y})\mathbf{R}_z\\
&-\sin(\pi J_{SR}t)[\sin\theta_1\sin(\pi\Omega_1 t)\cos(\pi\Omega_2 t)+\sin\theta_2\cos(\pi\Omega_1 t)\sin(\pi\Omega_2 t)]4\mathbf{S}_y(\mathbf{I}_{1y}\mathbf{I}_{2x}-\mathbf{I}_{1x}\mathbf{I}_{2y})\mathbf{R}_z\\
&-\cos(\pi J_{SR}t)[\sin\theta_1\sin(\pi\Omega_1 t)\cos(\pi\Omega_2 t)+\sin\theta_2\cos(\pi\Omega_1 t)\sin(\pi\Omega_2 t)]2\mathbf{S}_x(\mathbf{I}_{1y}\mathbf{I}_{2x}-\mathbf{I}_{1x}\mathbf{I}_{2y})\\
&-\sin(\pi J_{SR}t)[\sin(\theta_1-\theta_2)\sin(\pi\Omega_1 t)\sin(\pi\Omega_2 t)]2\mathbf{S}_y(\mathbf{I}_{1x}\mathbf{I}_{2x}+\mathbf{I}_{1y}\mathbf{I}_{2y})
\end{aligned}
$$

(C.7)

$$
\begin{aligned}
&\mathbf{S}_x(\mathbf{I}-4\mathbf{I}_{1z}\mathbf{I}_{2z})\mathbf{R}_z(t)\\
&=\cos(\pi J_{SR}t)[\cos(\pi\Omega_1 t)\cos(\pi\Omega_2 t)+\cos(\theta_1+\theta_2)\sin(\pi\Omega_1 t)\sin(\pi\Omega_2 t)]\mathbf{S}_x(\mathbf{I}-4\mathbf{I}_{1z}\mathbf{I}_{2z})\mathbf{R}_z\\
&-\sin(\pi J_{SR}t)[\cos\theta_1\sin(\pi\Omega_1 t)\cos(\pi\Omega_2 t)+\cos\theta_2\cos(\pi\Omega_1 t)\sin(\pi\Omega_2 t)]\mathbf{S}_x(\mathbf{I}_{1z}-\mathbf{I}_{2z})\\
&+\cos(\pi J_{SR}t)[\cos\theta_1\sin(\pi\Omega_1 t)\cos(\pi\Omega_2 t)+\cos\theta_2\cos(\pi\Omega_1 t)\sin(\pi\Omega_2 t)]2\mathbf{S}_y(\mathbf{I}_{1z}-\mathbf{I}_{2z})\mathbf{R}_z\\
&+\sin(\pi J_{SR}t)[\cos(\pi\Omega_1 t)\cos(\pi\Omega_2 t)-\cos(\theta_1+\theta_2)\sin(\pi\Omega_1 t)\sin(\pi\Omega_2 t)]\frac{1}{2}\mathbf{S}_y(\mathbf{I}-4\mathbf{I}_{1z}\mathbf{I}_{2z})\\
&-\cos(\pi J_{SR}t)[\sin(\theta_1+\theta_2)\sin(\pi\Omega_1 t)\sin(\pi\Omega_2 t)]4\mathbf{S}_y(\mathbf{I}_{1y}\mathbf{I}_{2x}-\mathbf{I}_{1x}\mathbf{I}_{2y})\mathbf{R}_z\\
&-\sin(\pi J_{SR}t)[\sin\theta_1\sin(\pi\Omega_1 t)\cos(\pi\Omega_2 t)-\sin\theta_2\cos(\pi\Omega_1 t)\sin(\pi\Omega_2 t)]4\mathbf{S}_x(\mathbf{I}_{1x}\mathbf{I}_{2x}+\mathbf{I}_{1y}\mathbf{I}_{2y})\mathbf{R}_z\\
&+\cos(\pi J_{SR}t)[\sin\theta_1\sin(\pi\Omega_1 t)\cos(\pi\Omega_2 t)-\sin\theta_2\cos(\pi\Omega_1 t)\sin(\pi\Omega_2 t)]2\mathbf{S}_y(\mathbf{I}_{1x}\mathbf{I}_{2x}+\mathbf{I}_{1y}\mathbf{I}_{2y})\\
&+\sin(\pi J_{SR}t)[\sin(\theta_1+\theta_2)\sin(\pi\Omega_1 t)\sin(\pi\Omega_2 t)]2\mathbf{S}_x(\mathbf{I}_{1y}\mathbf{I}_{2x}-\mathbf{I}_{1x}\mathbf{I}_{2y})
\end{aligned}
$$

(C.8)

$$\frac{1}{2}\mathbf{S}_y(\mathbf{I}-4\mathbf{I}_{1z}\mathbf{I}_{2z})(t)$$

$$\begin{aligned}
&= \cos(\pi J_{SR}t)[\cos(\pi\Omega_1 t)\cos(\pi\Omega_2 t)-\cos(\theta_1+\theta_2)\sin(\pi\Omega_1 t)\sin(\pi\Omega_2 t)]\frac{1}{2}\mathbf{S}_y(\mathbf{I}-4\mathbf{I}_{1z}\mathbf{I}_{2z})\\
&-\sin(\pi J_{SR}t)[\cos\theta_1\sin(\pi\Omega_1 t)\cos(\pi\Omega_2 t)+\cos\theta_2\cos(\pi\Omega_1 t)\sin(\pi\Omega_2 t)]2\mathbf{S}_y(\mathbf{I}_{1z}-\mathbf{I}_{2z})\mathbf{R}_z\\
&-\cos(\pi J_{SR}t)[\cos\theta_1\sin(\pi\Omega_1 t)\cos(\pi\Omega_2 t)+\cos\theta_2\cos(\pi\Omega_1 t)\sin(\pi\Omega_2 t)]\mathbf{S}_x(\mathbf{I}_{1z}-\mathbf{I}_{2z})\\
&-\sin(\pi J_{SR}t)[\cos(\pi\Omega_1 t)\cos(\pi\Omega_2 t)-\cos(\theta_1+\theta_2)\sin(\pi\Omega_1 t)\sin(\pi\Omega_2 t)]\mathbf{S}_x(\mathbf{I}-4\mathbf{I}_{1z}\mathbf{I}_{2z})\mathbf{R}_z\\
&-\cos(\pi J_{SR}t)[\sin\theta_1\sin(\pi\Omega_1 t)\cos(\pi\Omega_2 t)-\sin\theta_2\cos(\pi\Omega_1 t)\sin(\pi\Omega_2 t)]4\mathbf{S}_x(\mathbf{I}_{1x}\mathbf{I}_{2x}+\mathbf{I}_{1y}\mathbf{I}_{2y})\mathbf{R}_z\\
&+\sin(\pi J_{SR}t)[\sin(\theta_1+\theta_2)\sin(\pi\Omega_1 t)\sin(\pi\Omega_2 t)]4\mathbf{S}_y(\mathbf{I}_{1y}\mathbf{I}_{2x}-\mathbf{I}_{1x}\mathbf{I}_{2y})\mathbf{R}_z\\
&+\cos(\pi J_{SR}t)[\sin(\theta_1+\theta_2)\sin(\pi\Omega_1 t)\sin(\pi\Omega_2 t)]2\mathbf{S}_x(\mathbf{I}_{1y}\mathbf{I}_{2x}-\mathbf{I}_{1x}\mathbf{I}_{2y})\\
&-\sin(\pi J_{SR}t)[\sin\theta_1\sin(\pi\Omega_1 t)\cos(\pi\Omega_2 t)-\sin\theta_2\cos(\pi\Omega_1 t)\sin(\pi\Omega_2 t)]2\mathbf{S}_y(\mathbf{I}_{1x}\mathbf{I}_{2x}+\mathbf{I}_{1y}\mathbf{I}_{2y})
\end{aligned}$$

(C.9)

$$2\mathbf{S}_y(\mathbf{I}_{1z}-\mathbf{I}_{2z})\mathbf{R}_z(t)$$

$$\begin{aligned}
&= \cos(\pi J_{SR}t)[\cos(\pi\Omega_1 t)\cos(\pi\Omega_2 t)-\cos(\theta_1-\theta_2)\sin(\pi\Omega_1 t)\sin(\pi\Omega_2 t)]2\mathbf{S}_y(\mathbf{I}_{1z}-\mathbf{I}_{2z})\mathbf{R}_z\\
&-\sin(\pi J_{SR}t)[\cos\theta_1\sin(\pi\Omega_1 t)\cos(\pi\Omega_2 t)+\cos\theta_2\cos(\pi\Omega_1 t)\sin(\pi\Omega_2 t)]\frac{1}{2}\mathbf{S}_y(\mathbf{I}-4\mathbf{I}_{1z}\mathbf{I}_{2z})\\
&-\cos(\pi J_{SR}t)[\cos\theta_1\sin(\pi\Omega_1 t)\cos(\pi\Omega_2 t)+\cos\theta_2\cos(\pi\Omega_1 t)\sin(\pi\Omega_2 t)]\mathbf{S}_x(\mathbf{I}-4\mathbf{I}_{1z}\mathbf{I}_{2z})\mathbf{R}_z\\
&-\sin(\pi J_{SR}t)[\cos(\pi\Omega_1 t)\cos(\pi\Omega_2 t)-\cos(\theta_1-\theta_2)\sin(\pi\Omega_1 t)\sin(\pi\Omega_2 t)]\mathbf{S}_x(\mathbf{I}_{1z}-\mathbf{I}_{2z})\\
&-\cos(\pi J_{SR}t)[\sin\theta_1\sin(\pi\Omega_1 t)\cos(\pi\Omega_2 t)+\sin\theta_2\cos(\pi\Omega_1 t)\sin(\pi\Omega_2 t)]4\mathbf{S}_y(\mathbf{I}_{1y}\mathbf{I}_{2x}-\mathbf{I}_{1x}\mathbf{I}_{2y})\mathbf{R}_z\\
&+\sin(\pi J_{SR}t)[\sin(\theta_1-\theta_2)\sin(\pi\Omega_1 t)\sin(\pi\Omega_2 t)]4\mathbf{S}_x(\mathbf{I}_{1x}\mathbf{I}_{2x}+\mathbf{I}_{1y}\mathbf{I}_{2y})\mathbf{R}_z\\
&-\cos(\pi J_{SR}t)[\sin(\theta_1-\theta_2)\sin(\pi\Omega_1 t)\sin(\pi\Omega_2 t)]2\mathbf{S}_y(\mathbf{I}_{1x}\mathbf{I}_{2x}+\mathbf{I}_{1y}\mathbf{I}_{2y})\\
&+\sin(\pi J_{SR}t)[\sin\theta_1\sin(\pi\Omega_1 t)\cos(\pi\Omega_2 t)+\sin\theta_2\cos(\pi\Omega_1 t)\sin(\pi\Omega_2 t)]2\mathbf{S}_x(\mathbf{I}_{1y}\mathbf{I}_{2x}-\mathbf{I}_{1x}\mathbf{I}_{2y})
\end{aligned}$$

(C.10)

$$
\begin{aligned}
&4\mathbf{S}_x(\mathbf{I}_{1x}\mathbf{I}_{2x}+\mathbf{I}_{1y}\mathbf{I}_{2y})\mathbf{R}_z(t)\\
&=\cos(\pi J_{SR}t)[\cos(\pi\Omega_1 t)\cos(\pi\Omega_2 t)+\cos(\theta_1-\theta_2)\sin(\pi\Omega_1 t)\sin(\pi\Omega_2 t)]4\mathbf{S}_x(\mathbf{I}_{1x}\mathbf{I}_{2x}+\mathbf{I}_{1y}\mathbf{I}_{2y})\mathbf{R}_z\\
&+\sin(\pi J_{SR}t)[\cos\theta_1\sin(\pi\Omega_1 t)\cos(\pi\Omega_2 t)-\cos\theta_2\cos(\pi\Omega_1 t)\sin(\pi\Omega_2 t)]4\mathbf{S}_y(\mathbf{I}_{1y}\mathbf{I}_{2x}-\mathbf{I}_{1x}\mathbf{I}_{2y})\mathbf{R}_z\\
&+\cos(\pi J_{SR}t)[\cos\theta_1\sin(\pi\Omega_1 t)\cos(\pi\Omega_2 t)-\cos\theta_2\cos(\pi\Omega_1 t)\sin(\pi\Omega_2 t)]2\mathbf{S}_x(\mathbf{I}_{1y}\mathbf{I}_{2x}-\mathbf{I}_{1x}\mathbf{I}_{2y})\\
&+\sin(\pi J_{SR}t)[\cos(\pi\Omega_1 t)\cos(\pi\Omega_2 t)+\cos(\theta_1-\theta_2)\sin(\pi\Omega_1 t)\sin(\pi\Omega_2 t)]2\mathbf{S}_y(\mathbf{I}_{1x}\mathbf{I}_{2x}+\mathbf{I}_{1y}\mathbf{I}_{2y})\\
&-\cos(\pi J_{SR}t)[\sin(\theta_1-\theta_2)\sin(\pi\Omega_1 t)\sin(\pi\Omega_2 t)]\mathbf{S}_x(\mathbf{I}_{1z}-\mathbf{I}_{2z})\\
&-\sin(\pi J_{SR}t)[\sin\theta_1\sin(\pi\Omega_1 t)\cos(\pi\Omega_2 t)-\sin\theta_2\cos(\pi\Omega_1 t)\sin(\pi\Omega_2 t)]\mathbf{S}_x(\mathbf{I}-4\mathbf{I}_{1z}\mathbf{I}_{2z})\mathbf{R}_z\\
&+\cos(\pi J_{SR}t)[\sin\theta_1\sin(\pi\Omega_1 t)\cos(\pi\Omega_2 t)-\sin\theta_2\cos(\pi\Omega_1 t)\sin(\pi\Omega_2 t)]\frac{1}{2}\mathbf{S}_y(\mathbf{I}-4\mathbf{I}_{1z}\mathbf{I}_{2z})\\
&+\sin(\pi J_{SR}t)[\sin(\theta_1-\theta_2)\sin(\pi\Omega_1 t)\sin(\pi\Omega_2 t)]2\mathbf{S}_y(\mathbf{I}_{1z}-\mathbf{I}_{2z})\mathbf{R}_z
\end{aligned}
$$

(C.11)

$$
\begin{aligned}
&4\mathbf{S}_y(\mathbf{I}_{1y}\mathbf{I}_{2x}-\mathbf{I}_{1x}\mathbf{I}_{2y})\mathbf{R}_z(t)\\
&=\cos(\pi J_{SR}t)[\cos(\pi\Omega_1 t)\cos(\pi\Omega_2 t)+\cos(\theta_1+\theta_2)\sin(\pi\Omega_1 t)\sin(\pi\Omega_2 t)]4\mathbf{S}_y(\mathbf{I}_{1y}\mathbf{I}_{2x}-\mathbf{I}_{1x}\mathbf{I}_{2y})\mathbf{R}_z\\
&+\sin(\pi J_{SR}t)[\cos\theta_1\sin(\pi\Omega_1 t)\cos(\pi\Omega_2 t)-\cos\theta_2\cos(\pi\Omega_1 t)\sin(\pi\Omega_2 t)]4\mathbf{S}_x(\mathbf{I}_{1x}\mathbf{I}_{2x}+\mathbf{I}_{1y}\mathbf{I}_{2y})\mathbf{R}_z\\
&-\cos(\pi J_{SR}t)[\cos\theta_1\sin(\pi\Omega_1 t)\cos(\pi\Omega_2 t)-\cos\theta_2\cos(\pi\Omega_1 t)\sin(\pi\Omega_2 t)]2\mathbf{S}_y(\mathbf{I}_{1x}\mathbf{I}_{2x}+\mathbf{I}_{1y}\mathbf{I}_{2y})\\
&-\sin(\pi J_{SR}t)[\cos(\pi\Omega_1 t)\cos(\pi\Omega_2 t)+\cos(\theta_1+\theta_2)\sin(\pi\Omega_1 t)\sin(\pi\Omega_2 t)]2\mathbf{S}_x(\mathbf{I}_{1y}\mathbf{I}_{2x}-\mathbf{I}_{1x}\mathbf{I}_{2y})\\
&-\cos(\pi J_{SR}t)[\sin(\theta_1+\theta_2)\sin(\pi\Omega_1 t)\sin(\pi\Omega_2 t)]\mathbf{S}_x(\mathbf{I}-4\mathbf{I}_{1z}\mathbf{I}_{2z})\mathbf{R}_z\\
&-\sin(\pi J_{SR}t)[\sin\theta_1\sin(\pi\Omega_1 t)\cos(\pi\Omega_2 t)+\sin\theta_2\cos(\pi\Omega_1 t)\sin(\pi\Omega_2 t)]\mathbf{S}_x(\mathbf{I}_{1z}-\mathbf{I}_{2z})\\
&+\cos(\pi J_{SR}t)[\sin\theta_1\sin(\pi\Omega_1 t)\cos(\pi\Omega_2 t)+\sin\theta_2\cos(\pi\Omega_1 t)\sin(\pi\Omega_2 t)]2\mathbf{S}_y(\mathbf{I}_{1z}-\mathbf{I}_{2z})\mathbf{R}_z\\
&-\sin(\pi J_{SR}t)[\sin(\theta_1+\theta_2)\sin(\pi\Omega_1 t)\sin(\pi\Omega_2 t)]\frac{1}{2}\mathbf{S}_y(\mathbf{I}-4\mathbf{I}_{1z}\mathbf{I}_{2z})
\end{aligned}
$$

(C.12)

$$
\begin{aligned}
&2\mathbf{S}_x(\mathbf{I}_{1y}\mathbf{I}_{2x} - \mathbf{I}_{1x}\mathbf{I}_{2y})(t) \\
&= \cos(\pi J_{SR}t)[\cos(\pi\Omega_1 t)\cos(\pi\Omega_2 t) + \cos(\theta_1+\theta_2)\sin(\pi\Omega_1 t)\sin(\pi\Omega_2 t)]2\mathbf{S}_x(\mathbf{I}_{1y}\mathbf{I}_{2x} - \mathbf{I}_{1x}\mathbf{I}_{2y}) \\
&-\sin(\pi J_{SR}t)[\cos\theta_1\sin(\pi\Omega_1 t)\cos(\pi\Omega_2 t) - \cos\theta_2\cos(\pi\Omega_1 t)\sin(\pi\Omega_2 t)]2\mathbf{S}_y(\mathbf{I}_{1x}\mathbf{I}_{2x} + \mathbf{I}_{1y}\mathbf{I}_{2y}) \\
&-\cos(\pi J_{SR}t)[\cos\theta_1\sin(\pi\Omega_1 t)\cos(\pi\Omega_2 t) - \cos\theta_2\cos(\pi\Omega_1 t)\sin(\pi\Omega_2 t)]4\mathbf{S}_x(\mathbf{I}_{1x}\mathbf{I}_{2x} + \mathbf{I}_{1y}\mathbf{I}_{2y})\mathbf{R}_z \\
&+\sin(\pi J_{SR}t)[\cos(\pi\Omega_1 t)\cos(\pi\Omega_2 t) + \cos(\theta_1+\theta_2)\sin(\pi\Omega_1 t)\sin(\pi\Omega_2 t)]4\mathbf{S}_y(\mathbf{I}_{1y}\mathbf{I}_{2x} - \mathbf{I}_{1x}\mathbf{I}_{2y})\mathbf{R}_z \\
&+\cos(\pi J_{SR}t)[\sin(\theta_1+\theta_2)\sin(\pi\Omega_1 t)\sin(\pi\Omega_2 t)]\frac{1}{2}\mathbf{S}_y(\mathbf{I} - 4\mathbf{I}_{1z}\mathbf{I}_{2z}) \\
&+\sin(\pi J_{SR}t)[\sin\theta_1\sin(\pi\Omega_1 t)\cos(\pi\Omega_2 t) + \sin\theta_2\cos(\pi\Omega_1 t)\sin(\pi\Omega_2 t)]2\mathbf{S}_y(\mathbf{I}_{1z} - \mathbf{I}_{2z})\mathbf{R}_z \\
&+\cos(\pi J_{SR}t)[\sin\theta_1\sin(\pi\Omega_1 t)\cos(\pi\Omega_2 t) + \sin\theta_2\cos(\pi\Omega_1 t)\sin(\pi\Omega_2 t)]\mathbf{S}_x(\mathbf{I}_{1z} - \mathbf{I}_{2z}) \\
&-\sin(\pi J_{SR}t)[\sin(\theta_1+\theta_2)\sin(\pi\Omega_1 t)\sin(\pi\Omega_2 t)]\mathbf{S}_x(\mathbf{I} - 4\mathbf{I}_{1z}\mathbf{I}_{2z})\mathbf{R}_z
\end{aligned}
$$

(C.13)

$$
\begin{aligned}
&2\mathbf{S}_y(\mathbf{I}_{1x}\mathbf{I}_{2x} + \mathbf{I}_{1y}\mathbf{I}_{2y})(t) \\
&= \cos(\pi J_{SR}t)[\cos(\pi\Omega_1 t)\cos(\pi\Omega_2 t) + \cos(\theta_1-\theta_2)\sin(\pi\Omega_1 t)\sin(\pi\Omega_2 t)]2\mathbf{S}_y(\mathbf{I}_{1x}\mathbf{I}_{2x} + \mathbf{I}_{1y}\mathbf{I}_{2y}) \\
&-\sin(\pi J_{SR}t)[\cos\theta_1\sin(\pi\Omega_1 t)\cos(\pi\Omega_2 t) - \cos\theta_2\cos(\pi\Omega_1 t)\sin(\pi\Omega_2 t)]2\mathbf{S}_x(\mathbf{I}_{1y}\mathbf{I}_{2x} - \mathbf{I}_{1x}\mathbf{I}_{2y}) \\
&+\cos(\pi J_{SR}t)[\cos\theta_1\sin(\pi\Omega_1 t)\cos(\pi\Omega_2 t) - \cos\theta_2\cos(\pi\Omega_1 t)\sin(\pi\Omega_2 t)]4\mathbf{S}_y(\mathbf{I}_{1y}\mathbf{I}_{2x} - \mathbf{I}_{1x}\mathbf{I}_{2y})\mathbf{R}_z \\
&-\sin(\pi J_{SR}t)[\cos(\pi\Omega_1 t)\cos(\pi\Omega_2 t) + \cos(\theta_1-\theta_2)\sin(\pi\Omega_1 t)\sin(\pi\Omega_2 t)]4\mathbf{S}_x(\mathbf{I}_{1x}\mathbf{I}_{2x} + \mathbf{I}_{1y}\mathbf{I}_{2y})\mathbf{R}_z \\
&-\cos(\pi J_{SR}t)[\sin(\theta_1-\theta_2)\sin(\pi\Omega_1 t)\sin(\pi\Omega_2 t)]2\mathbf{S}_y(\mathbf{I}_{1z} - \mathbf{I}_{2z})\mathbf{R}_z \\
&-\sin(\pi J_{SR}t)[\sin\theta_1\sin(\pi\Omega_1 t)\cos(\pi\Omega_2 t) - \sin\theta_2\cos(\pi\Omega_1 t)\sin(\pi\Omega_2 t)]\frac{1}{2}\mathbf{S}_y(\mathbf{I} - 4\mathbf{I}_{1z}\mathbf{I}_{2z}) \\
&-\cos(\pi J_{SR}t)[\sin\theta_1\sin(\pi\Omega_1 t)\cos(\pi\Omega_2 t) - \sin\theta_2\cos(\pi\Omega_1 t)\sin(\pi\Omega_2 t)]\mathbf{S}_x(\mathbf{I} - 4\mathbf{I}_{1z}\mathbf{I}_{2z})\mathbf{R}_z \\
&+\sin(\pi J_{SR}t)[\sin(\theta_1+\theta_2)\sin(\pi\Omega_1 t)\sin(\pi\Omega_2 t)]\mathbf{S}_x(\mathbf{I}_{1z} - \mathbf{I}_{2z})
\end{aligned}
$$

(C.14)

The final state, Equation C.9, is the state representing heteronuclear polarization. In the end of the pulse sequence, a 90_x pulse rotate the state to the polarized heteronucleus, $\mathbf{S}_z(\mathbf{I} - 4\mathbf{I}_{1z}\mathbf{I}_{2z})$.

APPENDIX D

SOURCE CODE

As shown in Chapter II, III, and Appendix A and B, the product operator basis used to simulate the quantum spin states and their evolution under Hamiltonian are mostly represented by density operators. Matlab was used to simulate the spin evolutions and these codes are shown below.

D.1. Pulse programs for hyper-SHIELDED

In a 3 spin system (I_1I_2S), each quantum spin state could be represented by a 8x8 density matrix. The spin evolutions could therefore be represented by the evolution of density matrix. The hyper-SHIELDED sequence, as we described in Chapter II, is illustrated in Figure D.1.

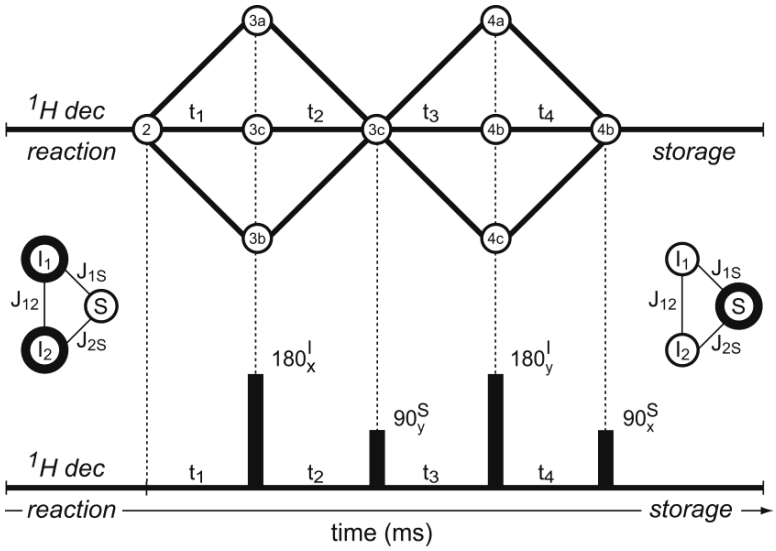

Figure D.1. Graphical depiction of evolution of density matrix components (upper graph) and the hyper - SHIELDED sequence (lower graph) for focusing parahydrogen singlet-states ($I_1 \cdot I_2$) into pure magnetization on an adjacent coupled (S) nucleus for strongly coupled I_1I_2S spin systems. Symbols ($3_{a\text{-}c}$, $4_{a\text{-}c}$) correspond to components of the density operator.

The effective pulses in hyper - SHIELDED are two 180° (+x) pulses on proton channel, with two 90° (+x and +y) pulses on ^{13}C channel. The Hamiltonian, initial density matrix, along with the evolution of states during the process are described in Chapter II. Below is the Matlab code to calculate the final density matrix after applying hyper-SHIELDED sequence to a given molecule with known scalar coupling constants.

```
Function [rou] = HyperSHIELDED(J,t)
% function to calculate the final density matrix after HyperSHIELDED
% Sequenceapplied to a spin system with given J coupling constants

% I1 represents one of the singlet protons
I1x=zeros(8);                    % I1x refers to the transverse x
I1x(1,4)=0.5;                    % component of the proton I1
I1x(2,6)=0.5;
I1x(3,7)=0.5;
```

```
I1x(4,1)=0.5;
I1x(5,8)=0.5;
I1x(6,2)=0.5;
I1x(7,3)=0.5;
I1x(8,5)=0.5;

I1y=zeros(8);                    % I1y refers to the transverse y
I1y(1,4)=-0.5*1i;                 % component of the proton I1
I1y(2,6)=-0.5*1i;
I1y(3,7)=-0.5*1i;
I1y(4,1)=0.5*1i;
I1y(5,8)=-0.5*1i;
I1y(6,2)=0.5*1i;
I1y(7,3)=0.5*1i;
I1y(8,5)=0.5*1i;

I1z=eye(8);                      % I1z refers to the longitudinal z
I1z(4,4)=-1;                     % component of the proton I1
I1z(6,6)=-1;
I1z(7,7)=-1;
I1z(8,8)=-1;
I1z=0.5*I1z;

% I2 represents the other singlet protons

I2x=zeros(8);                    % I2x refers to the transverse x
I2x(1,3)=0.5;                    % component of the proton I2
I2x(2,5)=0.5;
I2x(3,1)=0.5;
I2x(4,7)=0.5;
I2x(5,2)=0.5;
I2x(6,8)=0.5;
I2x(7,4)=0.5;
I2x(8,6)=0.5;

I2y=zeros(8);                    % I2y refers to the transverse y
I2y(1,3)=-0.5*1i;                 % component of the proton I2
I2y(2,5)=-0.5*1i;
I2y(3,1)=0.5*1i;
I2y(4,7)=-0.5*1i;
I2y(5,2)=0.5*1i;
I2y(6,8)=-0.5*1i;
I2y(7,4)=0.5*1i;
I2y(8,6)=0.5*1i;
```

```
I2z=eye(8);                         % I2z refers to the longitudinal z
I2z(3,3)=-1;                        % component of the proton I2
I2z(5,5)=-1;
I2z(7,7)=-1;
I2z(8,8)=-1;
I2z=0.5*I2z;

% S represents the heteronucleus

Sx=zeros(8);                        % Sx refers to the transverse x
Sx(1,2)=0.5;                        % component ofthe heteronucleus
Sx(2,1)=0.5;
Sx(3,5)=0.5;
Sx(4,6)=0.5;
Sx(5,3)=0.5;
Sx(6,4)=0.5;
Sx(7,8)=0.5;
Sx(8,7)=0.5;

Sy=zeros(8);                        % Sy refers to the transverse y
Sy(1,2)=-0.5*1i;                     % component of the heteronucleus
Sy(2,1)=0.5*1i;
Sy(3,5)=-0.5*1i;
Sy(4,6)=-0.5*1i;
Sy(5,3)=0.5*1i;
Sy(6,4)=0.5*1i;
Sy(7,8)=-0.5*1i;
Sy(8,7)=0.5*1i;

Sz=eye(8);                          % Sz refers to the longitudinal z
Sz(2,2)=-1;                         % component of the heteronucleus
Sz(5,5)=-1;
Sz(6,6)=-1;
Sz(8,8)=-1;
Sz=0.5*Sz;

% Used operators defined below

H=2*pi*(J(1)*(I1x*I2x+I1y*I2y+...   % Calculate Hamiltonian, assuming
I1z*I2z)+J(2)*I1z*Sz+J(3)*I2z*Sz);  %low field (strong homonuclear
                                    % coupling and weak heteronuclear
                                    % coupling regime)
```

```
rou0=I1x*I2x+I1y*I2y+I1z*I2z;% initial singlet-state operator

RI1pi=cos(pi/2)*eye(8)...
    +2*1i*sin(pi/2)*I1x; % The 180x pulse for proton I1

RI2pi=cos(pi/2)*eye(8)...% The 180x pulse for proton I2
    +2*1i*sin(pi/2)*I2x;

RSx=cos(pi/4)*eye(8)... % The 90x pulse for 13C
    +2*1i*sin(pi/4)*Sx;

RSy=cos(pi/4)*eye(8)...% The 90y pulse for 13C
    +2*1i*sin(pi/4)*Sy;

RIpi=RI1pi*RI2pi;              % The 180x pulse for both protons

Ut1=expm(-1i*H*(t(1)));          % Calculate the evolving operator
Ut2=expm(-1i*H*(t(2)));          % Calculate the evolving operator
Ut3=expm(-1i*H*(t(3)));         % Calculate the evolving operator
Ut4=expm(-1i*H*(t(4)));         % Calculate the evolving operator

rou=Ut1*rou0*conj(Ut1);% Calculate the spin state after
rou=inv(RIpi)*rou*(RIpi);% applying hyper-SHIELDED sequence
rou=Ut2*rou*conj(Ut2);
rou=inv(RSy)*rou*(RSy);
rou=Ut3*rou*conj(Ut3);
rou=inv(RIpi)*rou*(RIpi);
rou=Ut4*rou*conj(Ut4);
rou=inv(RSx)*rou*(RSx);

end
```

In a more general case, while a short a pulse is applied to any I_1I_2S spin system states in either proton or ^{13}C channel (or both) with specific pulse amplitude and phase, the evolved density matrix could be calculated from the codes below.

```
Function [rou] = ApplyPulse(rou0,J,phiH,AmpH,phiS,AmpS,t)

% Program used to calculate the effect of a tiny pulse on 3-spin density
% matrix

% Variables: Output: rou:  Calculated new density matrix
%          Input:  rou0: The former density matrix before applied pulse
%                  J:    The J coupling constants of the spin system;
%                        J(1) refers to 1H-1H coupling, J(2) and J(3)
%                        refers to 1H-13C couplings
%                  phiH: Phase of the pulse on 1H channel (radians),
%                        measured from +x axis, within [0,pi)
%                  AmpH: Amplitude of the pulse on 1H channel (T)
%                  phiS: Phase of the pulse on 13C channel (radians),
%                        measured from +x axis, within [0,pi)
%                  AmpS: Amplitude of the pulse on 13C channel (T)
%                  t:    length of the short pulse delta (s)


% Construct Product Basis Below. All basis constructed on the order of
% [|aaa>,|aab>,|aba>,|baa>,|abb>,|bab>,|bba>,|bbb>]. Here |a> and |b>
% represents spin-up and spin-down states, as |alpha> and |beta>. The
% order corresponds to proton I1, proton I2, carbon S |I1,I2,S>

% I1 represents one of the singlet protons

I1x=zeros(8);                    % I1x refers to the transverse x
I1x(1,4)=0.5;                    % component of the proton I1
I1x(2,6)=0.5;
I1x(3,7)=0.5;
I1x(4,1)=0.5;
I1x(5,8)=0.5;
I1x(6,2)=0.5;
I1x(7,3)=0.5;
I1x(8,5)=0.5;

I1y=zeros(8);                    % I1y refers to the transverse y
I1y(1,4)=-0.5*1i;                % component of the proton I1
I1y(2,6)=-0.5*1i;
I1y(3,7)=-0.5*1i;
I1y(4,1)=0.5*1i;
I1y(5,8)=-0.5*1i;
I1y(6,2)=0.5*1i;
```

```
I1y(7,3)=0.5*1i;
I1y(8,5)=0.5*1i;

I1z=eye(8);                         % I1z refers to the longitudinal z
I1z(4,4)=-1;                        % component of the proton I1
I1z(6,6)=-1;
I1z(7,7)=-1;
I1z(8,8)=-1;
I1z=0.5*I1z;

% I2 represents the other singlet protons

I2x=zeros(8);                       % I2x refers to the transverse x
I2x(1,3)=0.5;                       % component of the proton I2
I2x(2,5)=0.5;
I2x(3,1)=0.5;
I2x(4,7)=0.5;
I2x(5,2)=0.5;
I2x(6,8)=0.5;
I2x(7,4)=0.5;
I2x(8,6)=0.5;

I2y=zeros(8);                       % I2y refers to the transverse y
I2y(1,3)=-0.5*1i;                    % component of the proton I2
I2y(2,5)=-0.5*1i;
I2y(3,1)=0.5*1i;
I2y(4,7)=-0.5*1i;
I2y(5,2)=0.5*1i;
I2y(6,8)=-0.5*1i;
I2y(7,4)=0.5*1i;
I2y(8,6)=0.5*1i;

I2z=eye(8);                         % I2z refers to the longitudinal z
I2z(3,3)=-1;                        % component of the proton I2
I2z(5,5)=-1;
I2z(7,7)=-1;
I2z(8,8)=-1;
I2z=0.5*I2z;

% S represents the heteronucleus

Sx=zeros(8);                        % Sx refers to the transverse x
Sx(1,2)=0.5;                        % component ofthe heteronucleus
Sx(2,1)=0.5;
```

```
Sx(3,5)=0.5;
Sx(4,6)=0.5;
Sx(5,3)=0.5;
Sx(6,4)=0.5;
Sx(7,8)=0.5;
Sx(8,7)=0.5;

Sy=zeros(8);                        % Sy refers to the transverse y
Sy(1,2)=-0.5*1i;                     % component of the heteronucleus
Sy(2,1)=0.5*1i;
Sy(3,5)=-0.5*1i;
Sy(4,6)=-0.5*1i;
Sy(5,3)=0.5*1i;
Sy(6,4)=0.5*1i;
Sy(7,8)=-0.5*1i;
Sy(8,7)=0.5*1i;

Sz=eye(8);                          % Sz refers to the longitudinal z
Sz(2,2)=-1;                         % component of the heteronucleus
Sz(5,5)=-1;
Sz(6,6)=-1;
Sz(8,8)=-1;
Sz=0.5*Sz;

% Used Constants are defined below

gammaH=4.257*10^7;                   % The gyromagnetic ratio for 1H  (Hz/T)
gammaS=1.070*10^7;                   % The gyromagnetic ratio for 13C (Hz/T)

% Calculate the angle of rotation below

thetaH=2*pi*gammaH*AmpH*t;           % The angle of rotation for 1H;
thetaS=2*pi*gammaS*AmpS*t;           % The angle of rotation for 13C;

% Used operators defined below

H=2*pi*(J(1)*(I1x*I2x+I1y*I2y+...  % Calculate Hamiltonian, assuming
low
I1z*I2z)+J(2)*I1z*Sz+J(3)*I2z*Sz); % field (strong homonuclear coupling
% and weak heteronuclear coupling
% regime)

RI1=cos(thetaH/2)*eye(8)+2*1i*... % Calculate the rotation for proton I1
    sin(thetaH/2)*(cos(phiH)*I1x...
```

```
    +sin(phiH)*I1y);

RI2=cos(thetaH/2)*eye(8)+2*1i*...   % Calculate the rotation for proton
I2
    sin(thetaH/2)*(cos(phiH)*I2x...
    +sin(phiH)*I2y);

RS=cos(thetaS/2)*eye(8)+2*1i*...    % Calculate the rotation for
    sin(thetaS/2)*(cos(phiS)*Sx...  % heteronucleus 13C
    +sin(phiS)*Sy);

RI=RI1*RI2;                         % Calculate the rotation for both 1H

R=RI*RS;                            % Calculate the full expression of
% rotation

U=expm(-1i*H*(t/2));                % Calculate the evolving operator

% Calculate the evolved density matrix below

routemp=U*rou0*conj(U);           % Calculate the evolved density matrix
% for the first half time period

routemp=(R\routemp)*(R);          % Calculate the effect of the
% applied pulse

routemp=U*routemp*conj(U);        % Calculate the evolved density matrix
% after the next half time period

rou=routemp;                    % The final calculated density matrix

end
```

D.2. Pulse programs for I_1I_2SR spin system pulse sequence

As described in Chapter III, for an I_1I_2SR spin system, the Hamiltonian, each pulse and spin state could be represented by a 16x16 density matrix. The pulse to transfer polarization level, as in Chapter III, is illustrated in Figure D.2.

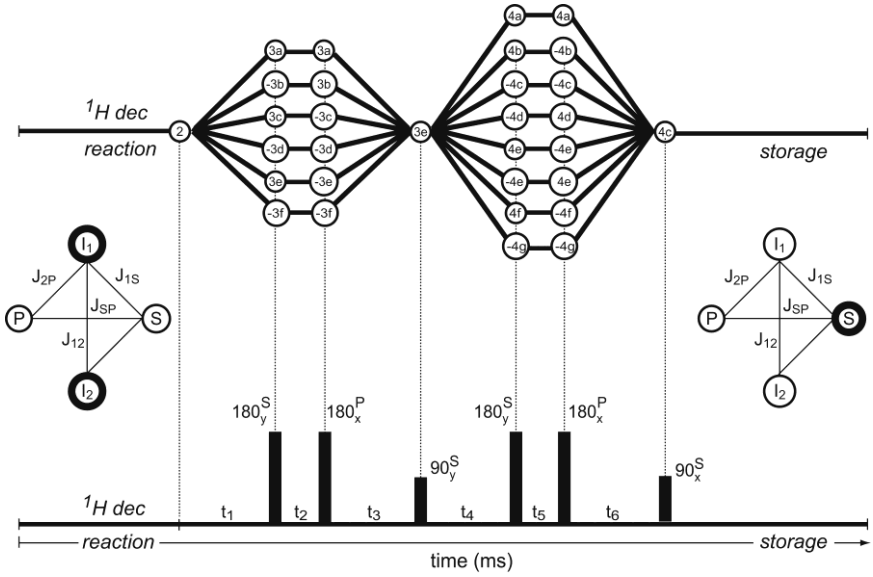

Figure D.2. Evolution of density matrix components (upper graph) and the associated pulse sequence (lower graph) for focusing parahydrogen singlet-states ($I_1 \cdot I_2$) into pure magnetization on an adjacent coupled (S) nucleus for I_1I_2SR spin systems in the strong coupling regime. Labels S and P refer generally to coupled S nucleus (for example, ^{13}C and ^{31}P). Symbols ($3_{a\text{-}f}$, $4_{a\text{-}g}$) correspond to components of the density operator.

In Figure D.2, the effective pulses are two 180 (+x) pulses on ^{13}C channel, two 180 (+x) pulses on proton channel, and two 90 (+x and +y) pulses on ^{13}C channel. The evolution of states, along with Hamiltonian and initial states are shown in Chapter III and Appendix B & C. Below is the Matlab code used to calculate the final density matrix after applying the pulse sequence to a given I_1I_2SR spin system with coupling constants.

```
Function [rou]= FourSpinHyperSHIELDED(J,t)
%Calculating final density matrix for 4 spin system with 2 protons and
%two heteronuclei
% J(1):I1-I2; J(2):I1-S;J(3):I1-R; J(4):I2-S; J(5):I2-R; J(6):S-R;
% Spin order transferred to S
% Output: rou: final density matrix
% Input:  J:   J coupling constants of the spin system, in the form of
%             [J12,J1S,J1R,J2S,J2R,JSR] (Hz)
```

```
%          t:  The time intervals (t(1)-t(6)) of the pulse sequence

% General Product Operators Defined Below
% I1 and I2 represent the two protons, while S and R represent the two
% heteronuclei

% The operators for one of the singlet protons I1
I1x=zeros(16);% I1x refers to the transverse x
I1x(1,5)=0.5;% component of proton I1
I1x(5,1)=0.5;
I1x(2,9)=0.5;
I1x(9,2)=0.5;
I1x(3,10)=0.5;
I1x(10,3)=0.5;
I1x(4,11)=0.5;
I1x(11,4)=0.5;
I1x(6,13)=0.5;
I1x(13,6)=0.5;
I1x(7,14)=0.5;
I1x(14,7)=0.5;
I1x(8,15)=0.5;
I1x(15,8)=0.5;
I1x(12,16)=0.5;
I1x(16,12)=0.5;

I1y=-1i*I1x;% I1y refers to the transverse y
I1y(5,1)=0.5*1i;% component of proton I1
I1y(9,2)=0.5*1i;
I1y(10,3)=0.5*1i;
I1y(11,4)=0.5*1i;
I1y(13,6)=0.5*1i;
I1y(14,7)=0.5*1i;
I1y(15,8)=0.5*1i;
I1y(16,12)=0.5*1i;

I1z=eye(16);% I1z refers to the longitudinal
I1z(5,5)=-1;% z component of proton I1
I1z(9,9)=-1;
I1z(10,10)=-1;
I1z(11,11)=-1;
I1z(13,13)=-1;
I1z(14,14)=-1;
I1z(15,15)=-1;
I1z(16,16)=-1;
```

```
I1z=0.5*I1z;

% The operators for one of the singlet protons I2
I2x=zeros(16);% I2x refers to the transverse x
I2x(1,4)=0.5;% component of proton I2
I2x(4,1)=0.5;
I2x(2,7)=0.5;
I2x(7,2)=0.5;
I2x(3,8)=0.5;
I2x(8,3)=0.5;
I2x(5,11)=0.5;
I2x(11,5)=0.5;
I2x(6,12)=0.5;
I2x(12,6)=0.5;
I2x(9,14)=0.5;
I2x(14,9)=0.5;
I2x(10,15)=0.5;
I2x(15,10)=0.5;
I2x(13,16)=0.5;
I2x(16,13)=0.5;

I2y=-1i*I2x;% I2y refers to the transverse y
I2y(4,1)=0.5*1i;% component of proton I2
I2y(7,2)=0.5*1i;
I2y(8,3)=0.5*1i;
I2y(11,5)=0.5*1i;
I2y(12,6)=0.5*1i;
I2y(14,9)=0.5*1i;
I2y(15,10)=0.5*1i;
I2y(16,13)=0.5*1i;

I2z=eye(16);% I2z refers to the longitudinal
I2z(4,4)=-1;% z component of proton I2
I2z(7,7)=-1;
I2z(8,8)=-1;
I2z(11,11)=-1;
I2z(12,12)=-1;
I2z(14,14)=-1;
I2z(15,15)=-1;
I2z(16,16)=-1;
I2z=0.5*I2z;

% S represents the first heteronuclei S
Sx=zeros(16);% Sx refers to the transverse x
```

```
Sx(1,3)=0.5;% component of heteronucleus S
Sx(3,1)=0.5;
Sx(2,6)=0.5;
Sx(6,2)=0.5;
Sx(4,8)=0.5;
Sx(8,4)=0.5;
Sx(5,10)=0.5;
Sx(10,5)=0.5;
Sx(7,12)=0.5;
Sx(12,7)=0.5;
Sx(9,13)=0.5;
Sx(13,9)=0.5;
Sx(11,15)=0.5;
Sx(15,11)=0.5;
Sx(14,16)=0.5;
Sx(16,14)=0.5;

Sy=-1i*Sx;% Sy refers to the transverse y
Sy(3,1)=0.5*1i;% component of heteronucleus S
Sy(6,2)=0.5*1i;
Sy(8,4)=0.5*1i;
Sy(10,5)=0.5*1i;
Sy(12,7)=0.5*1i;
Sy(13,9)=0.5*1i;
Sy(15,11)=0.5*1i;
Sy(16,14)=0.5*1i;

Sz=eye(16);% Sz refers to the longitudinal
Sz(3,3)=-1;% z component of heteronucleus S
Sz(6,6)=-1;
Sz(8,8)=-1;
Sz(10,10)=-1;
Sz(12,12)=-1;
Sz(13,13)=-1;
Sz(15,15)=-1;
Sz(16,16)=-1;
Sz=0.5*Sz;

% R represents the other heteronucleus R
Rx2=zeros(16);% Rx refers to the transverse x
Rx(1,2)=0.5;% component of heteronucleus R
Rx(2,1)=0.5;
Rx(3,6)=0.5;
Rx(6,3)=0.5;
```

```
Rx(4,7)=0.5;
Rx(7,4)=0.5;
Rx(5,9)=0.5;
Rx(9,5)=0.5;
Rx(8,12)=0.5;
Rx(12,8)=0.5;
Rx(10,13)=0.5;
Rx(13,10)=0.5;
Rx(11,14)=0.5;
Rx(14,11)=0.5;
Rx(15,16)=0.5;
Rx(16,15)=0.5;

Ry=-1i*Rx;% Ry refers to the transverse y
Ry(2,1)=0.5*1i;% component of heteronucleus R
Ry(6,3)=0.5*1i;
Ry(7,4)=0.5*1i;
Ry(9,5)=0.5*1i;
Ry(12,8)=0.5*1i;
Ry(13,10)=0.5*1i;
Ry(14,11)=0.5*1i;
Ry(16,15)=0.5*1i;

Rz=eye(16);% Rz refers to the longitudinal
Rz(2,2)=-1;% z component of heteronucleus R
Rz(6,6)=-1;
Rz(7,7)=-1;
Rz(9,9)=-1;
Rz(12,12)=-1;
Rz(13,13)=-1;
Rz(14,14)=-1;
Rz(16,16)=-1;
Rz=0.5*Rz;

% The 90 and 180 degree pulse operators for each spin calculated below
Rx90I1=(1/(sqrt(2)))*eye(16)…          % 90degree I1 pulse around x axis
+sqrt(2)*1i*I1x;
Rx180I1=2*1i*I1x;% 180degree I1 pulse around x axis
Ry90I1=(1/(sqrt(2)))*eye(16)…          % 90degree I1 pulse around y axis
+sqrt(2)*1i*I1y;
Ry180I1=2*1i*I1y;% 180degree I1 pulse around y axis

Rx90I2=(1/(sqrt(2)))*eye(16)…          % 90degree I2 pulse around x axis
+sqrt(2)*1i*I2x;
```

```
Rx180I2=2*1i*I2x;% 180degree I2 pulse around x axis
Ry90I2=(1/(sqrt(2)))*eye(16)…          % 90degree I2 pulse around y axis
+sqrt(2)*1i*I2y;
Ry180I2=2*1i*I2y;% 180degree I2 pulse around y axis

Rx90S=(1/(sqrt(2)))*eye(16)…           % 90degree S pulse around x axis
+sqrt(2)*1i*Sx;
Rx180S=2*1i*Sx;% 180degree S pulse around x axis
Ry90S=(1/(sqrt(2)))*eye(16)…           % 90degree S pulse around y axis
+sqrt(2)*1i*Sy;
Ry180S=2*1i*Sy;% 180degree S pulse around y axis

Rx90R=(1/(sqrt(2)))*eye(16)…           % 90degree R pulse around x axis
+sqrt(2)*1i*Rx;
Rx180R=2*1i*Rx;% 180degree R pulse around x axis
Ry90R=(1/(sqrt(2)))*eye(16)…% 90degree R pulse around y axis
+sqrt(2)*1i*Ry;
Ry180R=2*1i*Ry;% 180degree S pulse around y axis

Rx90H=Rx90I1*Rx90I2;% 90degree H pulse (I1 and I2)
                                        % around x axis
Rx180H=Rx180I1*Rx180I2;% 180degree H pulse (I1 and I2)
                                        % around x axis
Ry90H=Ry90I1*Ry90I2;% 90degree H pulse (I1 and I2)
                                        % around y axis
Ry180H=Ry180I1*Ry180I2;% 180degree H pulse (I1 and I2)
                                        % around y axis

% The initial density matrix and Hamiltonian calculated below
Sigma0=I1x*I2x+I1y*I2y;
H=2*pi*(J(1)*(I1x*I2x+I1y*I2y+I1z*I2z)+J(2)*I1z*Sz+J(3)*I1z*Rz...
    +J(4)*I2z*Sz+J(5)*I2z*Rz+J(6)*Sz*Rz);

% The evolution propagators defined below
Ut1=expm(-1i*H*t1);
Ut2=expm(-1i*H*t2);
Ut3=expm(-1i*H*t3);
Ut4=expm(-1i*H*t4);
Ut5=expm(-1i*H*t5);
Ut6=expm(-1i*H*t6);

% The evolution of density matrix with hyer-SHIELDED pulse sequence
sigma=Ut1*sigma0*conj(Ut1);
sigma=(Rx180S\sigma)*Rx180S;
```

```
sigma=Ut2*sigma*conj(Ut2);
sigma=(Rx180H\sigma)*Rx180H;
sigma=Ut3*sigma*conj(Ut3);
sigma=(Ry90S\sigma)*Ry90S;
sigma=Ut4*sigma*conj(Ut4);
sigma=(Rx180S\sigma)*Rx180S;
sigma=Ut5*sigma*conj(Ut5);
sigma=(Rx180H\sigma)*Rx180H;
sigma=Ut6*sigma*conj(Ut6);
sigma=(Rx90S\sigma)*Rx90S;
rou=sigma;

end
```

In the I_1I_2SR spin systems, the evolution of product operators becomes much more complicated than I_1I_2S spin systems. Therefore it is straightforward to calculate the polarization level from the density matrix directly. Below is the matlab code that is used to calculate the optimum time intervals of the pulse sequence to transfer polarization for an I_1I_2SR spin system with given scalar coupling constants. To minimize calculation, the time intervals are calculated in two independent steps as described in Chapter III.

```
function [tau,t] = fourspinHyperSHIELDED(J,dur)
%Calculating time intervals for 4 spin system with 2 H and 2 heteronucleai
% J(1):I1-I2; J(2):I1-S;J(3):I1-R; J(4):I2-S; J(5):I2-R; J(6):S-R;
% Spin order transferred to S
% Output: tau: The time interval parameters when choosing (I1z-I2z)Sz in
%            the first step, with tau(7) indicating final polarization
%            (seconds)
%        t:  The time interval parameters when choosing (I1yI2x-I1xI2y)Sz
%            in the first step, with t(7) indicating final polarization
%            (seconds)
% Input:  J:   J coupling constants of the spin system, in the form of
%            [J12,J1S,J1R,J2S,J2R,JSR] (Hz)
%        dur: Total duration of the pulse sequence (seconds)
```

```
% Product Operators Defined Below, with I1 and I2 represent the two protons,
% and S and R represent the two heteronuclei

% The operators for one of the singlet protons I1
I1x=zeros(16);                          % I1x refers to the transverse x
I1x(1,5)=0.5;                           % component of proton I1
I1x(5,1)=0.5;
I1x(2,9)=0.5;
I1x(9,2)=0.5;
I1x(3,10)=0.5;
I1x(10,3)=0.5;
I1x(4,11)=0.5;
I1x(11,4)=0.5;
I1x(6,13)=0.5;
I1x(13,6)=0.5;
I1x(7,14)=0.5;
I1x(14,7)=0.5;
I1x(8,15)=0.5;
I1x(15,8)=0.5;
I1x(12,16)=0.5;
I1x(16,12)=0.5;

I1y=-1i*I1x;                            % I1y refers to the transverse y
I1y(5,1)=0.5*1i;                        % component of proton I1
I1y(9,2)=0.5*1i;
I1y(10,3)=0.5*1i;
I1y(11,4)=0.5*1i;
I1y(13,6)=0.5*1i;
I1y(14,7)=0.5*1i;
I1y(15,8)=0.5*1i;
I1y(16,12)=0.5*1i;

I1z=eye(16);                            % I1z refers to the longitudinal
I1z(5,5)=-1;                            % z component of proton I1
I1z(9,9)=-1;
I1z(10,10)=-1;
I1z(11,11)=-1;
I1z(13,13)=-1;
I1z(14,14)=-1;
I1z(15,15)=-1;
I1z(16,16)=-1;
I1z=0.5*I1z;
```

```
% The operators for one of the singlet protons I2
I2x=zeros(16);                          % I2x refers to the transverse x
I2x(1,4)=0.5;                           % component of proton I2
I2x(4,1)=0.5;
I2x(2,7)=0.5;
I2x(7,2)=0.5;
I2x(3,8)=0.5;
I2x(8,3)=0.5;
I2x(5,11)=0.5;
I2x(11,5)=0.5;
I2x(6,12)=0.5;
I2x(12,6)=0.5;
I2x(9,14)=0.5;
I2x(14,9)=0.5;
I2x(10,15)=0.5;
I2x(15,10)=0.5;
I2x(13,16)=0.5;
I2x(16,13)=0.5;

I2y=-1i*I2x;                            % I2y refers to the transverse y
I2y(4,1)=0.5*1i;                        % component of proton I2
I2y(7,2)=0.5*1i;
I2y(8,3)=0.5*1i;
I2y(11,5)=0.5*1i;
I2y(12,6)=0.5*1i;
I2y(14,9)=0.5*1i;
I2y(15,10)=0.5*1i;
I2y(16,13)=0.5*1i;

I2z=eye(16);                            % I2z refers to the longitudinal
I2z(4,4)=-1;                            % z component of proton I2
I2z(7,7)=-1;
I2z(8,8)=-1;
I2z(11,11)=-1;
I2z(12,12)=-1;
I2z(14,14)=-1;
I2z(15,15)=-1;
I2z(16,16)=-1;
I2z=0.5*I2z;

% S represents the first heteronucleus S
Sx=zeros(16);                           % Sx refers to the transverse x
Sx(1,3)=0.5;                            % component of heteronucleus S
```

```
Sx(3,1)=0.5;
Sx(2,6)=0.5;
Sx(6,2)=0.5;
Sx(4,8)=0.5;
Sx(8,4)=0.5;
Sx(5,10)=0.5;
Sx(10,5)=0.5;
Sx(7,12)=0.5;
Sx(12,7)=0.5;
Sx(9,13)=0.5;
Sx(13,9)=0.5;
Sx(11,15)=0.5;
Sx(15,11)=0.5;
Sx(14,16)=0.5;
Sx(16,14)=0.5;

Sy=-1i*Sx;                              % Sy refers to the transverse y
Sy(3,1)=0.5*1i;                         % component of heteronucleus S
Sy(6,2)=0.5*1i;
Sy(8,4)=0.5*1i;
Sy(10,5)=0.5*1i;
Sy(12,7)=0.5*1i;
Sy(13,9)=0.5*1i;
Sy(15,11)=0.5*1i;
Sy(16,14)=0.5*1i;

Sz=eye(16);                             % Sz refers to the longitudinal
Sz(3,3)=-1;                             % z component of heteronucleus S
Sz(6,6)=-1;
Sz(8,8)=-1;
Sz(10,10)=-1;
Sz(12,12)=-1;
Sz(13,13)=-1;
Sz(15,15)=-1;
Sz(16,16)=-1;
Sz=0.5*Sz;

% R represents the other heteronuclei R
Rx2=zeros(16);                           % Rx refers to the transverse x
Rx(1,2)=0.5;                             % component of heteronucleus R
Rx(2,1)=0.5;
Rx(3,6)=0.5;
Rx(6,3)=0.5;
Rx(4,7)=0.5;
```

```
Rx(7,4)=0.5;
Rx(5,9)=0.5;
Rx(9,5)=0.5;
Rx(8,12)=0.5;
Rx(12,8)=0.5;
Rx(10,13)=0.5;
Rx(13,10)=0.5;
Rx(11,14)=0.5;
Rx(14,11)=0.5;
Rx(15,16)=0.5;
Rx(16,15)=0.5;

Ry=-1i*Rx;                                  % Ry refers to the transverse y
Ry(2,1)=0.5*1i;                             % component of heteronucleus R
Ry(6,3)=0.5*1i;
Ry(7,4)=0.5*1i;
Ry(9,5)=0.5*1i;
Ry(12,8)=0.5*1i;
Ry(13,10)=0.5*1i;
Ry(14,11)=0.5*1i;
Ry(16,15)=0.5*1i;

Rz=eye(16);                                % Rz refers to the longitudinal
Rz(2,2)=-1;                                % z component of heteronucleus R
Rz(6,6)=-1;
Rz(7,7)=-1;
Rz(9,9)=-1;
Rz(12,12)=-1;
Rz(13,13)=-1;
Rz(14,14)=-1;
Rz(16,16)=-1;
Rz=0.5*Rz;

% The 90 and 180 degree pulse operators for each spin calculated below
Rx90I1=(1/(sqrt(2)))*eye(16)…              % 90degree I1 pulse around x axis
+sqrt(2)*1i*I1x;
Rx180I1=2*1i*I1x;                          % 180degree I1 pulse around x axis
Ry90I1=(1/(sqrt(2)))*eye(16)…              % 90degree I1 pulse around y axis
+sqrt(2)*1i*I1y;
Ry180I1=2*1i*I1y;                          % 180degree I1 pulse around y axis

Rx90I2=(1/(sqrt(2)))*eye(16)…              % 90degree I2 pulse around x axis
+sqrt(2)*1i*I2x;
Rx180I2=2*1i*I2x;                          % 180degree I2 pulse around x axis
```

```
Ry90I2=(1/(sqrt(2)))*eye(16)…          % 90degree I2 pulse around y axis
+sqrt(2)*1i*I2y;
Ry180I2=2*1i*I2y;                      % 180degree I2 pulse around y axis

Rx90S=(1/(sqrt(2)))*eye(16)…           % 90degree S pulse around x axis
+sqrt(2)*1i*Sx;
Rx180S=2*1i*Sx;                        % 180degree S pulse around x axis
Ry90S=(1/(sqrt(2)))*eye(16)…           % 90degree S pulse around y axis
+sqrt(2)*1i*Sy;
Ry180S=2*1i*Sy;                        % 180degree S pulse around y axis

Rx90R=(1/(sqrt(2)))*eye(16)…           % 90degree R pulse around x axis
+sqrt(2)*1i*Rx;
Rx180R=2*1i*Rx;                        % 180degree R pulse around x axis
Ry90R=(1/(sqrt(2)))*eye(16)…% 90degree R pulse around y axis
+sqrt(2)*1i*Ry;
Ry180R=2*1i*Ry;                        % 180degree S pulse around y axis

Rx90H=Rx90I1*Rx90I2;                   % 90degree H pulse (I1 and I2)
                                       % around x axis
Rx180H=Rx180I1*Rx180I2;                % 180degree H pulse (I1 and I2)
                                       % around x axis
Ry90H=Ry90I1*Ry90I2;                   % 90degree H pulse (I1 and I2)
                                       % around y axis
Ry180H=Ry180I1*Ry180I2;                % 180degree H pulse (I1 and I2)
                                       % around y axis


% Initial Density Matrix for Each Step and Hamiltonian Defined Below
sigma0=I1x*I2x+I1y*I2y;% initial singlet-state
sigma1=Sx*(I1z-I2z);% the state after the 1st step
sigma2=2*Sx*(I2x*I1y-I1x*I2y);% another state after the 1st step
H=2*pi*(J(1)*(I1x*I2x+I1y*I2y+I1z*I2z)+J(2)*I1z*Sz+J(3)*I1z*Rz...
    +J(4)*I2z*Sz+J(5)*I2z*Rz+J(6)*Sz*Rz);
maxtime=dur/6;

% Calculate the Optimum Time Intervals (tau) for the First Step, each time
% interval (t1,t2,t3) are searched by the range from 0.1maxtime, 0.01
% maxtime, to 0.001 maxtime, sigma(4,4)+sigma(7,7) represents the
% coefficient of sigma1
for k1=1:10;
    t1=maxtime*0.1*k1;
    Ut1=expm(-1i*H*t1);
for k2=1:10;
```

```
       t2=maxtime*0.1*k2;
       Ut2=expm(-1i*H*t2);
for k3=1:10;
          t3=maxtime*0.1*k3;
          Ut3=expm(-1i*H*t3);
          sigma=Ut1*sigma0*conj(Ut1);
          sigma=(Rx180S\sigma)*Rx180S;
          sigma=Ut2*sigma*conj(Ut2);
          sigma=(Rx180H\sigma)*Rx180H;
          sigma=Ut3*sigma*conj(Ut3);
          F1(k1,k2,k3)=abs(sigma(4,4)+sigma(7,7));
end
end
end

[maxF1,maxind1]=max(F1(:));
[K1,K2,K3]=ind2sub(size(F1),maxind1);

for l1=1:20;
   t1=maxtime*(0.1*(K1-1)+*0.01*l1);
   Ut1=expm(-1i*H*t1);
for l2=1:20;
       t2=maxtime*(0.1*(K2-1)+*0.01*l2);
       Ut2=expm(-1i*H*t2);
for l3=1:20;
          t3=maxtime*(0.1*(K3-1)+*0.01*l3);
          Ut3=expm(-1i*H*t3);
          sigma=Ut1*sigma0*conj(Ut1);
          sigma=(Rx180S\sigma)*Rx180S;
          sigma=Ut2*sigma*conj(Ut2);
          sigma=(Rx180H\sigma)*Rx180H;
          sigma=Ut3*sigma*conj(Ut3);
          F2(l1,l2,l3)=abs(sigma(4,4)+sigma(7,7));
end
end
end

[maxF2,maxind2]=max(F2(:));
[L1,L2,L3]=ind2sub(size(F2),maxind2);

for m1=1:20;
   t1=maxitme*(0.1*(K1-1)+0.01*(L1-1)+0.001*m1);
   Ut1=expm(-1i*H*t1);
for m2=1:20;
```

```
       t2=maxitme*(0.1*(K2-1)+0.01*(L2-1)+0.001*m2);
       Ut2=expm(-1i*H*t2);
for m3=1:20;
          t3=maxitme*(0.1*(K3-1)+0.01*(L3-1)+0.001*m3);
          Ut3=expm(-1i*H*t3);
          sigma=Ut1*sigma0*conj(Ut1);
          sigma=(Rx180S\sigma)*Rx180S;
          sigma=Ut2*sigma*conj(Ut2);
          sigma=(Rx180H\sigma)*Rx180H;
          sigma=Ut3*sigma*conj(Ut3);
          F3(m1,m2,m3)=abs(sigma(4,4)+sigma(7,7));
end
end
end

[maxF3,maxind3]=max(F3(:));
[M1,M2,M3]=ind2sub(size(F3),maxind3);

% The optimum time intervals tau1, tau2, tau3
tau(1)=maxitme*(0.1*(K1-1)+0.01*(L1-1)+0.001*M1);
tau(2)=maxitme*(0.1*(K2-1)+0.01*(L2-1)+0.001*M2);
tau(3)=maxitme*(0.1*(K3-1)+0.01*(L3-1)+0.001*M3);

% Calculate the Optimum Time Intervals (tau) for the Second Step, each
% time interval (t4,t5,t6) are searched by the range from 0.1maxtime, 0.01
% maxtime, to 0.001 maxtime, imag(sigma(4,8))+imag(sigma(7,12))
% represents the coefficient of final state
for o1=1:10;
   t1=maxtime*0.1*o1;
   Ut1=expm(-1i*H*t1);
for o2=1:10;
       t2=maxtime*0.1*o2;
       Ut2=expm(-1i*H*t2);
for o3=1:10;
          t3=maxtime*0.1*o3;
          Ut3=expm(-1i*H*t3);
          sigma=Ut1*sigma1*conj(Ut1);
          sigma=(Rx180S\sigma)*Rx180S;
          sigma=Ut2*sigma*conj(Ut2);
          sigma=(Rx180H\sigma)*Rx180H;
          sigma=Ut3*sigma*conj(Ut3);
          F4(o1,o2,o3)=abs(imag(sigma(4,8))+imag(sigma(7,12)));
end
end
```

```
end

[maxF4,maxind4]=max(F4(:));
[O1,O2,O3]=ind2sub(size(F4),maxind4);

for p1=1:20;
   t1=maxtime*(0.1*(O1-1)+0.01*p1);
   Ut1=expm(-1i*H*t1);
for p2=1:20;
      t2=maxtime*(0.1*(O2-1)+0.01*p2);
      Ut2=expm(-1i*H*t2);
for p3=1:20;
         t3=maxtime*(0.1*(O3-1)+0.01*p3);
         Ut3=expm(-1i*H*t3);
         sigma=Ut1*sigma1*conj(Ut1);
         sigma=(Rx180S\sigma)*Rx180S;
         sigma=Ut2*sigma*conj(Ut2);
         sigma=(Rx180H\sigma)*Rx180H;
         sigma=Ut3*sigma*conj(Ut3);
       F5(p1,p2,p3)=abs(imag(sigma(4,8))+imag(sigma(7,12)));
end
end
end

[maxF5,maxind5]=max(F5(:));
[P1,P2,P3]=ind2sub(size(F5),maxind5);

for q1=1:20;
   t1=maxtime*(0.1*(O1-1)+0.01*(P1-1)+0.001*q1);
   Ut1=expm(-1i*H*t1);
for q2=1:20;
      t2=maxtime*(0.1*(O2-1)+0.01*(P2-1)+0.001*q2);
      Ut2=expm(-1i*H*t2);
for q3=1:20;
         t3=maxtime*(0.1*(O3-1)+0.01*(P3-1)+0.001*q3);
         Ut3=expm(-1i*H*t3);
         sigma=Ut1*sigma1*conj(Ut1);
         sigma=(Rx180S\sigma)*Rx180S;
         sigma=Ut2*sigma*conj(Ut2);
         sigma=(Rx180H\sigma)*Rx180H;
         sigma=Ut3*sigma*conj(Ut3);
      F6(q1,q2,q3)=abs(imag(sigma(4,8))+imag(sigma(7,12)));
end
end
```

```
end

[maxF6,maxind6]=max(F6(:));
[Q1,Q2,Q3]=ind2sub(size(F6),maxind6);

% The optimum time intervals tau4, tau5, tau6, tau7 represents final
% polarization level
tau(4)=maxtime*(0.1*(O1-1)+0.01*(P1-1)+0.001*Q1);
tau(5)=maxtime*(0.1*(O2-1)+0.01*(P2-1)+0.001*Q2);
tau(6)=maxtime*(0.1*(O3-1)+0.01*(P3-1)+0.001*Q3);
tau(7)=F3(M1,M2,M3)*F6(Q1,Q2,Q3);

% Calculate the Optimum Time Intervals (tau) for the First Step, each time
% interval (t1,t2,t3) are searched by the range from 0.1maxtime, 0.01
% maxtime, to 0.001 maxtime, imag(sigma(4,5))+imag(sigma(7,9))
% represents the coefficient of sigma2
for k1=1:10;
    t1=maxtime*0.1*k1;
    Ut1=expm(-1i*H*t1);
for k2=1:10;
        t2=maxtime*0.1*k2;
        Ut2=expm(-1i*H*t2);
for k3=1:10;
            t3=maxtime*0.1*k3;
            Ut3=expm(-1i*H*t3);
simga=Ut1*sigma0*conj(Ut1);
            sigma=(Rx180S\sigma)*Rx180S;
            sigma=Ut2*sigma*conj(Ut2);
            sigma=(Rx180H\sigma)*Rx180H;
            sigma=Ut3*sigma*conj(Ut3);
        F1(k1,k2,k3)=abs(imag(sigma(4,5)+imag(sigma(7,9))));
end
end
end

[maxF1,maxind1]=max(F1(:));
[K1,K2,K3]=ind2sub(size(F1),maxind1);

for l1=1:20;
    t1=maxtime*(0.1*(K1-1)+0.01*l1);
    Ut1=expm(-1i*H*t1);
for l2=1:20;
        t2=maxtime*(0.1*(K2-1)+0.01*l2);
        Ut2=expm(-1i*H*t2);
```

```
for l3=1:20;
          t3=maxtime*(0.1*(K3-1)+0.01*l3);
          Ut3=expm(-1i*H*t3);
          sigma=Ut1*sigma0*conj(Ut1);
          sigma=(Rx180S1\sigma)*Rx180S1;
          sigma=Ut2*sigma*conj(Ut2);
          sigma=(Rx180H\sigma)*Rx180H;
          sigma=Ut3*sigma*conj(Ut3);
       F2(l1,l2,l3)=abs(imag(sigma(4,5)+imag(sigma(7,9))));
end
end
end

[maxF2,maxind2]=max(F2(:));
[L1,L2,L3]=ind2sub(size(F2),maxind2);

for m1=1:20;
   t1=maxtime*(0.1*(K1-1)+0.01*(L1-1)+0.001*m1);
   Ut1=expm(-1i*H*t1);
for m2=1:20;
       t2=maxtime*(0.1*(K2-1)+0.01*(L2-1)+0.001*m2);
       Ut2=expm(-1i*H*t2);
for m3=1:20;
          t3=maxtime*(0.1*(K3-1)+0.01*(L3-1)+0.001*m3);
          Ut3=expm(-1i*H*t3);
          sigma=Ut1*sigma0*conj(Ut1);
          sigma=(Rx180S\sigma)*Rx180S;
          sigma=Ut2*sigma*conj(Ut2);
          sigma=(Rx180H\sigma)*Rx180H;
          sigma=Ut3*sigma*conj(Ut3);
  F3(m1,m2,m3)=abs(imag(sigma(4,5)+imag(sigma(7,9))));
end
end
end

[maxF3,maxind3]=max(F3(:));
[M1,M2,M3]=ind2sub(size(F3),maxind3);

% The optimum time intervals t1, t2, t3
t(1)=maxtime*(0.1*(K1-1)+0.01*(L1-1)+0.001*M1);
t(2)=maxtime*(0.1*(K2-1)+0.01*(L2-1)+0.001*M2);
t(3)=maxtime*(0.1*(K3-1)+0.01*(L3-1)+0.001*M3);

% Calculate the Optimum Time Intervals (tau) for the Second Step, each
```

```
% time interval (t4,t5,t6) are searched by the range from 0.1maxtime, 0.01
% maxtime, to 0.001 maxtime, imag(sigma(4,8))+imag(sigma(7,12))
% represents the coefficient of final state
for o1=1:10;
    t1=maxtime*0.1*o1;
    Ut1=expm(-1i*H*t1);
for o2=1:10;
       t2=maxtime*0.1*o2;
       Ut2=expm(-1i*H*t2);
for o3=1:10;
          t3=maxtime*0.1*o3;
          Ut3=expm(-1i*H*t3);
          sigma=Ut1*sigma2*conj(Ut1);
          sigma=(Rx180S\sigma)*Rx180S;
          sigma=Ut2*sigma*conj(Ut2);
          sigma=(Rx180H\sigma)*Rx180H;
          sigma=Ut3*sigma*conj(Ut3);
       F4(o1,o2,o3)=abs(imag(sigma(4,8))+imag(sigma(7,12)));
end
end
end

[maxF4,maxind4]=max(F4(:));
[O1,O2,O3]=ind2sub(size(F4),maxind4);

for p1=1:20;
    t1=maxtime*(0.1*(O1-1)+0.01*p1);
    Ut1=expm(-1i*H*t1);
for p2=1:20;
       t2=maxtime*(0.1*(O2-1)+0.01*p2);
       Ut2=expm(-1i*H*t2);
for p3=1:20;
          t3=maxtime*(0.1*(O3-1)+0.01*p3);
          Ut3=expm(-1i*H*t3);
          sigma=Ut1*sigma2*conj(Ut1);
          sigma=(Rx180S\sigma)*Rx180S;
          sigma=Ut2*sigma*conj(Ut2);
          sigma=(Rx180H\sigma)*Rx180H;
          sigma=Ut3*sigma*conj(Ut3);
       F5(p1,p2,p3)=abs(imag(sigma(4,8))+imag(sigma(7,12)));
end
end
end
```

```
[maxF5,maxind5]=max(F5(:));
[P1,P2,P3]=ind2sub(size(F5),maxind5);

for q1=1:20;
    t1=maxtime*(0.1*(O1-1)+0.01*(P1-1)+0.001*q1);
    Ut1=expm(-1i*H*t1);
for q2=1:20;
       t2=maxtime*(0.1*(O2-1)+0.01*(P2-1)+0.001*q2);
       Ut2=expm(-1i*H*t2);
for q3=1:20;
          t3=maxtime*(0.1*(O3-1)+0.01*(P3-1)+0.001*q3);
          Ut3=expm(-1i*H*t3);
          sigma=Ut1*sigma2*conj(Ut1);
          sigma=(Rx180S\sigma)*Rx180S;
sigma=Ut2*sigma*conj(Ut2);
          sigma=(Rx180H\sigma)*Rx180H;
          sigma=Ut3*sigma*conj(Ut3);
       F6(q1,q2,q3)=abs(imag(sigma(4,8))+imag(sigma(7,12)));
end
end
end

[maxF6,maxind6]=max(F6(:));
[Q1,Q2,Q3]=ind2sub(size(F6),maxind6);

% The optimum time intervals t4, t5, t6, t7 represents final
% polarization level
t(4)=maxtime*(0.1*(O1-1)+0.01*(P1-1)+0.001*Q1);
t(5)=maxtime*(0.1*(O2-1)+0.01*(P2-1)+0.001*Q2);
t(6)=maxtime*(0.1*(O3-1)+0.01*(P3-1)+0.001*Q3);
t(7)=F3(M1,M2,M3)*F6(Q1,Q2,Q3);

end
```

D.3. Monte Carlo model for high resolution J spectroscopy and resolution

As described in Chapter IV, we constructed a Monte Carlo statistical model to get high resolution scalar coupling spectroscopy in low inhomogeneous fields by fitting the experiment data to theory, also calculate the resolution with certain experimental error. Below are the Matlab codes for calculating both scalar coupling

constants and resolutions with certain experimental error. There are three major functions in the codes. The main function (Monte Carlo) calculates the final average scalar coupling constants range and resolution within 95% confidence interval by calling the FitMontecarlo function, which fits the experiment data with standard deviation to the theoretical equations, which is contained in function (FTMontecarlo). All three major functions are shown below.

Monte Carlo:

```
function [J12range,Jdeltarange,popJ1,popdelta,popsurf] =
Montecarlo(pol, Error)

% A function used to get the resolution of J-resolving spectroscopy
% with certain experimental error
% Output:  J12range: the calculated homonuclear coupling constant range
%                  with 95% confidence range
%          Jdeltarange: the calculated coupling asymmetry range Jdelta
%                     with 95% confidence range
%          popJ1:  the calculated frequency for each homonuclear
%                   coupling constant
%          popJdelta:  the calculated frequency for each coupling
                      asymmetry Jdelta
%          popsurf:    the calculated frequency for both couplings
% Input:  pol: experimental results of a set of polarization level

% set zero for outputs
for m=1:1000;
    popJ1(m)=0;
popdelta(m)=0;
end

for o=1:1000;
for p=1:1000;
popsurf(o,p)=0;
end
end

% Fit the results by calling the function FitMontecarlo and calculate the
% corresponding frequency
```

```
for l=1:10000;
    [y]=FitMontecarlo(pol, Error);
    CoJ1=round(100*y(1));
Codelta=round(50*y(2));
    popJ1(CoJ1)=popJ1(CoJ1)+1;
popdelta(Codelta)=popdelta(Codelta)+1;
popsurf(CoJ1,Codelta)=popsurf(CoJ1,Codelta)+1;
end

% Calculate the lower and upper range of J1 with 95% confidence interval
numdn=0;
formdn=1:1000;
numdn=numdn+popJ1(mdn);
if (numdn>249)
break;
end
end

numup=0;

formup=1000:-1:1;
numup=numup+popJ1(mup);
if (numup>249)
break;
end
end

J12range=[mdn/100,mup/100];

% Calculate the lower and upper range of Jdelta with 95% confidence interval
numdn=0;

formdn=1:1000;
numdn=numdn+popdelta(mdn);
if (numdn>249)
break;
end
end

numup=0;

formup=1000:-1:1;
numup=numup+popdelta(mup);
```

```
if (numup>249)
break;
end
end

Jdeltarange=[mdn/50,mup/50];

% Plot the J1 and Jdelta spectroscopy
plot(popJ1);
plot(popdelta);
end
```

FitMontecarlo:

```
function [x]=FitMontecarlo(pol, Error)
% A function used to fit experimental data with random deviation and get
% high resolution J spectroscopy

warning offall;
hold on;

% set starting fitting points
x0=[7.5,12.5,100];

% Fit the experimental data with theory (by calling FTMontecarlo function)
% and extract J1 and Jdelta

for k=1:1:47;
    R(k)=Error*(sqrt(3))*pol(k)*rand();
    P(k)=pol(k)-0.05*(sqrt(3))*pol(k)+R(k);
end
length (P)
xdata=[1:1:length(P)];
size(xdata);
x=lsqcurvefit(@FTMontecarlo, x0, xdata, P);

end
```

FTMontecarlo:

```
function [p] = FTMontecarlo(x,xdata)
```

```
% A function of theoretical values for J-dependent polarization, used for
% fitting experimental data and get J spectroscopy

% Define the fitting components
J12=x(1);
Jdiff=x(2);
scale=x(3);

% The time intervals of each group of experiment
t(1,:)=[0.0005, 0.05847, 0.0362, 0.02828];
t(2,:)=[0.00975, 0.05847, 0.0362, 0.02828];
t(3,:)=[0.02, 0.05847, 0.0362, 0.02828];
t(4,:)=[0.032, 0.05847, 0.0362, 0.02828];
t(5,:)=[0.04, 0.05847, 0.0362, 0.02828];
t(6,:)=[0.045, 0.05847, 0.0362, 0.02828];
t(7,:)=[0.05, 0.05847, 0.0362, 0.02828];
t(8,:)=[0.06, 0.05847, 0.0362, 0.02828];
t(9,:)=[0.07, 0.05847, 0.0362, 0.02828];
t(10,:)=[0.00975, 0.05847, 0.0362, 0.107];
t(11,:)=[0.09, 0.05847, 0.0362, 0.02828];
t(12,:)=[0.1, 0.05847, 0.0362, 0.02828];
t(13,:)=[0.1104, 0.05847, 0.0362, 0.02828];
t(14,:)=[0.12, 0.05847, 0.0362, 0.02828];
t(15,:)=[0.131, 0.05847, 0.0362, 0.02828];
t(16,:)=[0.00975, 0.008, 0.0362, 0.02828];
t(17,:)=[0.00975, 0.0204, 0.0362, 0.02828];
t(18,:)=[0.00975, 0.031, 0.0362, 0.02828];
t(19,:)=[0.00975, 0.041, 0.0362, 0.02828];
t(20,:)=[0.00975, 0.077, 0.0362, 0.02828];
t(21,:)=[0.00975, 0.086, 0.0362, 0.02828];
t(22,:)=[0.00975, 0.0965, 0.0362, 0.02828];
t(23,:)=[0.00975, 0.109, 0.0362, 0.02828];
t(24,:)=[0.00975, 0.121, 0.0362, 0.02828];
t(25,:)=[0.00975, 0.05847, 0.003, 0.02828];
t(26,:)=[0.00975, 0.05847, 0.011, 0.02828];
t(27,:)=[0.00975, 0.05847, 0.017, 0.02828];
t(28,:)=[0.00975, 0.05847, 0.023, 0.02828];
t(29,:)=[0.00975, 0.05847, 0.03, 0.02828];
t(30,:)=[0.00975, 0.05847, 0.04, 0.02828];
t(31,:)=[0.00975, 0.05847, 0.05, 0.02828];
t(32,:)=[0.00975, 0.05847, 0.056, 0.02828];
t(33,:)=[0.00975, 0.05847, 0.0614, 0.02828];
t(34,:)=[0.00975, 0.05847, 0.07, 0.02828];
t(35,:)=[0.00975, 0.05847, 0.08, 0.02828];
```

```
t(36,:)=[0.00975, 0.05847, 0.0865, 0.02828];
t(37,:)=[0.00975, 0.05847, 0.09, 0.02828];
t(38,:)=[0.00975, 0.05847, 0.1, 0.02828];
t(39,:)=[0.00975, 0.05847, 0.11, 0.02828];
t(40,:)=[0.00975, 0.05847, 0.12, 0.02828];
t(41,:)=[0.00975, 0.05847, 0.13, 0.02828];
t(42,:)=[0.00975, 0.05847, 0.0362, 0.004];
t(43,:)=[0.00975, 0.05847, 0.0362, 0.012];
t(44,:)=[0.00975, 0.05847, 0.0362, 0.05];
t(45,:)=[0.00975, 0.05847, 0.0362, 0.063];
t(46,:)=[0.00975, 0.05847, 0.0362, 0.0786];
t(47,:)=[0.00975, 0.05847, 0.0362, 0.094];

% The parameters in the theoretical equations
delta=Jdiff/(2*J12);
omega=J12*(sqrt(1+delta^2));
theta=asin(1/(sqrt(1+delta^2)));

% The calculated J-sensitive theoretical polarization level
for n=1:1:length(xdata);
    p(n)=((sin(theta)*sin(2*theta)*sin(2*pi*omega*t(n,2))...
        +cos(theta)*cos(2*theta)*cos(2*pi*omega*t(n,1))...
        *sin(2*pi*omega*t(n,2))...
        -cos(theta)*sin(2*pi*omega*t(n,1))*cos(2*pi*omega*t(n,2)))...

*(0.25*sin(4*theta)+0.25*sin(4*theta)*cos(2*pi*omega*t(n,3))...
        *cos(2*pi*omega*t(n,4))+sin(2*theta)*(((sin(theta))^2)...

*cos(2*pi*omega*t(n,3))-((cos(theta))^2)*cos(2*pi*omega*t(n,4)))...
        +cos(theta)*sin(theta)*sin(2*pi*omega*t(n,3))...
        *sin(2*pi*omega*t(n,4))))...
        -(0.5*sin(2*theta)*(cos(2*theta)...
        +2*((sin(theta))^2)*cos(2*pi*omega*t(n,2))...
        -2*((cos(theta))^2)*cos(2*pi*omega*t(n,1))...
        +cos(2*theta)*cos(2*pi*omega*t(n,1))*cos(2*pi*omega*t(n,2))...
        +sin(2*pi*omega*t(n,1))*sin(2*pi*omega*t(n,2)))...
        *(cos(theta)*cos(2*pi*omega*t(n,3))*sin(2*pi*omega*t(n,4))...
        -sin(theta)*sin(2*theta)*sin(2*pi*omega*t(n,3))...
        -cos(theta)*cos(2*theta)*sin(2*pi*omega*t(n,3))...
        *cos(2*pi*omega*t(n,4))))*scale;
end
end
```

REFERENCES

1. Bloch, F., W.W. Hansen, and M.E. Packard, *Nuclear Induction.* Physical Review, 1946. **69**: p. 1.

2. Purcell, E.M., H.C. Torrey, and R.V. Pound, *Resonance Absorption by Nuclear Magnetic Moments in a Solid.* Physical Review, 1946. **69**(1-2): p. 2.

3. Albert, K., *On-line use of NMR detection in separation chemistry.* Journal of Chromatography A, 1995. **703**(1–2): p. 123-147.

4. Bendel, P., *Biomedical applications of 10B and 11B NMR.* NMR Biomed, 2005. **18**(2): p. 74-82.

5. Ernst, R.R. and G. Bodenhausen, *Principles of Nuclear Magnetic Resonance in One and Two Dimensions*. 1987, Oxford: Clarendon Press.

6. Kitaygorodskiy, A., et al., *NMR Detection of Single-Walled Carbon Nanotubes in Solution.* Journal of the American Chemical Society, 2005. **127**(20): p. 7517-7520.

7. Widmer, H. and W. Jahnke, *Protein NMR in biomedical research.* Cellular and molecular life sciences : CMLS, 2004. **61**(5): p. 580-599.

8. Wu, N., et al., *Nanoliter Volume Sample cells for 1H NMR: Application to Online Detection in Capillary Electrophoresis.* Journal of the American Chemical Society, 1994. **116**(17): p. 7929-7930.

9. Larmor, J., *A dynamical theory of the electric and luminiferous medium Part II. Theory of electrons.* Proceedings of the Royal Society, 1895. **58**(222).

10. Gottlieb, H.E., V. Kotlyar, and A. Nudelman, *NMR Chemical Shifts of Common Laboratory Solvents as Trace Impurities.* The Journal of Organic Chemistry, 1997. **62**(21): p. 7512-7515.

11. Jacobsen, N.E., *NMR Spectroscopy Explained*. 2007: John Wiley & Sons.

12. Shen, Y., et al., *Consistent blind protein structure generation from NMR chemical shift data.* Proceedings of the National Academy of Sciences, 2008. **105**(12): p. 4685-4690.

13. Burt, S.R., *MRI of Heterogeneous Hydrogenation Reactions Using Para-hydrogen Polarization*, 2008, University of California, Berkeley: Berkeley.

14. McRobbie, D. and M.A. Foster, *Cardiac response to pulsed magnetic fields with regard to safety in NMR imaging.* Physics in Medicine and Biology, 1985. **30**(7): p. 695.

15. Reid, A., F.W. Smith, and J.M.S. Hutchison, *Nuclear magnetic resonance imaging and its safety implications: follow-up of 181 patients.* British Journal of Radiology, 1982. **55**(658): p. 784-786.

16. Saunders, R.D. and H. Smith, *Safety aspects of NMR clinical imaging.* British medical bulletin, 1984. **40**(2): p. 148-154.

17. Smith, F.W., *Safety of NMR imaging.* Lancet, 1982. **1**(8278): p. 974.

18. Zeeman, P., *The Effect of Magnetization on the Nature of Light Emitted by a Substance.* Nature, 1897. **55**(1424): p. 347.

19. Shankar, R., *Principles of Quantum Mechanics*. 2 ed. 1994: Springer.

20. Laws, D.D., H.M. Bitter, and A. Jerschow, *Solid-state NMR spectroscopic methods in chemistry.* Angew Chem Int Ed Engl, 2002. **41**(17): p. 3096-129.

21. Schmidt-Rohr, K. and H.W. Spiess, *Multidimensional Solid-state NMR and Polymers*. 1994, London: Academic Press.

22. Farrow, N.A., et al., *Backbone Dynamics of a Free and a Phosphopeptide-Complexed Src Homology 2 Domain Studied by 15N NMR Relaxation.* Biochemistry, 1994. **33**(19): p. 5984-6003.

23. Peng, J.W. and G. Wagner, *Mapping of spectral density functions using heteronuclear NMR relaxation measurements.* Journal of Magnetic Resonance

(1969), 1992. **98**(2): p. 308-332.

24. Swift, T.J. and R.E. Connick, *NMR-Relaxation Mechanisms of O^{17} in Aqueous Solutions of Paramagnetic Cations and the Lifetime of Water Molecules in the First Coordination Sphere.* Journal of Chemical Physics, 1962. **37**(2): p. 307.

25. Tjandra, N., et al., *Rotational diffusion anisotropy of human ubiquitin from 15N NMR relaxation.* Journal of the American Chemical Society, 1995. **117**(50): p. 12562-12566.

26. Wansapura, J.P., et al., *NMR relaxation times in the human brain at 3.0 tesla.* Journal of Magnetic Resonance Imaging, 1999. **9**(4): p. 531-538.

27. Wittebort, R.J. and A. Szabo, *Theory of NMR relaxation in macromolecules: Restricted diffusion and jump models for multiple internal rotations in amino acid side chains.* The Journal of Chemical Physics, 1978. **69**(4): p. 1722-1736.

28. Brex, P.A., et al., *Lesion heterogeneity in multiple sclerosis: a study of the relations between appearances on T1 weighted images, T1 relaxation times, and metabolite concentrations.* Journal of Neurology, Neurosurgery & Psychiatry, 2000. **68**(5): p. 627-632.

29. Mlynárik, V., S. Gruber, and E. Moser, *Proton T1 and T2 relaxation times of human brain metabolites at 3 Tesla.* NMR in Biomedicine, 2001. **14**(5): p. 325-331.

30. Van Walderveen, M.A.A., et al., *Neuronal damage in T1-hypointense multiple sclerosis lesions demonstrated in vivo using proton magnetic resonance spectroscopy.* Annals of Neurology, 1999. **46**(1): p. 79-87.

31. Wang, H.Z., S.J. Riederer, and J.N. Lee, *Optimizing the precision in T1 relaxation estimation using limited flip angles.* Magnetic Resonance in Medicine, 1987. **5**(5): p. 399-416.

32. Dunn, T.C., et al., *T2 Relaxation Time of Cartilage at MR Imaging: Comparison with Severity of Knee Osteoarthritis1.* Radiology, 2004. **232**(2): p. 592-598.

33. Fullerton, G.D., I.L. Cameron, and V.A. Ord, *Orientation of tendons in the*

magnetic field and its effect on T2 relaxation times. Radiology, 1985. **155**(2): p. 433-435.

34. Nieminen, M.T., et al., *T2 relaxation reveals spatial collagen architecture in articular cartilage: A comparative quantitative MRI and polarized light microscopic study.* Magnetic Resonance in Medicine, 2001. **46**(3): p. 487-493.

35. Pervushin, K., et al., *Attenuated T2 relaxation by mutual cancellation of dipole–dipole coupling and chemical shift anisotropy indicates an avenue to NMR structures of very large biological macromolecules in solution.* Proceedings of the National Academy of Sciences, 1997. **94**(23): p. 12366-12371.

36. Stanisz, G.J., et al., *T1, T2 relaxation and magnetization transfer in tissue at 3T.* Magnetic Resonance in Medicine, 2005. **54**(3): p. 507-512.

37. Blum, K., *Density Matrix Theory and Applications, Physics of Atoms and Molecules*. 1981: Plenum Press.

38. Cavanagh, J., et al., *Protein NMR Spectroscopy*. 1 ed. 1996: Academic Press.

39. Nielsen, M.A. and I.L. Chuang, *Quantum Computation and Quantum Information*. 2000: Cambridge University Press.

40. Hore, P., J.A. Jones, and S. Wimperis, *NMR: The Toolkit*. 2000, Oxford: Oxford Chemistry Primers.

41. Claridge, T., *High-resolution NMR Techniques in Organic Chemistry*. 1999: Pergamon.

42. Tycko, R., *Broadband Population Inversion.* Physical Review Letters, 1983. **51**(9): p. 775-777.

43. Wimperis, S., *Broadband, Narrowband, and Passband Composite Pulses for Use in Advanced NMR Experiments.* Journal of Magnetic Resonance, Series A, 1994. **109**(2): p. 221-231.

44. Nishimura, D.G., *Principles of Magnetic Resonance Imaging.* 1996.

45. Hoult, D.I. and R.E. Richards, *The signal-to-noise ratio of the nuclear magnetic resonance experiment.* Journal of Magnetic Resonance (1969), 1976. **24**(1): p. 71-85.

46. Gomori, J.M., et al., *NMR Relaxation Times of Blood: Dependence on Field Strength, Oxidation State, and Cell Integrity.* Journal of Computer Assisted Tomography, 1987. **11**(4): p. 684-690.

47. Hoult, D.I., C.N. Chen, and V.J. Sank, *The field dependence of NMR imaging. II. Arguments concerning an optimal field strength.* Magnetic Resonance in Medicine, 1986. **3**(5): p. 730-746.

48. Tkáč, I., et al., *In vivo 1H NMR spectroscopy of the human brain at high magnetic fields: Metabolite quantification at 4T vs. 7T.* Magnetic Resonance in Medicine, 2009. **62**(4): p. 868-879.

49. Vaughan, J.T., et al., *7T vs. 4T: RF power, homogeneity, and signal-to-noise comparison in head images.* Magnetic Resonance in Medicine, 2001. **46**(1): p. 24-30.

50. Pathria, R.K., *Statistical Mechanics*. 2 ed. 1997: Elsevier Pte Ltd.

51. Carver, T.R. and C.P. Slichter, *Polarization of Nuclear Spins in Metals.* Physical Review, 1953. **92**(1): p. 212-213.

52. Bowers, C.R. and D.P. Weitekamp, *Transformation of symmetrization order to nuclear-spin magnetization by chemical reaction and nuclear magnetic resonance.* Phys Rev Lett, 1986. **57**(21): p. 2645-2648.

53. Maly, T., et al., *Dynamic nuclear polarization at high magnetic fields.* The Journal of Chemical Physics, 2008. **128**(5): p. 052211-19.

54. Gallagher, F.A., et al., *Production of hyperpolarized [1,4-13C2]malate from [1,4-13C2]fumarate is a marker of cell necrosis and treatment response in tumors.* Proceedings of the National Academy of Sciences, 2009. **106**(47): p. 19801-19806.

55. Günther, H., *NMR Spectroscopy*. 2 ed. 1994: John Wiley & Sons.

56. Ferdia, A.G., et al., *Magnetic resonance imaging of pH in vivo using hyperpolarized 13C-labelled bicarbonate.* Nature, 2008. **453**(7197): p. 940-943.

57. Gabellieri, C., et al., *Therapeutic Target Metabolism Observed Using Hyperpolarized 15N Choline.* Journal of the American Chemical Society, 2008. **130**(14): p. 4598-4599.

58. Gore, J.C., et al., *Magnetic resonance in the era of molecular imaging of cancer.* Magnetic Resonance Imaging, 2011. **29**(5): p. 587-600.

59. Albers, M.J., et al., *Hyperpolarized ^{13}C lactate, pyruvate, and alanine: noninvasive biomarkers for prostate cancer detection and garding.* Cancer Res., 2008. **68**(20): p. 8.

60. Day, S.E., et al., *Detecting tumor response to treatment using hyperpolarized 13C magnetic resonance imaging and spectroscopy.* Nature Medicine, 2007. **13**(11): p. 1382-1387.

61. Witney, T.H., et al., *A comparison between radiolabeled fluorodeoxyglucose uptake and hyperpolarized (13)C-labeled pyruvate utilization as methods for detecting tumor response to treatment.* Neoplasia, 2009. **11**(6): p. 8.

62. Herzberg, G., *Molecular Spectra and Molecular Structure*. Vol. 1. 1950: Van Nostrand Reinhold Company.

63. de Angelis, M., et al., *Test of the Symmetrization Postulate for Spin-0 Particles.* Physical Review Letters, 1996. **76**(16): p. 2840-2843.

64. Modugno, G., M. Inguscio, and G.M. Tino, *Search for Small Violations of the Symmetrization Postulate for Spin-0 Particles.* Physical Review Letters, 1998. **81**(22): p. 4790-4793.

65. Sakurai, J.J., *Modern Quantum Mechanics*. 1994: Addison-Wesley.

66. Levine, I.N., *Molecular Spectroscopy*. 1975: John Wiley & Sons.

67. Hollas, J.M., *Modern Spectroscopy*. 3 ed. 1996: John Wiley & Sons.

68. Banwell, C.N., *Fundamentals of Molecular Spectroscopy*. 1983: McGraw-Hill Book Company (UK) Limited.

69. Silvera, I.F., *The solid molecular hydrogens in the condensed phase: Fundamentals and static properties.* Reviews of Modern Physics, 1980. **52**(2): p. 393-452.

70. Anwar, M.S., *NMR Quantum Information Processing Using Para-hydrogen*, 2004, University of Oxford: Oxford.

71. Balling, L.C. and J.J. Wright, *Use of angular‐momentum selection rules for laser isotope separation.* Applied Physics Letters, 1976. **29**(7): p. 411-413.

72. Matsumoto, Y., L.H. Spangler, and D.W. Pratt, *On the origin of the rotational state dependence of the decay of intermediate case molecules. Role of angular momentum selection rules in intersystem crossing.* Chemical Physics Letters, 1983. **98**(4): p. 333-339.

73. Xie, J. and R.N. Zare, *Selection rules for the photoionization of diatomic molecules.* The Journal of Chemical Physics, 1990. **93**(5): p. 3033-3038.

74. Turkevich, J. and P.W. Selwood, *Solid Free Radical as Catalyst for Ortho—Para Hydrogen Conversion1a.* Journal of the American Chemical Society, 1941. **63**(4): p. 1077-1079.

75. Emmett, P.H. and R.W. Harkness, *THE CONVERSION OF PARA HYDROGEN TO ORTHO HYDROGEN OVER IRON SYNTHETIC AMMONIA CATALYSTS.* Journal of the American Chemical Society, 1932. **54**(1): p. 403-404.

76. Feng, B., et al., *A pulsed injection parahydrogen generator and techniques for quantifying enrichment.* Journal of Magnetic Resonance, 2012. **214**(0): p. 258-262.

77. Goldman, M. and H. Johannesson, *Conversion of a proton pair para order into 13C polarization by rf irradiation, for use in MRI.* Comptes Rendus Physique, 2005. **6**(4–5): p. 575-581.

78. Bouchard, L.-S., et al., *NMR Imaging of Catalytic Hydrogenation in Microreactors with the Use of para-Hydrogen.* Science, 2008. **319**(5862): p. 442-445.

79. Eisenschmid, T.C., et al., *Para hydrogen induced polarization in hydrogenation reactions.* Journal of the American Chemical Society, 1987. **109**(26): p. 8089-8091.

80. Kating, P., et al., *Nuclear singlet/triplet mixing during hydrogenations with parahydrogen: an in situ NMR method to investigate catalytic reaction mechanisms and their kinetics. 2. Homogeneous hydrogenation of 1,4-dihydro-1,4-epoxynaphthalene using different rhodium catalysts.* The Journal of Physical Chemistry, 1993. **97**(50): p. 13313-13317.

81. Barkemeyer, J., et al., *Heteronuclear Polarization Transfer Using Selective Pulses during Hydrogenation with Parahydrogen.* Journal of Magnetic Resonance, Series A, 1996. **120**(1): p. 129-132.

82. Sengstschmid, H., et al., *A New Excitation Sequence to Observe the PASADENA Effect.* Journal of Magnetic Resonance, Series A, 1996. **120**(2): p. 249-257.

83. Carson, P.J., C.R. Bowers, and D.P. Weitekamp, *The PASADENA Effect at a Solid Surface: High-Sensitivity Nuclear Magnetic Resonance of Hydrogen Chemisorption.* Journal of the American Chemical Society, 2001. **123**(47): p. 11821-11822.

84. Pravica, M.G. and D.P. Weitekamp, *Net NMR alignment by adiabatic transport of parahydrogen addition products to high magnetic field.* Chemical Physics Letters, 1988. **145**(4): p. 255-258.

85. Natterer, J. and J. Bargon, *Parahydrogen induced polarization.* Progress in Nuclear Magnetic Resonance Spectroscopy, 1997. **31**(4): p. 293-315.

86. Bowers, C.R., *Para-hydrogen And Synthesis Allow Dramatic Enhanced Nuclear Alignment*, 1991, California Institute of Technology.

87. Buntkowsky, G., J. Bargon, and H.-H. Limbach, *A Dynamic Model of Reaction Pathway Effects on Parahydrogen-Induced Nuclear Spin*

Polarization. Journal of the American Chemical Society, 1996. **118**(36): p. 8677-8683.

88. Bouchard, L.-S., et al., *Para-Hydrogen-Enhanced Hyperpolarized Gas-Phase Magnetic Resonance Imaging.* Angewandte Chemie International Edition, 2007. **46**(22): p. 4064-4068.

89. Waddell, K., *Parahydrogen Production and Polarizer.* U.S. Patent Application, 2011. **61**(478): p. 193.

90. Eisenberg, R., *Parahydrogen-induced polarization: a new spin on reactions with molecular hydrogen.* Accounts of Chemical Research, 1991. **24**(4): p. 110-116.

91. Canet, D., et al., *Para-hydrogen enrichment and hyperpolarization.* Concepts in Magnetic Resonance Part A, 2006. **28A**(5): p. 321-330.

92. Ienco, A., et al., *Activation of Molecular Hydrogen over a Binuclear Complex with Rh2S2 Core: DFT Calculations and NMR Mechanistic Studies.* Journal of the American Chemical Society, 2004. **126**(38): p. 11954-11965.

93. Zhou, R., et al., *Parahydrogen derived illumination of pyridine based coordination products obtained from reactions involving rhodium phosphine complexes.* Dalton Transactions, 2005. **0**(23): p. 3773-3779.

94. López-Serrano, J., S.B. Duckett, and A. Lledós, *Palladium-Catalyzed Hydrogenation: Detection of Palladium Hydrides. A Joint Study Using Para-Hydrogen-Enhanced NMR Spectroscopy and Density Functional Theory*. Journal of the American Chemical Society, 2006. **128**(30): p. 9596-9597.

95. Johansson, E., et al., *Perfusion assessment with bolus differentiation: A technique applicable to hyperpolarized tracers.* Magnetic Resonance in Medicine, 2004. **52**(5): p. 1043-1051.

96. Goldman, M., et al., *Design and implementation of 13C hyper polarization from para-hydrogen, for new MRI contrast agents.* Comptes Rendus Chimie, 2006. **9**(3–4): p. 357-363.

97. Maki, J.H., T.L. Chenevert, and M.R. Prince, *Three-dimensional*

Contrast-enhanced MR Angiography. Topics in Magnetic Resonance Imaging, 1996. **8**(6): p. 322-344.

98. Golman, K. and J.S. Petersson, *Metabolic Imaging and Other Applications of Hyperpolarized 13C1.* Academic radiology, 2006. **13**(8): p. 932-942.

99. Månsson, S., et al., *13C imaging—a new diagnostic platform.* European Radiology, 2006. **16**(1): p. 57-67.

100. Fuchs, F., G. Laub, and K. Othomo, *TrueFISP—technical considerations and cardiovascular applications.* European Journal of Radiology, 2003. **46**(1): p. 28-32.

101. Golman, K., et al., *Molecular imaging with endogenous substances.* Proceedings of the National Academy of Sciences, 2003. **100**(18): p. 10435-10439.

102. Norris, D.G. and J.M.S. Hutchison, *Concomitant magnetic field gradients and their effects on imaging at low magnetic field strengths.* Magnetic resonance imaging, 1990. **8**(1): p. 33-37.

103. Jóhannesson, H., O. Axelsson, and M. Karlsson, *Transfer of para-hydrogen spin order into polarization by diabatic field cycling.* Comptes Rendus Physique, 2004. **5**(3): p. 315-324.

104. Ardenkjaer-Larsen, J.H., et al., *Increase in signal-to-noise ratio of > 10,000 times in liquid-state NMR.* Proceedings of the National Academy of Sciences of the United States of America, 2003. **100**(18): p. 10158-10163.

105. Golman, K., et al., *Metabolic imaging by hyperpolarized 13C magnetic resonance imaging for in vivo tumor diagnosis.* Cancer Res, 2006. **66**(22): p. 10855-60.

106. Carver, T.R. and C.P. Slichter, *Experimental Verification of the Overhauser Nuclear Polarization Effect.* Physical Review, 1956. **102**(4): p. 975-980.

107. Overhauser, A.W., *Polarization of Nuclei in Metals.* Physical Review, 1953. **92**(2): p. 411.

108. Albers, M.J., et al., *Hyperpolarized 13C lactate, pyruvate, and alanine: noninvasive biomarkers for prostate cancer detection and grading.* Cancer Res, 2008. **68**(20): p. 8607-15.

109. Day, S.E., et al., *Detecting tumor response to treatment using hyperpolarized 13C magnetic resonance imaging and spectroscopy.* Nat Med, 2007. **13**(11): p. 1382-7.

110. Golman, K. and J.S. Petersson, *Metabolic imaging and other applications of hyperpolarized 13C1.* Acad Radiol, 2006. **13**(8): p. 932-42.

111. Bowers, C.R. and D.P. Weitekamp, *Para-Hydrogen and Synthesis Allow Dramatically Enhanced Nuclear Alignment.* Journal of the American Chemical Society, 1987. **109**(18): p. 5541-5542.

112. Bowers, C.R. and D.P. Weitekamp, *Transformation of Symmetrization Order to Nuclear-Spin Magnetization by Chemical-Reaction and Nuclear-Magnetic-Resonance.* Physical Review Letters, 1986. **57**(21): p. 2645-2648.

113. Adams, R.W., et al., *Reversible interactions with para-hydrogen enhance NMR sensitivity by polarization transfer.* Science, 2009. **323**(5922): p. 1708-11.

114. Goldman, M., et al., *Hyperpolarization of 13C through order transfer from parahydrogen: a new contrast agent for MRI.* Magn Reson Imaging, 2005. **23**(2): p. 153-7.

115. Kadlecek, S., et al., *Optimal transfer of spin-order between a singlet nuclear pair and a heteronucleus.* J Magn Reson, 2011. **205**(1): p. 9-13.

116. Neumann, J.v., *Mathematical Foundations of Quantum Mechanics*. 1955, Princeton, NJ: Princeton Univ. Press.

117. Waddell, K.W., A.M. Coffey, and E.Y. Chekmenev, *In Situ Detection of PHIP at 48 mT: Demonstration Using a Centrally Controlled Polarizer.* Journal of the American Chemical Society, 2010. **133**(1): p. 97-101.

118. Coffey, A.M., et al., *A large volume double channel 1H–X RF probe for*

hyperpolarized magnetic resonance at 0.0475 T. Journal of Magnetic Resonance, 2012. **220**(0): p. 94-101.

119. Goldman, M., et al., *Hyperpolarization of 13C through order transfer from parahydrogen: A new contrast agent for MRI.* Magnetic resonance imaging, 2005. **23**(2): p. 153-157.

120. Bowers, C.R. and D.P. Weitekamp, *Parahydrogen and synthesis allow dramatically enhanced nuclear alignment.* Journal of the American Chemical Society, 1987. **109**(18): p. 5541-5542.

121. Kadlecek, S., et al., *Optimal transfer of spin-order between a singlet nuclear pair and a heteronucleus.* Journal of Magnetic Resonance, 2010. **205**(1): p. 9-13.

122. Sarkar, R., et al., *Proton NMR of 15N-Choline Metabolites Enhanced by Dynamic Nuclear Polarization.* Journal of the American Chemical Society, 2009. **131**(44): p. 16014-16015.

123. Reineri, F., et al., *15N Magnetic Resonance Hyperpolarization via the Reaction of Parahydrogen with 15N-Propargylcholine.* Journal of the American Chemical Society, 2012. **134**(27): p. 11146-11152.

124. Cai, C., et al., *Efficient Transformation of Parahydrogen Spin Order into Heteronuclear Magnetization.* The Journal of Physical Chemistry B, 2012.

125. Reineri, F., et al., *Effect of low and zero magnetic field on the hyperpolarization lifetime in parahydrogenated perdeuterated molecules.* J Magn Reson, 2009. **200**(1): p. 15-20.

126. Lowenstein, J., *Methods in Enzymology, Volume 13: Citric Acid Cycle*. Vol. 13. 1969, Boston: Academic Press.

127. Krebs HA, W.P., *Kreb's citric acid cycle: half a century and still turning*. 1987, London: Biochemical Society.

128. Lane, N., *Life Ascending: The Ten Great Inventions of Evolution*. 2009, New York: W.W.Norton & Co.

129. H.A., K. and J. W.A., *The role of citric acid in intermediate metabolism in animal tissues.* Enzymologia, 1937. **4**: p. 148-156.

130. Reineri, F., et al., *Effect of low and zero magnetic field on the hyperpolarization lifetime in parahydrogenated perdeuterated molecules.* Journal of Magnetic Resonance, 2009. **200**(1): p. 15-20.

131. Tadanki, S., et al., *Double tuning a single input probe for heteronuclear NMR spectroscopy at low field.* Journal of Magnetic Resonance, 2012. **223**(0): p. 64-67.

132. Patt, S.L. and J.N. Shoolery, *Attached proton test for carbon-13 NMR.* Journal of Magnetic Resonance (1969), 1982. **46**(3): p. 535-539.

133. Crews, P., et al., *Residually coupled attached proton test in the 13C NMR assignment of natural products.* Magnetic Resonance in Chemistry, 1985. **23**(8): p. 684-687.

134. Radel, P.A. and S.B. Kahl, *A useful modification of the attached proton test 13C NMR experiment: Unambiguous peak assignments for carbons with large 1J(CH) values.* Tetrahedron Letters, 1996. **37**(37): p. 6623-6626.

135. Morris, G.A., *Sensitivity enhancement in nitrogen-15 NMR: polarization transfer using the INEPT pulse sequence.* Journal of the American Chemical Society, 1980. **102**(1): p. 428-429.

136. Blinka, T.A., B.J. Helmer, and R. West, *Polarization Transfer NMR Spectroscopy for Silicon-29: The INEPT and DEPT Techniques*, in *Advances in Organometallic Chemistry*, F.G.A. Stone and W. Robert, Editors. 1984, Academic Press. p. 193-218.

137. Duckett, S.B., C.L. Newell, and R. Eisenberg, *More than INEPT: parahydrogen and INEPT + give unprecedented resonance enhancement to carbon-13 by direct proton polarization transfer.* Journal of the American Chemical Society, 1993. **115**(3): p. 1156-1157.

138. Fyfe, C.A., et al., *INEPT Experiments in Solid-State NMR.* Journal of the American Chemical Society, 1995. **117**(41): p. 10397-10398.

139. Weigelt, J. and G. Otting, *1H-Detected INEPT-INADEQUATE at Natural 13C Abundance.* Journal of Magnetic Resonance, Series A, 1995. **113**(1): p. 128-130.

140. Kao, H.-M. and C.P. Grey, *INEPT Experiments Involving Quadrupolar Nuclei in Solids.* Journal of Magnetic Resonance, 1998. **133**(2): p. 313-323.

141. Elena, B., et al., *Proton to Carbon-13 INEPT in Solid-State NMR Spectroscopy.* Journal of the American Chemical Society, 2005. **127**(49): p. 17296-17302.

142. Pegg, D.T. and M.R. Bendall, *Two-dimensional DEPT NMR spectroscopy.* Journal of Magnetic Resonance (1969), 1983. **55**(1): p. 114-127.

143. Gençten, A., T. Özdoğan, and F. Köksal, *A Product Operator Theory of 2D Dept J-Resolved NMR Spectroscopy for IS N Spin System (I = 1/2, S = 1).* Spectroscopy Letters, 1998. **31**(5): p. 981-987.

144. Yamada, T. and H. Ono, *Rapid liquefaction of lignocellulosic waste by using ethylene carbonate.* Bioresource Technology, 1999. **70**(1): p. 61-67.

145. Brar, A.S., K. Dutta, and S.K. Hekmatyar, *Stereochemical and compositional assignment of acrylonitrile/methyl methacrylate copolymers by DEPT and inverse HECTOR NMR spectroscopy.* Journal of Polymer Science Part A: Polymer Chemistry, 1998. **36**(7): p. 1081-1092.

146. Marion, D. and K. Wüthrich, *Application of phase sensitive two-dimensional correlated spectroscopy (COSY) for measurements of 1H-1H spin-spin coupling constants in proteins.* Biochemical and Biophysical Research Communications, 1983. **113**(3): p. 967-974.

147. Rance, M., et al., *Improved spectral resolution in COSY 1H NMR spectra of proteins via double quantum filtering.* Biochemical and Biophysical Research Communications, 1983. **117**(2): p. 479-485.

148. Griesinger, C., O.W. Sørensen, and R.R. Ernst, *Practical aspects of the E.COSY technique. Measurement of scalar spin-spin coupling constants in peptides.* Journal of Magnetic Resonance (1969), 1987. **75**(3): p. 474-492.

149. Griesinger, C., et al., *Clean TOCSY for proton spin system identification in macromolecules.* Journal of the American Chemical Society, 1988. **110**(23): p. 7870-7872.

150. Kim, Y. and J.H. Prestegard, *Measurement of vicinal couplings from cross peaks in COSY spectra.* Journal of Magnetic Resonance (1969), 1989. **84**(1): p. 9-13.

151. Maier, R., *Cooler synchrotron COSY — Performance and perspectives.* Nuclear Instruments and Methods in Physics Research Section A: Accelerators, Spectrometers, Detectors and Associated Equipment, 1997. **390**(1–2): p. 1-8.

152. Meissner, A., J.ø. Duus, and O.W. Sørensen, *Spin-State-Selective Excitation. Application for E.COSY-Type Measurement ofJHHCoupling Constants.* Journal of Magnetic Resonance, 1997. **128**(1): p. 92-97.

153. Abdel-Bary, M., et al., *Evidence for a narrow resonance at 1530 MeV/c2 in the K0p-system of the reaction pp→Σ+K0p from the COSY-TOF experiment.* Physics Letters B, 2004. **595**(1 – 4): p. 127-134.

154. Cavanagh, J. and M. Rance, *Sensitivity improvement in isotropic mixing (TOCSY) experiments.* Journal of Magnetic Resonance (1969), 1990. **88**(1): p. 72-85.

155. Hwang, T.L. and A.J. Shaka, *Cross relaxation without TOCSY: transverse rotating-frame Overhauser effect spectroscopy.* Journal of the American Chemical Society, 1992. **114**(8): p. 3157-3159.

156. Kay, L.E., et al., *A Gradient-Enhanced HCCH-TOCSY Experiment for Recording Side-Chain 1H and 13C Correlations in H2O Samples of Proteins.* Journal of Magnetic Resonance, Series B, 1993. **101**(3): p. 333-337.

157. Logan, T., et al., *A general method for assigning NMR spectra of denatured proteins using 3D HC(CO)NH-TOCSY triple resonance experiments.* Journal of Biomolecular NMR, 1993. **3**(2): p. 225-231.

158. Anderson, R.C., J.P. Stokes, and M.J. Shapiro, *Structure determination in combinatorial chemistry: Utilization of Magic Angle Spinning HMQC and*

TOCSY NMR spectra in the structure determination of Wang-bound lysine. Tetrahedron Letters, 1995. **36**(30): p. 5311-5314.

159. Kevin, H.G., et al., *An (H)C(CO)NH-TOCSY pulse scheme for sequential assignment of protonated methyl groups in otherwise deuterated 15N, 13C-labeled proteins.* Journal of Biomolecular NMR, 1996.

160. Nunes, M.T., V.M.S. Gil, and J. Ascenso, *The conformation of succinic acid in aqueous solution studied by 1h and 13c nmr.* Tetrahedron, 1981. **37**(3): p. 611-614.

161. Price, D.J., J.D. Roberts, and W.L. Jorgensen, *Conformational Complexity of Succinic Acid and Its Monoanion in the Gas Phase and in Solution: Ab Initio Calculations and Monte Carlo Simulations.* Journal of the American Chemical Society, 1998. **120**(37): p. 9672-9679.

162. Roberts, J.D., *Fascination with the Conformational Analysis of Succinic Acid, as Evaluated by NMR Spectroscopy, and Why†.* Accounts of Chemical Research, 2006. **39**(12): p. 889-896.

163. Chekmenev, E.Y., et al., *PASADENA Hyperpolarization of Succinic Acid for MRI and NMR Spectroscopy.* Journal of the American Chemical Society, 2008. **130**(13): p. 4212-4213.